Modified nucleotides and nucleic acids for the discovery of antiretroviral agents targeting HIV-1 reverse transcriptase

Alexander S. Wahba

Department of Chemistry, McGill University

Montreal, QC, Canada

May, 2010

A thesis submitted to McGill University in partial fulfillment of the requirements of the degree of Doctor of Philosophy

Dedicated to the memory of Henena "Margo" Marguerite Wahba
December 7, 1930 – June 29, 2005

Teta Margo wanted most in life to bring together
those she loved in peace and happiness

She loved all, and was loved by all

Copyright statement

Abstract

The reverse transcriptase (RT) of the human immunodeficiency virus (HIV) has both polymerase and ribonuclease H (RNase H) activity, and is a key enzyme in the HIV life cycle as it converts the viral RNA genome into double-stranded DNA. A series of studies built around the theme of chemically modified nucleic acids are described in order to: (1) better understand the biochemical processes of reverse transcription in HIV-1, (2) synthesize antiretroviral agents directed to novel targets on HIV-1 (RT), and (3) develop screening methods incorporating fluorescent nucleobase analogues to uncover new drug candidates.

We demonstrated how chemically modified nucleic acid hairpins inhibited the RNase H activity of HIV-1 RT. For example, substituting natural RNA for 2'-deoxy-2'-fluoro-ribonucleotides, 2'-deoxy-2'-fluoro-arabinonucleotides, locked nucleic acids or conjugation of cholesterol at the 5'-terminus modulated the potency of hairpins for RNase H activity. Biochemical methods indicated that the substrate for HIV-1 RT, a short primer-long template, may be bound at the polymerase domain with its trajectory diverted away from the RNase H domain by the presence of the synthetic hairpins. Furthermore, the binding of hairpins to HIV-1 RT had no adverse affects on the potency of chain terminators such as 3'-azido-3'-deoxythymidine (AZT), a widely used antiviral agent. This discovery supports a model where the RNase H activity can be an antiretroviral target independent of the rest of RT.

We synthesized 6-phenylpyrroloribocytidine (PhpC), a novel fluorescent cytidine analogue incorporated into RNA. The PhpC-containing RNA formed native-like duplex structures with complementary strands and fluorometrically reported upon binding to complementary RNA and DNA strands. PhpC was shown to rank among the brightest fluorescent cytidine analogues based on quantum yields. RNA containing PhpC was cleaved by HIV-1 RT RNase H with a 14-fold increase in fluorescence intensity. In contrast to the same fluorescein/DABCYL containing oligonucleotides used in older RNase H assays to screen for inhibitors, PhpC containing RNA did not disrupt catalytic activity of the enzyme. Furthermore, the PhpC RNase H assay was implemented on 96-well microplate format, the first example among fluorescent nucleobase analogues.

Small interfering RNAs (siRNAs) containing PhpC were synthesized and shown to possess enhanced thermal stability and good gene-silencing activity. Due to their emissive properties, the biodistribution of PhpC-containing siRNAs could be monitored by fluorescence microscopy and were shown to accumulate in the cytoplasm in HeLa cells.

We synthesized a series of oligonucleotide primers with 3'-terminated nucleosides of varying sugar conformations. This was accomplished on solid supports using a methodology that avoids the direct coupling of phosphoramidite building blocks. The synthesis of an analogous AZT 3'-terminated primer was accomplished using AZT 5'-H-phosphonate with greater ease, speed and yield compared to traditional enzymatic approaches. We tested the primers as substrates for RT-catalyzed nucleotide excision, the phenotypic mechanism of drug resistance in HIV strains carrying thymidine analogue mutations (TAMs). We determined that in general RNA-like sugar conformations are poorly excised by HIV-1 RT, while DNA-like sugar conformations are quickly excised. Fluorescence-based nucleotide excision assays incorporating the emissive nucleobase analogues PhpC and 2-AP were explored. The rate of nucleotide excision could be monitored in 96-well microplate format for the PhpC-containing assay only.

Abrégé

La transcriptase inverse (RT) du virus de l'immunodéficience humaine de type 1 (VIH-1) possède deux activités: polymérase et ribonucléase H (RNase H), en faisant l'enzyme clé pour le cycle de vie du VIH puisqu'elle convertit l'ARN viral génome en ADN à double brins. Des études portant sur des acides nucléiques modifiés chimiquement sont ici décris afin de : (1) mieux comprendre les procédés biochimiques sous-tendant la transcription inverse du virus d'immunodéficience humaine de type 1 (VIH-1), (2) synthétiser des agents antirétroviraux dirigés contre de nouvelles cibles de la transcriptase inverse (RT) du VIH-1, et (3) développer des méthodes de criblage incorporant des analogues de nucléobase fluorescente afin de découvrir de nouveaux candidats thérapeutiques.

Nous avons ainsi démontré comment de petits acides nucléiques modifiés (épingles) inhibent l'activité ribonucléase (RNase H) de la RT VIH-1. Par exemple, la substitution de l'ARN naturel par des 2'-fluoro-2'-désoxyribonucléotides, 2'-fluoro-2'-désoxyarabinonucléotides, acides nucléiques verrouillés ou la conjugaison du cholestérol à l'extrémité 5', ont modulé la puissance de l'épingle face à l'activité de la RNase H. Des méthodes biochimiques ont démontré que le substrat de la RT VIH-1, un double brin de ADN amorceur-gabarit, peut être lié au domaine polymérase lorsque sa trajectoire est déviée du domaine RNase H par la présence d'épingles. De surcroît, la liaison des épingles à la RT VIH-1 n'a eu aucun effet négatif sur la puissance de terminateurs de chaîne tels que le 3'-azido-3'-désoxythymidine (AZT), un agent antirétroviral largement utilisé. Cette découverte supporte le modèle selon lequel l'activité de RNase H représente une cible antirétrovirale indépendante du reste de la RT.

Nous avons synthétisé la 6-phénylpyrroloribocytidine (PhpC), un nouvel analogue fluorescent de la cytidine incorporé dans l'ARN. Cet ARN contenant de la PhpC a formé des structures ressemblant à des brins doubles natifs ayant des branches complémentaires et est reconnu par fluorométrie après liaison à une branche d'ARN ou d'ADN complémentaire. Se basant sur son rendement quantique, la PhpC se révéla un des analogues fluorescents de la cytidine les plus lumineux. Mais encore, l'ARN contenant de la PhpC fût coupé par la RNase H de la RT VIH-1, augmentant quatorze

fois l'intensité de la fluorescence. Contrairement aux mêmes oligonucléotides contenant de la fluorescéine/DABCYL utilisés dans d'anciennes expériences de criblage d'inhibiteurs, l'ARN contenant de la PhpC n'a pas rompu l'activité catalytique de l'enzyme. De plus, l'expérience PhpC-RNase H a pu être appliquée sur un format de microplaque de 96 puits, le premier exemple d'une telle application parmi les analogues fluorescents de nucléobase.

De petits ARNs interférents (*siRNAs*) contenant de la PhpC furent synthétisés et démontrèrent une stabilité thermale améliorée et une bonne activité d'extinction de gènes. À cause de leurs propriétés émissives, la biodistribution des siRNAs contenant de la PhpC a pu être suivie par microscopie à fluorescence, illustrant une accumulation dans le cytoplasme des cellules HeLa.

Nous avons aussi synthétisé une série d'amorces d'oligonucléotides ayant un nucléoside terminé en 3' avec des conformations variées de sucre. Ceci fût accompli grâce à l'utilisation d'une méthodologie divergente de phosphitylation/couplage sur colonne qui évite la synthèse de composants individuels de phosphoramidite. Ainsi, la synthèse d'un analogue d'amorce de l'AZT terminé en 3' fut réalisée en employant un AZT 5'-H-phosphonate avec une plus grande facilité, rapidité et un meilleur rendement comparé aux approches traditionnelles enzymatiques. Nous avons testés ces amorces en tant que substrats pour l'excision d'un nucléotide dirigée par la RT, le mécanisme phénotypique de la résistance aux médicaments dans les souches de VIH portant des mutations sur les analogues de thymidine (TAMs). Nous avons également déterminé qu'en général, les conformations de sucre ressemblant à l'ARN sont pauvrement excisées par la RT VIH-1, tandis que celle ressemblant à l'ADN sont rapidement excisées. Des expériences mesurant l'excision de nucléotides fluorescents incorporant les analogues de nucléobase PhpC et 2-AP ont été explorées. Le rythme de l'excision des nucléotides a pu être suivi seulement dans les plaques de 96 puits contenant de la PhpC.

Acknowledgements

I have been very fortunate to have met Professor Damha in my first semester at McGill, and later on, joining his research group. He has been my greatest mentor throughout my academic career and a role-model for scholarly excellence. I thank him for his constant support, motivation, encouragement, for always demanding my very best and confidence in my capacities as a scientist.

I also thank Professor Damha for amassing a lab group of wonderful individuals to whom I owe so much of my success: Sandra, Kazim, Rami, Maria, Anna, Anne, Katya, Min, Mohamed, Karolina, Robert, Paul, David, Jon, Siara, Benedicte, Jeremy, Matt, Pascal, Dilip, Nuria, Jean-Christophe, Adam, Glen, Malik, Julia, Paula, Fereshteh, Maryam, Jovanka and Nerea. Thanks to your shared knowledge and camaraderie, you helped me surmount the obstacles of doing research, and it is because of teamwork that I obtain a Ph.D. I am also grateful for the students I have supervised, Jennifer, Jeremy S. and Kim, you showed me the joys of teaching science.

I must give a special thank you to Dr. Katya Viazozkina, who taught us her mastery of oligonucleotide synthesis. Without her help, we would have been lost. Dr. David Sabatino, I am always grateful for your willingness to help me, both in the lab and in the classroom dating back to Champlain. To Robert Donga as well, for teaching me how to run columns. I want to thank the original members of the B-D crew, Pascal Gallant, Glen Deleavey and Adam Katolik for the good times, and Matthew Hassler as well for putting himself up for charity. I want to thank all the members who helped me at the end of my degree, especially the new members who were patient with me as I finished my final experiments and let me use their office space. Finally, I must single out Dr. Jonathan Watts and Dr. Jeremy Lackey, two colleagues who have made a tremendous impact on my academic and personal lives. Each of your presence helped create the perfect learning environment, and I already miss discussing science and running new ideas by each other. Jon, your kindness is unsurpassed, and I am so fortunate to have worked by your side. Jeremy, your motivation and swagger is infectious. I am indebted to you for looking out for my best interests.

I have been very fortunate to have worked with world-class collaborators who have allowed me to share their work. I have much to thank Professor Robert H.E. Hudson from the University of Western Ontario, who introduced me to fluorescent nucleobases and brought my Ph.D. to another level. I greatly appreciate him trusting my ideas and being constantly available to discuss our projects. I thank Professor Michael Parniak and his lab group for providing materials and expertise in RNase H, and also inviting me to the University of Pittsburgh. I also appreciate his post-doc, Dr. Tatiana Ilina for befriending me during my stay and willing to continue the nucleotide excision studies. I also must thank Dr. Matthias Götte for adopting me in his lab to learn his novel biochemical techniques and his support throughout my graduate studies. I thank his lab group, especially Bruno and Sue, for their time, materials and exchanging ideas. I am grateful for Kalle Gehring and Tara Sprules for tremendous time spent on doing protein NMR experiments, despite the heavy usage of the instrument. I also thank Dr. Orval Mamer and Dr. Marcos Di Falco for their work analyzing and interpreting protein MS data. I thank Georgios Rizis for carrying out the DLS experiments. Finally, I appreciate all the help from Professor Jerry Pelletier and a big thank you to Dr. Francis Robert for always willing to run luciferase assays.

I am grateful to many Professors in our wonderful Department of Chemistry. I thank Dr. Karine Auclair for giving me access to her lab and the use of the plate reader and CD spectroscopy and Dr. Bruce Lennox for the use of the fluorescence spectrometer. Dr. Tony Mittermaier, for using his lab to carry out the cross-link experiments. Dr. Youla Tsantrizos for always providing sound scientific advice and helping me decide to make the switch to Chemistry. Dr. Gonzalo Cosa for teaching me fluorescence and Dr. William Galley for teaching me physical chemistry. The late Dr. George Just, who always encouraged me to get my first paper out, for saying a good scientist must be good at reporting his work. I appreciate many discussions with Dr. Jean-Christophe Leroux, and his objectivity. I especially am grateful to Professor James Gleason, for making certain that I learned organic chemistry, and always keeping us on our toes.

I am very grateful for having a wonderful staff in Chemistry that allowed me to carry out my research: Chantal Marotte, Sandra Aerssen, Allison McCaffrey, Faye Nurse, Carole Brown, Robert Workman, Louis Godbout and Colleen McNamee. There are three indispensable individuals in chemistry; Fred Kluck, Georges Kopp and Rick Rossi. We could not function without you. Also Nadim Saade and Antisar Hlil for their assistance with MS and Dr. Claire Brown and Alex Spurmanis from the McGill Imaging Facility.

No two people in the world have provided constant support as much as my parents. I could not ask for more, and you made sure I never had to. On so many occasions they took care of other aspects of my life, and cleared their agenda's for me. I am always grateful, even if I was rushing out the door and did not look like it. My success is theirs and because of them. I also share my success with my brothers, my other two biggest fans, along with the other Wahba clan members, Claudia, Vanessa, Kali, Gabi and Tristan. This is the end of an era, and I will miss living by your side.

I have been blessed with special friends that encouraged me throughout my studies. First, Christophe and Sabine, my dearest friends, always looked out for my best interests, especially Christophe with his magic LC columns. Tony and Stephane, my good friends, thanks for pulling me out of the lab when I needed to loosen up.

I have to thank little Yuri the cat, for being my loyal companion and a source of comfort, especially those late nights coming home from the lab.

Finally, I have much to thank Nancy, who was by my side from the start and at the end. I especially appreciate her enduring my late nights while writing this thesis. But most of all, her courage and dedication in the face of her own adversity are an inspiration. She showed me that it is never too late to achieve your goals.

Alexander Sean Wahba

Table of Contents

List of Figures

List of Schemes

List of Tables

Abbreviations

A	adenosine
Å	Angstrom
a.u.	arbitrary units
A_{260}	UV absorbance at 260 nm
Ac2O	acetic anhydride
ACN	acetonitrile
Ade	adenine
AIDS	acquired immune deficiency syndrome
AMP	adenosine 5'-monophosphate
ANA	arabinonucleic acid
AON	antisense oligonucleotide
2-AP	2-aminopurine
APS	ammonium persulfate
ATP	adenosine 5'-triphosphate
AZT	3'-deoxy-3'-azidothymidine
B	base
BDF	base discriminating fluorophore
bp	base pair
Bz	benzoyl
C	cytidine
CD	circular dichroism
cDNA	complementary DNA
CE	2-cyanoethyl
Cyt	cytosine
d	doublet
DABCYL	4-(4-dimethylaminophenyl) azobenzoyl; para-methyl red)
DCI	4,5-dicyanoimidazole
DCM	dichloromethane
dd	doublet of doublets

ddC	2',3'-dideoxycytidine
ddI	2',3'-dideoxyinosine
ddT	2',3'-dideoxythymidine
DEPC	diethylpyrocarbonate
DHBNH	dihydroxy benzoyl naphthyl hydrazone
DIPEA	*N*,*N*-diisopropylethylamine
DMAP	4-(dimethylamino)pyridine
DMEM	Dulbecco's modified Eagle medium
DMF	*N*,*N*-dimethylformamide
DMSO	dimethylsulfoxide
DMT	4,4'-*O*-dimethoxytrityl
DNA	2'-deoxyribonucleic acid
dNTP	2'-deoxyribonucleoside 5'-triphosphate
ds	double-stranded
dT	2'-deoxythymidine
DTT	dithiothreitol (*threo*-1,4-dimercapto-2,3-butanediol)
E. coli	*Escherichia coli*
ESI-MS	electrospray ionization mass spectrometry
Et	ethyl
EtOAc	ethyl acetate
EtOH	ethanol
ETT	5-(ethylthio)-1H-tetrazole
2'F-ANA	2'-deoxy-2'-fluoroarabinonucleic acid
2'F-araN	2'-deoxy-2'-fluoroarabinonucleoside
FBS	fetal bovine serum
FP	fluorescence polarization
2'F-RNA	2'-deoxy-2'-fluororibonucleic acid
FRET	fluorescence resonance energy transfer
G	guanosine
Gua	guanosine
HeLa	Henrietta Lacks immortal cells

HI	HIV integrase
HIV	human immunodeficiency virus
HIV-1	human immunodeficiency virus type 1
HPLC	high performance (or high pressure) liquid chromatography
HSQC	heteronuclear single quantum correlation spectroscopy (NMR)
J	scalar coupling constant (in Hz)
LNA	locked nucleic acid, *i.e.* containing 2'-*O*,4'-*C*-methylene-bicyclo
MALDI	matrix-assisted laser desorption/ionization (mass spectrometry)
Me	methyl
MeOH	methanol
MepC	6-methylpyrrolocytidine
miRNA	micro RNA
MMT	4-monomethoxytrityl
MOMpC	6-methoxymethylpyrrolocytidine
mRNA	messenger RNA
MS	mass spectrometry
NEt_3	triethylamine
NMP	*N*-methylpyrrolidinone (*i.e.*, 1-methyl-2-pyrrolidinone)
NMR	nuclear magnetic resonance spectroscopy
NNRTI	non-nucleoside reverse transcriptase inhibitor
NRTI	nucleoside analog reverse transcriptase inhibitor
NTP	nucleoside 5'-triphosphate
ODU	optical density units, defined as the hypothetical A260 of a solution
PAGE	polyacrylamide gel electrophoresis
PBS	primer binding site
pC	pyrrolocytidine
PCR	polymerase chain reaction
PI	polydispersity index
PhpC	6-phenylpyrrolocytidine
PO	phosphodiester (linkage)
PPT	polypurine tract

PS	phosphorothioate (linkage)
R_f	retention factor (in TLC)
r.f.u.	relative fluorescence units
r.t.	room temperature
RET	resonance energy transfer
RISC	RNA-induced silencing complex
RNA	ribonucleic acid
RNAi	RNA interference
RNase H	ribonuclease H
rNTP	ribonucleoside 5'-triphosphate
rRNA	ribosomal RNA
RT	reverse transcriptase
SELEX	systematic evolution of ligands by exponential enrichment
shRNA	short hairpin RNA
siRNA	small interfering RNA
ss	single-stranded
SVPDE	snake venom phosphodiesterase, a 3'-exonuclease
t	triplet
T	thymidine
TAM	thymidine analogue mutation
TBAF	tetrabutylammonium fluoride
TBDMS	terbutyldimethylsilyl
TCA	trichloroacetic acid
TEA	triethylamine
TEAA	triethylammonium acetate
TEMED	*N*,*N*,*N*',*N*'-tetramethylethylenediamine
THF	tetrahydrofuran
Thy	thymine
TLC	thin-layer chromatography
TLR	toll-like receptor
T_m	melting temperature

Tris	tris(hydroxtmethyl)aminomethane
tRNA	transfer RNA
U	uridine
Ura	uracil
UV	ultraviolet (spectroscopy)
WT	wild type
Φ	quantum yield
ε	extinction coefficient
λ	wavelength

Chapter 1. Introduction

Nucleic acids play central roles in cellular processes.[1] The study of their chemical structure is thus important to understanding their function in biology and furthering their development as tools for medicine, diagnostics, forensics or materials sciences. This thesis describes a series of studies built around the theme of chemically modified nucleic acids and their biological effects. Two unifying themes run throughout all of the experiments in this thesis. The first is the theme of progress toward nucleotide and oligonucleotide-based therapeutics, specifically, inhibitors of the reverse transcriptase (RT) enzyme of the human immunodeficiency virus (HIV),[2,3] the causative agent of the acquired immunodeficiency syndrome (AIDS). The second is the development of new fluorescence-based tools for studying nucleic acids and cellular processes.

1.1 Nucleic Acid Structure and Function[1]

1.1.1 The discovery of the DNA double helix

As advances in biology and medicine benefit from chemistry, they are often the source of motivation for much work done in the physical sciences. In 1944, Oswald Avery identified deoxyribonucleic acids (DNA) as the material responsible for hereditary characters[4] and inspired investigators to elucidate its structure. In 1953 Francis Crick and James Watson answered this call, and they published their model for the double helix structure of DNA.[5] Based on X-ray crystallographic data from Maurice Wilkins[6], Rosalind Franklin[7] and experimental results from other researchers, they refined their hypothesis by simply using cardboard and metal molecular models. The implications of their discovery for chemistry are perhaps overshadowed by their impact on biology as it *"suggests a possible copying mechanism for the genetic material"*. This model for the replication of DNA, the substance of genes,[8] brought nucleic acids into the spotlight of biology and ultimately revolutionized our understanding of life. Table 1.1 illustrates key discoveries, in chronological order, that led to Watson and Crick's DNA double helix model, contributions from biologists and chemists alike.

Table 1.1. Chronology of key discoveries that led to the elucidation to the structure of the DNA double helix.

1868	Friedrich Miescher isolated cell nuclei and named the material nuclein. He later observed that it was very acidic.[1]
1889	Richard Altman isolated the first protein-free nuclein and referred to the material as *nucleic acids*.[1]
1900-30's	Pheobus Levene studied the structure of nucleic acids and their monomers. His many contributions included coining the term *nucleotide*, describing the 2'-deoxy-D-ribose sugar, the nucleobases and the phosphodiester linkage.[9]
1923	Frederick Griffiths discovered a "transforming principle" that transferred hereditary traits among bacteria.[10]
1944	Oswald Avery discovered that Griffith's transforming principle was DNA.[4]
1947	Based on titration studies, John Gulland predicted hydrogen bonds between bases and that the phosphate groups are accessible to solvent but not the amine groups.[11]
1947	Astbury looked at the first X-rays of DNA, obtained by Einar Hamerstein, and observed a 3.4 Å repeat along the fiber axis, like a ladder with steps.[12]
1949	Erwin Chargaff observed that the amount of adenine is equal to the amount of thymine, and the amount of guanine is equal to the amount of cytosine. This formed the groundwork for elucidating base-pairing.[13]
1953	Rosalind Franklin obtained very clean X-ray crystals of DNA that suggested the structure contains two fibers.[7] She also observed that DNA has two forms, a shorter A-form and a more elongated B-form under greater humidity.[14]
1953	James Watson and Francis Crick presented their molecular model for the structure of DNA.[5] They later provided more detail on the copying mechanism of genetic material.[8] Along with Maurice Wilkins, who provided X-ray crystallography data describing the helix geometry,[6] they obtained the 1962 Nobel Prize in Medicine. Unfortunately, Rosalind Franklin had died by this time, but her contributions were unquestionably deserving of the prize.

1.1.2 Nucleic acid structure[15]

Nucleic acids are biopolymers that can reach several million units long. Each monomer unit is called a nucleotide, and includes three components: a pentose sugar, a phosphate group and a nitrogen-containing basic heterocycle (nucleobase). The structure and numbering scheme for nucleotides is depicted in Figure 1.1.1. Monomers without the phosphate group are called nucleosides. There are four possible nucleobases: adenine, guanine, cytosine and either thymine or uracil in DNA and RNA respectively. The nucleobases are attached to the anomeric carbon (C-1') of the sugar by a β linkage at the N-1 nitrogen for pyrimidines or N-9 nitrogen for purines.

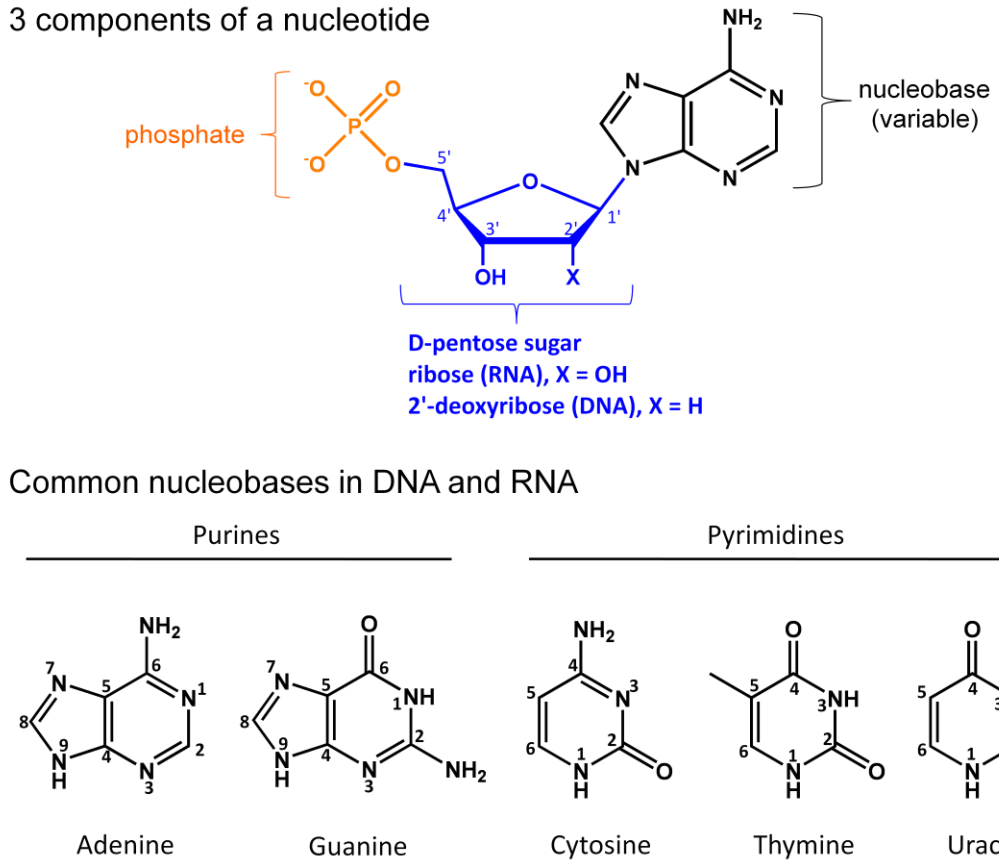

Figure 1.1.1 Structure and numbering of nucleotide sugar and the five common natural nucleobases. The phosphate is attached at the 5' carbon of the pentose, and the nucleobase is attached at the 1' carbon via a β linkage. The nucleotide depicted is adenosine 5'-monophosphate (AMP) if the sugar is D-ribose (X=OH) or 2'-deoxyadenosine 5'-monophosphate (dAMP) if the sugar is D-2-deoxyribose (X=H).

Nucleotides are linked together into linear nucleic acid polymers by phosphodiester linkages between the 3' and 5' oxygens of the pentose sugars (Figure 1.1.2). The sequence of nucleotides in DNA and RNA, referred to as the primary structure, is designated from the 5' to 3' end. DNA and RNA are the carriers of genetic information, and the variability in the sequence of the nucleobases makes up the coding. Single-stranded nucleic acids are capable of folding into higher ordered structures, such as a double-stranded helix (Figure 1.3). This double helix can be compared to a winding staircase or a ladder, with the sugar-phosphate backbone consisting of the rails on the exterior running in opposite 5' to 3' directions, and the variable nucleobases in the middle stacked one on top of the other like steps. In this configuration, the negatively charged phosphate backbone is exposed to the polar solvent, and the hydrophobic nucleobases are hidden in the inner core of the helix. The nucleic acids strands are held together by non-covalent forces, predominantly hydrogen bonds (H-bonds) between the nucleobases and π-stacking with neighboring bases. The H-bonding between nucleobases is called "base pairing", and occurs between "complementary bases" according to the model proposed by Watson and Crick; adenine with thymine and guanine with cytosine (Figure 1.1.2). The A·T base

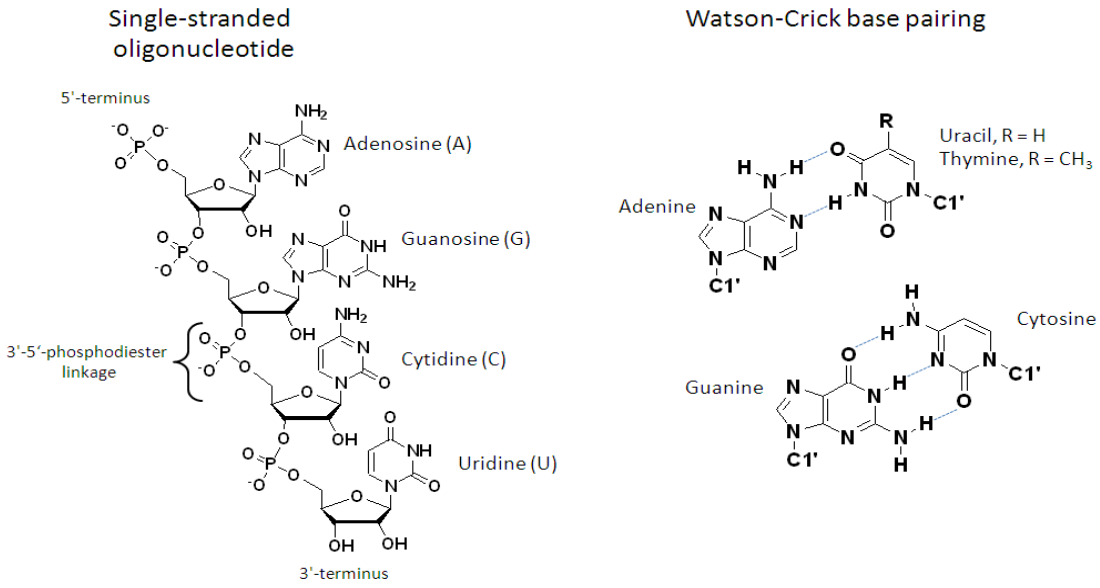

Figure 1.1.2. (Left) RNA tetramer 5'-rAGCU-3' showing the phosphodiester internucleotide linkages. (Right) Watson-Crick base pairing between A and U/T and between G and C. Hydrogen bonds are indicated by dotted lines.

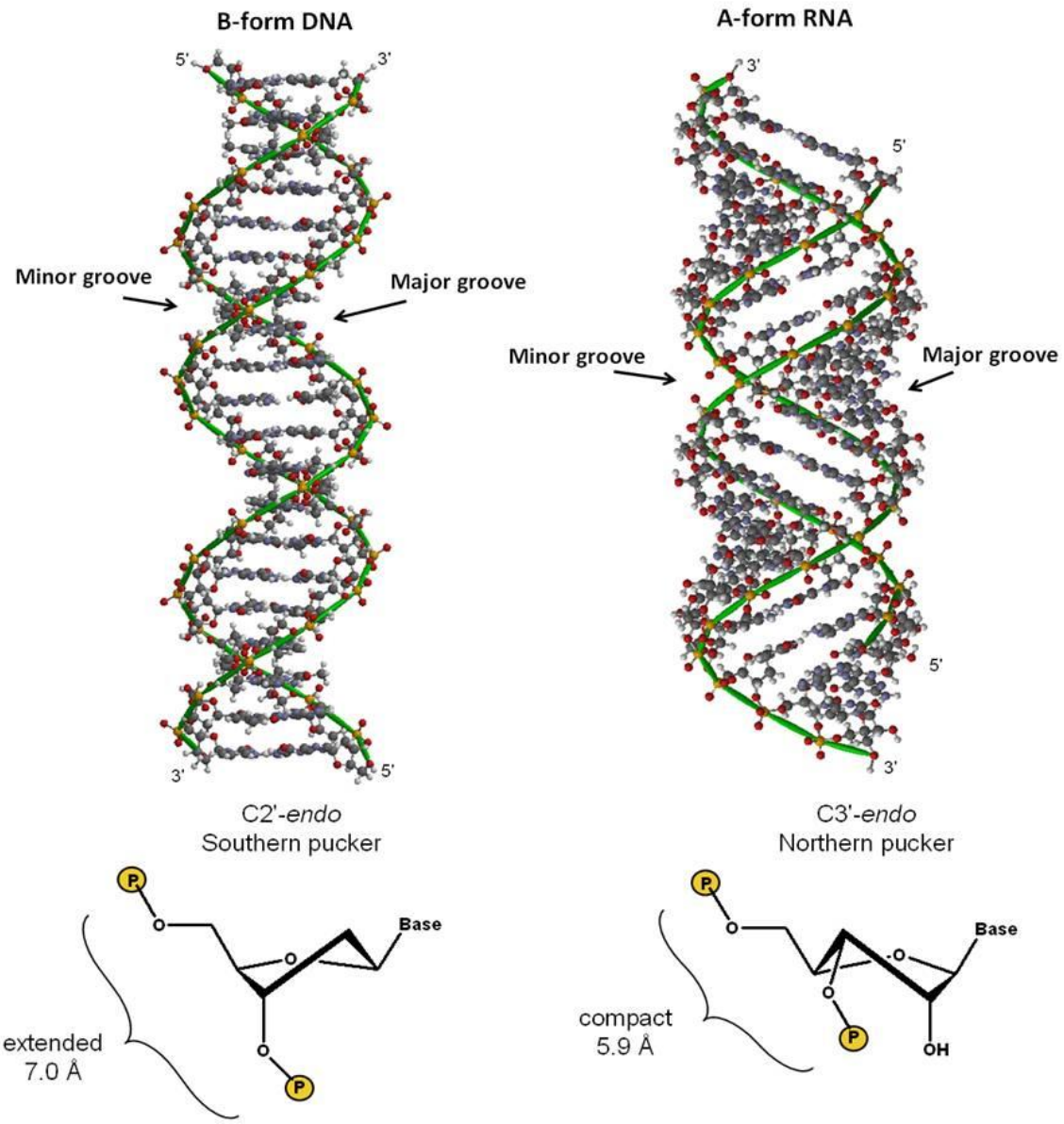

Right-handed	**Helix sense**	Right-handed
10	**Residues per turn**	11
3.4 Å	**Rise per base pair**	2.6 Å
6 °	**Base tilt**	20 °
23.7 Å	**Helix diameter**	25.5 Å
wide and deep	**Major groove**	narrow and deep
narrow and deep	**Minor groove**	wide and shallow

Figure 1.1.3. Average helical conformation and structural parameters of double-stranded B-form DNA and double-stranded A-form RNA. Preferred sugar conformations of each helix are indicated underneath with the distances between adjacent internucleotide phosphates.[1] Models were constructed using Spartan 08 v.1.2.0.

pair forms 2 hydrogen bonds, and the G·C base pair forms 3 hydrogen bonds. A mismatch incurs a penalty to the thermodynamic stability of the double-stranded nucleic acid. This preference for the A·T and G·C pairing is the basis for the copying of genetic information.

Nucleic acids are dynamic macromolecules that can undergo conformational changes. In solution, the average structure of double-stranded DNA is a right-handed B-form helix, while double-stranded RNA forms a right-handed A-form helix (Figure 1.1.3). B-form DNA has a relatively longer geometry; with 10 base pairs per turn of the helix and a diameter of 23.7 Å. A-form duplexes are more compact with 11 residues per helix turn and a helix diameter of 25 Å.

Conformational differences between double-stranded A-form and B-form helices are influenced by differences at the nucleotide level. The pentose sugar ring twists to relieve strain, causing some atoms to protrude above and below the plane of the ring. This puckering can also be described numerically using two parameters; the phase angle, P, indicates which part of the ring is most out of plane, and the maximum puckering amplitude, Ψ_{max}, describes the extent of the displacement.[16] The continuum of sugar puckering conformations (P values) can be intuitively illustrated using a cardinal point system called the pseudorotational wheel (1.1.4).[16] The most stable pseudorotomer of the nucleotides in RNA and DNA fall within the northern (P = 0° - 36°, centered on C3'-*endo*) and southern coordinates (P = 144° - 180°, centered on C2'-*endo*). In solution, nucleosides and nucleotides

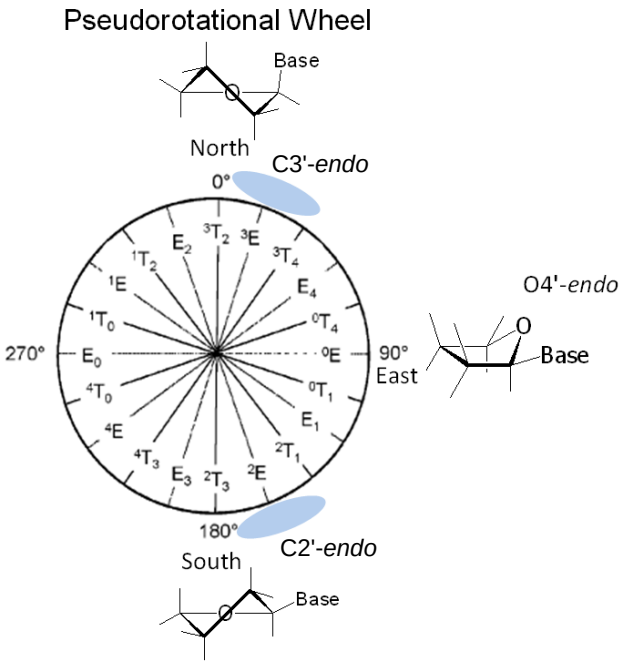

Figure 1.1.4. The pseudorotational wheel illustrates the various conformations adopted by nucleotide sugars. The blue areas denote the most stable puckers of natural nucleotides. The E (envelope) and T (twist) designate the atom(s) most displaced in the ring.

rapidly equilibrate between the North and South sugar puckers, passing through the East sugar pucker (O4'-*endo)*. Depending on the nature of the substituents on the sugar ring (e.g. RNA vs. DNA), nucleotides can show preference for certain puckering configurations.[17-19]

RNA duplexes adopt a compact A-form helix with the flanking phosphates close together (5.9 Å, Figure 1.1.3).[20] DNA duplexes are more flexible but adopt predominantly the longer B-form helix (interphosphate distances of 7.0 Å, Figure1.1.4). In less hydrated environments, DNA can also adopt an A-form helix.[14] Hybrid duplexes containing RNA bound to DNA form an intermediate helix. This hybrid has more A-form character as the flexible DNA strand adapts its sugar configuration to that of RNA to allow the formation of a stable duplex.[20]

RNA is less flexible than DNA. It forms thermodynamically more stable duplexes[20-23] and a range of higher ordered functional structures.[1,24] In the cell, RNA is biosynthesized as a single covalent chain instead of a double strand, and is thus free to fold into an array of self-complementary hairpins, bulges and internal loops. RNA secondary structures can also be stabilized by unusual base pairing, such as the extra-stable UUCG tetraloop that is widespread in natural RNA hairpins (Figure 1.1.5).[25,26] The tetraloop is stabilized by a U1·G4 Wobble base pair that stacks with C3, while the neighboring U2 twists away into the solvent to allow room for this configuration (Figure 1.1.5). In addition, the G4 in the tetraloop adopts a *syn* orientation (Figure 1.1.6) allowing the associated nucleobase O-6 oxygen to hydrogen bond with the ribose 2'-OH of the paired U-1.[27-29]

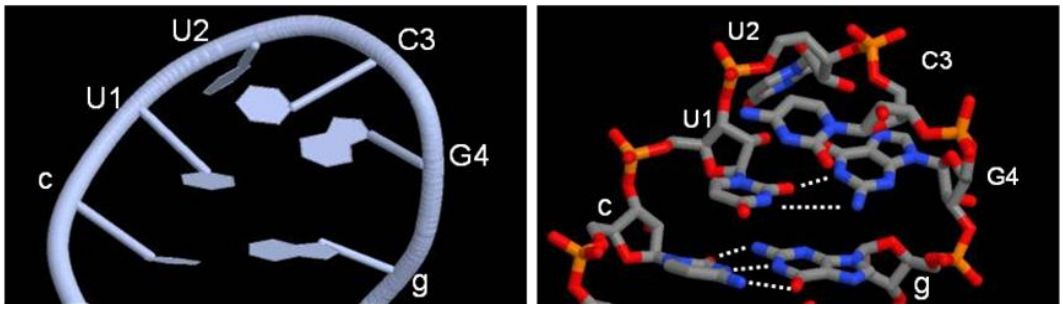

Figure 1.1.5. Cartoon (left) and tube (right) diagrams of the extra stable UUCG tetraloop (numbered 5'-U_1-U_2-C_3-G_4-3'). C3 stacks on top of U1 and G4, while U2 twists into the solvent. Dotted white lines represent hydrogen bond base pairing. G4 adopts a *syn* glycosidic torsion angle to allow the G·U base pair. Structure generated through Jmol using PDB code 2koc.

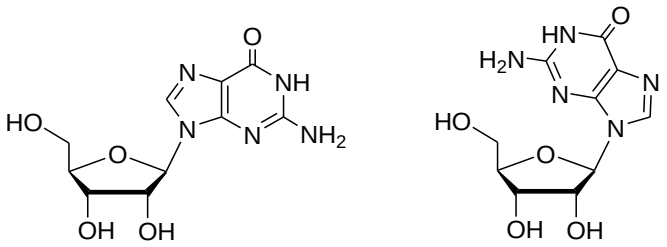

Figure 1.1.6. *Anti* (left) and *syn* (right) glycosidic bond conformations of guanosine.

1.1.3 Nucleic acids in the cell

Nature's choice of DNA over RNA for the long-term storage of information offers advantages in chemical stability. In solution, DNA has a half life of 10^9 years, versus RNA with a half life of 10^2 years.[30] RNA is more susceptible to internal cleavage because the 2'-hydroxyl group in ribose promotes a transesterification with the adjacent 3'-phosphoester bond, cleaving the oligonucleotide into two products, one with a strained 2',3'-cyclic phosphate, and one with a free 5'-hydroxyl (Figure 1.1.7).[31]

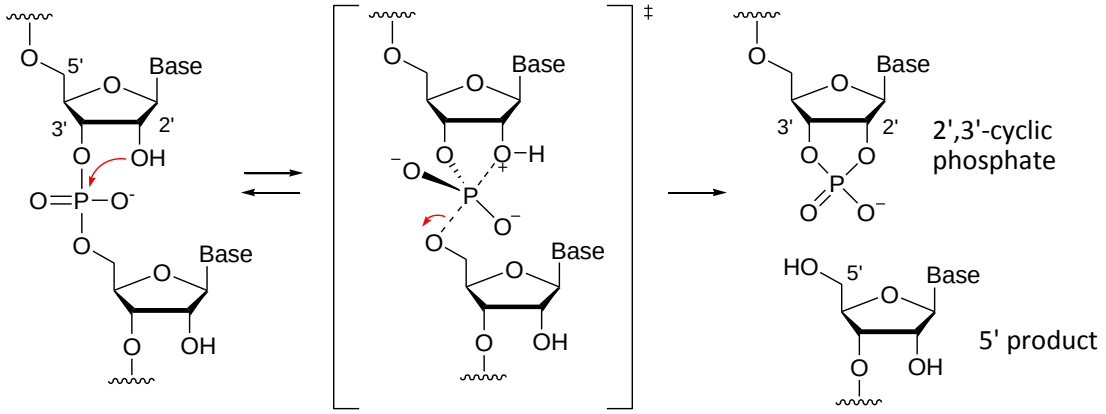

Figure 1.1.7. Self-cleavage of an RNA strand initiated by the 2'-hydroxyl group adjacent to the 3'-phosphodiester bond generating a 2',3'-cyclic phosphate product.

Genomic DNA is found in the cell nucleus, densely coiled with proteins into chromosomes in mammalian cells. A DNA strand can be copied into two identical daughter strands during DNA replication, a process carried out by enzymes called DNA polymerases.[32] RNA polymerases[33] are responsible for the synthesis of RNA from genomic DNA. Both enzymes catalyze the formation of the phosphodiester bonds in the sugar-phosphate backbone from the 5' to the 3' direction. Polymerization occurs from the 3'-hydroxyl of a primer strand annealed to a longer template strand, which directs the identity of the nucleotide unit to be added through Watson-Crick

base pairing. RNA polymerases use ribonucleoside 5'-triphosphates (rNTPs) as substrates, while DNA polymerases use 2'-deoxynucleoside 5'-triphosphates (dNTPs).

Nucleases are enzymes that break apart the phosphodiester linkages of nucleic acids. They are important in the metabolism of nucleic acids and can protect the cell from nucleic acids derived from pathogens. Nucleases capable of cleaving the phosphodiester bond in the middle of strands are called endonucleases, while exonucleases cleave from the 3' or 5' termini.

The *central dogma* of molecular biology is a simple illustration to explain the manner genes are expressed in cells (Figure 1.1.8); from DNA, to messenger RNA (mRNA),[34] which serves as an intermediary disposable copy,[35,36] to proteins, which carry out cellular functions.[37] In this model, proteins cannot be used as a template for converting the information back to nucleic acids, the carriers of the information. The DNA that is located in the cell nucleus is converted into single-stranded RNA in a process called *transcription*. This nascent RNA transcript (called pre-mRNA) is processed in the nucleus into mature mRNA by post-transcriptional modifications. These include adding a 7-methylguanosine triphosphate 5'-cap, polyadenylation of the 3'-terminus, and removal of non-coding RNA sequences (introns) while joining together the coding RNA sequences (exons) by a process called splicing.[38,39] The mature mRNA is transported to ribosomes[40] in the cytoplasm where it serves as a template for peptide biosynthesis, termed *translation*. The ribosomes are composed of catalytic RNAs (ribozymes)[41-43] called ribosomal RNA (rRNA) and synthesizes the peptide using highly ordered transfer RNA (tRNA)[44] which delivers the amino acids. In the last decade, researchers have discovered other forms of RNA transcribed from non-coding genes in the nucleus, such as micro RNAs (miRNA) and piwi-interacting RNAs (piRNA), which can regulate translation.[45-47]

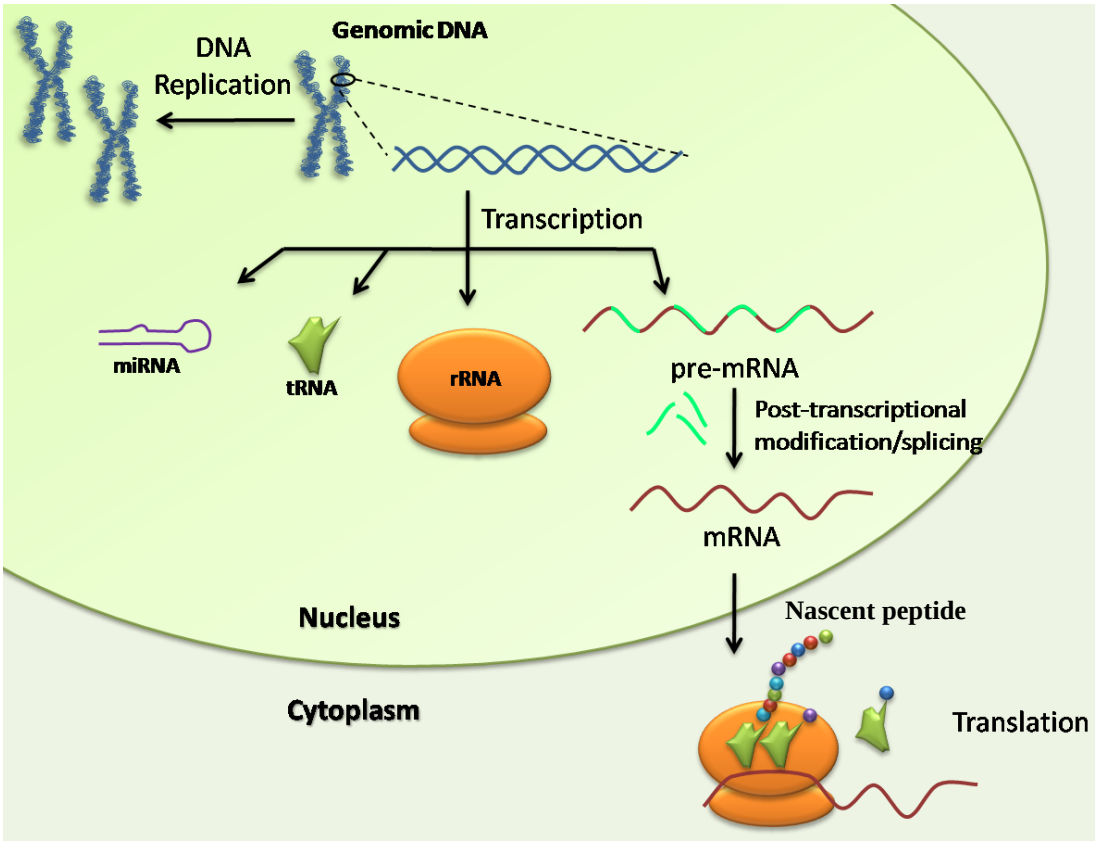

Figure 1.1.8. Flow of genetic information inside a cell.

In summary, the versatility of the cellular functions demonstrated by nucleic acids is unprecedented amongst biomolecules. They can store genetic information (DNA, viral RNA), serve as an intermediary template for protein synthesis (mRNA), perform catalysis (rRNA, splicing and other ribozymes), fold into distinct functional structures (tRNA) and are involved in signaling and regulation of gene expression (miRNA, piRNA).

1.2 HIV Reverse Transcriptase

The human immunodeficiency virus (HIV), the causative agent of AIDS,[2,3] is a global epidemic with 33 million individuals infected worldwide.[48] HIV is a retrovirus: its genetic information is encoded and transmitted by RNA. The process of reverse transcription, whereby viral genomic RNA is converted into double-stranded DNA,[49,50] is thus central to the HIV life cycle. This process involves several steps, all of which are catalyzed by a multifunctional enzyme called HIV reverse transcriptase (RT),[51] which has DNA polymerase and ribonuclease H (RNase H) activities.[52]

Reverse transcription takes place in the cytoplasm after the HIV virus particle fuses with the host CD4+ T cell. RT RNA-dependant DNA polymerization of the minus DNA strand (the DNA strand complementary to the RNA genome) is initiated by a host tRNA binding to the single-stranded RNA genome at the primer binding site (PBS) (Figure 1.2.1).[53] A short strand of DNA is synthesized, then a portion of the RNA dissociates from the degradation of the R region of the RNA template and binds to a different complementary region on the 5'-end of the viral RNA template (this is called a "strand transfer").[54] Synthesis of a full-length RNA•DNA hybrid ensues. The RNase H activity of RT degrades the RNA strand of the hybrid duplex except for an A/G rich region called the polypurine tract (PPT).[55] The PPT serves as the primer in plus-strand DNA-dependant DNA polymerization which involves a second strand transfer (Figure 1.2.1). The double-stranded DNA product is incorporated into the host genome by another viral enzyme, HIV integrase (HI).

1.2.1 Reverse Transcriptase Structure

RT is a heterodimeric protein that contains a 66 kDa subunit (p66) and a 51 kDa subunit (p51) derived from the same viral gene.[51] The p66 subunit houses the nucleic acid binding cleft, the polymerase and RNase H activity (Figure 1.2.2).[56,57] The p51 subunit serves structural roles in RT, and is identical in sequence to p66 but lacks the 15 kDa C-terminal RNase H domain. The three dimensional structure of the amino-terminal polymerase domain can be compared to a right hand that grasps the nucleic acid substrate, and the subdomains are named the palm, finger and thumb accordingly. A connection domain bridges the N-terminal polymerase domain and the

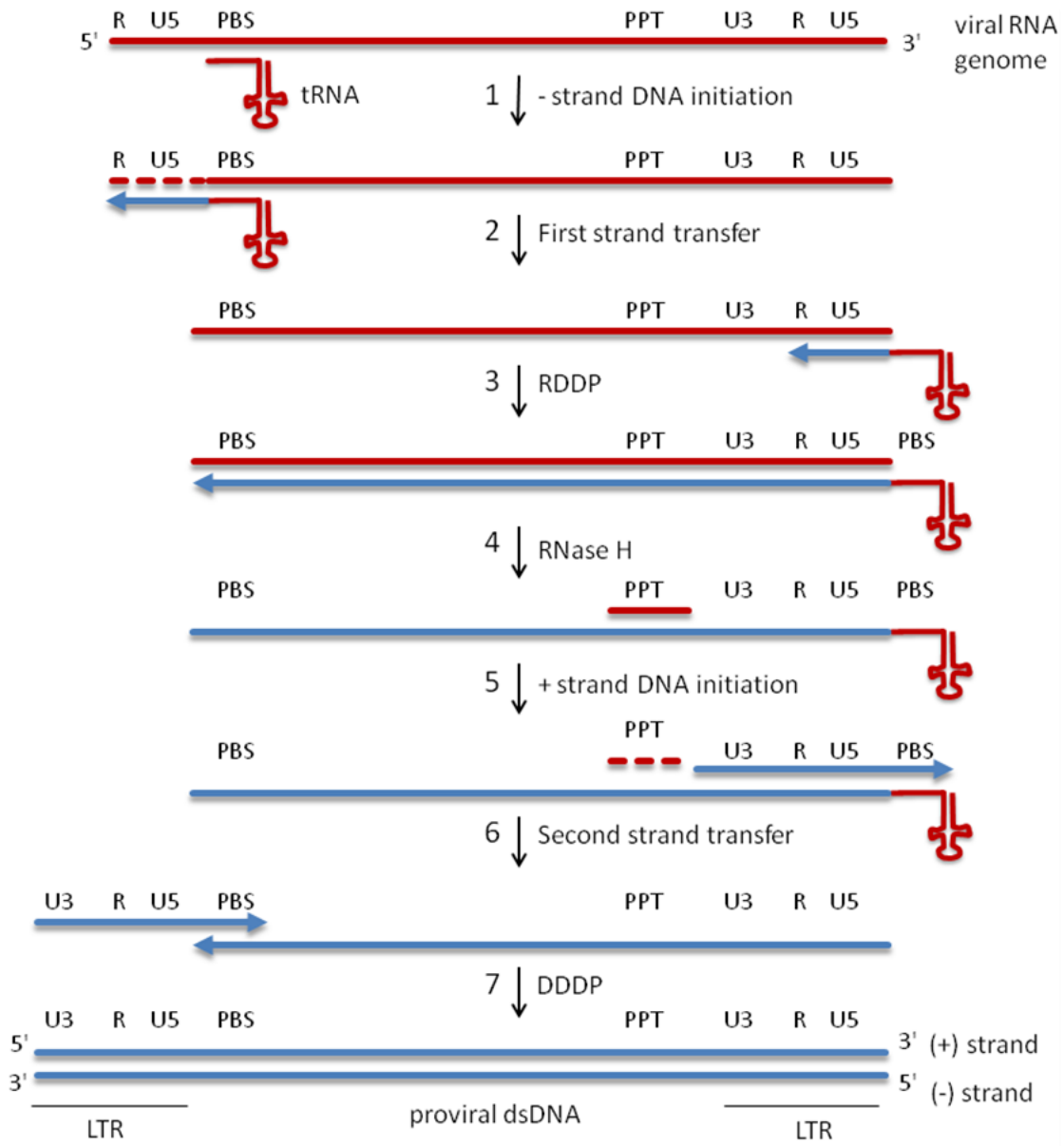

Figure 1.2.1. Schematic diagram of reverse transcription (adapted from Katz and Skalka).[53] RNA is depicted in red, DNA is depicted in blue. A host cell $tRNA^{lys3}$ binds to the primer binding site (PBS) of the viral RNA genome. *Step 1*: Minus-strand DNA synthesis is initiated close to the 5'-terminus of the RNA genome. *Step 2*: RT RNase H degrades the RNA genome U5 and repeat (R) regions freeing the primer to bind to the R region of the 3'-terminus. *Step 3*: RNA-dependent DNA polymerization (RDDP) of the minus-strand. *Step 4*: RT RNase H activity degrades the RNA genome except for the polypurine tract (PPT). *Step 5*: The PPT serves as a primer for plus-strand initiation. *Step 6*: The PPT and tRNA primers are removed and the second strand transfer allows the plus-strand PBS to bind the minus-strand PBS. The second strand transfer occurs in intramolecular fashion. *Step 7*: DNA-dependent DNA polymerization of the plus-strand DNA and the long-terminal repeats (LTR; U3, R and U5 regions) necessary for integrating into the host genome by HI.

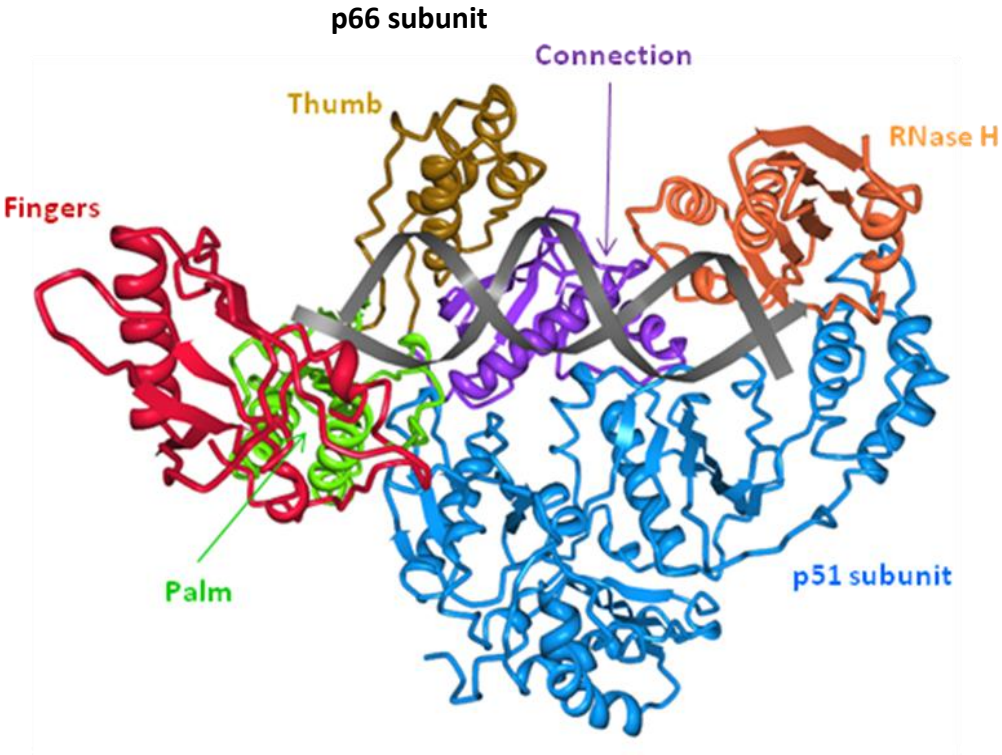

Figure 1.2.2. Structure of RT bound to a DNA duplex (grey) in the nucleic acid binding cleft. The p66 subunit contains the fingers (red), plam (green), thumb (brown), connection (purple), and RNase H (orange) domains. The p51 subunit is depicted in blue. Figure generated using JMOL, PDB code 2HMI.

C-terminal RNase H domain. The nucleic acid substrate spans the 70 Å (17-18 nt long) of the nucleic acid binding cleft making contact with the polymerase, RNase H and connection domains (Figure 1.2.2).

1.2.2 Polymerase activity

The polymerase activity of HIV RT is responsible for the synthesis of the minus-strand and plus-strand DNA. As with most DNA polymerases, the substrate for reverse transcriptase is a recessed primer bound to a template and deoxynucleoside triphosphates (dNTPs). Prior to polymerization, the primer-template duplex binds to RT forming a binary complex (Figure 1.2.3). The 3'-nucleotide of the primer occupies the primer site (P-site) of the polymerase domain.[57] The addition of a dNTP to the nucleotide site (N-site) forms a stable tight-binding ternary complex.[58,59] The fingers domain closes down on the dNTP forming a catalytically competent conformation.[60] Two Mg^{2+} ions coordinate to the dNTP phosphate groups and assist the 3'-hydroxyl group of the primer to attack the α-phosphate in S_N2 fashion, creating a new

phosphodiester bond.[61,62] The release of pyrophosphate (PP_i),[63] the leaving group, is followed by translocation of the incorporated nucleotide from the N-site to the P-site.[64,65]

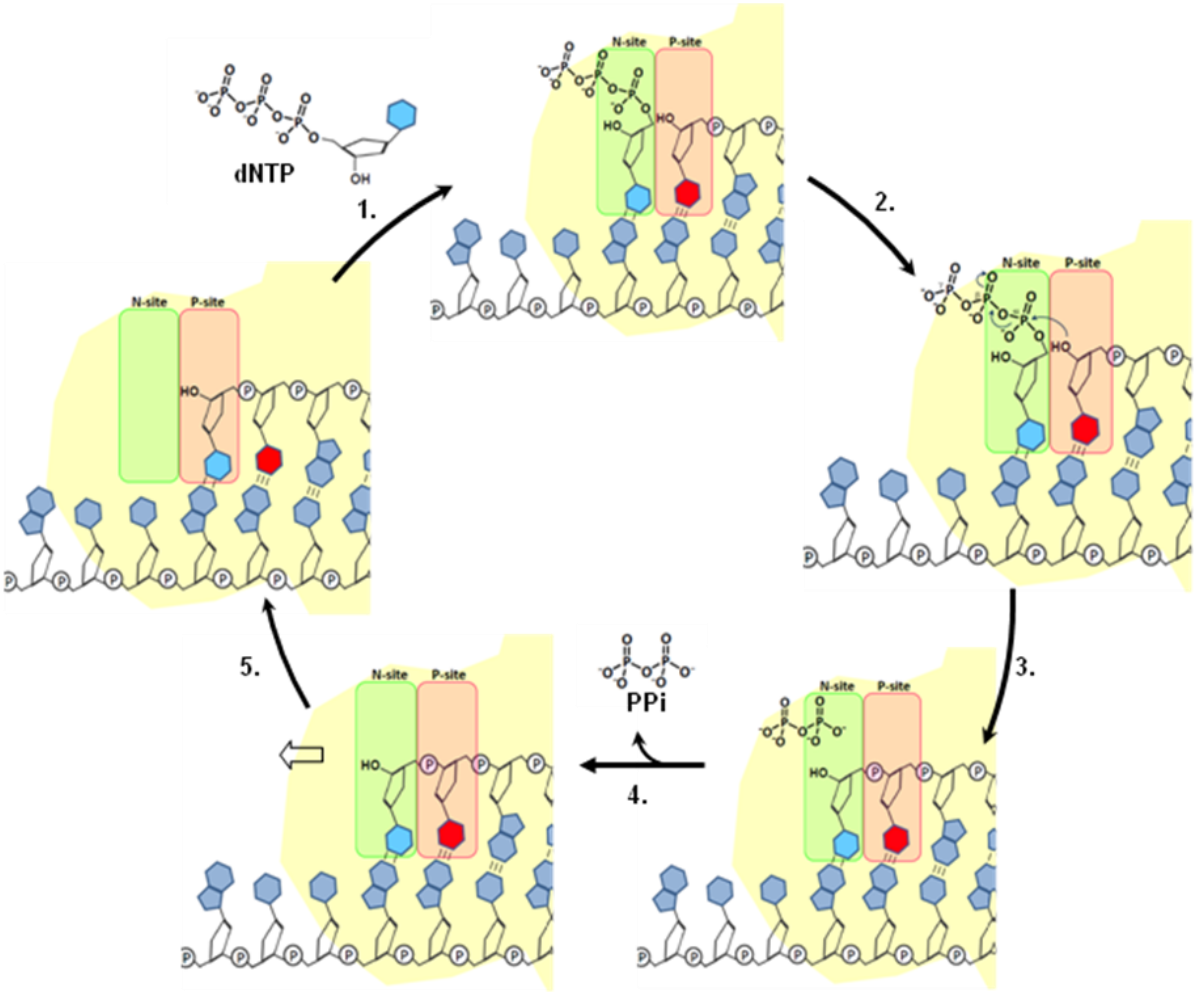

Figure 1.2.3. Polymerization cycle of RT as described in the text. The terminal 3'-hydroxyl of the primer occupies the P-site (shaded red) *Step 1*. dNTP binding to N-site (shaded green) of binary complex. *Step 2*. Formation of stable ternary complex. *Step 3*. Catalysis. *Step 4*. Release of pyrophosphate. *Step 5*. Translocation from N-site to P-site.

1.2.3. RNase H activity

RNase H is a ubiquitous endoribonuclease that selectively cleaves the phosphodiester backbone of the RNA strand in an RNA•DNA hybrid duplex.[66] The selectivity for RNA•DNA hybrids is believed to depend on the trajectory of the AB-form helix backbone and the width of the minor groove.[67-69] However, HIV-1 RT RNase H activity has been known to cleave RNA•RNA hybrids in stalled complexes.[70] The isolated RNase H domain of HIV-1 RT is inactive, as it requires contacts in the primer grip and connection domain to bind to its substrate.[71] Adding a basic loop found in the RNases H of other organisms compensates for the absence of the other domains and allows the isolated RNase H domain to have catalytic activity.[72] The active site of most RNases H, including HIV-1 RT RNase H, contains a highly conserved DEDD catalytic motif.[71,73] These negatively charged amino acids coordinate a two-metal ion cleavage mechanism with water as the nucleophile.[74-76] The product is a 3'-hydroxyl and a 5'-phosphate from the scissile phosphate (Figure 1.2.4).

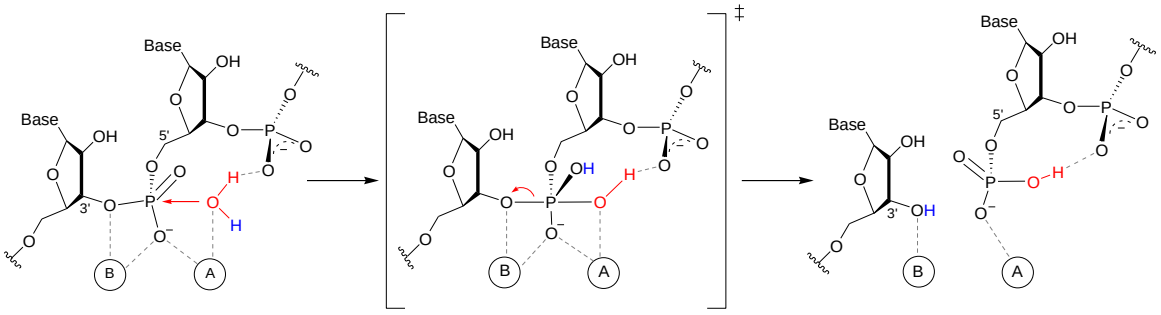

Figure 1.2.4. Two-metal ion assisted reaction mechanism of RNase H mediated cleavage of an RNA strand. The two Mg^{2+} cations are depicted as circles A and B. Mg^{2+} A assists nucleophilic attack of a water molecule (red and blue). Both Mg^{2+} ions stabilize the pentavalent transition state with the nucleophile and leaving group at the apical positions. The products formed are a 3'-hydroxyl and a 5'-phosphate.

Different kinds of RNase H cleavage events occur during reverse transcription (Figure 1.2.5).[77] In a polymerase-dependent mode, RNase H cleavage is directed by the 3'-terminus of the DNA primer. During polymerization, RNase H cuts the RNA template during pausing events generating cuts approximately 15-20 nucleotides away from the P-site of the polymerase domain. In a polymerase-independent mode,

RNase H cleavage occurs due to positioning at the 5'-terminus of the RNA strand, generating cuts 7-21 nucleotides from the P-site, or in a non-directed non-specific fashion within large segments of RNA•DNA duplexes.[77]

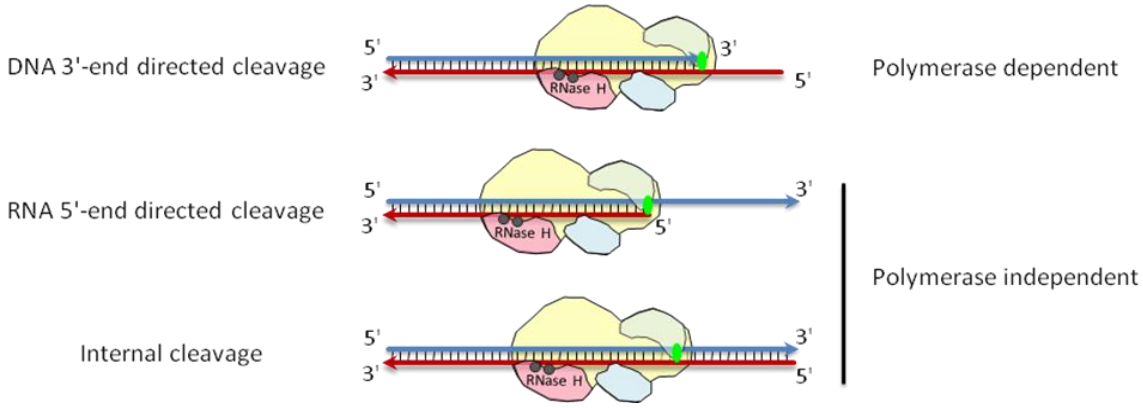

Figure 1.2.5. Modes of HIV-1 RT binding during RNase H cleavage. Red bars, RNA; blue bars, DNA; grey circles, RNase H catalytic site; green oval, N-site.

1.2.4. Reverse Transcriptase Drugs

Drug development for HIV remains an area of intense research as there is still no cure or vaccine to eradicate the epidemic. There are currently 25 FDA-approved drugs to combat HIV that target various stages of the viral life cycle.[78] Half of these agents are directed towards RT, a testament to its key role for infectivity. The two classes of RT inhibitors in clinical use disrupt the polymerase activity of RT. These are nucleoside (or nucleotide) reverse transcriptase inhibitors (NRTIs) and non-nucleoside reverse transcriptase inhibitors (NNRTIs). Although the RNase H activity is also required for virus infectivity,[79] no such inhibitory agents have matured past pre-clinical development.[80]

NRTIs are structural analogs of the natural dNTPs used during DNA polymerization (Figure 1.2.6). These compounds act as chain terminators because they lack a 3'-hydroxyl group on the sugar ring. The incorporation of a single chain-terminator is thus sufficient to arrest polymerization forming a dead-end complex upon translocation to the P-site (Figure 1.2.7).[81] NRTIs may be incorporated by other polymerases and as such pose a toxic risk to non-infected host cells. For this reason, developing NRTIs specific for RT are paramount for prolonged use by HIV-infected

patients. Most NRTIs are administered as nucleosides, and must first be converted to triphosphates by host kinases, presenting another obstacle for their successful incorporation by RT.[82,83] Kinases prefer nucleosides that adopt a southern sugar conformation,[84] while polymerases (including RT) prefer to incorporate nucleotides in a northern sugar pucker.[62,85] Finally, NRTI triphosphates must compete with the high concentration of natural dNTPs for incorporating into RT. RT's low fidelity and lack of proofreading ability work in favour of the incorporation of modified dNTPs.[86] However, they also contribute to RT's ability to rapidly mutate and develop resistance against NRTIs.

The first compound approved for the treatment of HIV was 3'-azido-3'-deoxythymidine (AZT) in 1987 (Figure 1.2.6).[87] AZT is the only NRTI to contain a functional group appended to the 3' position of the sugar ring. 2',3'-dideoxyinosine (ddI) and 2',3'-dideoxycytidine were the next compounds approved; both are very similar to natural RT substrates except for the missing 3'-hydroxyl group.[88] ddI is metabolized to 2',3'-dideoxyATP in the body and is less toxic than ddA. 2',3'-didehydro-2',3'-dideoxythymidine (d4T) and abacavir, (1S,4R)-4-[-2-amino-6(cyclopropylamino)-9H-Purin-9yl]-2-cyclopentene-1-methanol (ABC), are analogues that contain an alkene in the sugar ring. d4T is quickly processed by thymidylate kinase to obtain high intracellular levels of d4TTP.[89,90] ABC, which contains a carbocyclic ring, is phosphorylated by adenosine phosphotransferase before being metabolized by AMP deaminase eventually forming a dGTP analogue.[91] L-β-2',3'-Dideoxy-3'-thiacytidine (3TC),[92] and its 5-fluoro analogue FTC[93] contain an oxathiolane ring in the opposite configuration of deoxyribose and show minimal side effects at clinical doses. 3TC was the first compound used in combination therapy with AZT. Tenofovir isopropyl fumarate (9-[2-(phosphonomethoxy propyl] adenine, TDF) is an acyclic analogue with a 5'-phosphonate diester.[94] It is an AMP analogue thus it bypasses the first kinase phosphorylation required by traditional nucleoside analogues. The liphophilic groups on the ester improve cellular uptake and are cleaved by cellular esterases to form the free nucleotide phosphonate tenofovir.

Nucleoside (or nucleotide) RT inhibitors (NRTIs)

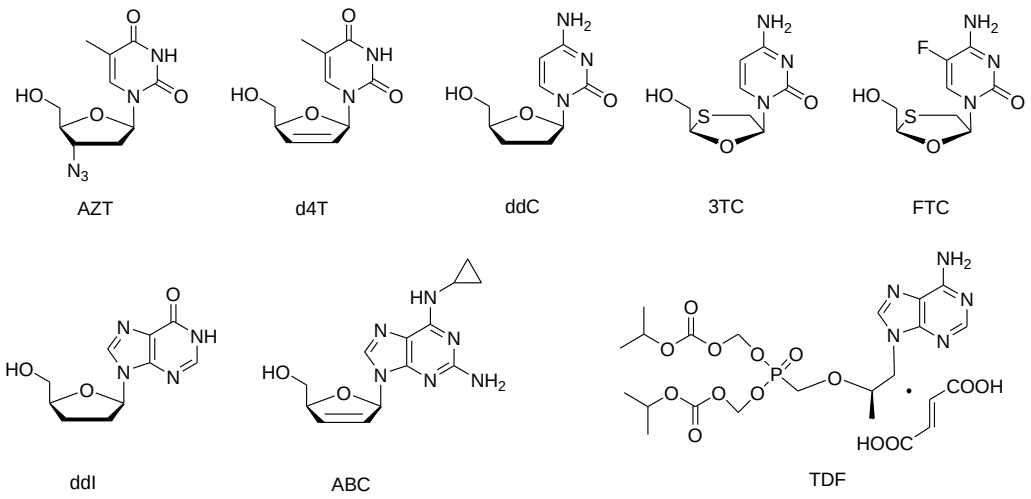

Non-nucleoside RT inhibitors (NNRTIs)

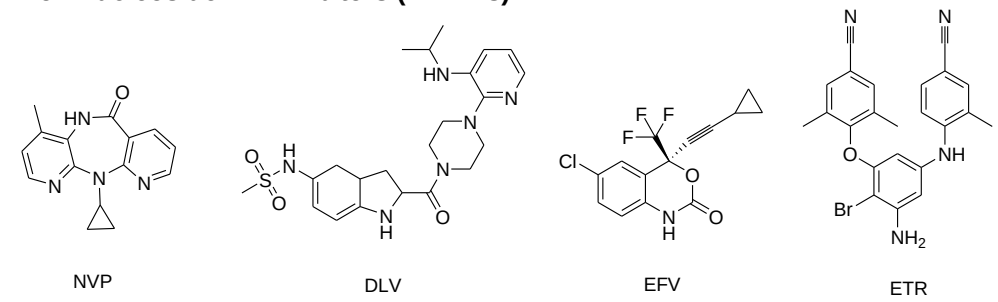

Figure 1.2.6. FDA approved inhibitors of HIV reverse transcriptase

The NNRTIs are a diverse class of molecules with a shared mechanism of action. They are noncompetitive inhibitors of polymerase activity that bind to a hydrophobic pocket in the palm domain of the p66 subunit.[56] There are four NNRTIs approved for clinical use (Figure 1.2.6); nevirapine (NVP), delavirdine mesylate (DLV), efavirenz (EFV) and etravirine (ETR).[80] These compounds all have π-stacking and hydrogen bonding capabilities necessary to interact with the hydrophobic NNRTI binding pocket (NNIBP). NNRTI binding has been observed to reduce the mobility of the thumb domain and impact the formation of a competent ternary complex for polymerization.[56,95] Studies have also demonstrated that nevirapine binding to RT increases RNase H activity,[96] which has been implicated in decreasing resistance mechanisms.[97,98] RT mutations that confer resistance to NNRTIs usually introduce

steric barriers to restrict access to the NNIBP or remove favourable interactions for drug binding.[99]

1.2.5 NRTI Drug Resistance

Treatment insensitivity is a major concern in HIV therapy. Mutations that confer resistance to antiviral agents develop quickly due to HIV's fast replication rate and low polymerase fidelity.[86,100,101] Under the selective pressure of HIV-therapy, these drug-resistant variants become the dominant species[102] and newly infected patients are left with fewer treatment options. Thus monotherapy is not an option for prolonged use, and current treatment relies on combination therapy to restrain the development of drug resistance. When several drugs, typically three, are taken in combination, the approach is known as highly active antiretroviral therapy, or HAART.

There are two general mechanisms by which HIV can develop resistance towards NRTIs: discrimination and nucleotide excision.[101] The first method involves higher discrimination towards the incorporation of NRTI triphosphates, without compromising the incorporation for natural dNTPs. This enhanced recognition may be due to steric hindrance, such as with the M184I/V mutation that confers resistance towards 3TC and FTC.[59,103] Modeling studies showed that the branched side-chains clash with the larger sulphur atom on the oxathiolane ring, preventing incorporation. However, steric hindrance may not explain discrimination against ddI or ddC, as these NRTIs are sterically smaller than their natural counterparts.[104]

In the second mechanism of resistance, RT can rescue DNA synthesis by excising the chain-terminated nucleotide at the 3'-terminus of the primer strand.[105,106] Mutations associated with this mechanism are called thymidine analogue mutations (TAMs) as they were first observed in AZT resistant patients following monotherapy.[107] The model for excision involves ATP or pyrophosphate binding close to the N-site, and carrying out the opposite reaction of incorporation to release the NRTI triphosphate. This is only possible if there is no incoming dNTP occupying the N-site, and the chain-terminated complex translocates back to the N-site. Indeed, the rate of nucleotide excision is correlated to the incidence of the NRTI occupying

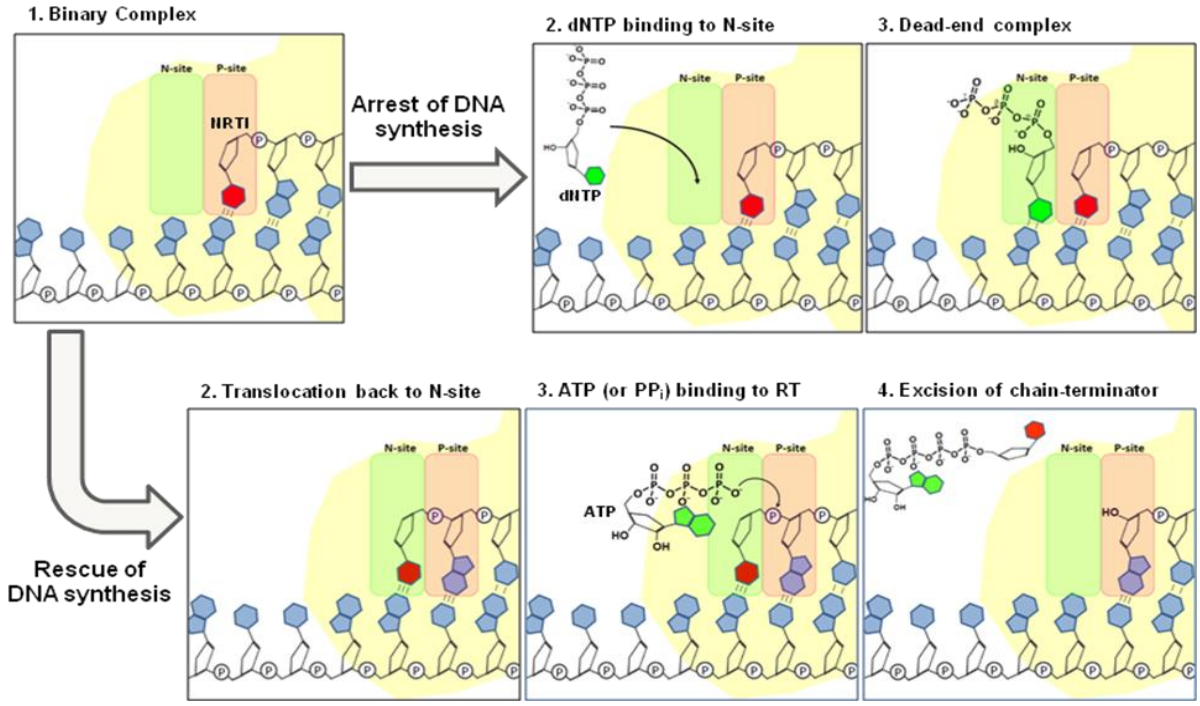

Figure 1.2.7. Cartoon depicting the competition between the arrest and rescue of DNA synthesis following the incorporation of an NRTI. The NRTI (red nucleotide) occupies the P-site (shaded red) in the chain-terminated binary complex (*Box 1*). The next dNTP binds to the N-site (shaded green) (*Box 2*, top) leading to the formation of a dead-end complex and arrest of DNA synthesis (*Box 3*, top). Conversely, the chain-terminator can translocate back to the N-site (*Box 2*, bottom). ATP or pyrophosphate (PP_i) bind close to the N-site (*Box 3*, bottom), allowing the excision of the chain terminator and rescue of DNA synthesis (*Box 4*, bottom).

the N-site.[63,65] It has been suggested that the higher propensity for AZT excision is due to the bulky azido-group preventing the binding of the next dNTP in the N-site to form the dead-end complex.[108] However, the azido group has been shown not to be the major determinant in excision[109] and TAM's have shown to provide resistance to other NRTIs as well.[110]

Mutations that resensitize RT towards AZT by decreasing excision also exist, such as the 3TC and FTC resistant mutation M184I/V, illustrating the success of combination therapy.[111] NNRTI resistant mutations have shown the same effect,[112,113] and combined with NRTIs can act in synergy to inhibit RT polymerase activity. Combination therapy thus typically includes two NRTIs and an NNRTI or a drug that targets HIV protease, the enzyme that cleaves viral polypeptides into functional

proteins.[78] Although there are many stages in the viral life cycle that are necessary for virulence, current therapy relies heavily on RT and protease inhibitors. Some other targets, such as inhibitors to prevent virus entry into cells and inhibitors of HIV integrase, have recently been approved for therapeutic use by regulatory bodies. It is essential to continue research in the identification and validation of new HIV targets as the occurrence of multidrug resistant HIV strains can impart cross-resistant phenotypes for several variants of a therapeutic class of compounds.

1.3 Therapeutic/Biological applications of oligonucleotides

Owing to Watson-Crick base paring, an oligonucleotide can be designed to bind a very specific region of genomic DNA or messenger RNA. This complementary strand is often referred to as an "antisense strand", as it binds in an *anti*parallel fashion to the target *sense* sequence. When coupled to a reporter, an antisense strand can identify the presence of a gene of interest inside tissue by *in-situ* hybridization[114] or on a membrane by a Southern Blot.[115] With this concept in mind, in 1978 Zamecnik and Stephenson (Harvard Medical School) demonstrated that a synthetic antisense oligodeoxynucleotide could bind to a sequence specific nucleic acid *in vivo* to block translation of a viral mRNA (Rous sarcoma virus).[116] This groundbreaking discovery opened the door to a possible therapeutic pathway that could selectively target various diseases by repressing genes of interest. The following section will discuss several hybridization-mediated techniques to disrupt gene function in *vivo*. These techniques are widely used to study the roles of genes in living systems, and there is great interest in their development into therapeutic applications.[117]

1.3.1 Antisense oligonucleotides

Gene silencing strategies using oligonucleotides generally direct the arrest of translation, the process of making proteins from mRNA. Antisense oligonucleotides (AONs) are short single-stranded nucleic acids designed to bind complementary mRNA strands coding for a protein, thereby disrupting translation. The silencing mechanism can take many forms. It was initially believed that the AON-mRNA duplex formed a *steric block* that prevented the ribosomal machinery from reading the genetic code. Later, it was shown that pre-mRNA splicing could be altered resulting

in the production of non-functional proteins,[118] or could direct misspliced mRNA to form the correct protein.[119] We now know that antisense oligonucleotides composed of single-stranded DNA or DNA analogues can also recruit endogenous RNase H to cleave the mRNA•AON hybrid duplex.[120,121]

RNases H are present in all mammalian cells and are involved in DNA replication and repair. As discussed previously, they selectively degrade the RNA strand in RNA-DNA hybrid duplexes.[122] Thus DNA AONs are necessary to activate this enzyme-assisted silencing pathway. One clear advantage of the RNase H-mediated pathway over the steric block approach is the capability of one AON eliciting the destruction of several mRNA molecules in a multiple turnover fashion. A well designed AON will bind to target mRNA, elicit mRNA cleavage by recruiting RNase H and de-anneal from the degraded products to target another mRNA (Figure 1.3.1).[117]

1.3.2 RNA interference

In the late 1990's Andrew Fire (Carnegie Institute of Washington), Craig Mello (U. Massachusetts Medical School) and co-workers were experimenting with antisense oligonucleotides composed of single-stranded and double-stranded RNA targeting the *unc* gene of *Caenorhabditis elegans* (*C. elegans*).[123] To their great surprise, they obtained very potent gene silencing with the double-stranded RNA, comprised of the sense and antisense strands, compared to either strand individually. This "RNA interference" by double-stranded RNA was also evident in the progeny of the nematodes, leading them to conclude the signal was amplified by an endogenous pathway different from classic AONs. The expression of virtually any gene can be disrupted by RNA interference by delivering double-stranded RNA corresponding to that gene's sequence.[124] RNAi is proving an indispensable tool in elucidating the function of genes and presents a possible route to silence genes for therapeutic purposes.

RNA interference is triggered by double-stranded RNA in the cell. An enzyme called Dicer cuts the RNA into short interfering RNAs (siRNAs), 21-23-nt long double-stranded fragments with 2-nt overhangs at the 3'-terminus (Figure 1.3.1).[125,126] The siRNA can then become incorporated into the RNA-induced silencing complex,

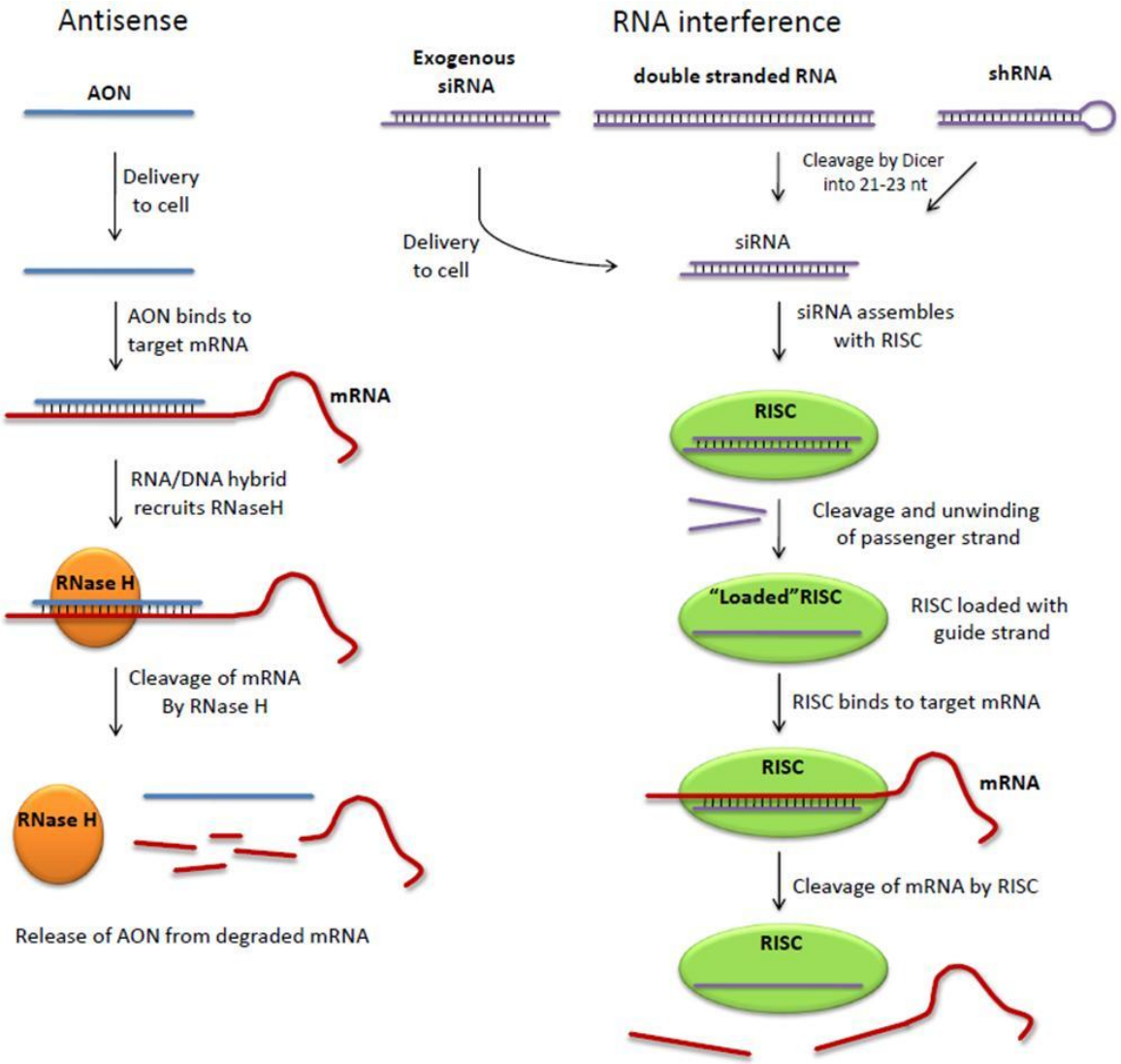

Figure 1.3.1. Schematic diagram of antisense and RNA interference mediated gene silencing pathways in the cell. *Antisense:* Synthetic antisense oligonucleotides (AONs) introduced in the cell can elicit target mRNA destruction by recruiting the activity of RNase H. *RNA interference:* Double-stranded RNA can be processed by Dicer into 21-23-nt short interfering RNA (siRNAs). Alternativley, synthetic siRNAs can be delivered into the cell. The siRNA gets incorporated into the RNA induced silencing complex (RISC) which discards the passenger strand and forms a "loaded" complex that binds and cleaves mRNA complementary to the guide strand.

or RISC,[127] which unwinds the RNA duplex discarding the sense strand (also called *passenger strand*) and loads the antisense strand (also called *guide strand*) into the complex. The RISC complex binds to mRNA that has sequence complementarity to the loaded antisense strand (Figure 1.3.1). This binding coordinates the cleavage of the mRNA near the center of the guide strand[128] by a nuclease embedded in RISC called Argonaute 2 (Ago2),[129] thus rendering the mRNA incapable of carrying out its

function. Like the RNase H-mediated antisense approach, siRNA gene silencing is a multiple turnover process.

The origin of the RNA molecules that trigger RNAi can be synthetic 21-23 nt siRNAs or short hairpin RNA (shRNA) introduced into the cell,[128] double-stranded RNA from pathogens or micro RNAs (miRNAs) from a related gene-regulating pathway.[45] Micro RNAs are endogenously transcribed and processed by a nuclear protein, Drosha,[46] into long double-stranded RNA hairpins (pre-miRNAs). If the hairpins have mismatches, they get converted to micro RNAs (miRNAs) capable of regulating translation.[130] RNA interference is found in all organisms but the exact machinery and functions may vary among species. RNAi may have arisen as a means to control transposable elements in the cell,[131] regulate gene expression through miRNAs or degrade viral genomic RNA.[132] In some species, the interference signal can be amplified by polymerases,[133] cross over to other cells,[134] or act at the transcriptional level by modifying chromatin.[135] HIV and some other viruses have adapted to a cellular environment where small RNA-mediated gene regulation is important. In some cases viruses suppress endogenous RNAi,[136-138] while in other cases they can co-opt the pathway for their own benefit.[139] Micro RNAs have even been implicated in controlling viral reservoirs of latent HIV.[140,141]

1.3.3 Aptamers and functional nucleic acids

Aptamers are another class of synthetic nucleic acids with great promise for diagnostic[142] and therapeutic[143] applications. Unlike other oligonucleotide tools which rely solely on Watson-Crick base pairing with their targets, aptamer function is mediated by their folding into three dimensional structures. Aptamers, derived from *aptu*s in Latin meaning "to fit",[144] can be engineered to have high binding affinity for their target molecules. Aptamers have been found in natural mRNA (called ribo-switches)[145-147] or can be generated by *in vitro* selection through a process called SELEX (selective evolution of ligands by exponential enrichment).[144,148] A random library of 10^{15} oligonucleotide sequences is passed through a solid-support tethered to a ligand or receptor. Only the oligonucleotides that fold into structures that "*fit*" the target will be retained on the support, while those that have no affinity wash through. The retained oligonucleotides are eluted off the column, amplified by the polymerase

chain reaction (PCR), and reintroduced to the column. Generally 6 to 15 rounds of this selection process are required to obtain a pool of oligonucleotides that show high affinity and specificity for the target molecule. The identity of the aptamers is determined by cloning the pool of oligonucleotides in bacteria and sequencing. SELEX can yield aptamers that rival antibodies in terms of binding affinity and specificity. For example, an aptamer was generated with high-affinity for theophylline (K_d=100 nM) but had 10 000 times less affinity to caffeine, a molecule that differs by a single methyl group.[149]

Aptamers have been selected for a wide range of molecular targets such as small molecules, nucleotides, amino acids, antibiotics, proteins and even unicellular pathogens.[150,151] Competitive inhibitory aptamers have been generated towards nucleic acid processing enzymes involved in diseases, such as HIV-1 RT[152] and the HIV Rev protein.[153] Aptamers targeting proteins that do not normally bind nucleic acids, such as thrombin and vascular endothelial growth factor (VEGF),[154] have proven to be viable chemotherapeutic agents in the clinic.[155,156] Aptamers show promise as delivery tools to shuttle other therapeutic agents to their site of action, such as siRNAs in prostate cancer cells.[157] Inspired by the catalytic cellular functions of RNA, such as the self-splicing hammerhead ribozyme (RNAzyme),[158] SELEX has also generated functional nucleic acids with catalytic activity. A very well known example is the Joyce 10-23 deoxyribozyme (DNAzyme)[159] that catalyzes the cleavage of RNA between any A-U or G-U sequence and was proposed to be competent for translation arrested gene-silencing.[160] This strategy has largely been abandoned since RNAzymes and DNAzymes lag behind siRNA and antisense pathways in their catalytic efficiency and their ability to function at cellular Mg^{2+} concentrations.[161]

1.3.4 Chemical modifications

Oligonucleotides present a straightforward means to selectively interrupt a target gene in light of Watson-Crick base pairing, or by the very specific ligand affinity evolved through SELEX. However, these compounds are presented with the same pharmacokinetic obstacles as other chemotherapeutic agents. According to Lipinski's Rule of Five,[162] oligonucleotides fare extremely poorly as potential chemotherapeutic agents due to their large size, the charged phosphate backbone and multiple H-

bonding sites. These properties make it difficult for oligonucleotides to enter the cell, the site of action for antisense and siRNA oligonucleotides, and can be degraded by nucleases in the extracellular environment. These shortcomings can be alleviated through chemically modifying nucleic acids to impart drug-like properties.[117,163,164]

Many nucleoside and nucleic acid analogs have been developed to improve the therapeutic profile of oligonucleotides. As nucleic acids are normally metabolized by the body, modifications often aim to prevent oligonucleotides from being degraded by non-specific nucleases or eliciting an immune response, yet allow them to bind to target mRNA and be recognized by the cellular enzymes of the antisense and/or RNAi machinery. For antisense oligonucleotides, modifications that mimic DNA (South sugar puckers) are necessary to form the RNA-DNA hybrid duplexes recognized by RNase H and lead to target mRNA cleavage. Chemical modifications can enhance duplex stability between the AON and mRNA, thus enhancing drug-target binding affinity. To this end, the use of "gapmer" constructs with AONs containing a small RNase H compatible tract of DNA flanked by RNA wings benefit from the greater binding affinity between RNA•RNA duplexes compared to RNA•DNA.[165] Nucleotide analogs that mimic RNA are generally better in siRNAs since double-stranded RNA is the trigger for RNA interference.[164,166]

To date, there are two FDA-approved oligonucleotide drugs, and both employ chemical modifications at various sites on nucleic acids. Vitravene,[167,168] an antisense oligonucleotide approved to combat cytomegalovirus (CMV) retinitis in AIDS patients, is a 21-nt DNA oligonucleotide with phosphorothioate internucleotide linkages. These modified backbones contain phosphate groups with sulphur replacing a non-bridging oxygen (Figure 1.3.2), improving the resistance towards degradation by nucleases while retaining RNase H activity.[169,170] Macugen®,[155,156] an RNA aptamer that binds to VEGF for the treatment of wet age-related macular degeneration, incorporates 2'-*O*-Me-RNA and 2'-deoxy-2'-fluororibose analogs, an unnatural terminal 3'-3'-linked dT, and a lipophilic lysine N-linked to two polyethylene glycol (PEG) molecules at the 5'-end. Placing hydrophobic groups at the ends of oligonucleotides protects them from exonucleases and increases their cell permeability.[171,172] The 2'-*O*-Me-RNA and 2'F-RNA analogs (Figure 1.3.2) are RNA-

mimics that are more resistant to endonucleases.[165,173,174] The replacement of the 2'-hydroxyl group by fluorine enhances gauche effects that strongly favour the North sugar pucker, and improves thermostability of nucleic acid duplexes.[174] Finally, the addition of large hydrophobic groups, such as PEG, at the 5'-terminus imparts better bioavailability.

Two other noteworthy oligonucleotide modifications with good therapeutic potential are locked nucleic acids (LNA) and 2'-deoxy-2'-fluoroarabinonucleic acids (2'F-ANA) (Figure 1.3.2). Locked nucleic acids have a methylene bridge between the 2'-hydroxyl group and the C4' carbon "locking" the nucleoside into a North sugar pucker, leading to tremendous enhancements in duplex binding affinity.[175-177] The lack of a 2'-OH group also enhances stability of LNA to hydrolysis and RNases.[178] LNA is finding many uses in biotechnology as a replacement for RNA with tighter binding affinity.[179]

The 2'F-ANA analogue is the 2' epimer of 2'F-RNA. The fluorine causes gauche effects that favor the southern sugar pucker, so the nucleoside tends to adopt South-East sugar conformation making it a DNA mimic.[19,180,181] 2'F-ANA oligonucleotides show enhanced binding affinity to target RNA, and are among the very few sugar modifications that can elicit RNase H cleavage of mRNA.[182-184] 2'F-ANA also has extended nuclease resistance and is in preclinical development for the treatment of chronic obstructive pulmonary disease.[185,186]

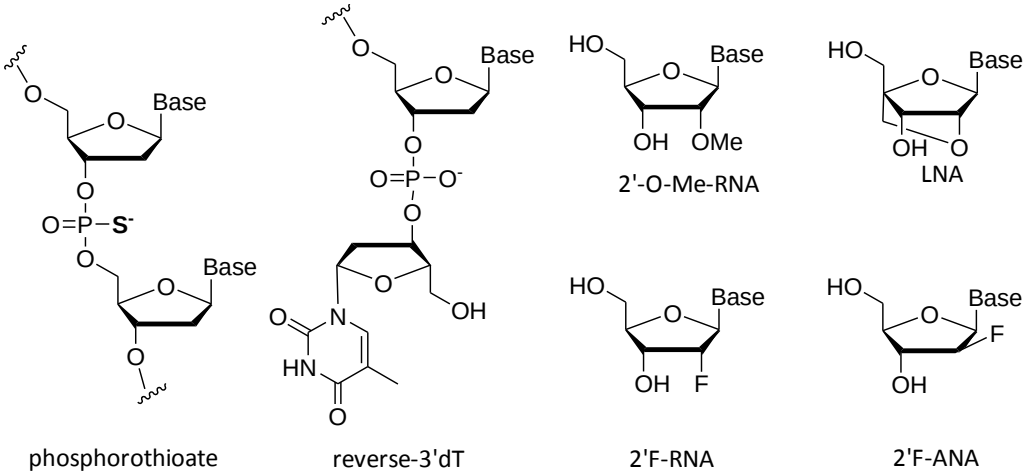

Figure 1.3.2. Examples of common nucleotide modifications incorporated in oligonucleotide therapeutic applications.

1.4 Solid-phase synthesis of oligonucleotides

Advances in our understanding of nucleic acids and their development into diagnostic tools and therapeutic agents have been made possible by preparing large quantities of oligonucleotides to test *in vitro* and *in vivo*, including in the clinical setting. Facile oligonucleotide synthesis has also enabled the development of invaluable tools in biotechnology such as the polymerase chain reaction (PCR)[187] and the fabrication of DNA[188] and RNA microarrays.[189]

The quick and cost effective chemical synthesis of DNA and RNA on large scale is now possible thanks to the development of automated solid-phase oligonucleotide synthesis. The multiple reactive groups present on nucleotides, such as the phosphate group, the sugar hydroxyls and the exocyclic amines on the nucleobases, contribute to the challenge in oligonucleotide synthesis, demanding clever and novel protecting group strategies. Considering the complexity of nucleic acids, it is remarkable that their synthesis can now be automated. This technology is the result of extensive work by brilliant researchers.

Oligonucleotides are generally synthesized from the 3' to the 5' direction in order to utilize the greater nucleophilicity of the 5'-hydroxyl group. This is in contrast to the biosynthesis of nucleic acids in which 5'-triphosphates are the reactive building blocks and the synthesis proceeds in the 3' to 5' direction. For chemical synthesis, each building block contains the sugar, the nucleobase, and an activated phosphorus at the 3'-end, and only four building blocks are needed to synthesize a natural DNA or RNA strand. The first polynucleotide synthesized was dTpT by Meselson and Todd (University of Cambridge) in 1955[190] where 3'-*O*-benzoyl protected thymidine was coupled to 5'-*O*-benzoylthymidine-3'-phosphoryl chloride. Base protecting groups are not required on thymidine since there are no reactive exocyclic amines. Khorana (University of Wisconsin) pioneered much of the chemistry that allowed the synthesis of longer oligonucleotides, culminating in the synthesis of the gene for alanine tRNA.[191] He introduced the mild acid-cleavable trityl protecting group on the 5'-hydroxyl[192] of nucleoside 3' phosphate building blocks, and more stable nucleobase exocyclic amine protecting groups benzoyl (for A and C) and isobuturyl (for G) (Figure 1.4.1).[193] This allowed the oligonucleotides to be built in a cycle of 5'-*O*-trityl

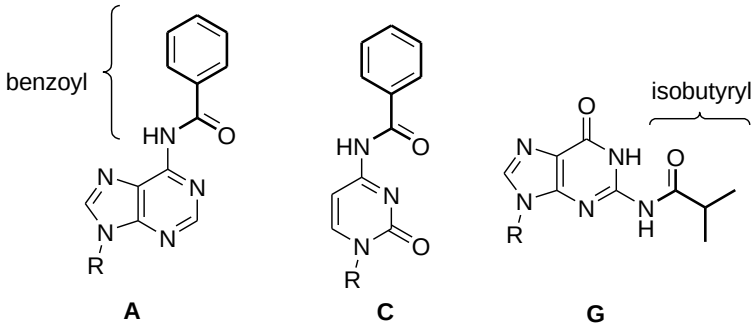

Figure 1.4.1. Exocyclic amine protecting groups in nucleobases.

deprotection followed by coupling of another phosphate building block, and removal of all base protecting groups at the end of the synthesis is achieved in ammonia. Letsinger (Northwestern University) devised the phosphotriester approach by introducing a β-cyanoethyl protecting group on the phosphate which produced neutral molecules soluble in organic solvents that were far easier to isolate and purify by column chromatography.[194] Later, he opted to remove a phosphate oxygen to give phosphite triester (phosphorus III) building blocks which greatly increased coupling times.[195] Oxidizing the newly formed P(III) sugar-phosphate bond to a phosphate triester is easily accomplished in iodine/water and is necessary to prevent acid-mediated strand cleavage in the ensuing detritylation. The chlorophosphite building blocks proved so reactive they suffered from limited shipping capability and had to be used on site. This was remedied by Beaucage and Caruthers (University of Colorado

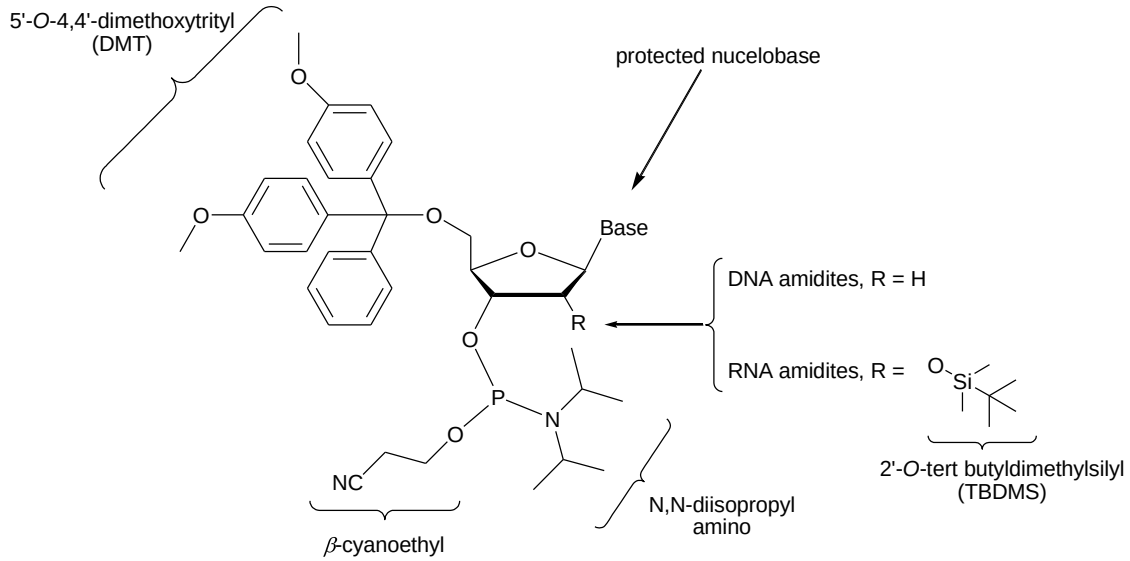

Figure 1.4.2. Structure of phosphoramidite building blocks used in solid phase oligonucleotide synthesis.

at Boulder) who replaced the chlorine for N,N-diisopropylethylamine to the phosphorus to give hydrolytically stable phosphoramidite building blocks (Figure 1.4.2).[196] During the coupling step of the synthesis cycle, the phosphoramidite is activated with a very weak acid, 1H-tetrazole or 4,5-dicyanoimidazole (DCI), in the presence of the 5'-hydroxyl of the growing chain. These heterocycles are not acidic enough to remove the 5'-*O*-trityl group of the phosphoramidite.

To this day, the phosphoramidite approach is the most utilized method for oligonucleotide synthesis. The building blocks are depicted in Figure 1.3.2 and the synthetic scheme is illustrated in Figure 1.4.3. Letsinger was also the first to experiment with oligonucleotide synthesis on solid support,[197] eliminating the need for separation and purification between cycles, which led to the first automated DNA/RNA synthesizer, or "gene machine", by his former student Kelvin Ogilvie (McGill University).[198] Alkylamine functionalized controlled-pore glass (CPG)[199] is generally the solid support conjugated to the first 5'-*O*-dimethoxytrityl protected building block via a succinyl linker.[200] There are four steps in the synthesis cycle. It begins with the removal of the 5'-*O*-dimethoxytrityl group of the support-bound nucleoside with 3%TCA. This is followed by the coupling step; a tetrazole or DCI activated phosphoramidite building block forms a phosphite triester bond with the free 5'-hydroxyl. The third step, capping, acetylates any unreacted 5'-hydroxyl groups to halt the accumulation of by-products. The fourth step is the oxidation of the phosphite triester to an acid stable phosphate triester. It was demonstrated that performing the capping step prior to oxidation is necessary to prevent the formation of branched adducts on the O-6 position of guanine.[201] It is usually necessary to remove the DMT group of the last coupled nucleotide, but if left intact can be beneficial for purification by reverse-phase (RP) HPLC. At the end of the last cycle and detritylation, the oligonucleotide is cleaved from the solid support in ammonium hydroxide. This treatment also removes the exocyclic nucleobase protecting groups and the β-cyanoethyl protecting on the phosphate. The automated solid-phase synthesis of oligodeoxynucleotides gives excellent coupling yields (>99% per step), requires little manual labour, can be performed on very small scale (nmol) and

consumes little material compared to solution phase. The synthesis of DNA is very quick, lasting approximately 7.5 minutes per cycle.

The synthesis of RNA has proven more challenging as the presence of the 2'-hydroxyl requires the control of yet another protecting group. The synthesis of the building block requires selective protection of the 2'-hydroxyl group over the 3'-hydroxyl. In addition, many protecting groups introduced at the 2'-hydroxyl can isomerize to the 3' position if careful conditions are not met, further complicating the task. The introduction of 2'-hydroxyl protecting groups also generally adds steric bulk to the phosphoramidite building blocks, which contributes to lower stepwise coupling yields afforded in RNA synthesis (98.5% per step) and longer reaction times (approximately 15 minutes per cycle). Although there are many 2'-hydroxyl protecting groups that have led to the successful synthesis of RNA,[202] the most widely utilized is the *tert*-butyldimethylsilyl (TBDMS, Figure 1.4.2) protection group introduced by Ogilvie (McGill University).[203,204] It is resistant to the conditions in the DNA synthesis cycle and only requires an extra step for its removal after the deprotection and cleavage from the solid support. This is generally accomplished with a fluoride source, such as tetra-n-butylammonium fluoride (TBAF) or triethylamine trihydrofluoride (NEt_3:3HF or TREAT-HF).[205] The robustness of the 2'-*O*-TBDMS protecting group was demonstrated by Ogilvie by synthesizing a functional 77-mer tRNA molecule.[206]

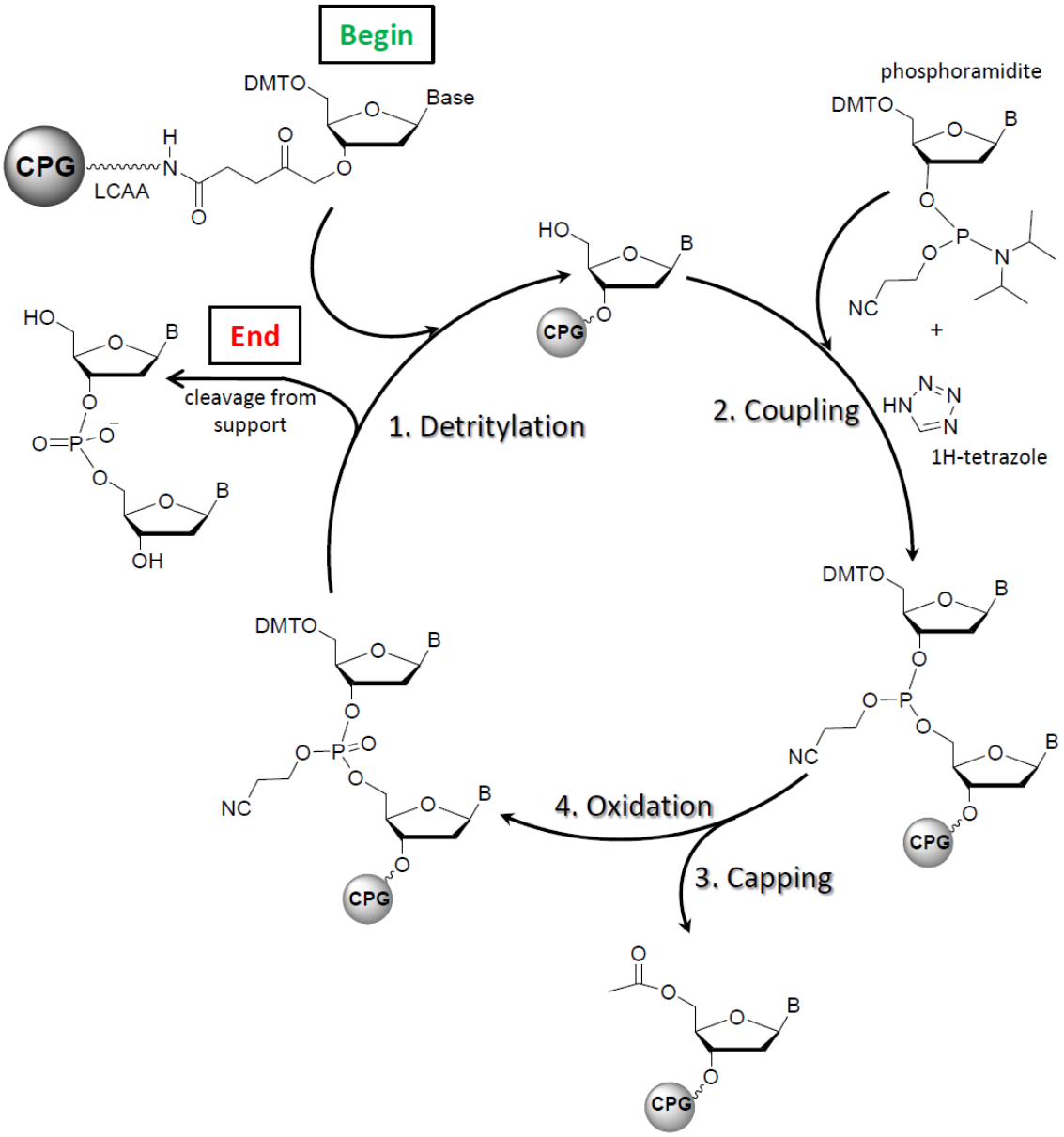

Figure 1.4.3. Solid-phase synthesis cycle using the phosphoramidite approach. The first building block is attached to the controlled pore glass (CPG) solid support through a long chain alkylamine (LCAA)/succinyl linker. Conditions: 1. Detritylation, 3% TCA, DCM 2. Coupling, 0.25 M tetrazole (or DCI), phosphoramidite, ACN 3. Capping, Ac_2O, imidazole, pyridine, ACN 4. Oxdation, 0.02 M I_2, pyridine, H_2O, THF. After the final cycle and detritylation, NH_4OH is used to cleave the oligonucleotide from the solid support, remove the base protecting groups, and remove the β-cyanoethyl groups on phosphorus.

1.5 Physical properties and characterization of nucleic acids

Due to their large size and the limited material obtained from syntheses, characterization of oligonucleotides by conventional means such as mass spectrometry (MS), nuclear magnetic resonance (NMR) and crystallography is not always readily achieved. Fortunately, nucleic acids can be characterized using a variety of other techniques that make use of their physical and spectroscopic properties. These methods can provide information quickly and often require little material. For example, the ultraviolet absorbance of the nucleobases in oligonucleotides can be used for quantitation, determining the denaturation temperature of nucleic acid duplexes, and can provide information about helical geometry using only nanomolar quantities. An electric current can be utilized to move negatively charged oligonucleotides through a matrix. Thus, gel electrophoresis is useful for both analytical and preparative purposes, and can be used to assess the size and shape of nucleic acids and their binding affinity for proteins. When labeled with radioactive phosphorus (^{32}P or ^{33}P), oligonucleotides can be analyzed at sub-picomolar quantities using gel electrophoresis. Fluorescence labeling is now replacing radioactive probes as a safer alternative to radiation, and offers the ability to observe multiple luminophores with different emission wavelengths for multiple analyses. In addition, gel-free fluorescence techniques exist that can be used in real-time, for single molecule detection or in a high throughput format. This section presents the principles behind these techniques, which are used throughout this thesis for a variety of purposes.

1.5.1 Absorbance

The nucleobases of RNA and DNA absorb ultraviolet light with a maximum absorption (λ_{max}) around 260 nm (Table 1.5.1).[207] It is possible to quantitate nucleic acids in aqueous media from the measured absorbance according to the Beer-Lambert law:

$$A = \varepsilon_\lambda \ell c \qquad (1)$$

where A is absorbance, the amount of light absorbed by the sample defined by log(incident light intensity/transmitted light intensity), ε_λ is the molar extinction coefficient for a given nucleic acid sequence at a specific wavelength in $M^{-1}cm^{-1}$, ℓ is

the path length the light travels in the sample media in cm, and c is the concentration of the sample in M. The ε_{260} values for the nucleotides in RNA and DNA are listed in Table 1.5.1.[208,209]

Table 1.5.1. Maximum absorbance and extinction coefficients of RNA and DNA nucleotides.[208,209]

Nucleotide	λ_{max} (nm)	ε_{260} ($cm^{-1}M^{-1}$)
A/dA	259	15340
G/dG	252	12160
C/dC	271	7600
U	262	10210
T	267	8700

The maximum absorption of heteropolymeric nucleic acids falls close to 260 nm, roughly the average of the λ_{max} values in Table 1.5.1. One would assume that the molar extinction coefficient of an oligonucleotide can be estimated from the sum of the ε_{260} values of the individual constituent monomers. However, the ε_{260} of polymeric single-stranded, and to greater extent double-stranded oligonucleotides, are less than the sum of the individual ε_{260} of the constituent nucleobases, a phenomenon known as hypochromism.[210] Hypochromism arises when there is a parallel arrangement of dipoles running in opposite directions, such that the induced dipole reduces the intensity of the transition dipole (Figure 1.5.1).[211] For the nucleobases, the transition dipoles run in the plane of the heterocyclic rings. In RNA and DNA, the nucleobase transition dipoles are stacked one on top of the other like a deck of cards, in a parallel arrangement favorable for hypochromism. When transitioning from single-stranded to double-stranded nucleic acids, more hypochromism arises because the direction of the transition and induced dipoles of paired nucleobases run in opposite directions in a quasi parallel arrangement (Figure 1.5.1).[212] Aside from hypochromism, the ε_{260} of each individual nucleobase is influenced by the identity of the neighboring bases.[213,214] Therefore, in order to calculate the molar extinction coefficient of single-stranded oligonucleotides, it is customary to employ a nearest neighbor approximation using the equation shown below (equation (2)).[213] This

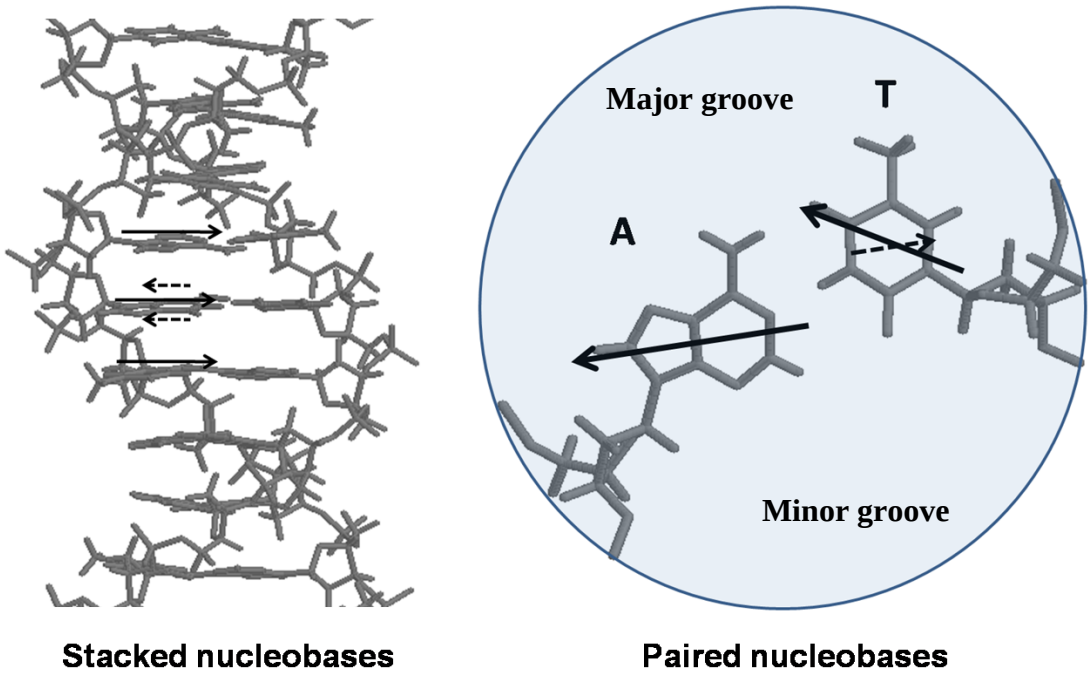

Figure 1.5.1. Interaction between transition dipoles (solid arrows) and induced dipoles (dotted arrows) of neighboring nucleobases in DNA that causes hypochromism. The dipoles in stacked nucleobases (left image) are parallel in a card/pack arrangement. In paired nucelobases (right image), the orientation of the induced dipole from A (dotted arrow) opposes the transition dipole of T.

method accounts for sequence variability and utilizes the measured ε_{260} values for all 16 dinucleotide combinations.

$$\varepsilon_{260} = \sum_{n-1}^{1} (\varepsilon_{260}\text{dinucleotide}) - \sum_{n-1}^{2} (\varepsilon_{260}\text{nucleoside}) \qquad (2)$$

Integrated DNA Technologies (Coralville, Iowa) provides a free tool to calculate the sequence specific ε_{260} of single-stranded RNA or DNA that uses equation (2) and is available on the World Wide Web:

http://www.idtdna.com/ANALYZER/Applications/OligoAnalyzer/Default.aspx.

1.5.2 Thermal denaturation studies[215]

Nucleic acid secondary structure can be disrupted by physical or chemical means, often referred to as denaturation. An example of denaturation occurs when double-stranded DNA, an ordered state, is broken into two single strands, a disordered state. This process is reversible, and the two single strands can anneal again to form the native duplex if the denaturing conditions are removed. Denaturation can be accomplished by heating, changing pH, varying solvent or salt concentration or by introducing a chemical denaturant such as urea.

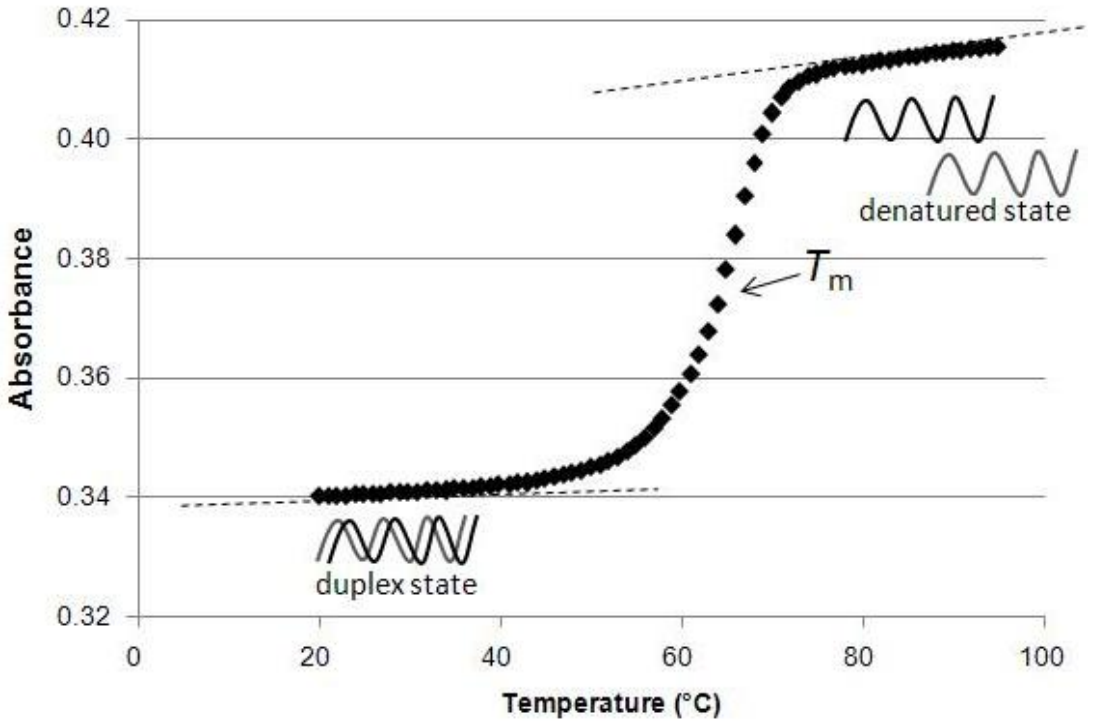

Figure 1.5.2. Thermal denaturation curve of an 18-mer RNA-DNA hybrid duplex with a melting temperature of 65 °C. The x-axis is temperature in degrees centigrade, and the y-axis is absorbance units measured at 260 nm ultraviolet light (UV_{260}). The nucleic acid is predominantly double-stranded (duplex state) at low temperatures, and the absorbance exhibits hypochromism (lower absorbance). At high temperature, the secondary structure is disrupted, the two strands dissociate, and the absorbance increases from reduction of hypochromism. The melting temperature (T_m) is indicated by the black arrow, and can be determined by the mid-point between the low temperature baseline and the high temperature baseline (dotted lines).

Monitoring the denaturation of nucleic acids while increasing temperature yields a thermal denaturation curve, also called a melting curve, and can provide information about the physical properties of nucleic acids. Nucleic acid differences in UV_{260}

absorbance between double-stranded and single-stranded forms presents a practical means to follow denaturation.[216] Figure 1.5.2 depicts a typical plot of absorbance as a function of temperature for a double-stranded bimolecular nucleic acid. At low temperature, the nucleic acid exists predominantly in the native duplex form and exhibits lower absorbance due to hypochromism. When the sample is heated, denaturation occurs and the absorbance progressively rises as the population of dissociated oligonucleotides increases. The absorbance reaches a plateau indicating that all the nucleic acids are in a single-stranded state. The mid-point of the steep transition indicates when there is an equal population of duplexed and denatured nucleic acids, referred to as the melting temperature (T_m). This value is calculated as halfway between the upper and lower baselines. In melting curves where no high temperature baseline can be obtained, the T_m can be estimated as the peak value of a plot of the first derivative of the melting curve versus temperature.[215]

The melting temperature provides a quantitative measure of the strength of a nucleic acid duplex and/or the stability of nucleic acid secondary structure. The magnitude of the T_m value is used to compare the thermostability of different duplexes and can evaluate if nucleotide modifications disrupt base pairing or base stacking by decreases in T_m. Melting curves can also distinguish unimolecular duplexes, such as hairpins, from bi-molecular duplexes by monitoring T_m at varying concentrations[215] and detect non Watson-Crick base pairing structures such as G-quadruplexes by monitoring UV_{295} absorbance.[217]

1.5.3 Circular Dichroism Spectroscopy[15]

Circular dichroism (CD) spectroscopy is a technique that can provide structural information about nucleic acids in solution. A CD signal is detected when chromophores contain repetitive chirality, such as with the right-handed B-form DNA double helix. Molar circular dichroism is defined as the result of subtracting the extinction coefficient of circularly polarized light in the counterclockwise direction from the extinction coefficient in the clockwise direction ($\Delta\varepsilon$). A CD spectrum is graphically plotted as units of $\Delta\varepsilon$ or molar ellipticity as a function of wavelength. CD spectra give information about the global conformation of nucleic acids. With the appropriate reference spectra, CD can differentiate nucleic acid single strands, double

strands, A-form or B-form duplexes, right or left handed helices, and G-quadruplexes.[218]

The CD spectra of A-form and B-form duplexes display some characteristic traits. B-form DNA displays a positive maximum around 280 nm, crosses the x-axis (cross-over point) around 260 nm, and continues to a negative maximum around 250 nm.[218] The magnitude of the A-form DNA and RNA positive maximum is generally greater than B-form, appearing around 265 nm, cross–over point closer to 240 nm, and has a negative maximum close to 210 nm.[15] G-quadruplexes also have a distinctive CD signature with a positive maximum close to 295 nm.[219]

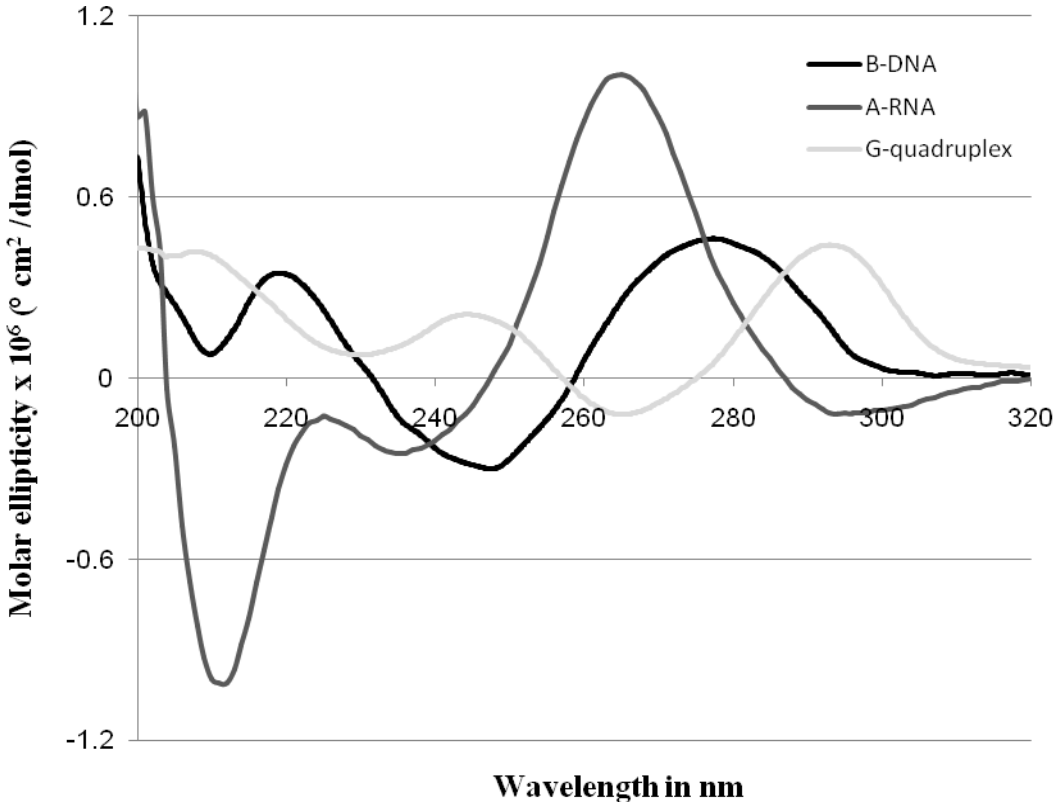

Figure 1.5.3. Circular dichroism spectra of different nucleic acid structures. The black line represents a typical B-form DNA CD spectra, the dark grey line represents A-form RNA, and the light grey line represents a G-quadruplex.

1.5.4 Gel Electrophoresis[220]

Gel electrophoresis is a technique whereby charged molecules, such as nucleic acids, are driven through a gel matrix made of agarose or polyacrylamide under an electric field. The velocity of molecules in the gel depends on their size, shape and charge. Larger and less compact molecules will experience greater frictional forces and migrate slower in the gel, whereas molecules with a greater net charge and compact size will migrate faster. Due to the phosphate groups in their backbone, nucleic acids are negatively charged at neutral pH and migrate towards the positive electrode in an electric field. Using denaturing conditions, nucleic acids form straight rods and regardless of their length will have the same shape and similar charge density (provided the oligonucleotide is greater than 5 units long). Such conditions conveniently allow the separation of nucleic acids based on their size alone.

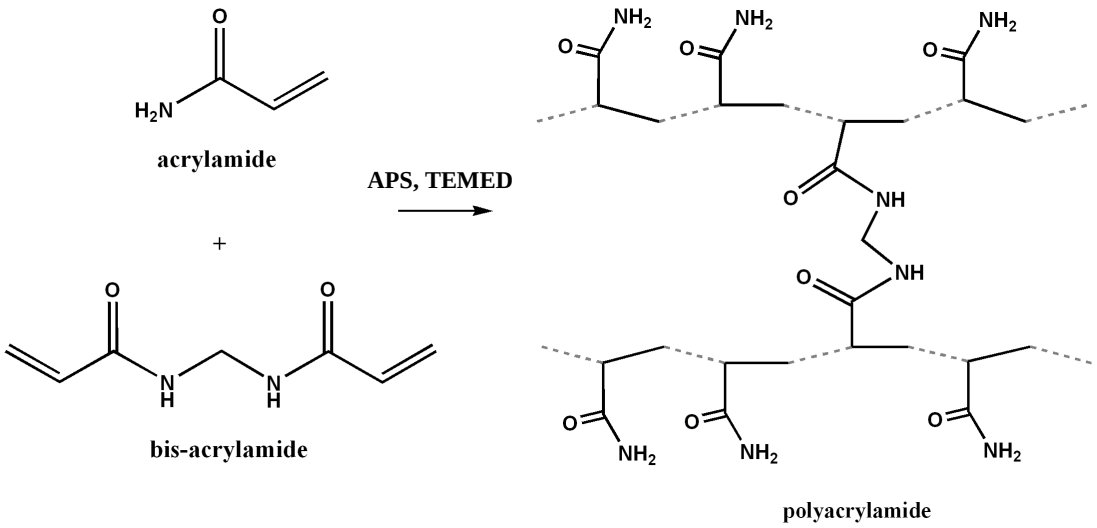

Figure 1.5.4. Formation of polyacrylamide from its monomers, acrylamide and bisacrylamide. The free radical catalyzed reaction is performed with ammonium persulfate (APS) and the initiator and *N*,*N*,*N*',*N*'-tetramethylethylenediamine (TEMED) as the stabilizer.

Electrophoresis of nucleic acids larger than 200 nucleotides long is generally done in agarose gels, while for shorter nucleic acids, such as synthetic oligonucleotides, polyacrylamide gel electrophoresis (PAGE) is used. PAGE is employed for both the purification and analysis of synthetic oligonucleotides. The gel is made from the polymerization of acrylamide and bis-acrylamide (Figure 1.5.4) and forms pores 1-2 nm wide depending on the ratio of the two building blocks and the concentration of

polyacrylamide which usually lies between 6 and 24%. Higher concentrations of acrylamide will retard the migration of the nucleic acids more and are necessary to analyze and purify shorter oligonucleotides (20-5 nucleotides in length). One gel can accommodate up to 60 samples (as in sequencing gels) or a large quantity of a single sample (usually for purification purposes). Each sample is placed in a different trough at the top of the gel, referred to as a "well" (Figure 1.5.5A).

PAGE can be carried out under native conditions, where the secondary structures remain intact, or denaturing conditions, where all the oligonucleotides dissociate into straight single strands. Denaturing conditions are achieved by preparing the polyacrylamide gel with 7M urea, which disrupts hydrogen bonding. In addition, samples can be denatured prior to loading on the gel by heating to 95 °C in formamide. Denaturing PAGE resolves oligonucleotides at single nucleotide resolution (Figure 1.5.5A) and can be used to determine the length of an oligonucleotide if run alongside controls of known length. Preparative denaturing PAGE allows the purification of synthetic oligonucleotides from the failure sequences after solid-phase synthesis; the thick slowest moving band is usually the full-length product (Figure 1.5.5B).

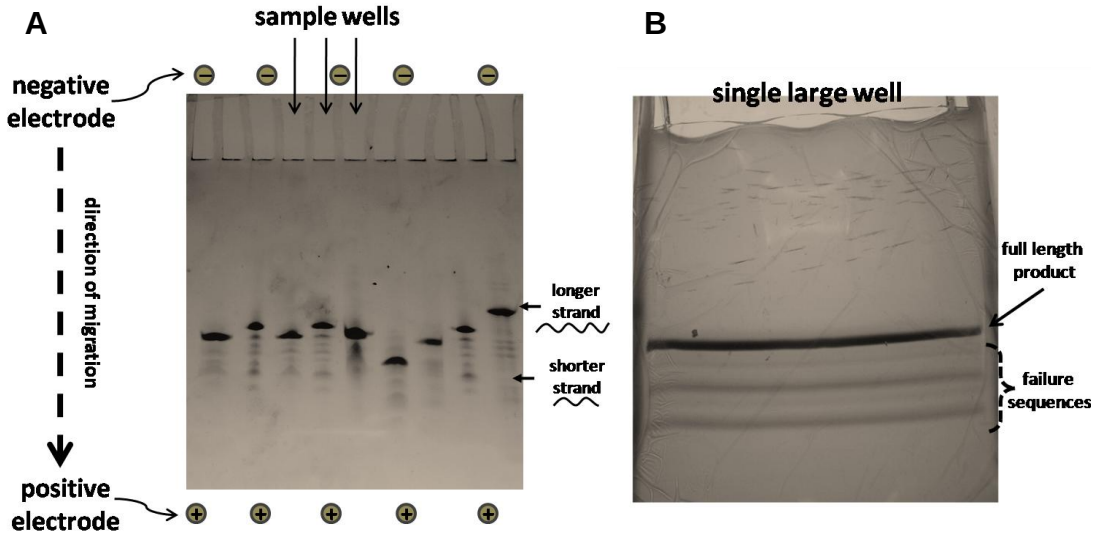

Figure 1.5.5. A. An example of an analytical 24% denaturing PAGE (7M urea) visualized by Stains-All. Each well contains a single sample. The oligonucleotides are migrate from the negative electrode (top of the gel) to the positive electrode (bottom of gel) with longer oligonucleotides migrating slower. B. An example of a preparative 24% denaturing PAGE (7M urea) visualized by UV-shadowing. The full-length product appears as a larger slower moving band compared to the shorter failure sequences which migrate quicker.

Nucleic acids are easily visualized in PAGE by a variety of methods depending on the amount of material loaded on the gel. Preparative gels, which can accommodate up to 1 mg of material, can be visualized by UV-shadowing on a thin layer chromatography (TLC) plate that contains a fluorescent indicator with 254 nm light. Analytical gels can be visualized by UV-shadowing with as little as 2 μg of material per well. Alternatively, the chemical dye Stains-All (Sigma-Aldrich)[221,222] can be used for detecting down to 100 ng of material per well. Oligonucleotides can be labeled with radioactive phosphorus-32 (^{32}P) on the 3' or 5' terminus and visualized by autoradiography. This method provides great sensitivity with little modifications to the DNA structure, but also poses a safety hazard as ^{32}P emits β-particles. Fluorescent tags are a safer alternative to ^{32}P with sensitivity down to pg quantities. However, unlike ^{32}P-labelling which can be done post-synthetically, fluorescent tagging must be planned beforehand.

1.5.5 Fluorescence Spectroscopy[223]

When a molecule becomes excited by light energy, photons, it can relax through a variety of pathways. These energy-releasing pathways can either be non-radiative or radiative. Examples of non-radiative pathways are the loss of energy as heat or chemical energy. In the radiative pathways, the energy can be released as light of a lower energy (longer wavelength), which is fluorescence. Molecules that fluoresce are often called fluorophores. The fraction of the photons absorbed by a molecule that are emitted as fluorescence is known as the quantum yield (Φ). The five common nucleobases (A, C, G, T and U) have very low quantum yields, on the order of 10^{-4}, which corresponds to undetectable levels of fluorescence by conventional means, and consequently do not interfere with the measurements of highly emissive fluorescent probes.[224] Thus, fluorescent techniques are useful to study the structure and dynamics of nucleic acids.

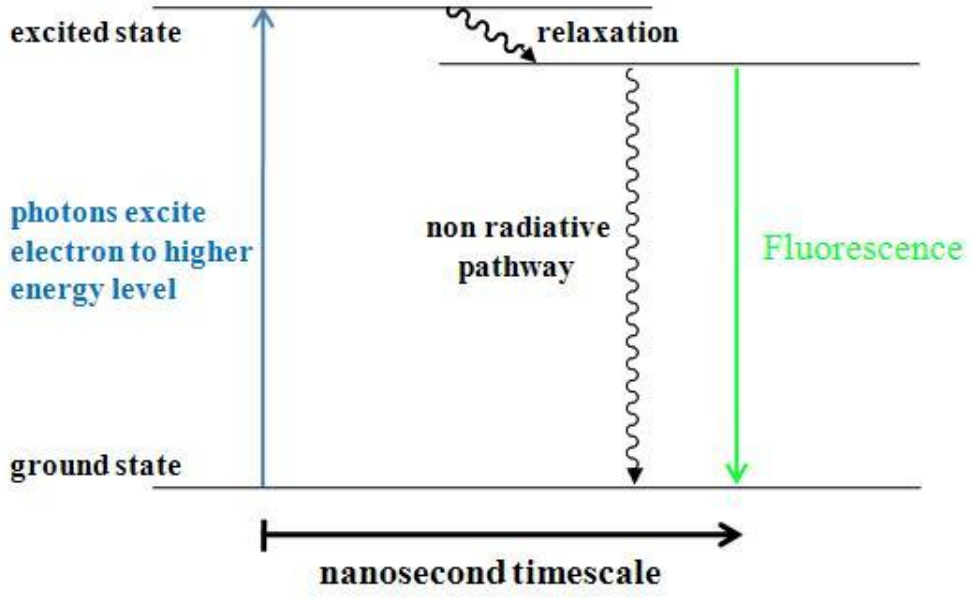

Figure 1.5.6. This simplified Jablonski diagram illustrates the events that lead to fluorescence emission. Photons promote an electron from the ground state to an excited state (excitation). The electron equilibrates to the lowest vibrational level. It can then relax back to the ground state by radiative pathways, such as fluorescence (emission), or non-radiative pathways. The events that occur during fluorescence last on the order of nanoseconds.

The events leading to fluorescence emission are readily described in a Jablonski diagram as illustrated in Figure 1.5.6. Photons that are absorbed by a molecule can promote an electron at the ground state to an excited state. This process is so quick (10^{-15}s) that it is not accompanied by any rearrangement of atoms in the molecule. The excited electron relaxes to the lowest vibrational level (10^{-12}s) of the first excited state, after which fluorescence emission can take place when the electron returns to the ground state. The average time the electron remains in an excited state prior to fluorescence emission is known as the excited state lifetime or fluorescence lifetime. The fluorescence lifetime is an intrinsic property of a fluorescent molecule and is usually on a nanosecond (10^{-9}s) timescale.

The energy from an excited state fluorescent molecule can be absorbed by interacting with another molecule, called a quencher, which allows the fluorophore to return to the ground state without emitting fluorescence. Another process that decreases emission intensity of an excited fluorophore is resonance energy transfer (RET) also known as Förster resonance energy transfer (FRET). FRET is possible

when the emission spectrum of a fluorophore (termed the donor) overlaps with the absorption spectrum of another molecule (termed the acceptor) and the excited state energy is transferred from the donor to acceptor (Figure 1.5.7). If the acceptor is a fluorophore, it may release the excited state energy acquired from the donor as fluorescence emission. There are three factors that determine the efficiency of energy transfer: 1) the distance between the donor and the acceptor (the Förster distance), 2) the overlap between the emission spectrum of the donor and the absorption spectrum of the acceptor, and 3) the orientation of the transition dipoles of the donor with respect to the acceptor. FRET is an invaluable tool to map distances in biological macromolecules, such as proteins and nucleic acids.[225]

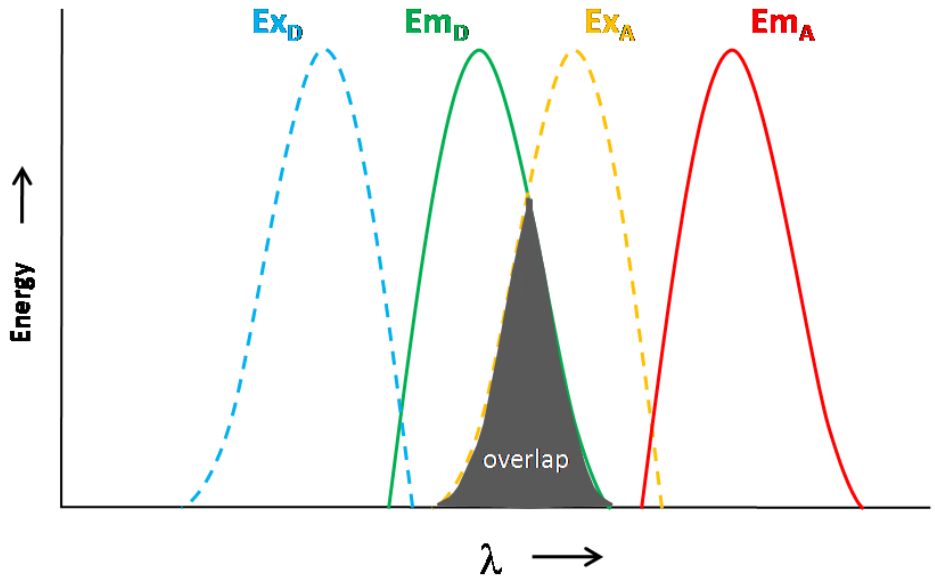

Figure 1.5.7. Representation of the excitation and emission spectra of fluorescent molecules undergoing fluorescent resonance energy transfer (FRET). The excitation and emission spectra of the donor are shown as the blue and green curves respectively (Ex_D and Em_D). The excitation and emission spectra of the acceptor fluorophore are shown as the orange and red curves respectively (Ex_A and Em_A). FRET can occur when there is spectral overlap between the donor emission spectra and the acceptor excitation spectra. If all the conditions for FRET are met, exciting at the donor fluorophore would produce emission of the acceptor fluorophore.

Another useful tool for studying biological macromolecules is fluorescence polarization (FP) (essentially the same as fluorescence anisotropy). FP can give information about the size of molecules attached to fluorescent moieties. As discussed in section 1.5.1, molecules that absorb light have an excitation transition dipole.

Fluorescent molecules have an emission transition dipole as well. Light passed through a polarizing filter (polarizer) oscillates in a single orientation. A molecule will absorb the most energy when its transition dipole is parallel with the polarization axis of the excitation light and the least when it is perpendicular. A fluorescent molecule will also mostly emit light with waves oriented parallel to the emission transition dipole. During the time a fluorescent molecule is in the excited state, which lasts for nanoseconds, it may rotate such that the emission dipole has changed orientation with respect to the excitation transition dipole (depolarization) (Figure 1.5.8). Smaller molecules have more rotational diffusion in this timeframe than larger ones in solution, and have a greater propensity for depolarization (Figure 1.5.8). Thus fluorescence polarization is retained for large molecules with limited motion, and fluorescence depolarization is observed for smaller molecules undergoing more Brownian motion. Figure 1.5.8 illustrates how fluorescence polarization and depolarization can be used to evaluate the size of biological molecules.

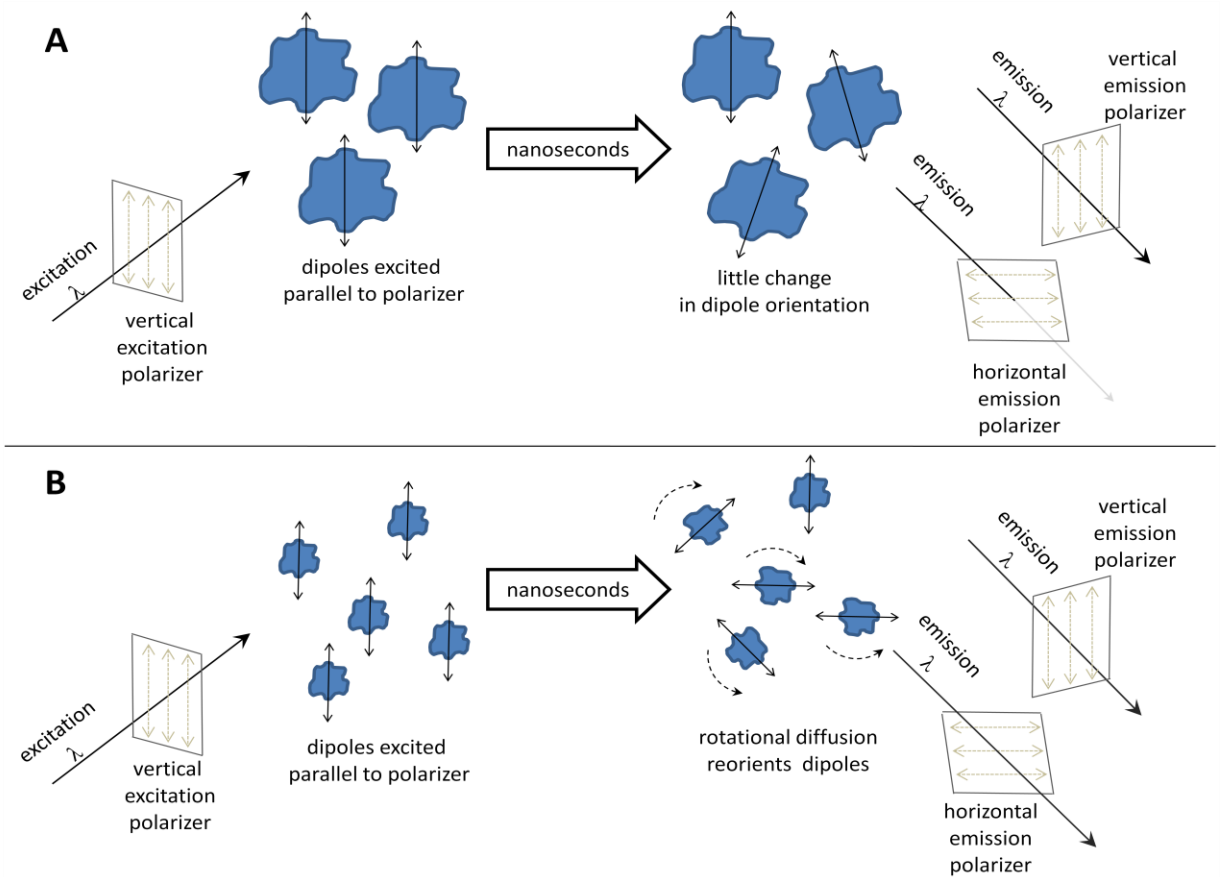

Figure 1.5.8. Comparison of fluorescence polarization for large and small molecules. **A**. Plane polarized light excites the fluorophores with transition dipoles (double arrows) parallel to the axis of the polarizer. Large molecules rotate slowly at the nanosecond timescale such that the transition dipoles remain in nearly the same orientation during emission, thus the emitted light remains polarized. The fluorescent light will pass through the emission polarizer oriented parallel emission dipole, and blocked by polarizers oriented perpendicular. **B.** When smaller fluorophores are in the excited state, they undergo more rotational diffusion in nanoseconds and the orientation of the transition dipoles changes, thus the emitted light is depolarized. Some fluorescent light will pass through both parallel and perpendicular oriented emission polarizers.

1.6 Thesis objectives

This research laboratory has a long-standing interest in chemically modified nucleotides and oligonucleotides and their structural and biological consequences. Sugar-modified nucleic acids such as arabinonucleic acids (ANA),[226] 2'F-ANA,[226] unlocked nucleic acids,[227] 2'-fluoro-4'-thioarabinonucleic acids[166] and oxepane nucleic acids (ONA)[228] have been tested as substrates for RNase H. These studies have helped identify structural properties necessary to elicit RNase H activity, such as flexibility and sugar pucker conformation,[229] and has implications for antisense oligonucleotides, and more recently siRNA-mediated gene-silencing. The RNase H activity of RT is also a potential antiretroviral target as this function is a requirement for HIV-1 infectivity.[79] This research group demonstrated that double-stranded RNA can inhibit the activity of *E. coli* and HIV-1 RT RNase H.[230] Small nucleic acid hairpins and dumbbells were also shown to preferentially inhibit the RNase H activity of RT over the polymerase activity.[231,232] The mechanism of this inhibition was not clearly identified.

Chapter 2 of this thesis aims to synthesize second-generation nucleic acid hairpins containing chemical modifications with improved stability and potency towards HIV-1 RT RNase H. In addition, studies designed to elucidate the mechanism of action of hairpin inhibition are carried out.

Chapter 3 describes a high throughput method to screen for inhibitors of RNase H using 6-phenylpyrrolocytidine (PhpC), a novel fluorescent nucleobase analogue. To evaluate PhpC as a chemical modification in RNA, its structural properties are determined by thermal denaturation experiments and circular dichroism spectroscopy.

Chapter 4 further investigates the properties of PhpC as a modification for gene-silencing oligonucleotides. siRNAs containing PhpC are evaluated for their ability to repress the luciferase gene in HeLa cells. The use of PhpC-siRNAs as a fluorescent reporter to monitor cellular localization is explored.

Chapter 5 investigates if there is a relationship between sugar conformation and nucleotide excision by HIV-1 RT. To this end, primers containing various chemical modifications at the 3'-terminus are synthesized and tested for excision. Since

inhibitors of nucleotide excision present a novel therapeutic target for RT, a high throughput screen to identify such agents using fluorescent nucleobases is explored.

Chapter 2. Inhibition of HIV-1 RT RNase H Activity by Chemically Modified Nucleic Acid Hairpins

2.1 Introduction

2.1.1 Current HIV therapy

Acquired immunodeficiency syndrome (AIDS), caused by the human immunodeficiency virus (HIV), has become one of the most lethal chronic diseases for which no cure has yet been identified.[233,234] HIV-1 reverse transcriptase (RT) is a key enzyme that plays an essential and multifunctional role in the life cycle of the virus. HIV-1 RT converts the viral single-stranded RNA genome into DNA following the entry of the virus into the cytoplasm of the host cell. The enzyme displays DNA polymerase activity on both RNA and DNA templates, and a ribonuclease H (RNase H) activity on RNA•DNA hybrids.[52,235] It also plays a role at specific steps during the complicated process of reverse transcription, including strand transfer and the removal of RNA primers. As a result, RT has been a prominent target in the discovery and development of antiviral agents that suppress HIV infection.[236] Of the numerous lead compounds studied, only those that specifically target HIV-1 RT or the HIV-1 protease enzyme, and, more recently, the cell entry and integrase process, have been approved for HIV therapy.[78] The common nucleoside reverse transcriptase inhibitors (NRTIs), *e.g.* AZT, 3TC, and d4T, and non-nucleoside reverse transcriptase inhibitors (NNRTIs) (nevirapine, efavirenz, and delavirdine) effectively block viral DNA replication and slow the onset and progression of AIDS.[56,237,238] Despite the tremendous success associated with antiretroviral combination therapy, which may also include inhibitors of the viral protease,[239] the development of resistance cannot be prevented and accounts for a major cause of treatment failure.[240] As a result, much effort is now directed at identification of drugs against novel (non-RT) HIV targets.[241]

2.1.2 RNase H as an antiretroviral target

HIV-1 RT provides additional unique targets for antiretroviral drug discovery. RT-associated ribonuclease H (RNaseH) is needed to degrade the RNA component of the RNA•DNA hybrid duplex intermediate formed during reverse transcription, in

order to free the DNA strand for use as template to form the final viral double strand DNA intermediate. Mutations in the RNase H domain of RT lead to a marked decrease in the level of virus proliferation, an indication of the crucial role of RNase H during the retroviral cycle.[79,242] Point mutations at the active site completely block replication of the virus.[79] HIV-1 RT RNase H is therefore a logical target for antiretroviral intervention, yet there are no such inhibitors in clinical development, and indeed very few have been identified.[104,243] There is some debate as to whether RNase H inhibitors can compromise the effectiveness of NRTIs. It has been proposed that reducing the degradation of the RNA template by RNase H will allow more time for RT to bind to the RNA template-DNA primer, increasing the rate of nucleotide excision (and hence drug resistance).[97,98] Indeed, recent studies on virus mutations in patients with thymidine analogue mutations (TAMs) and mutations in the connection domain offer conflicting results supporting this hypothesis.[244-246]

The development of potent and selective inhibitors of RNase H will help determine if this target is valid for antiretroviral therapy. Only a handful of small molecule compounds have shown very specific inhibition towards the RNase H activity of HIV-1 RT (Figure 2.1).[104] N-Acylhydrozones were the first compounds to show potent inhibition to RNase H.[247] One such analogue, dihydroxy benzoyl naphthyl hydrazone (DHBNH, Figure 2.1), shows specific inhibition towards the RNase H activity even though it binds close to the NNRTI binding site as revealed by X-ray crystallography.[248] Another class of potent RNase H inhibitor, the diketo acids, demonstrated synergy for reverse transcription with clinically approved RT inhibitors.[96,249,250] With the advent of better screening techniques for inhibitors of RNase H,[251-253] some other promising lead compounds have been described such as the hydroxylated tropolones[254,255] and more recently vinylogous ureas.[256]

Nucleic acid duplexes offer an alternative to small molecules for targeting RNase H, and should be well-suited for this task since they constitute the natural substrate of RNase H. The advent of SELEX (Systematic Evolution of Ligands by Exponential Enrichment)[144,148] opened the door to a quick and efficient method of obtaining nucleic acid ligands, better known as "aptamers" (from the Latin, *aptus*, meaning 'to fit'). The culmination of this discovery has thus far been the development of the

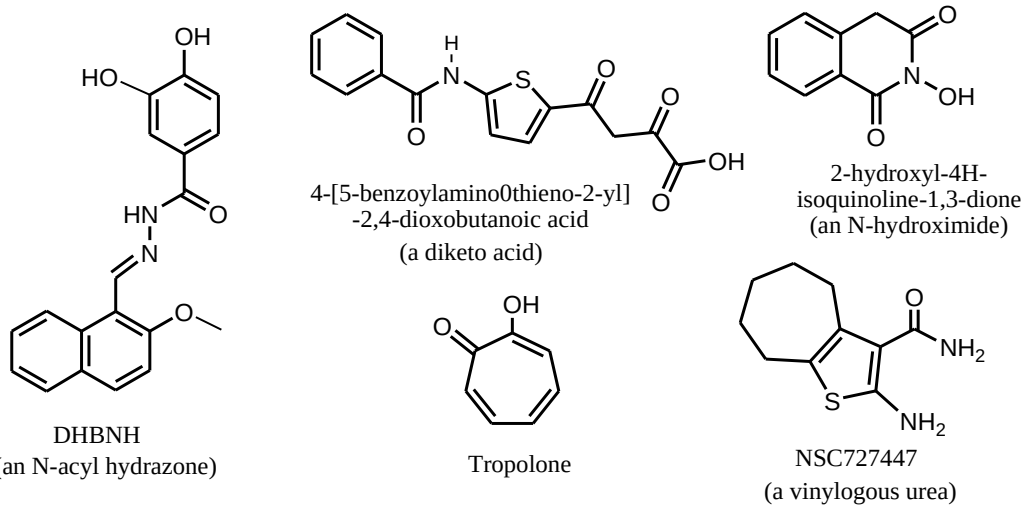

Figure 2.1. Classes of RNase H inhibitors. 1, N-acyl hydrazones; 2, diketo acids; 3, N-hydroxmides; 4, tropolones; 5, vinylogous ureas.

aptamer Macugen® for the treatment of wet age-related macular degeneration.[155,156] SELEX has also been utilized to generate aptamers that inhibit HIV RT with high binding affinity (K_d in nM range).[152,257-262] Aptamers targeting the RNase H domain have also been generated, demonstrating good potency in cell culture,[263,264] but this potency may be due partly to inhibition of polymerase activity.

2.1.3 Modified nucleic acid hairpins to target RNase H activity and probe binding requirements

Our group reported that short nucleic acid hairpins interfere with the function of RT-associated RNase H without affecting the DNA polymerase activity (Figure 2.2). Specifically, short hairpins (4 base pairs)[231,232] and dumbbells (8-10 base pairs)[231] effectively inhibited the RNase H activity of HIV-1 RT with IC_{50} values in the low micromolar range. Although the folded (hairpin) architecture of these compounds made them somewhat resistant to degradation by ubiquitous cellular nucleases, application of these (and antisense and siRNA) compounds *in vivo* and their possible use as therapeutics face some key hurdles such as delivery, cellular uptake and enhanced biostability.

These shortcomings can in principle be addressed through chemical modification of the sugar-phosphate backbone, thus generating nucleic acid analogues with improved properties over the native nucleotides. Indeed, several nucleic acid analogues such as DNA or RNA phosphorothioates,[265] 2',5'-linked RNA,[266] LNA,[176] 2'-OMe-RNA,[267,268]

2'F-RNA[174] and 2'F-arabinonucleic acids (2'F-ANA)[269] have been examined as a means to improve the biostability of antisense and siRNA oligonucleotides. The attraction of some of these modifications derives from their ability to simultaneously increase the strength of a hybrid and resistance to nucleases. For these reasons, we hypothesized that these modifications would also improve the efficiency of hairpin molecules directed against HIV-1 RT RNase H.

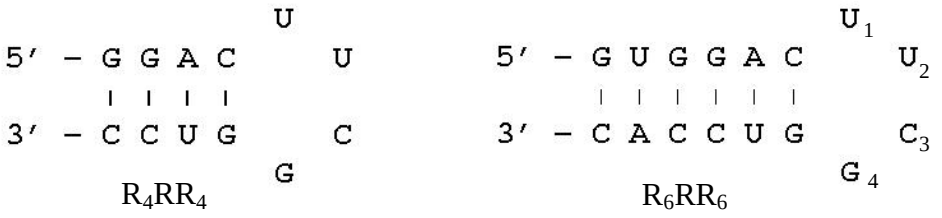

Figure 2.2. Native hairpins R_4RR_4 (right) and R_6RR_6 (left). The residues in the loop are designated U_1-U_2-C_3-G_4 from 5' to 3' as depicted on R_6RR_6.

Previous work in the Damha lab suggested that the hairpins may bind selectively to the RNase H domain, a rather peculiar finding since most of the contacts between HIV-1 RT and its RNA•DNA hybrid substrate lie outside the RNase H domain.[270,271] The discovery of nucleic acids that do indeed selectively bind to RNase H would greatly aid our understanding of how the virus recognizes different substrates to carry out its functions.[225,272] As a result, we undertook footprinting and protein-nucleic acid cross-linking experiments to determine the mode by which these hairpins bind to reverse transcriptase.[273,274] We demonstrate that RNA hairpins can perturb only the contacts in the RNase H domain and, consequently, do not interfere with potency of a chain terminator such as AZT.

2.2 Results and Discussion

2.2.1 Design of Oligonucleotides

This section describes how we planned to improve the potency, thermostability and biostability of hairpins through chemical modifications. Since HIV-1 RT binds tightly to long nucleic acids, we will maintain the conservative size of the hairpins by incorporating helix geometries that show preferential binding to RNase H, such as the natural substrate RNA•DNA hybrid duplex.[67-69] Given that RNase H also has high

affinity towards nucleic acid duplexes with A-form helices over B-form helices,[275] we incorporated 2'F-RNA and LNA segments (and combinations of these) in the stem and loop regions of hairpins, as these modifications preserve key structural features of the native ribonucleotides (North or C3'-*endo* sugar pucker) (Figure 2.3). In addition, 2'F-RNA and LNA modifications are known to enhance nuclease resistance and the overall thermodynamic stability of RNA duplexes. Therefore, hairpins containing these two modifications were prepared and these are listed in Table 2.1 (hairpins X-6, X-8, X-17, X-17-C, X-18, X-18-C, X-20, X-20-C, Si-12).

Since the eventual destination of our compounds would be inside a cell, other modifications that enhance biostability and bioavailability were contemplated. Among those considered were 2',5'-internucleotide linkages, 2'-deoxy-2'-fluoroarabinonucleotide (2'F-ANA), "reversed dT" (3'3'dT) and cholesterol units (Figure 2.3). When conjugated at the 5'- or 3'-termini of an oligonucleotide, the cholesterol (chol) moiety has the added advantage of potentially enhancing cellular uptake.[276,277]

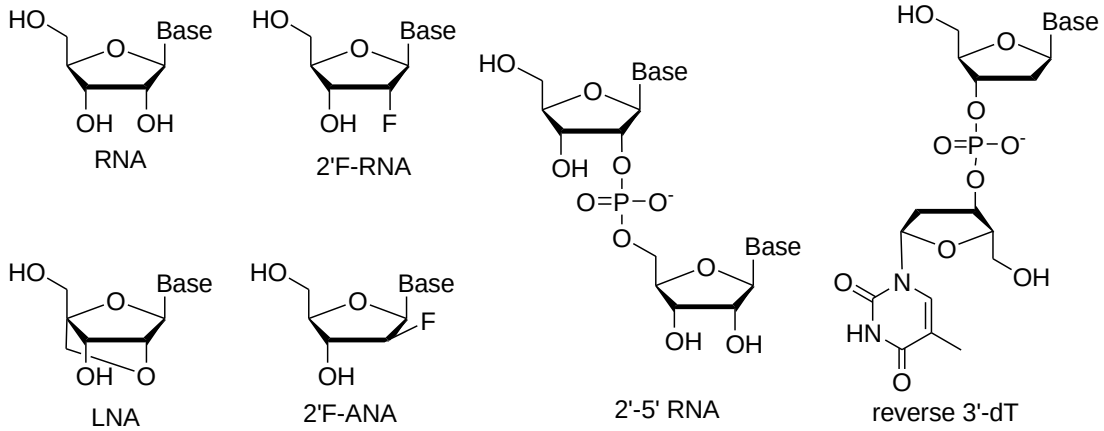

Figure 2.3. Chemical modifications employed in this study.

As there is evidence that longer nucleic acids are more potent inhibitors of HIV-1 RT's RNase H than shorter ones,[231,266] we also synthesized hairpins with stem regions of varying length (1-4 base pairs; see Table 2.1). In order to ensure sufficient stability for the hairpins containing only 2 and 4 base pairs, we incorporated LNA residues at various positions within R_2RR_2 and R_4RR_4 (Table 2.2).

The loop sequence selected for our initial studies was the known tetraloop UUCG, which displays extrastability by virture of very specific hydrogen bonding and

stacking interactions within the loop. As described in the Introduction (Chapter 1), the first U_1 residue in the rUUCG loop adopts a northern sugar pucker and it hydrogen bonds to the G_4 residue forming a U•G *wobble* base pair; these two nucleotides also hydrogen bond via the uridine 2'OH (rU) and the guanine lactam's O6 atom. Furthermore the third C residue in the loop stacks with the G•U *wobble* pair further contributing to the overall "extra" stability of the hairpin loop.[26,28]

Table 2.1. Hairpins screened for inhibition against HIV-1 RT RNase H activity.

Entry	Code	Sequence	IC_{50} (μM)	T_m (°C)
1	R_6RR_6	5'- GUGGAC UUCG GUCCAC - 3'	> 50	83
2	R_4RR_4	5'- GGAC UUCG GUCC - 3'	> 50	73
3	R_3RR_3	5'- GAC UUCG GUC - 3'	> 50	59
4	R_2RR_2	5'- AC UUCG GU – 3'	> 50	32
5	R_1RR_1	5'- C UUCG G - 3'	> 50	16
6	X-4	5'- GGAC UUCG GUCC - 3'3'dT	> 50	75
7	X-5	5'- GGA***C*** UUCG G***UCC*** - 3'3'dT	> 50	87
8	X-6	5'- GGA***C U***UCG G***UCC*** - 3'3'dT	37	80
9	X-7	5'- GUCAGUGGAC UUCG GUCCACUGAC - 3'3'dT	2.1	nd
10	X-8	5'- GGA***C UUC***G G***UCC*** - 3'3'dT	> 50	74
11	X-10	5'- GUGGAC UUCG GUCCAC - 3'3'dT	15	81
12	X-10-C	chol - 5'- GUGGAC UUCG GUCCAC - 3'3'dT	0.18	85
13	X-11	5'- GUGGAC <u>UUCG</u> GUCCAC - 3'3'dT	19	nd
14	X-11-C	chol - 5'- GUGGAC UUCG GUCCAC - 3'3'dT	0.2	nd
15	X-12	5'- <u>GUGGAC</u> <u>UUCG</u> gtccac - 3'3'dT	36	nd
16	X-13	5'- <u>GUGGAC</u> <u>UUCG</u> *gtccac* - 3'3'dT	32	60
17	X-13-C	chol - 5'- <u>GUGGAC</u> <u>UUCG</u> *gtccac* - 3'3'dT	17	81
18	X-14	5'- *gtggac* UUCG *gtccac* - 3'3'dT	32	84
19	X-14-C	chol - 5'- *gtggac* UUCG *gtccac* - 3'3'dT	1.5	> 95
20	X-15	5'- *GUGGAC* UUCG *GUCCAC* - 3'3'dT	nd	> 95
21	X-17	5'- GUGGAC ***T***UCG GUCCAC - 3'3'dT	20	80
22	X-17-C	chol - 5'- GUGGAC ***T***UCG GUCCAC - 3'3'dT	0.73	85
23	X-18	5'- GUGGAC **T**UCG GUCCAC - 3'3'dT	21	81
24	X-19	5'- gtggac UUCG gtccac - 3'	> 50	64
25	X-19-C	chol - 5'- gtggac UUCG gtccac - 3'	nd	72
26	X-20	5'- *gtggac* ***U***UCG *gtccac* - 3'3'dT	35	81
27	X-20-C	chol - 5'- *gtggac U*UCG *gtccac* - 3'3'dT	0.3	> 95
28	X-21	5'- GAUCAC UUCG GCCUGG - 3'3'dT	32	30
29	X-22	5'- **GATCAC TTCG GCCTGG** - 3'3'dT	>50	inc

Legend: UPPER CASE, RNA; lower case, DNA; <u>UNDERLINE,</u> 2'-5' linked RNA; **BOLD,** LNA; *italic lower case,* 2'F-ANA; ***BOLD ITALIC***, 2'F-RNA; 3'3'dT, 3' reversed dT; chol, 5'- cholesterol. IC_{50}s were calculated as described in the Methods section. T_m values are an average of at least three runs with standard deviation within +/- 1 °C. nd = not determined. inc = inconclusive.

The natural 3',5'-linked rUUCG loop has been shown to be a key structural motif for enhancing the potency of the nucleic acid hairpins.[232] The unnatural 2',5'-linked $rU_1U_2C_3G_4$ RNA loop is also highly stabilizing, and also undergoes (a) U_1•G_4 *wobble* base pairing, with both nucleotide residues in the anti-conformation, (b) extensive base stacking, and (c) sugar-base and sugar-sugar contacts, all of which contribute to the extra stability of this hairpin loop structure.[278] While replacement of the native 3',5'-rUUCG loop of RNA hairpins with a 2',5'-linked rUUCG loop is known to decrease potency of RNA hairpins against RT RNase H, the 2',5'-loop confers superior nuclease resistance compared to the 3',5'- rUUCG loop.[232] Therefore, we also synthesized a series of hairpins containing the 2',5'-rUUCG loop (X-11, X-12, X-15, X-16 and X-17; Table 2.1).

Table 2.2. Short LNA hairpins screened for inhibition against HIV-1 RT RNase H activity.

Entry	Code	Sequence	IC_{50} (μM)	T_m (°C)
1	R_4RR_4	5'- GGAC UUCG GUCC - 3'	> 50	73
2	R_2RR_2	5'- AC UUCG GU – 3'	> 50	32
3	Si-01	5'- A**C** UUCG G**U** - 3'	> 50	78
4	Si-02	5'- **A**C UUCG G**U** - 3'	> 50	66
5	Si-03	5'- **AC** UUCG **GU** - 3'	> 50	inc
6	Si-04	5'- **AC U**UCG **GU** - 3'	> 50	inc
7	Si-05	5'- **AC U**UC**G GU** - 3'	> 50	inc
8	Si-06	5'- AC **U**UC**G** GU - 3'	> 50	inc
9	Si-07	5'- **C** UUCG **G** - 3'	> 50	inc
10	Si-08	5'- **C U**UC**G G** - 3'	> 50	inc
11	Si-09	5'- **AC** UUCG GU - 3'	> 50	64
12	Si-10	5'- AC UUCG **GU** - 3'	> 50	inc
13	Si-11	5'- AC UUCG G**U** - 3'	> 50	55
14	Si-12	5'- GGAC **U**UCG GUCC - 3'	> 50	73
15	Si-13	5'- GGAC **U**UC**G** GUCC - 3'	> 50	69
16	Si-14	5'- GGAC UUC**G** GUCC - 3'	> 50	68

Legend: UPPER CASE, RNA; **BOLD,** LNA. IC_{50}s were calculated as described in the Methods section. T_m values are an average of at least three runs with standard deviation within +/- 1 °C. inc = inconclusive.

Finally, in order to thoroughly investigate the sequence dependence of the stem region on hairpin potency, a library of 64 hairpins based on X-4 (Table 2.1) with every possible permutation on the first three nucleotides was prepared (Table 2.3).

The physicochemical properties and inhibitory potency of these compounds towards HIV-1 RT RNase H are described in the following sections.

Table 2.3. Library of 64 hairpins screened for their anti-HIV-1 RT RNase H (RNH) potency.

CODE	Sequence [a]										% RNase H activity[b]
L1-53	U	A	G	C	UUCG	G	C	U	A	3'-3'dT	33
L1-37	C	A	G	C	UUCG	G	C	U	G	3'-3'dT	34
L1-24	G	U	G	C	UUCG	G	C	A	C	3'-3'dT	39
L1-61	U	A	U	C	UUCG	G	A	U	A	3'-3'dT	41
L1-10	A	G	C	C	UUCG	G	G	C	U	3'-3'dT	48
L1-21	G	A	G	C	UUCG	G	C	U	C	3'-3'dT	52
L1-45	C	A	U	C	UUCG	G	A	U	G	3'-3'dT	53
L1-32	G	U	U	C	UUCG	G	A	A	C	3'-3'dT	54
L1-13	A	A	U	C	UUCG	G	A	U	U	3'-3'dT	54
L1-40	C	U	G	C	UUCG	G	C	A	G	3'-3'dT	54
L1-62	U	G	U	C	UUCG	G	A	C	A	3'-3'dT	55
L1-09	A	A	C	C	UUCG	G	G	U	U	3'-3'dT	55
L1-31	G	C	U	C	UUCG	G	A	G	C	3'-3'dT	56
L1-34	C	G	A	C	UUCG	G	U	C	G	3'-3'dT	58
L1-47	C	C	U	C	UUCG	G	A	G	G	3'-3'dT	58
L1-43	C	C	C	C	UUCG	G	G	G	G	3'-3'dT	58
L1-23	G	C	G	C	UUCG	G	C	G	C	3'-3'dT	59
L1-44	C	U	C	C	UUCG	G	G	A	G	3'-3'dT	60
L1-07	A	C	G	C	UUCG	G	C	G	U	3'-3'dT	60
L1-20	G	U	A	C	UUCG	G	U	A	C	3'-3'dT	61
L1-19	G	C	A	C	UUCG	G	U	G	C	3'-3'dT	61
L1-28	G	U	C	C	UUCG	G	G	A	C	3'-3'dT	61
L1-26	G	G	C	C	UUCG	G	G	C	C	3'-3'dT	61
L1-18	G	G	A	C	UUCG	G	U	C	C	3'-3'dT	62
L1-46	C	G	U	C	UUCG	G	A	C	G	3'-3'dT	62
L1-30	G	G	U	C	UUCG	G	A	C	C	3'-3'dT	62
L1-15	A	C	U	C	UUCG	G	A	G	U	3'-3'dT	62
L1-36	C	U	A	C	UUCG	G	U	A	G	3'-3'dT	62
L1-12	A	U	C	C	UUCG	G	G	A	U	3'-3'dT	64
L1-05	A	A	G	C	UUCG	G	C	U	U	3'-3'dT	64
L1-42	C	G	C	C	UUCG	G	G	C	G	3'-3'dT	64
L1-56	U	U	G	C	UUCG	G	C	A	A	3'-3'dT	64
L1-55	U	C	G	C	UUCG	G	C	G	A	3'-3'dT	64
L1-29	G	A	U	C	UUCG	G	A	U	C	3'-3'dT	64
L1-48	C	U	U	C	UUCG	G	A	A	G	3'-3'dT	64
L1-35	C	C	A	C	UUCG	G	U	G	G	3'-3'dT	64
L1-52	U	U	A	C	UUCG	G	U	A	A	3'-3'dT	65
L1-58	U	G	C	C	UUCG	G	G	C	A	3'-3'dT	65
L1-14	A	G	U	C	UUCG	G	A	C	U	3'-3'dT	65
L1-16	A	U	U	C	UUCG	G	A	A	U	3'-3'dT	65
L1-41	C	A	C	C	UUCG	G	G	U	G	3'-3'dT	65
L1-04	A	U	A	C	UUCG	G	U	A	U	3'-3'dT	66
L1-17	G	A	A	C	UUCG	G	U	U	C	3'-3'dT	66

L1-03	A	C	A	C	UUCG	G	U	G	U	3'-3'dT	66
L1-25	G	A	C	C	UUCG	G	G	U	C	3'-3'dT	67
L1-39	C	C	G	C	UUCG	G	C	G	G	3'-3'dT	67
L1-51	U	C	A	C	UUCG	G	U	G	A	3'-3'dT	67
L1-27	G	C	C	C	UUCG	G	G	G	C	3'-3'dT	68
L1-33	C	A	A	C	UUCG	G	U	U	G	3'-3'dT	68
L1-22	G	G	G	C	UUCG	G	C	C	C	3'-3'dT	68
L1-64	U	U	U	C	UUCG	G	A	A	A	3'-3'dT	68
L1-54	U	G	G	C	UUCG	G	C	C	A	3'-3'dT	69
L1-11	A	C	C	C	UUCG	G	G	G	U	3'-3'dT	70
L1-50	U	G	A	C	UUCG	G	U	C	A	3'-3'dT	70
L1-57	U	A	C	C	UUCG	G	G	U	A	3'-3'dT	71
L1-02	A	G	A	C	UUCG	G	U	C	U	3'-3'dT	71
L1-08	A	U	G	C	UUCG	G	C	A	U	3'-3'dT	72
L1-06	A	G	G	C	UUCG	G	C	C	U	3'-3'dT	73
L1-60	U	U	C	C	UUCG	G	G	A	A	3'-3'dT	73
L1-38	C	G	G	C	UUCG	G	C	C	G	3'-3'dT	73
L1-59	U	C	C	C	UUCG	G	G	G	A	3'-3'dT	76
L1-49	U	A	A	C	UUCG	G	U	U	A	3'-3'dT	76
L1-63	U	C	U	C	UUCG	G	A	G	A	3'-3'dT	77
L1-01	A	A	A	C	UUCG	G	U	U	U	3'-3'dT	79

[a]Variable residues are in black and fixed residues in grey. Hairpins are organized from most potent to least potent. [b] These values represent the average of two experiments run in duplicate at a single concentration of 100 μM. Hairpin L1-18 (shaded) is identical to X-04 (Table 2.1). Note that hairpins contain a reversed dT at the 3'-terminus (3'3'dT).

2.2.2 Structural/Stability study of hairpins (T_m/CD)

The thermal stabilities of the modified hairpins were verified through UV_{260} melting studies. Hairpins with longer stems showed higher melting temperature (T_m) values as expected (Table 2.1, $R_6RR_6 > R_4RR_4 > R3RR_3 > R_2RR_2 > R_1RR_1$). Also as expected, the replacement of ribonucleotides in the stem for 2'F-RNA residues (Table 2.1, X-4 vs. X-5; X-10 vs. X-15), LNA residues (Table 2.2, R_2RR_2 vs. Si-01, Si-02, Si-09 and Si-09) and 2'F-ANA residues (Table 2.1, X-10 vs. X-14) caused increases in thermal stability. These observations are likely the result of the increased rigidity of these modifications. In other words, the modified sugar rings are pre-organized in a way that is compatible with A-form (2'F-RNA and LNA) or AB-like duplex conformations (2'F-ANA) thereby lowering the entropic penalty that results when a single strand folds into a more ordered hairpin structure. Replacement of 2'F-rU or LNA-U for the first rU in the tetraloop, $\underline{U_1}$-U_2-C_3-G_4, did not affect thermal stability (compare X-17 and X-18 to X-10, Table 2.1; and Si-12 to R_4RR_4, Table 2.2). This is

expected given that sugar pucker remains unaltered by these substitutions (C3'-*endo*).[26,28,279] One may argue that the loss of the sugar 2'-hydroxyl in the first loop residue (rU), through 2'F-RNA (or LNA) insertions could lead to some destabilization.[279] As this was not the case, it is possible that loss of the 2'-OH:O6 hydrogen bonding is compensated by the conformationally more rigid 2'F-rU units which better conform to the well structured tetraloop. The only stem modification that demonstrated significant destabilizing effects compared to the native RNA and DNA structures was the 2'F-ANA·2'-5' RNA stem hairpin X-13 (Table 2.1). This is somewhat expected since 2'-5' RNA binds unfavorably with DNA,[280] and 2'F-ANA is a rigid mimic of DNA. Thus the 2'F-ANA segment may not readily alter its conformation to accommodate the complementary 2'-5' RNA strand.

It was also noted that adding a 3' reversed thymidine did not change the T_m drastically. The thermostability of cholesterol conjugates versus their non-cholesterol counterparts demonstrated significantly higher T_m values. The greatest increase was observed between hairpin X-13 and X-13-C (entries 16 vs 17; $\Delta T_m > 20°C$ increase). Previous work on oligonucleotides bearing cholesterol conjugations showed destabilization when placed at the terminus of one strand, but better mismatch discrimination and T_m increases up to 13°C were observed when the cholesterol unit was placed on the same end of both strands compared to unmodified controls.[281] The nature of this stabilization was attributed to hydrophobic interactions, which we believe is also responsible for the extra stability of the cholesterol hairpins in the present study.

Circular dichroism (CD) spectroscopy was used to qualitatively probe the helix geometry of nucleic acid duplexes to ascertain if a given helix has more "RNA character" (an A-form helix), "DNA character" (B-form helix), or an intermediate thereof (I-like or AB-like). CD profiles of RNA hairpins and hairpins containing RNA-like modifications in their stems display classic A-form helix CD profiles with a maximum peak around 260 nm (Figure 2.5A). Hairpins containing DNA and DNA-like modifications (X-19, Table 2.1**)** exhibited CD spectra of the classical B-form with a maximum peak at 280 nm that crosses the x-axis at 250 nm, as expected. All other hairpins, gave AB-like CD profiles with broad peaks at 270 nm and crossing the

x-axis at 245 nm. 2'F-ANA·2'-5' RNA stem hairpins (Table 2.1, X-13 and X-13-C)

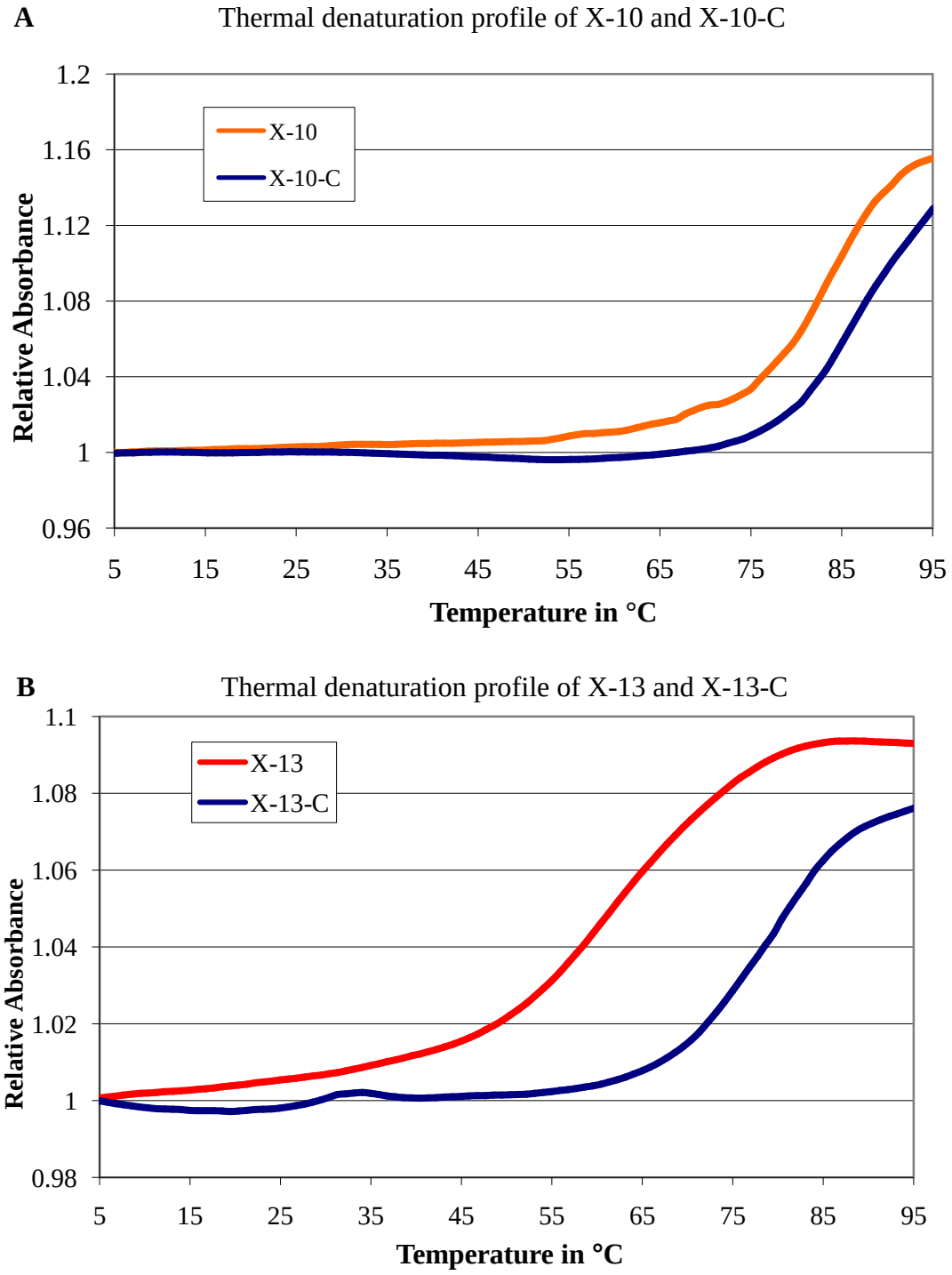

Figure 2.4. Representative thermal denaturation curves of nucleic acid hairpins monitored by UV_{260}. In both examples, the cholesterol increases the melting temperature. A) RNA hairpin X-10 and X-10-C. B) 2'-5' RNA/2'F-ANA stem hairpins X-13 and X-13-C.

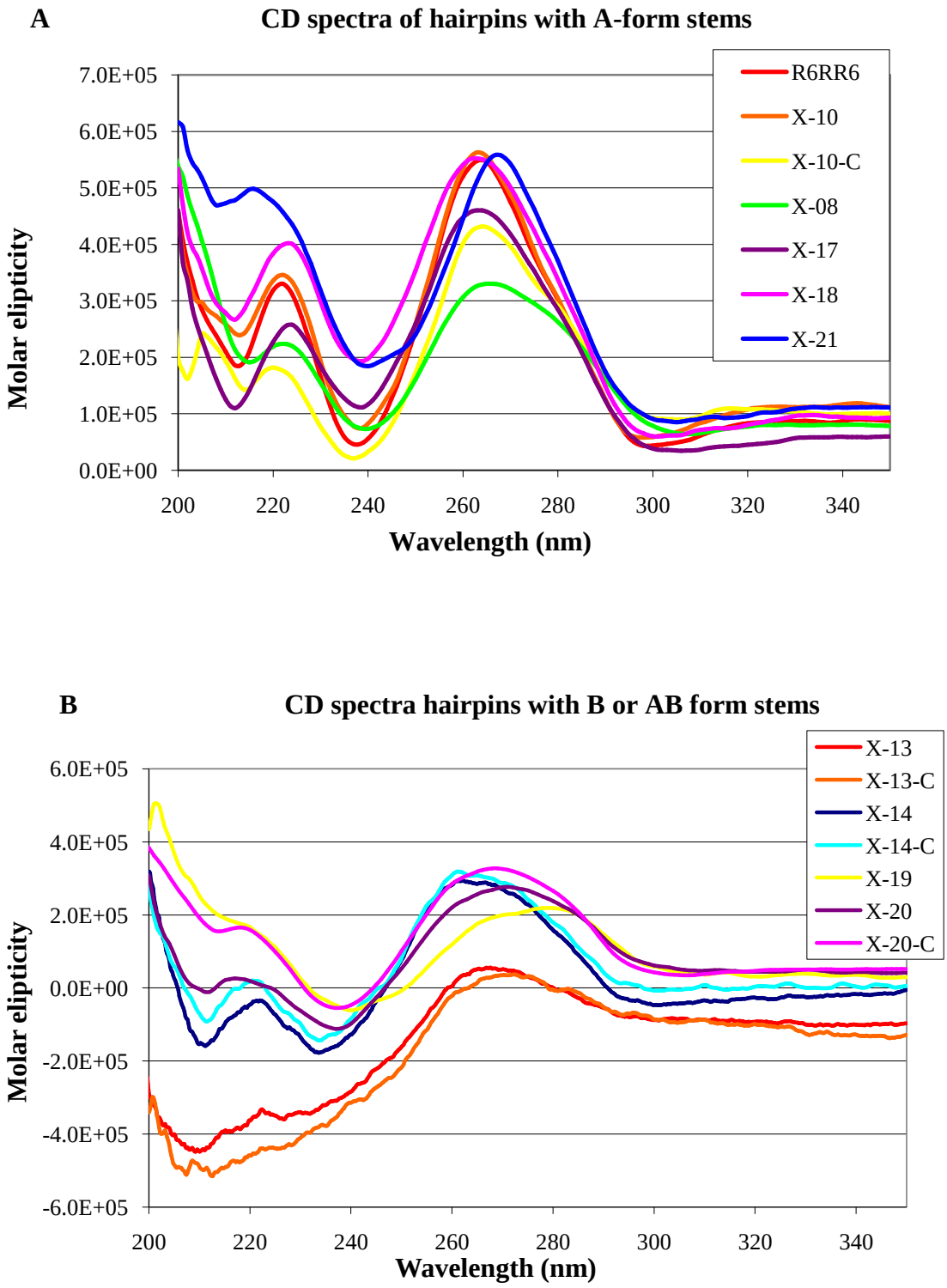

Figure 2.5. Circular dichroism spectra of hairpins with various modifications to the stem. A) Hairpins containing nucleic acids with A-form (RNA-like) helices in the stem. B) Hairpins containing nucleic acids with B-form (DNA-like) or AB-like (RNA•DNA hybrid like) helices in the stem.

gave CD spectra with a weak peak at 270 nm and crossed the x-axis at 280 and 260 nm, consistent with weaker binding between 2'-5' RNA and 2'F-ANA. In all instances, the cholesterol conjugated hairpins and their respective non-cholesterol variants gave CD spectra identical in shape suggesting that the cholesterol unit stabilizes the helices without altering the global conformation of the conjugated nucleic acid hairpin.

2.2.3 Serum stability assays

Chemically modified nucleosides were introduced to possibly increase resistance of hairpins to nucleases. Native hairpins and hairpins modified with reversed dT 3'-termini (such as X-10 and X-12) and unnatural 2'-5' linkages (such as X-12) were incubated in fetal bovine serum (FBS) to assess their stability to nucleases in biological media. The stability of the hairpins was compared to an 18-nucleotide long DNA single strand. Intact full-length hairpins were still present after 48 hours of incubation in serum, (Figure 2.6) whereas no full-length single-stranded DNA remained after 6 hours. This is primarily due to the hairpins being very short and double-stranded, two properties that already make the hairpins relatively nuclease resistant compared to linear oligonucleotide based therapeutics such as antisense DNAs and siRNAs.

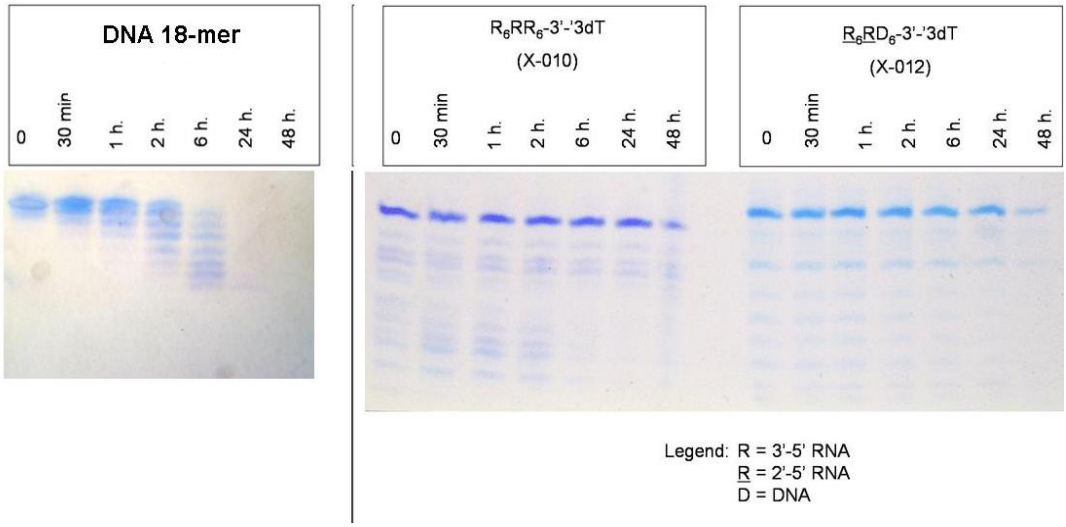

Figure 2.6. Denaturing PAGE of a nucleic acid serum stability assay in 10% FBS. An 18-nucleotide single-stranded DNA (5'-AGCTCCCAGGCTCAGATC-3') was used as a control against hairpins X-10 and X-12. Incubation times are indicated above corresponding wells. After 24 hours, all full length hairpins remain intact while none of the single-stranded DNA 18-mer remained.

2.2.4 HIV-1 RT RNase H inhibition assays

The potency of hairpins towards HIV-1 RT RNase H activity was tested using a gel-based method and a fluorescence-based method. The inhibitors were first screened using the former method as it required less material than fluorescent assays (Figure 2.7). From the preliminary screening, IC_{50} values of only the most potent inhibitors shown in Table 2.1 were determined under steady-state conditions in fluorescent assays (Figure 2.8). This assay incorporates a 3'-terminal fluorescein labeled RNA hybridized to a 5'-terminal DABCYL labeled DNA that quenches the fluorescent signal.[251] Upon RNase H treatment, the 3'-terminal fluorescein RNA is cleaved from the RNA•DNA hybrid and a concomitant increase in fluorescence emission is observed. We noted marked differences in absolute IC_{50} values from our previous reports,[231,232] and the assays employed in the current study. However, the relative RNase H potencies among different hairpins are consistent regardless of the testing method. We also compared the potency of the hairpin inhibitors to DHBNH (IC_{50} = 0.2 μM), a well characterized RNase H inhibitor we obtained from the lab of Dr. Michael A. Parniak from the University of Pittsburgh.[248] The most potent inhibitors, X-10-C and X-20-C, had comparable RNase H potency to DHBNH. We identified certain trends on the relationship between the structure of the hairpin inhibitors (Table 2.1-2.3) and their potency. These are depicted in Figure 2.9 and are summarized as follows.

Sequence modifications: The 64 hairpin library with varying stem sequences was tested for RNase H inhibition in fluorescent assays, the results of which are summarized in Table 2.3. The loop closing base pair was kept as G•C because it has been shown to be important to thermostability.[232,282] The most potent inhibitor from this mini-library, L1-53, was 2-fold more potent than the hairpin containing the original sequence, L1-18. Testing the four most potent hairpins from the screen and L1-18 in a dose-dependent manner showed potencies above 50 μM. There does not appear to be any clear trends on the relationship between sequence and RNase H potency (Table 2.2). However, we noted that seven out of the ten least potent hairpins are A-U rich.

Modifications to the stem: Stem composition has a profound effect on potency. Hairpins with longer stem lengths are more potent inhibitors. The hairpins tested with the same helix geometry but with varying length can be placed in order of increasing potency as follows (subscript in the name denotes stem length); X-07 (10 bp stem)> R_6RR_6 > R_4RR_4 > R_3RR_3 > R_2RR_2 > R_1RR_1 (Table 2.1). Helix geometry is another property of the stem that was probed through sugar modifications. Hairpins with stems that adopt A-form helix geometry generally are more potent. Stems containing 2'F-ANA inserts, which assume AB-form helices, showed reduced potency compared to RNA stems (Table 2.1, X-14), but better potency than the corresponding DNA hairpin (Table 2.1, X-19). This can be explained from the perspective of the 2'F-ANA•2'F-ANA stem mimicking the helix geometry of the natural RNA•DNA substrate, as suggested by CD spectroscopy (Figure 2.5). Overall, the most potent hairpins were those possessing RNA, and modifications that mimic RNA, consistent with previous studies by our group.[231,232]

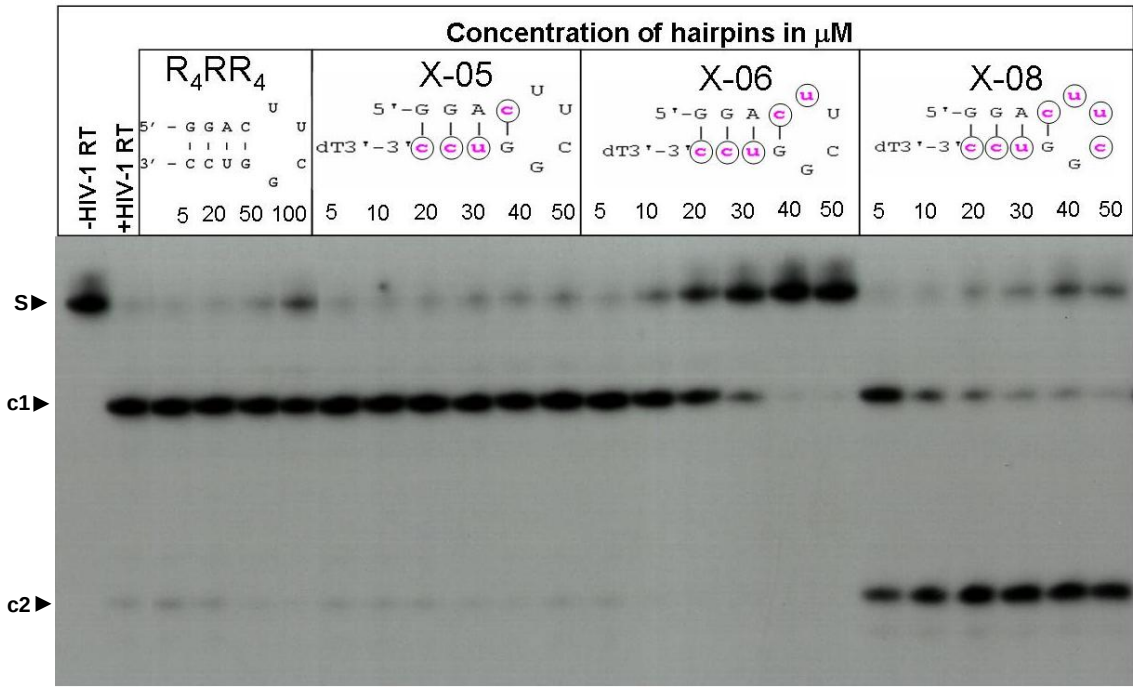

Figure 2.7. Example of a gel-based assay used to evaluate the inhibitory potency of various RNA hairpin inhibitors towards the polymerase independent RNase H activity of HIV-1 RT. Circled residues indicate 2'F-RNA insertions. Note the change in cleavage pattern by X-08. Arrowheads indicate the substrate (**s**), first cleavage product (**c1**) and second cleavage product (**c2**).

Termini modifications: Modifications on the 3' terminus of hairpins with a reversed dT gave surprisingly greater potency for all hairpins. For example, X-10 is over three times more potent than R_6RR_6 (**Table 2.1**, entry 11 vs. 1). This is remarkable given that the only difference is a terminal 3'-3'-linked dT unit. Although these results are difficult to explain, we note that RNase H activity of HIV-1 RT can be influenced by positioning to different ends of the primer-template.[77] It is not clear if RT can recognize the presence of two 5'-termini in light of the 3'-3' linkage, or that it binds better to the RNA-DNA junction, or simply that the extra nucleotide places itself in a binding pocket.

Conjugation of cholesterol to the 5'-end of hairpins also had a profound effect on inhibitory potency towards RNase H. All hairpins with cholesterol conjugates were better inhibitors than their non-cholesterol counterparts. Adding a cholesterol on the 5'-end increased the potency by 20-100 fold. The most potent of all hairpins tested are the cholesterol containing hairpins X-10-C (RNA duplex) and X-20-C (2'F-ANA duplex), with IC_{50} values of 0.18 μM and 0.30 μM, respectively. It is unlikely that these effects are due to the cholesterol moiety alone since RNase H activity was unchanged in the presence of saturating concentrations of cholesterol (2 μM). In addition, RNA•DNA hybrids bearing 3' terminal cholesterol conjugations have previously indicated no change in RNase H activity.[283]

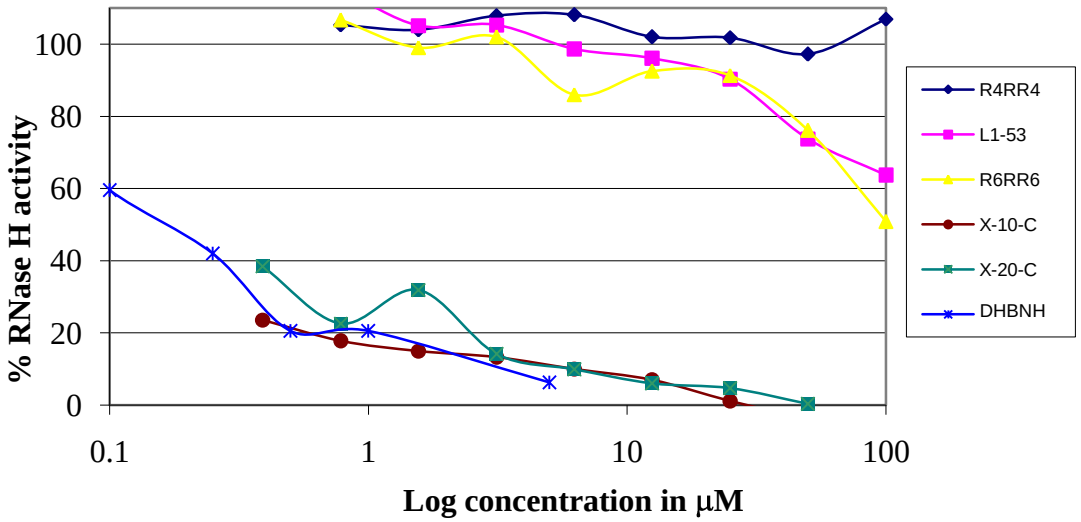

Figure 2.8. Results from a fluorescent RNase H assay. The blue curve represents the inhibition profile of the control RNase H inhibitor DHBNH.

Loop modifications: Replacement of the U1 loop residue with 2'F-rU led to an increase in potency. This trend was observed in two instances (Table 2.1), when comparing hairpin X-5 with X-6 (> 2 fold increase) and X-14-C and X-20-C (5 fold increase). If three 2'F-rN units are incorporated in the tetraloop (U1, U2, and C3), both T_m value and potency of the hairpin are compromised (X-8 vs. X-6, Table 2.1) and a different RNase H cleavage pattern is observed (Figure 2.7). At lower concentrations of X-8 (10-20 μM, Figure 2.7), the proportion of 10-mer to 14-mer cleavage products increases in a concentration dependant manner. Only after observing this change in cleavage pattern does inhibition appear. The reason for this interesting phenomenon is unclear. It does not seem to be related to the changes in the helix geometry of the stem as CD spectra showed no significant changes in helix structure from unmodified controls. Changes in RNase H cleavage patterns have been observed in other instances, notably with NNRTI binding [96] or with modifying the substrate for base-modified nucleotides.[284]

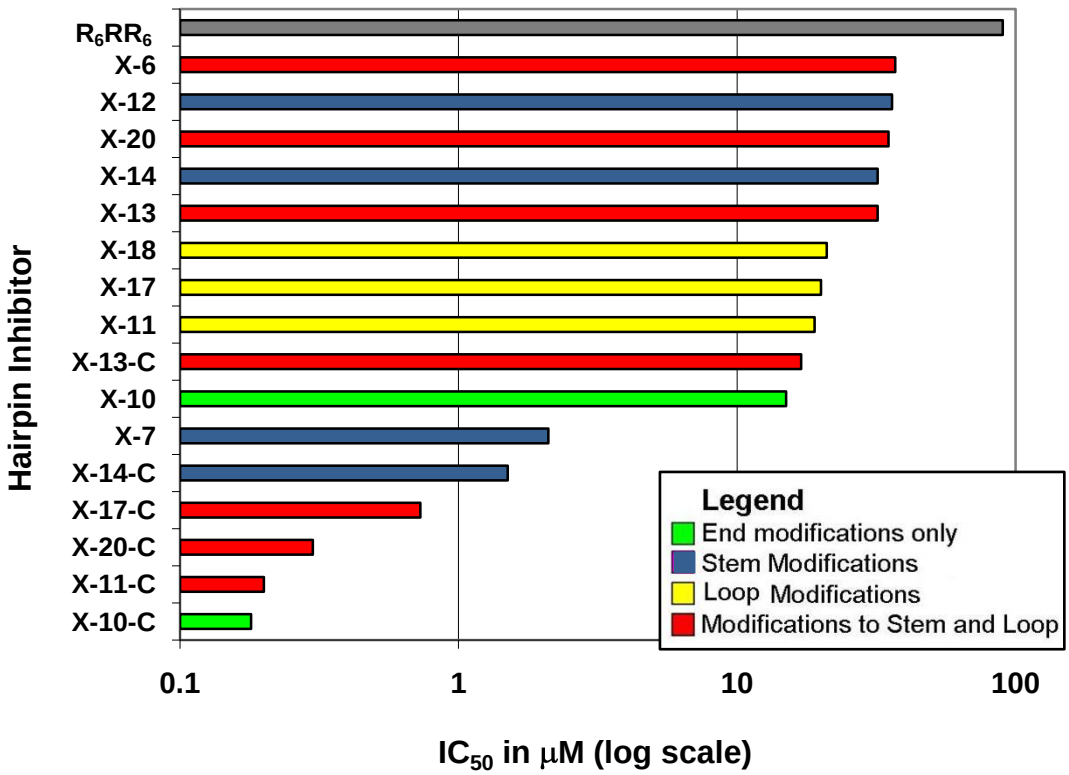

Figure 2.9. Graphical representation of the potency towards HIV-1 RNase H activity and the nature of the chemical modifications on nucleic acid hairpins. The unmodified RNA hairpin R_6RR_6 is indicated with a grey bar. All other hairpins were modified with at least a terminal 3'3'-linked dT unit.

2.2.5 Mechanistic studies using site-specific footprints

The following site-specific footprinting studies were designed to provide mechanistic information on the RT-substrate binary complex in the presence of hairpins. In traditional footprinting experiments, hydroxyl radicals destroy the nucleic acids that are exposed to solvent leaving the protected portion bound by a nucleic acid binding protein intact. Iron and peroxynitrite mediated footprints on HIV-1 RT work by producing site-specific cuts on the template strand of the nucleic acid substrate.[274] The peroxynitrite-mediated method uses the thiol group on cysteine 280 in the thumb domain of HIV-1 RT to generate a sulphur radical that cuts the template 8 residues upstream from the nucleotide binding site (Figure 2.10A). The iron-mediated method introduces Fe^{2+} in the divalent cation binding site in the RNase H domain of HIV-1 RT, located 18 nucleotides away from the nucleotide binding site.[273] At low concentrations of iron, the generation of hydroxyl radicals is localized only at the RNase H domain (Figure 2.10B). Both methods rely on the template being in close proximity to the site where the hydroxyl radicals are generated and thus the presence of a footprint indicates that the substrate is binding at these specific locations on HIV-

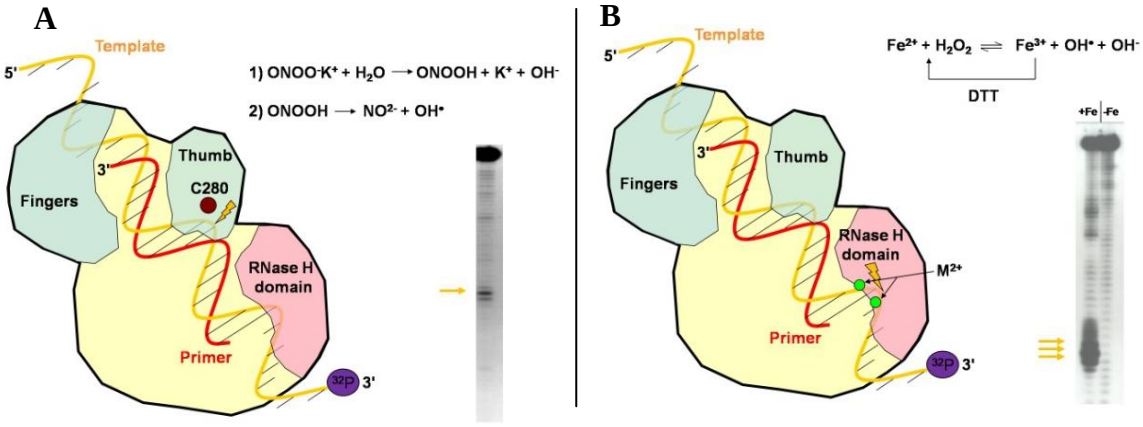

Figure 2.10. Depiction of the location and conditions used to obtain site-specific footprints. Footprints are generated by cuts (orange lightning) on the 3'-^{32}P-radiolabeled template strand (orange strand, 57-nt long) duplexed to a DNA primer (red strand 20-nt long). The polymerase active site is between the fingers and the thumb subdomains (cyan). A. Peroxynitrite-mediated footprinting forms a thiol radical at cysteine 280 in the thumb domain (red circle). A denaturing PAGE showing the footprint is depicted at the right (orange arrow). B. The iron-mediated footprints are obtained by Fe^{2+} binding to the divalent cation binding site (green circles) in the RNase H domain (magenta). A denaturing PAGE showing the footprint is depicted at the right (orange arrows).

1 RT. Using these methods, we verified if the hairpins could disrupt these nucleic acid-protein interactions by the disappearance of the footprints.

The primer-template used in these studies is derived from the viral polypurine tract. This region is resistant to RNase H degradation and is necessary for + strand initiation in the viral life cycle. This property enabled us to study the interactions of hairpins with both RNA•DNA and DNA•DNA primer-template RT substrates. Both footprints showed different levels of attenuation in the presence of hairpins (Figure 2.11). None of the hairpins tested disturbed the peroxynitrite-generated footprint up to 100 μM. In contrast, even hairpins that inhibit RNase H activity weakly were able to show concentration dependant disruption of the footprint generated at the RNase H domain when using the iron method. The relative attenuation of the disruption of the Fe^{2+}-mediated footprint correlates with the potency of hairpins. R_4RR_4 had previously

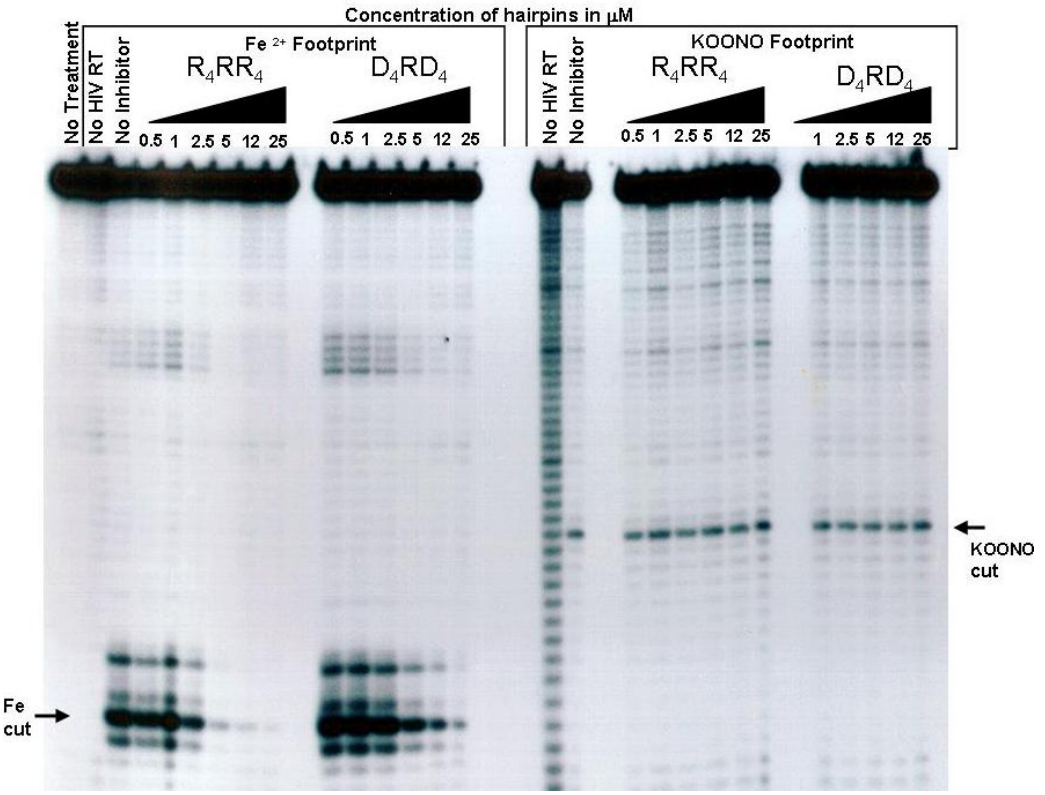

Figure 2.11. Denaturing gel of a site-specific footprinting assay using both methods on a modest (R_4RR_4) and a very weak (D_4RD_4) RNase H inhibitor. The iron-mediated footprints generated on the DNA template migrate faster, while KOONO mediated footprints migrate slower. Iron-mediated cuts are attenuated by the presence of hairpins while KOONO mediated cuts persist.

been shown to modestly inhibit RNase H activity, while its DNA stem derivative D_4RD_4 was shown to inhibit poorly[232] and the iron footprints correlate with this trend.

We verified how other hairpins of varying potency affect the iron-mediated footprints as illustrated in Figure 2.12. Second generation hairpins incorporating a terminal 3'3'-linked dT unit and incorporations of 2'F-RNA nucleotides also disrupted the iron footprint in correlation to their RNase H potency. A very long stemmed hairpin (X-07) completely abolished footprints at 5 μM while shorter hairpins showed complete removal of footprints at 25 μM. The only exception to this trend of footprint attenuation correlating to RNase H potency was with the cholesterol conjugated hairpins. Although they showed significantly greater RNase H inhibition in both gel-based and fluorescence assays, the attenuation to the footprint pattern was the same as that of their non-cholesterol containing variants.

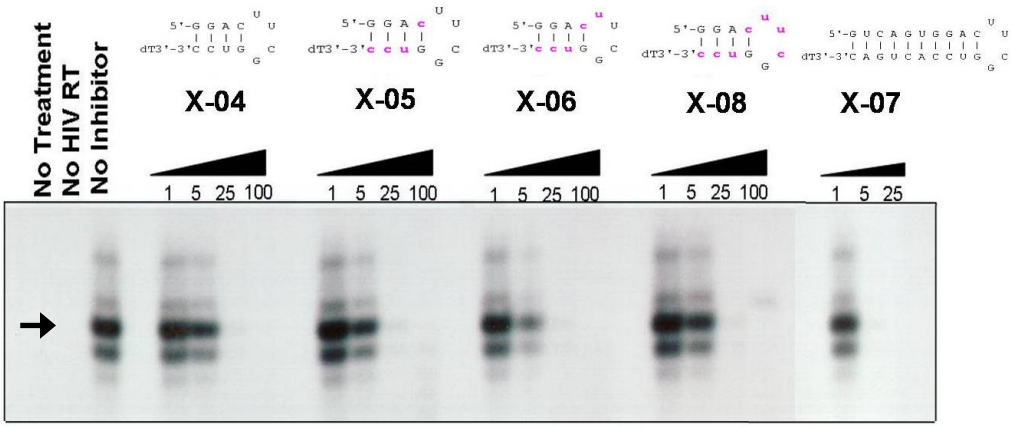

Figure 2.12. 8% denaturing PAGE analysis of iron-mediated site-specific footprint of HIV-1 RT (arrow) in the presence of different concentrations of hairpins. Hairpins that were best at attenuating footprints were also more potent towards HIV-1 RT RNase H activity. The concentration of hairpin in μM is indicated below the triangles.

Experiments where the double-stranded DNA substrate is replaced with an RNA·DNA PPT primer-template to more accurately mimic the complex formed during RNase H cleavage were performed. Footprints were attenuated to the same extent as with the DNA·DNA primer-template. However, the intensity of the footprint with the RNA·DNA primer template was less prominent than with a DNA•DNA substrate (Figure 2.12). We also tested whether the order of adding the substrate and hairpins to RT, or adding both simultaneously, affected the footprints with no changes

being observed. Experiments attempting to generate an iron footprint on a ^{32}P-labeled RNA hairpin inhibitor failed to generate any cuts. We cannot ascertain if this is because the hairpins are binding away from the RNase H domain, or the helical trajectory of the hairpin backbone is at an unfavorable distance from the Fe^{2+} cut site.

A secondary cut was also observed in the iron footprints. It had initially been assumed that these secondary cuts were due to sequence-specific cleavage from the free-radical induced Fe^{2+} reaction on the template or from Fe^{2+} ions binding in the Mg^{2+} binding pocket in the polymerase domain's active site. This may not be the case since it has been observed that RNA hairpin inhibitors are capable of suppressing this cut to the same extent as the major Fe footprint (Figure 2.11 and 2.13). Since there is an excess of HIV-1 RT relative to primer-template, we believe that a second enzyme binds to the substrate and an iron-mediated cut occurs also in this other RNase H active site, and thus is also suppressed by the hairpins.

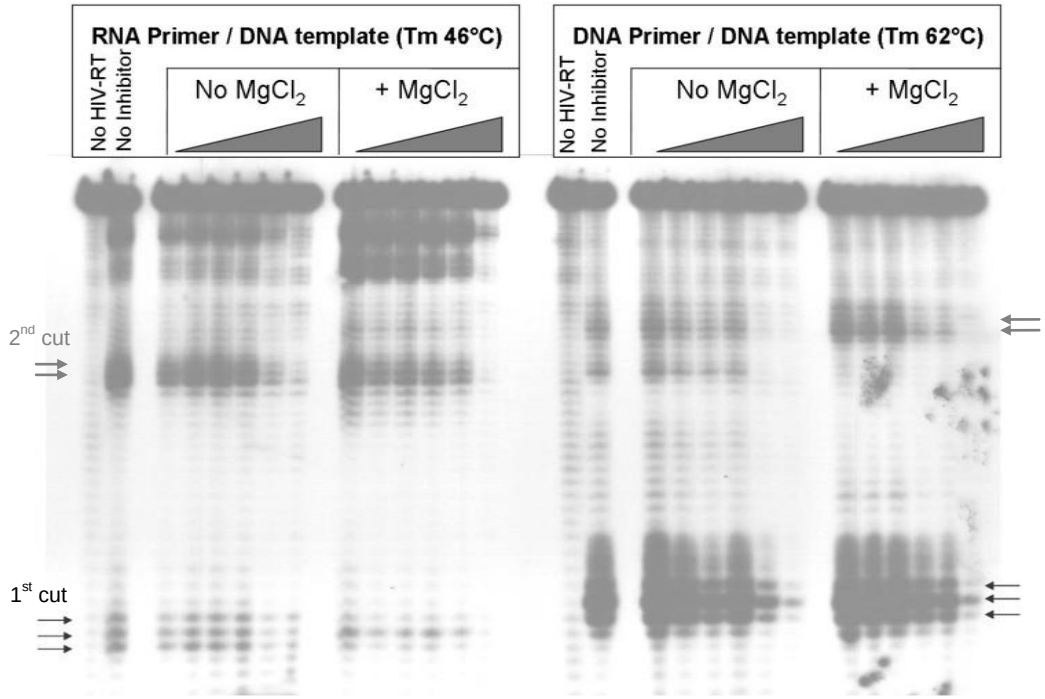

Figure 2.13. Comparison of iron-mediated site-specific footprints with an RNA primer and a DNA primer on a DNA template in the absence and presence of Mg^{2+} ions and increasing concentrations of hairpin X-10 (0.5, 1, 2.5, 5, 10 and 25 μM). Primary footprints are indicated by black arrows, and secondary footprints are indicated by grey arrows. The extent of the attenuation of the footprint is roughly the same regardless of the nature of the primer.

2.2.6 Strand transfer assays

It is a major challenge to develop compounds that block the RT-associated RNase H activity in a highly specific fashion without affecting the polymerase active center.[104] Such compounds, if found, could in principle be used in combination with existing NRTIs and/or NNRTIs in order to maximize synergistic effects. Unfortunately, compounds that inhibit the RNase H activity of HIV-1 RT in cell-free assays may also block the RT-associated polymerase activity, and, as a consequence, these compounds could diminish the beneficial effects of both classes of existing RT inhibitors. We thus probed the effects of the hairpins on the other steps of reverse transcription.

The strand transfer assay illustrated in Figure 2.14 follows several steps of reverse transcription including RNA-dependent DNA polymerase activity (RDDP), RNase H activity, removal of the remaining RNA template from the primer, binding of the acceptor DNA template to the primer and DNA-dependent DNA polymerase activity (DDDP). Figure 2.14 illustrates that increasing the concentration of RNA hairpin X-10 causes a build-up of the initial primer (P) and consequently the production of less final product (2). X-10 did not significantly affect the conversion of product (1) to product (2) as the ratio of these two remained approximately 3:1 until the highest concentration of hairpin was added (Figure 2.14, 60 μM). This suggests that X-10 inhibits the RDDP activity, but does not greatly disrupt DDDP activity. However, this does not necessarily indicate that the hairpins outcompete the DNA·RNA primer-template more than the DNA·DNA primer-template for the polymerase active. Work by others has shown that DNA·RNA hybrids bind tighter to HIV-1 RT than DNA·DNA primer-templates.[271] Furthermore, the site-specific footprinting experiments indicated that the primer-template is still bound to the polymerase active site in the presence of hairpins, suggesting they are not directly competing for this site. We also note that the reduced RDDP is not associated with increased pausing of polymerase activity, as none was detected (Figure 2.14). Recent single-molecule fluorescence studies demonstrated that RT can toggle between polymerase and RNase H binding modes with DNA·RNA primer-templates, but only assume a polymerase binding mode with DNA·DNA primer-templates.[225,272] A possible mechanism of

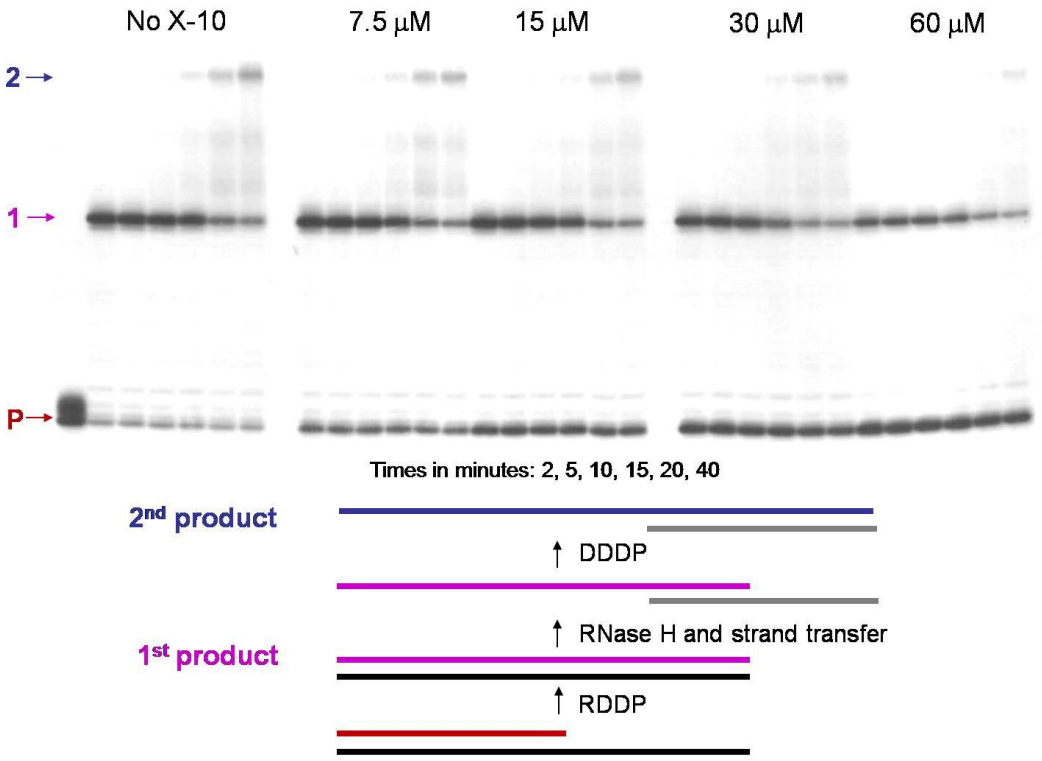

Figure 2.14. Strand transfer assay in the presence of increasing concentrations of hairpin X-10. The initial primer (indicated by a red **P** on the gel, red line in the scheme) is annealed to the RNA template (black in scheme). The first product from the RDDP activity (indicated by the violet **1** on the gel, violet line in scheme) a double-stranded RNA/DNA hybrid processed by the RNase H activity of RT. The primer is further elongated to the second product (indicated by the blue **2** on the gel, the blue line on the scheme) after successful strand transfer of the acceptor template.

inhibition where hairpin binding to RT favours the RNase H mode of binding with DNA·RNA hybrid primer-templates may exist.[225] In a separate experiment, we observed that the RNase H cleavage of the RNA template was not affected by 60 μM of X-10 and was inhibited by 50% with 60 μM X-10-C. This suggests that the hairpins may have different potencies for the various modes of HIV-1 RT RNase H activity (DNA 3'-end directed vs. RNA 5'-end directed vs. internal cleavage).

2.2.7 Polymerase activity and chain-termination assays

In order to further determine whether our RNase H hairpin inhibitors were directly affecting the DNA polymerase of HIV-1 RT, the effects on the DNA-dependent DNA polymerase reactions were tested with a 5'-^{32}P-DNA primer-DNA template duplex (Figure 2.15). We also tested if chain-termination by the anti-HIV drug 3'-azido-3'-deoxythymidine (AZT) is affected in the presence of our hairpin inhibitors. As shown

in Figure 2.15, hairpins lacking a 5'-cholesterol had no affect on both DDDP activity and chain termination up to 50 μM. In sharp contrast, cholesterol conjugated hairpins significantly compromised DNA polymerase activity. The most potent hairpins for RNase H activity, X-10-C and X-20-C, caused extensive inhibition of polymerase activity at 20 μM, and also reduced the rate of incorporation of AZT 5'-triphosphate. We postulate that the aggregation of 5'-cholesterol moieties may play a role in polymerase inhibition, discussed further in section 2.3.1. Therefore, it appears that cholesterol conjugation alters the selectivity of hairpin inhibitors from affecting only RNase H activity to also affecting polymerase activity. Although this was not the intention, we are thus presented with the challenge of tuning of the selectivity of cholesterol conjugated molecules.

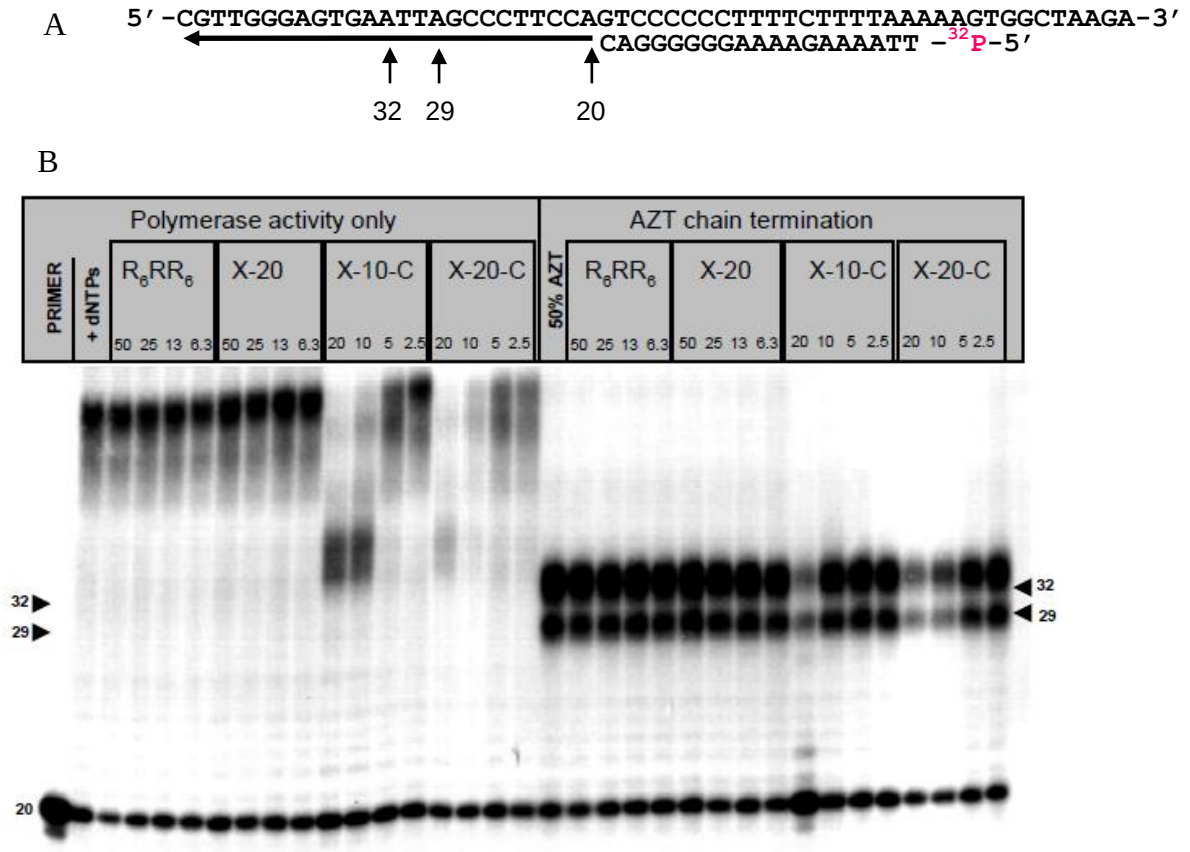

Figure 2.15. A. ^{32}P-labeled DNA primer and DNA template used for the primer extension assays. Arrows indicate residues where chain-termination was observed. B. Denaturing gel of primer-extension products in the presence of hairpins with and without AZT-chain termination.

2.2.8 UV Cross-linking experiments

To further confirm that the RNA hairpins were binding specifically to the RNase H domain of HIV-1 RT, and to help determine the exact location of binding, we conducted hairpin-RNase H cross-linking assays. In a typical cross-linking experiment, the protein is covalently attached to a nucleic acid of interest, the resulting protein-nucleic acid adduct degraded by proteases, and the peptide fragments generated are identified by mass spectrometry. In our assays, cross-links were initially obtained by irradiating various 5'-^{32}P-labeled hairpins or a control 17-nt dT homopolymer with UV_{260} light with either HIV-1 RT or an active isolated RNase H domain. Typically, the isolated RNase H domain of HIV-1 RT does not retain activity, but adding a basic containing loop from *E. coli* RNase H domain restores activity with Mn^{2+} ions.[72] Hairpins of 6-bp in the stem and the control dT 17-mer were successfully cross-linked to both the intact HIV-1 RT and the isolated RNase H domain (Figure 2.16 and 2.17). Shorter hairpins, such as those containing LNA in the stem (Si-02, S0-09, Si-10 and Si-13), did not cross-link to either enzyme. Based on the MW ladder, cross-links on HIV-1 RT appear to be on the p66 subunit, which is consistent with our previous observations.[231] Unfortunately, the yield of cross-linked to uncross-linked nucleic acid was extremely low, as observed by autoradiography, sufficient material could not be obtained for trypsin/MS analysis.

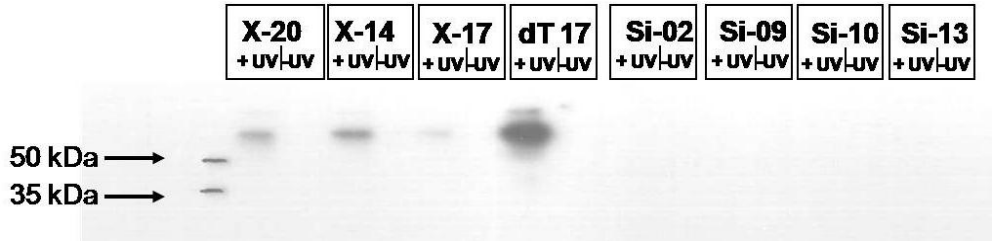

Figure 2.16. UV cross-linking of HIV-1 RT to hairpins using 260 nm light.

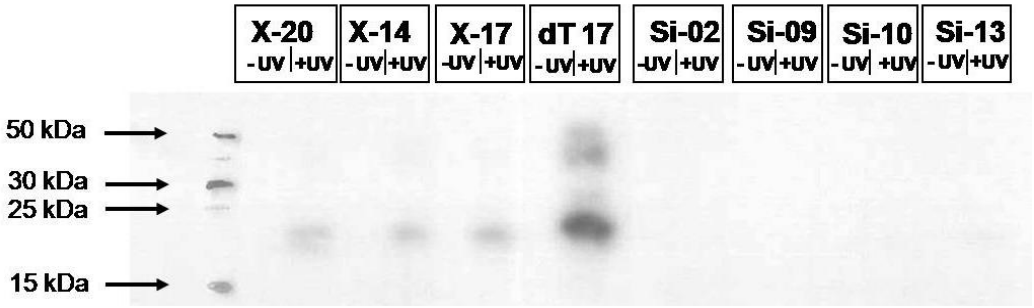

Figure 2.17. UV cross-linking of the isolated RNase H domain of HIV-1 RT to hairpins using 260 nm light.

With the aid of a phenyl azide photo-affinity label conjugated to the 5'-termini of the hairpin, we were able to obtain cross-links in higher yields. Under UV_{365} light, the phenyl azide turns into a reactive nitrene that can form covalent adducts with nucleophilic amino acid residues on the protein such as lysine.[285] Conjugating the hairpins with phenyl azide was easily achieved in aqueous buffer and in a site-specific manner by modifying one of the phosphodiester (PO) linkages into a more nucleophilic phosphorothioate (PS) (Figure 2.18). When both PO and PS linkages are present, only the latter reacts with *p*-azidophenacyl bromide[286] to generate the oligonucleotide alkylated with the photoreactive group at a defined position. Thus, we synthesized four hairpins derived from X-14 that contain the phenyl azide at different positions along the oligonucleotide backbone (Figure 2.18). This way, should the hairpin bind to its target in a specific orientation we hoped to generate cross-links on different parts of HIV-1 RT or the active isolated RNase H domain. Hairpin X-14

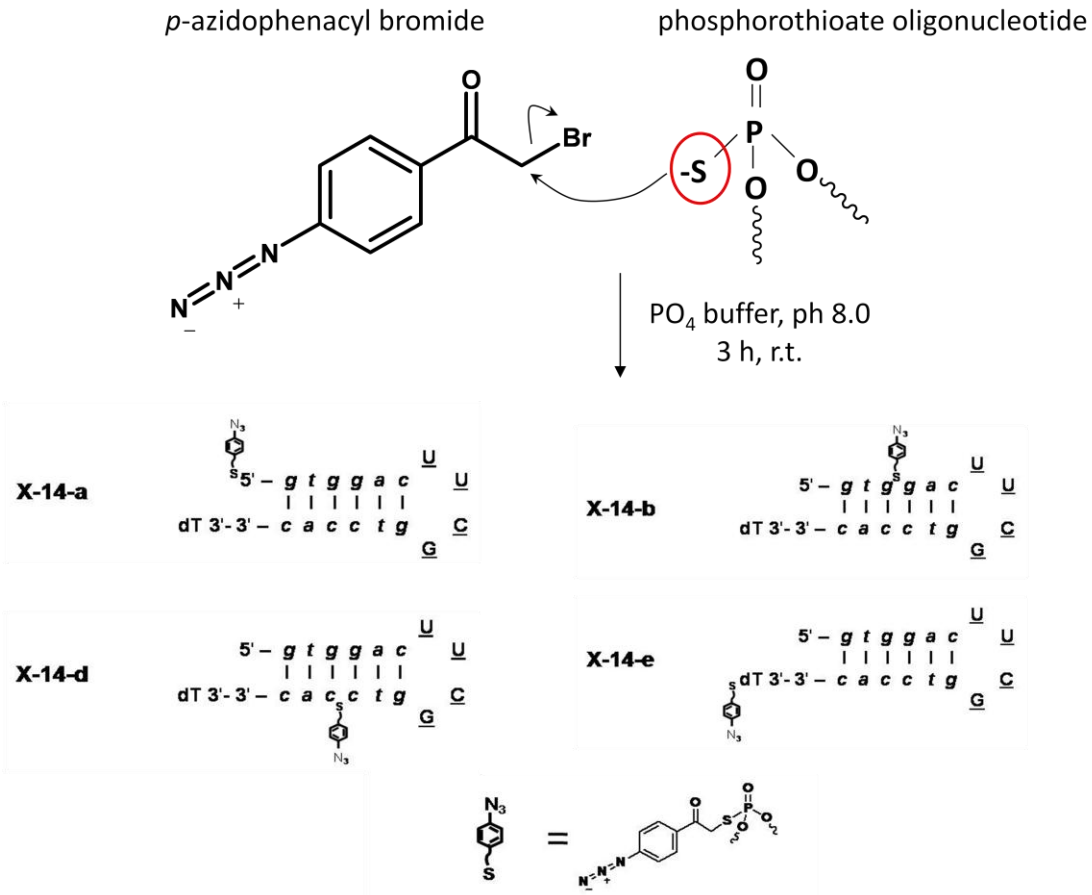

Figure 2.18. Synthesis of hairpins containing a photoreactive phenyl azide. Legend: lower case, DNA. underlined, 2'-5' RNA. *italics*, 2'F-ANA.

was a suitable candidate for alkylation with the phenyl azide because it showed good inhibition *in vitro*, generated the most cross-links without the aid of a photoreactive group, and contains a 2'F-ANA stem that lacks 2'-hydroxyl groups, thus leading to more stable phosphotriesters. This last point was confirmed by our inability to synthesize a variant of X-14 alkylated in the 2'-5' RNA loop of the hairpin, presumably due to 3'-OH mediated cleavage of the vicinal 2',5'-phosphotriester linkage. In this case, the products obtained after alkylation were that of a hairpin truncated at the site of the phosphotriester as confirmed by HPLC and MS. While a solution to this problem would be to introduce the 2'-O-Me or 2'-deoxyribose modification in the loop or the stem region, e.g. hairpins X-10 or X-17, these modifications severely impair the potency of RNA hairpins towards RNase H.[232]

The two hairpins with the photoreactive group at their termini, X-14-a and X-14-e, generated the highest yielding cross-links (50%) with the isolated RNase H domain as determined by SDS-PAGE and Coomasie blue staining (Figure 2.19). Variants of both X-14-a and X-14-e that were not alkylated with phenyl azide did not generate cross-links. No cross-links were detected when the photoreactive groups were placed in the stem region. In order to verify that cross-linking was specific to RNase H, we incubated X-14-a with either lysozyme or the homeodomain protein PBX under the same conditions. No higher molecular weight species which would signify the production of cross-links was detected. We next attempted to cross-link X-14-a and X-14-e to the intact HIV-1 RT enzyme (Figure 2.20). When HIV-1 RT and hairpins were mixed and allowed to react (1:40 enzyme/hairpin ratio), multiple cross-links were generated with both the p51 and p66 subunits. This would suggest that more than one point of contact and/or binding site exists for the RNA hairpins. We found it necessary to decrease the ratio of hairpin to protein by eight fold (i.e., 5:1) to resolve the major products and excise these bands for mass analysis. Based on four experiments, three slower moving bands appeared above the p66 band, (the middle band being the most abundant), and two slower moving bands above p51 (the lower band being most abundant). In general, X-14-e seemed to generate more cross-links than X-14-a (Figure 2.19 and 2.20).

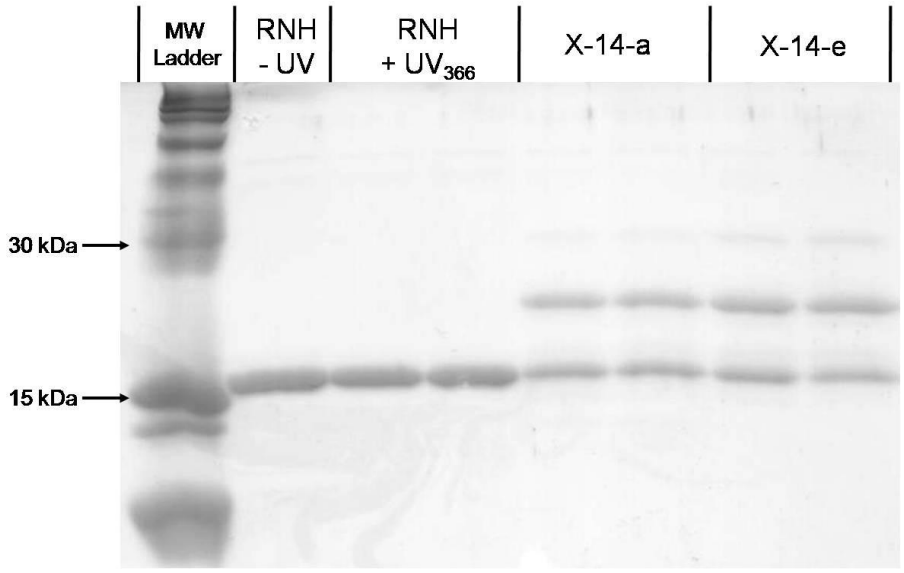

Figure 2.19. UV photo cross-linking of the isolated RNase H domain of HIV-1 RT to hairpins conjugated to a phenyl azide moiety under 366 nm light. The slower moving bands in lanes X-14-a and X-14-e correspond with the weight of the RNase H domain bound to the hairpin (16.6 kDa + 5.6 kDa = 22.2 kDa) according to the Rainbow™ MW marker.

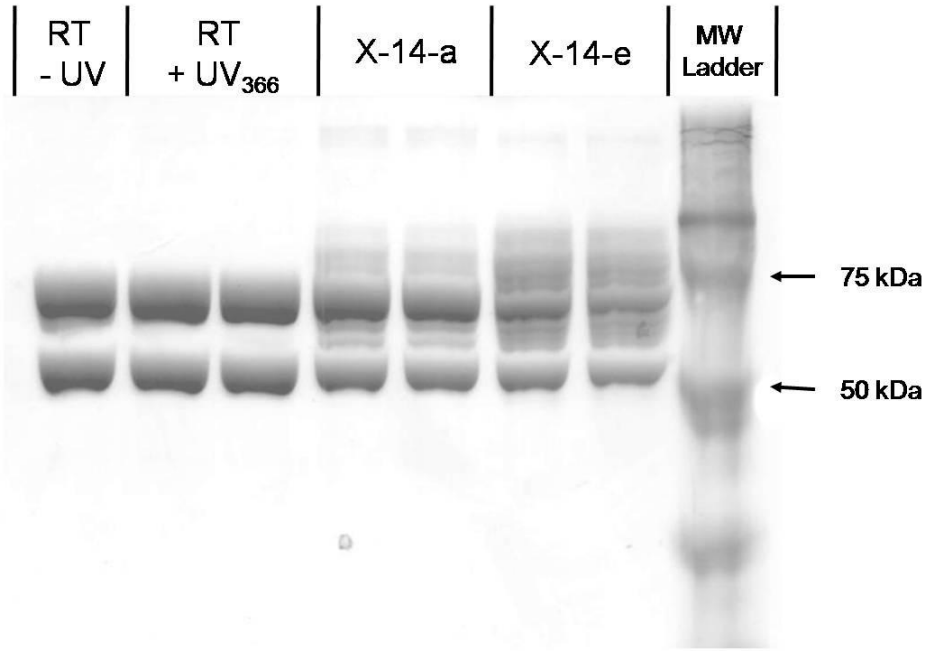

Figure 2.20. UV photo cross-linking of HIV-1 RT to hairpins conjugated with phenyl azide under 366 nm light. Multiple lower mobility bands appear above the unconjugated p51 and p66 domains. Based on the appearance of bands over 75 kDa mMW marker, it is assumed that two or more hairpins cross-linked to the p66 domain under these conditions (66 kDA+ 2 X 5.6 kDa = 77.2 kDa).

2.2.9 In-gel Digest and Mass Analysis

The HIV-1-RT-hairpin and RNase H-hairpin cross links were subjected to in-gel digestions by incubating the gel slices to a solution of trypsin or chymotrypsin for 16 hours at 37 ^{o}C. The peptide fragments were eluted from the gel by immersing the gels in acetonitrile. The mass of the eluted peptide fragments were determined by Maldi-Q/TOF MS. The only samples with peptides that corresponded with the simulated digests with peptidases were those containing the isolated RNase H domain treated with trypsin. Roughly 50% of the peptides from the simulated trypsin digest were observed by MS. We then compared the trypsin digest of the unmodified RNase H domain with the cross-linked samples. In the cross-linked samples, the most abundant fragments (MW= 1713) showed a decrease in relative abundance compared to the second most-abundant fragment (Figure 2.23). Assuming that this fragment is involved in cross-links with the hairpin molecules, the mass corresponds to the peptide fragment that includes the histidine containing loop of the RNase H domain,[72] close to the catalytic site in the folded enzyme (Figure 2.22). Although we were unable to directly observe the resultant MS peak that would support the hypothesis that the hairpins cross-link to the histidine containing peptide fragment, we note that both X-14-a and X-14-e gave the same fingerprint pattern. Since an additional appendage was incorporated into X-14 (to afford either X-14-a and X-14-e), one could argue that we may have created a bias for the enzyme to bind more favorable to these conjugates. Future experiments should examine the effect of these conjugates, the 5'-cholesterol hairpins, and other terminal phosphate modifications on binding and inhibitory activity against RNase H. Unfortunately, the cross-link experiments depleted all X-14-a, X-14-b, X-14-d and X-14-e such that insufficient material remained to carry out inhibition assays. We also recognize that

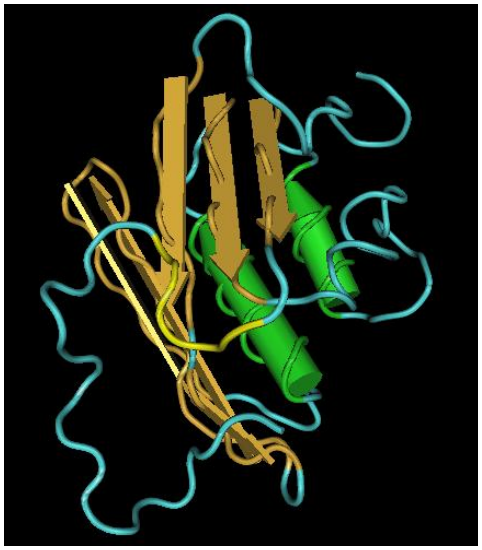

Figure 2.21. Structure of the isolated RNase H domain with the histidine containing loop highlighted in yellow.

deducing binding sites based on the decrease of peak intensities is ambiguous, therefore obtaining MS data of the peptide-nucleic acid conjugate itself will be necessary to unequivocally identify the binding site of the hairpins.

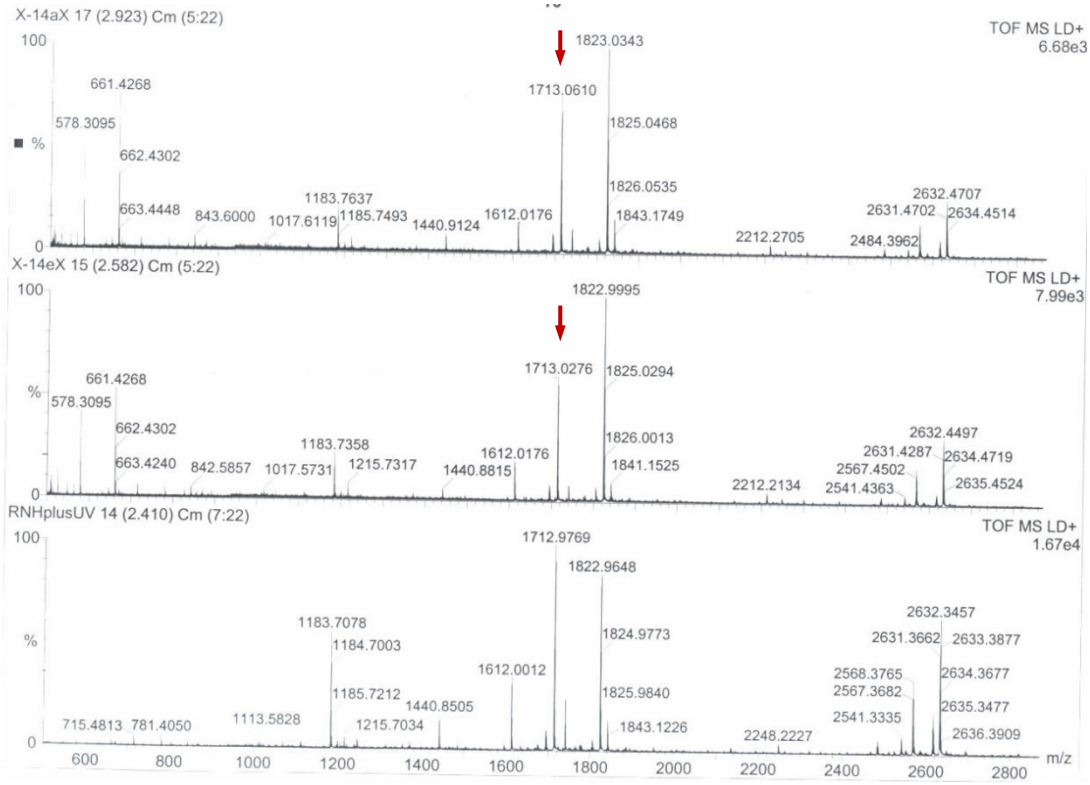

Figure 2.22. MS analysis peptides obtained from in-gel trypsin digests of the isolated RNase H domain of HIV-1 RT. The top spectrum is the RNase H domain cross-linked with hairpin X-14-a, the middle spectrum is the RNase H domain cross-linked with hairpin X-14-e, and the bottom spectrum is the unconjugated RNase H domain. The arrow indicates the peak corresponding to the histidine containing loop.

2.2.10 NMR of RNase H and hairpins

We attempted to use protein NMR to measure the binding affinity of the isolated RNase H domain of HIV-1 RT with a hairpin. The active isolated RNase H domain from wild-type HIV-1 RT maintains proper folding but is not functional. An ^{15}N-labeled sample of the same active recombinant RNase H domain of HIV-1 RT used in the cross-linking experiments was obtained from Dr. Michael A. Parniak from the University of Pittsburgh. This enzyme harbors the basic loop of *E. coli* RNase I and is catalytically active in the presence of Mn^{2+}.[72] The potency of various hairpins towards the activity of this enzyme showed similar trends to the full HIV-1 RT; hairpins with longer stems are better inhibitors, and cholesterol conjugated hairpins show the most

potency. Our goal was to follow the 2-D ^{1}H-^{15}N heteronuclear single quantum coherence (HSQC) spectrum of the recombinant RNase H protein with increasing amounts of hairpin X-10-C. Peaks in the NMR spectrum that shift position are believed to interact with the nucleic acid. The 2-D ^{1}H-^{15}N HSQC spectrum of the recombinant RNase H prior to adding any hairpin is depicted in Figure 2.23A. This spectrum looks similar to that of the unmodified RNase H domain,[287] with extra peaks originating from the basic loop of *E. coli* RNase H I. One equivalent of hairpin X-10-C was added to give the spectrum shown in Figure 2.23B. This spectrum is dramatically altered with most peaks grouped in the same region, greatly resembling an aggregated or denatured protein. We verified that this was not due to variations in pH or salt concentration in the sample containing the hairpin. We were able to remove X-10-C from the protein by washing with phosphate buffer (80 mM, pH 7.0) through a 10 kDa Microcon molecular weight cut-off centrifugal filter. The resulting NMR structure closely resembled the protein prior to adding hairpin. Next, two non-cholesterol containing hairpins were titrated with the recombinant RNase H domain, X-10 and X-07. In both cases, there were no changes in the NMR spectra titrated with up to 10 equivalents of X-10 and 6 equivalents of X-07. Since the sample preparation of all hairpins was the same, we can conclude that the aggregation in Figure 2.23B is due to the cholesterol moiety on X-10-C, as its non-conjugated homologue had no effect on the NMR spectrum. We then subjected X-10 and X-10-C for dynamic light scattering (DLS) analysis at similar concentrations used in the NMR experiments. X-10 did not show any scattering, whereas X-10-C showed the presence of particles 100-300 nm in diameter with a polydispersity index (PI) of 1.8 and 3.5 at 80 μM and 20 μM concentrations respectively. Although X-07, X-10 and X-10-C all exhibited potency for the RNase H activity of the isolated RNase H domain, clearly, the unconjugated hairpins are very weak binders under the NMR conditions. Studies have shown that most of the contacts between the primer-template of HIV-1 RT occur away from the RNase H domain.[271] Therefore, it should come as no surprise that nucleic acids have difficulty binding to the isolated RNase H domain. Furthermore, we note that the conditions in the inhibition assays use Mn^{2+} as the divalent cation, whereas NMR experiments were conducted in a buffer containing Mg^{2+} ions. Mn^{2+} is

paramagnetic and incompatible with NMR as it disrupts the acquisition of the other nuclei. Future experiments will titrate the natural RNA•DNA substrate with the recombinant RNase H domain to verify proper NMR conditions where nucleic acid-protein contacts are made.

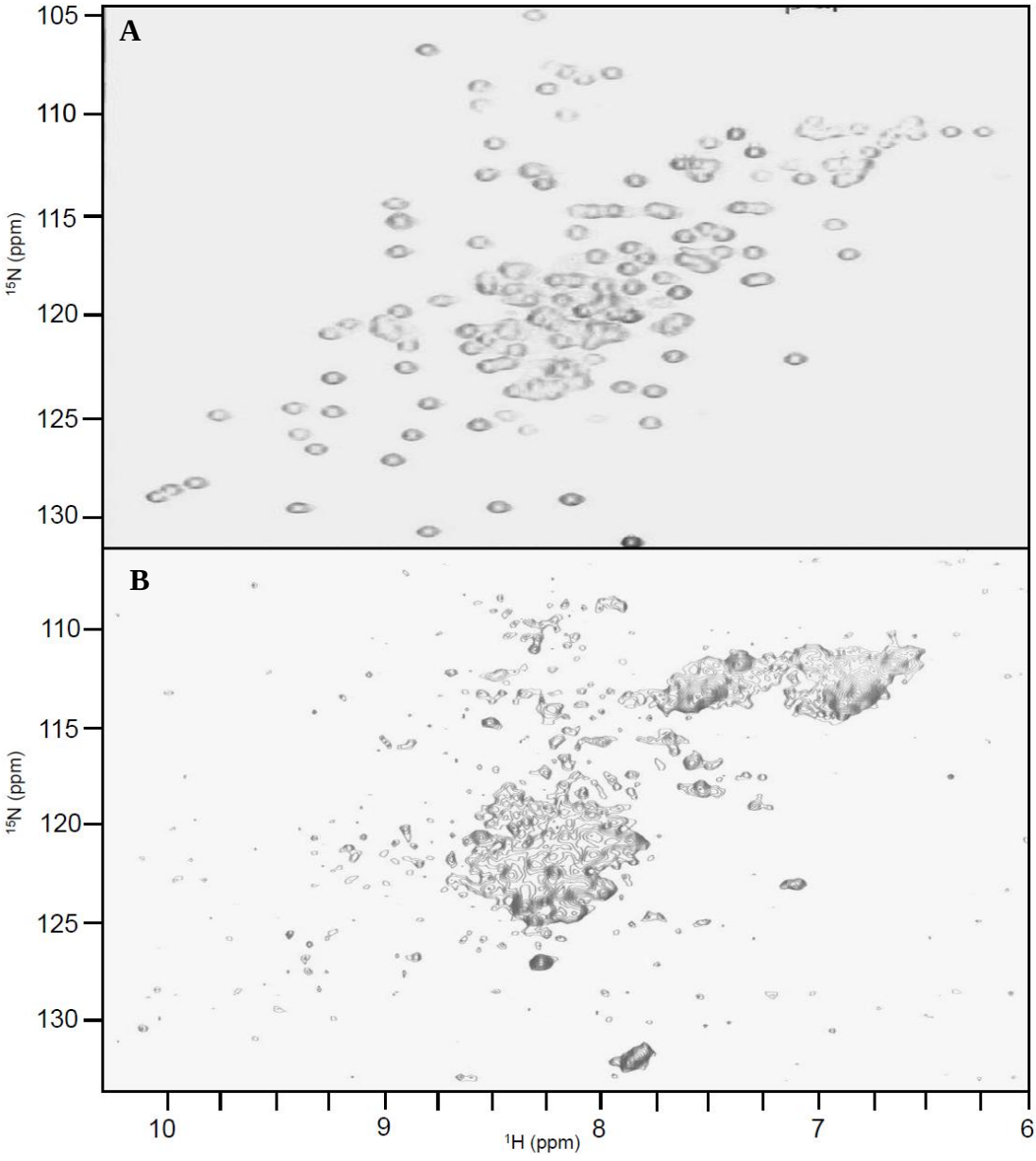

Figure 2.23. ^{1}H-^{15}N HSQC NMR spectra of the recombinant RNase H domain of HIV-1 RT. A. 0.6 mM RNase H in the absence of hairpin inhibitors in a buffer consisting of 25 mM Tris-HCl pH 6.8, 25 mM NaCl, 5 mM $MgCl_2$ and 10% D_2O. B. Identical conditions to A but with 1 equivalent of X-10-C

2.3 Conclusion and Future Directions

2.3.1 Conclusions

The RNA hairpins described herein offer some interesting properties for the purpose of targeting the RNase H activity of HIV-1 RT as an antiretroviral agent. Just as chain-terminators compete with natural dNTPs in the polymerase domain, we designed nucleic acid hairpins that compete with the RNA·DNA substrate of the RNase H domain of HIV-1 RT. This work shows that hairpin structure can be tuned to enhance their nuclease stability, potency and modulation of the RNase H cleavage pattern. Preliminary nuclease stability assays on some hairpin inhibitors confirmed previous reports[231] that, even in the native (unmodified ribose) form, they are highly stabilized against serum nucleases. The thermostability of hairpins does not appear to be directly related with their potency towards RNase H. Based on the melting temperatures, most hairpins should be in the duplex form at physiological conditions. The degree of inhibition appears to correlate with helix conformation; an A-type helical arrangement shows greater potency for RNase H activity. The greatest advantages displayed by chemically modifying the stem/loop region of hairpins were with RNase H potency. Modifying the hairpin loop at the U1- position by a 2'F-rU or LNA residue (X-17, X-18 and si-12) did not affect the T_m, however, in some instances it increased the potency towards RNase H (X-06 and X-20-C). Interestingly, adding more 2'F-rN nucleotides in the loop (X-8) lowered the T_m but modulated the RNase H cleavage pattern.

Another modification that showed marked benefits to the potency of the hairpins was the addition of a reversed 3'3'-linked dT unit. This single modification alone increased the RNase H potency of otherwise unmodified hairpins (e.g., R_4RR_4 and R_6RR_6). This observation suggests that just like the natural RNase H substrates, the terminus may play a role on catalysis or the mode of binding to HIV RT. The modification with the greatest impact to thermal stability and potency was a 5'-cholesterol unit. Although our intent with this modification was on making hairpin inhibitors more cell-permeable and more resistant towards 5'-exonucleases, we observed in all cases a dramatic enhancement in hairpin potency and thermal stability ($\Delta T_m > 20°C$). Site-specific footprinting experiments showed that hairpins likely

disrupt protein-nucleic acid interactions at the RNase H active site and not in the polymerase domain. This appeared to also be the case for the cholesterol-conjugated hairpins.

The most potent cholesterol-hairpin conjugate, X-10-C (IC_{50} = 0.18 μM), matched the potency of a well known RNase H inhibitor (DHBNH).[248] This somewhat contrasts previous reports showing that cholesterol-oligonucleotide DNA conjugates lower infectivity of HIV-1 by inhibiting both RT polymerase activity and entry of the virus particle into the cell,[171,288] with very little impact on RNase H activity. We observed that cholesterol conjugation also inhibited HIV-1 RT's DNA polymerase activity, albeit to a lesser degree. Dynamic light scattering experiments suggest that cholesterol-hairpin conjugates aggregate, and hence their mechanism of action may differ from that of unconjugated inhibitors. NMR experiments demonstrated that the isolated RNase H enzyme aggregates in the presence of X-10-C. Therefore we propose that cholesterol conjugated hairpins follow a "dual" mechanism of action. The non-polar cholesterol moieties would aggregate together, whereas the hairpin component binds to the RNase H active site like their non-cholesterol analogues. The formation of this hairpin-RNase H "aggregate" could then explain why the site-specific footprint binding assays showed that cholesterol and non-cholesterol hairpins bind to the RNase H domain to the same extent despite differences in potency. This aggregation in turn would also disrupt RNase H activity, in addition to polymerase activity to some degree as indicated by our primer extension assays.

From these observations we propose a binding model containing HIV-1 RT, the primer-template substrate and the hairpin inhibitors as illustrated in Figure 2.24. *We propose that the short hairpins are binding to RT in such a manner as to change the trajectory of the primer-template so that it no longer passes in proximity to the RNase H active site.* Recent studies suggest that RT is unable to simultaneously engage the primer-template at both the polymerase active site and the RNase H domain.[289] As RT exhibits tighter binding events with the primer-template close to the polymerase site,[271] the RNase H domain would be free to bind the hairpins. The site-specific footprinting experiments support this model, and have proven a useful method for elucidating the status of primer-template-RT interactions at the two catalytic

domains.[65,274] For this reason, elucidating the precise location where the hairpins bind to RT, through techniques such as NMR and UV cross-linking/MS, will help validate our model. We are aware that even though the hairpins disrupt RNA-dependent DNA polymerase activity, this does not necessarily mean they bind at the polymerase domain.

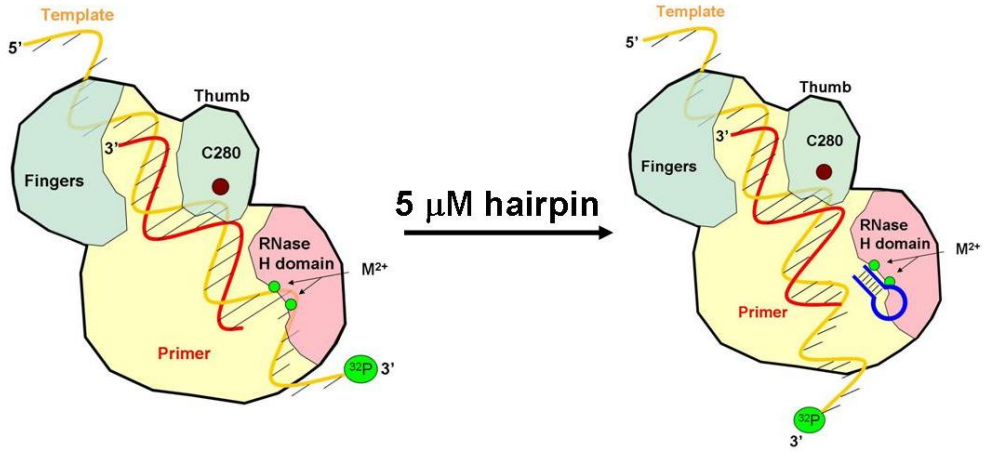

Figure 2.24. Cartoon depicting the binding of a DNA primer-DNA template bound to HIV-1 RT and the effect of adding RNA hairpins to the trajectory of the double-stranded substrate.

2.3.2 Future work

We have demonstrated through chemical modifications, we can improve the potency of short nucleic acid hairpins against the RNase H activity of HIV-1 RT, with varying consequences on selectivity against polymerase activity. Hairpins with dangling 3-3' linkages as well as natural 5'-3' linkages should be further investigated given that a single dangling reversed thymidine greatly increased potency perhaps by directing binding to RT in a similar manner as a DNA·RNA substrate duplex. As controls, circular RNAs or RNA dumbbells could help assess the importance of the 5' and 3' termini on the recognition and selectivity for the polymerase activity. These structures would be shorter versions of the long RNA dumbbells previously demonstrated by our laboratory to be more potent than RNA hairpins against RNase H activity, with minimal inhibition of polymerase activity.[231] A study of the termini should also compare the potency and selectivity of hairpins containing 5' and 3' phosphates. Finally, a more thorough study of loop modifications may reveal other increases in potency or changes in RNase H cleavage patterns.

Future work should also focus on supporting (or disproving) our hypothesized model of hairpin-RNase H binding (Figure 2.24). Single-molecule FRET has recently been employed to probe the orientation RT binds on the primer-template.[225,272] This method could presumably be used to localize where the hairpins bind on HIV-1 RT.

We attempted to address this question by cross-linking the hairpin with HIV-1 RT, but the results were inconclusive as we were unable to directly detect the mass of the peptide-hairpin adduct. To work around this problem, one could treat the hairpin-HIV-1 RT adducts first with aqueous base, and then with trypsin/chymotrypsin. The RNA portion would be degraded under the basic conditions to generate the RT bound to a single 5'-phosphate-ribonucleotide-2',3'cyclic phosphate residue. Digestion with trypsin/chymotrypsin would then generate peptide fragments, one of which will be attached to the nucleoside diphosphate. This peptide-phosphate-ribonucleotide-phosphate fragment would contain fewer negative phosphates which would make it much easier to analyze by MS. Hopefully this will allow for ready identification of a peak(s) that "moves" or "disappears" rather than "diminishes" in the mass spectrum.

2.4 Experimental methods

Chemicals and solvents were ACS grade or higher and were purchased from Sigma-Aldrich or Thermo-Fisher. Autoclaved Millipore water treated with diethylpyrocarbonate (DEPC)[290] was used to manipulate RNA and prepare aqueous buffers.

2.4.1 Synthesis of cholesterol phosphoramidite

The cholesterol phosphoramidite was prepared as previously described.[291] A 50 mL round bottom flask containing cholesterol (1 g, 2.6 mmol) was evacuated on high vacuum overnight, purged with argon, and dissolved in freshly distilled DCM (10 mL). Dry diisopropylethylamine (1.3 mL, 7.5 mmol) and diisopropylamino-(2-cyanoethyl)-phosphoramidic chloride (625 μL, 2.7 mmol) were added and the reaction was stirred for one hour. At the end of this time, the reaction was washed with 5% $NaHCO_3$, extracted with DCM and dried over sodium sulphate and loaded on a silica gel column neutralized in 2.5 % triethylamine in hexane. The purified phosphoramidite diastereomer was eluted in 6:4 hexane-ethyl acetate, rotary

evaporated and dried overnight on high vacuum to give the product as a thick white oil (1.35 g, 89 % yield). ^{31}P NMR (200 MHz, CD_3CN) δ= 146.3 (d, 2P) ppm. ESI-TOF: m/z 587.6 $[M + H]^+$

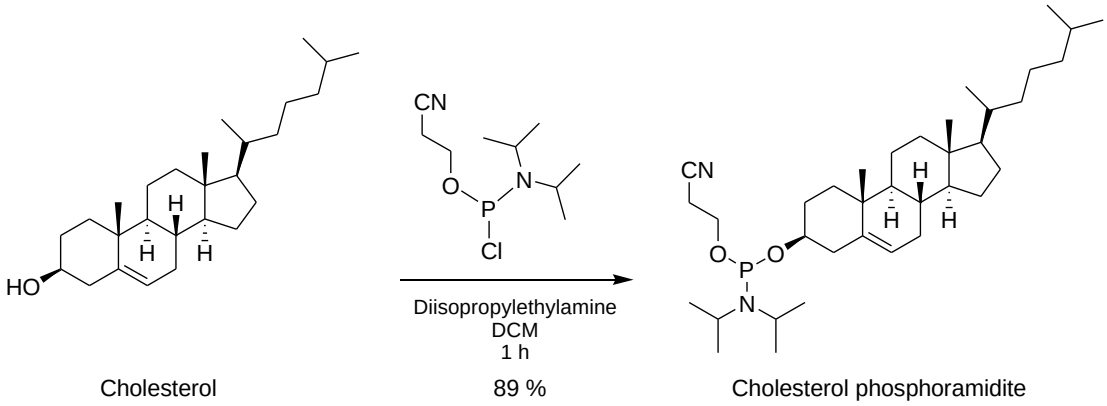

Scheme 2.1. Synthesis of cholesterol phosphoramidite from cholesterol.

2.4.2 Synthesis and purification of oligonucleotides

Unmodified DNA, RNA and 2'-5' RNA amidites, 3'-phosphate-ON CPG, 5'-phosphate-ON reagent and 3'-fluorescein CPG were purchased from Chemgenes (Cambridge, MA). 2'-F RNA and FANA amidites were obtained from Rasayan Inc. Solid-phase oligonucleotide synthesis was performed on an Applied Biosystems ABI 3400 synthesizer using previously published methods.[292] A 0.1 M solution of 3-amino-1,2,4-dithiazole-5-thione (ADTT) in dry acetonitrile was the sulfurizing reagent used to form phosphorothioate linkages.[293] Half the CPG from the synthesized hairpins were cleaved from the solid support while the other half was left on the synthesizer for an extra coupling with the cholesterol phosphoramidite with a coupling time of 30 minutes in distilled dichloromethane to a final concentration of 0.10 mM of the amidite. Oligonucleotides were purified on 24 % preparative denaturing PAGE using an SE600 gel apparatus or by anion-exchange HPLC on a Waters PROTEIN-PAK DEAE 5PW (7.5 x 150 mm) HPLC column and Waters 1525 dual pump HPLC (Waters) using a 0-30% gradient of 1M $LiClO_4$ in water in 30 minutes. Purified samples were desalted by size exclusion chromatography on G-25 Sephadex (GE-Healthcare) and quantified spectrophotometrically using a Cary 300 Beckman spectrophotometer. Purified oligonucleotides were confirmed by ESI-TOF

MS at the Concordia University Mass Spectrometry facility (Table 2.4). Primers and templates for footprint and chain-extension assays were purchased from Invitrogen. LNA containing oligonucleotides described in Table 2.2 were prepared by Signe Inglev Stefanssen. The hairpins of various stem length described in Table 2.3 were synthesized by the University of Calgary DNA Lab Services.

Table 2.4. Selected ESI mass spectral data of hairpins in the current study.

Entry	Code	Sequence	Mass calculated	Mass observed
1	X-10	5'- GUGGAC UUCG GUCCAC - 3'3'dT	5377.3	5390.2
2	X-11-C	chol - 5'- GUGGAC UUCG GUCCAC - 3'3'dT	5825.9	5855.9
3	X-13	5'- GUGGAC UUCG *gtccac* - 3'3'dT	5403.3	5401.8
4	X-14	5'- *gtggac* UUCG *gtccac* - 3'3'dT	5429.3	5427.5
5	X-17	5'- GUGGAC *T*UCG GUCCAC - 3'3'dT	5395.2	5391.8
6	X-18	5'- GUGGAC **T**UCG GUCCAC - 3'3'dT	5403.3	5401.7
7	X-19	5'- gtggac UUCG gtccac - 3'	4873.2	4910.7
8	X-20	5'- *gtggac U*UCG *gtccac* - 3'3'dT	5447.3	5443.3
9	X-20-C	chol - 5'- *gtggac U*UCG *gtccac* - 3'3'dT	5895.9	5892.2
10	X-21	5'- GAUCAC UUCG GCCUGG - 3'3'dT	5377.2	5376.0
11	X-14-a	phenylazide-pS-5'- *gtggac* UUCG *gtccac* - 3'3'dT	5684.5	5682.7
12	X-14-e	5'- *gtggac* UUCG *gtccac* - 3'3'dT-pS-phenylazide	5684.5	5682.5

Legend: UPPER CASE, RNA; lower case, DNA; UNDERLINE, 2'-5' linked RNA; **BOLD,** LNA; *italic lower case*, 2'F-ANA; ITALIC UPPER CASE, 2'F-RNA; 3'3'dT, 3' reversed dT; chol, 5'- cholesterol.

2.4.3 Thermal denaturation studies

Thermal denaturation curves were obtained on a Cary 300 Beckman spectrophotometer equipped with a 6 X 6 multi-cell block Peltier adapter under a stream of nitrogen. 0.5 OD units were dissolved in a phosphate buffer (10 mM $NaPO_4$ pH 7.0), thermally denatured at 95°C for 5 minutes and annealed by slow cooling to room temperature, followed by storage at 4°C overnight. Thermal denaturation curves were obtained by monitoring the absorbance at 260 nm during a temperature change of 0.5 °C per minute, recording points at 1°C intervals from 4°C to 95°C. The melting temperature values (T_m) were obtained using the first derivative method from the Cary UV Software version 2.3. The T_m values for LNA containing oligonucleotides described in Table 2.2 were obtained by Signe Inglev Stefanssen.

2.4.4 Circular dichroism (CD) studies

Samples for circular dichroism were prepared in the same manner as for the thermal denaturation studies. CD spectra were obtained using a Jasco 800 circular dichroism spectrometer. Three scans were acquired at 20°C at a rate of 50 nm per minute from 350 nm to 190 nm. The data was averaged, baseline-subtracted and smoothed using the Spectra Manager software provided by the manufacturer.

2.4.5 Serum stability studies

Hairpins of interest (0.4 ODUs) were suspended in 200μl of 10% FBS in Dulbecco's modified Eagle Medium (Invitrogen) and incubated at various times in a 37 °C water bath. Reactions were stopped by removing 30 μl aliquots from the bath and freezing immediately on dry ice. After all time points were collected, samples were evaporated to dryness and resuspended in 5 μl of 50% gel loading buffer in water and loaded on a 24% analytical polyacrylamide gel. Degradation products were visualized by UV shadowing and Stains-All (Sigma-Aldrich).

2.4.6 Screening for RNase H inhibitors

Wild type p66/p51 HIV-1 RT was prepared as previously described [52]. The activity of HIV-1 RT RNase H in the presence of hairpin inhibitors was tested with a 5'-^{32}P-labeled 18-mer RNA•DNA substrate (RNA 5'-^{32}P-GAUCUGAGCGGAGCU-3', DNA 5'-AGCTCCCAGGCTCAGATC-3') derived from the gag-pol region of the HIV-1 genome. Duplexes were formed by combining the RNA and DNA in a 1:1.2 ratio respectively and annealed by heating to 95°C followed by slow cooling to room temperature. The RNase H reactions were carried out in a Tris buffer (50 mM Tris-HCl, pH 7.8, 60 mM KCl, 5 mM $MgCl_2$, 0.1 mM DTT and 0.01% Tween-20) with a final concentration of 5 nM of HIV-1 RT. The buffer containing HIV-1 RT was added to dissolved hairpin inhibitors and pre-incubated at 37°C for 10 minutes (16 μl volume), and to this was added 4 μl of the labeled RNA•DNA substrate (50 nM final concentration) in the same buffer. Reactions were carried out for 10 minutes and subsequently quenched by the addition of an equal volume of gel loading buffer (98% deionized formamide, 10 mM EDTA, 0.1 mg/mL bromophenol blue, and 0.1 mg/mL xylene cyanol) followed by heating to 95°C for 5 min. Cleavage products were resolved on 16% denaturing polyacrylamide gels and visualized by autoradiography.

Relative HIV-1 RNase H activity was quantified by densitometry of the autoradiograph using UN-SCAN-IT v. 4.1 (Silk Scientific Corporation).

2.4.7 RNase H kinetic assays

Kinetic parameters for the RNase H inhibitors were determined using a fluorescence based assay developed by Parniak and co-workers [251]. Briefly, a 3'-fluorescein labeled derivative of the same 18-mer RNA substrate used in the gel-based assays was combined with its 5'-DABCYL modified DNA complement. All solutions were pre-incubated at 37 °C. Aliquots of 40 μl of substrate, under identical buffer conditions as those of the gel-based assays, were dispensed into 96-well plates containing 10 μl of water or hairpins with concentrations varying from 0.1 μM to 100 μM. Reactions were initiated by the addition of 50 μl of HIV-1 RT in the same buffer but with the addition of $MgCl_2$ (5 mM final concentration) and stopped at various time points by adding 50 μl 0.5 M EDTA. Resulting fluorescence was measured on a Molecular Devices Gemini XS spectrofluorometer with an excitation wavelength of 490 nm and an emission wavelength of 520 nm.

2.4.8 Site-specific footprint assays

Site-specific footprints were obtained using a double-stranded DNA primer-template derived from the polypurine tract (PPT) of HIV-1 RT (primer: 5'-TTAAAAGAAA AGGGGGGACT-3'; template 5'-CGTTGGGAGT GAATTAGCCC TTCCAGTCCC CCCTTTTCTT TTAAAAAGTG GCTAAGA-3'). The 3' end of the template strand was ^{32}P-labeled using terminal deoxynucleotidyl transferase (MBI Fermentas) according to the manufacturer's protocol. To maximize the footprinting on the template strand, a ratio of 1:3:6 template to primer to HIV-1 RT (2.7 pmoles, 8.1 pmoles and 16.2 pmoles respectively) was employed. Reactions were carried out in 20 μl volumes in a 120 mM cacodylic acid-sodium cacodylate buffer (pH 7.0, 20 mM NaCl, 6 mM $MgCl_2$, and 2 mM DTT). HIV-1 RT, hairpin inhibitors and primer-template substrates were pre-incubated for 10 minutes before Fe^{2+}-mediated and KOONO-mediated footprints were generated as previously described [65]. For Fe^{2+}-mediated footprints, 4 μl of a freshly prepared 0.5 mM solution of iron ammonium sulfate was added to each reaction for five minutes. For KOONO-mediated footprints, 2 μl KOONO was added to each reaction. All reactions were stopped by

the addition of 100 μl of a solution containing 10% 3M ammonium acetate in cold 2-propanol and 0.1 μg/μl tRNA. Reactions were subsequently centrifuged for 30 minutes at 13 000 rpm at 4°C. The supernatant was removed and the pellet was washed with 100 μl 80% ethanol stored at -20 °C. The products were resuspended in 10 μl gel loading buffer and heated to 95 °C for 5 minutes, resolved using an 8% denaturing polyacrylamide gel and the bands were visualized using autoradiography. Relative attenuation of footprints by hairpin inhibitors was quantified by densitometry using UN-SCAN-IT v. 4.1 (Silk Scientific Corporation).

2.4.9 Strand transfer assays

Assays were run according to previously published protocols.[294,295] Briefly, 20 nM of the 5'-^{32}P-labeled 22-nt DNA primer (5'-GCATCTGGGG CTCGCAAATT TG-3') hybridized to the 40-nt RNA template (5'-AGGUGAGUGA GAUGAUAACA AAUUUGCGAG CCCCAGAUGC) and 400 nM of the 43-nt DNA acceptor template (5'-GAGCTGCTTG AATTCTGCGT ACTAGGTGAG TGAGATGATA ACA) were pre-incubated at 37°C in a buffer containing 50 mM Tris-HCl pH 7.8, 60 mM KCl, 0.5 mM DTT and 0.01% Tween-20 and 10 nM HIV-1 RT in the presence of hairpin inhibitors at indicated concentrations. Reactions were initiated by the addition of 1 μM of each dNTP and 6 mM $MgCl_2$ (final concentrations). Aliquots were withdrawn at the indicated times and added to an equal volume of 100 mM EDTA in gel loading buffer (98% deionized formamide in 10X TBE, 0.1 mg/mL bromophenol blue, 0.1 mg/mL xylene cyanol), heated for 5 minutes at 95°C and resolved on a 16% denaturing PAGE. Product bands were visualized by autoradiography.

2.4.10 Chain-termination assays

DNA-dependant DNA polymerase reactions were carried out using the 5'-^{32}P-DNA PPT-20 primer and the DNA PPT-57 template (0.5 pmoles per reaction). Primer-template substrates were annealed by heating to 95°C in reaction buffer and cooling to room temperature over two hours. 5μM of each dNTP was added to 20 nM HIV-1 RT in a buffer containing 50mM Tris-HCl (pH 7.5), 60 mM KCl, 2 mM DTT, and 6 mM $MgCl_2$. Reactions were initiated by the addition of 4 μl of substrate to a final volume of 20 μl and run for 10 minutes before being stopped by adding an equal volume of gel loading buffer and heating for 5 minutes at 95°C. Products were

resolved on 16% denaturing polyacrylamide gels and visualized by autoradiography. For chain termination assays the previous protocol was used with the exception of using of 2.5 mM TTP and 2.5 AZTTP instead of 5 mM TTP.

2.4.11 UV cross-linking experiments

Protein-nucleic acid cross-links were generated by irradiating hairpins with 6-fold excess protein under UV_{260} light for 30 minutes in an ice bath in Tris buffer (50 mM Tris-HCl pH 7.8, 60 mM KCl, 5 mM $MgCl_2$). Alternatively, higher yielding cross-links can be obtained with phosphorothioate hairpins alkylated with *p*-azidophenacyl bromide [286,296-298]. Phosphorothioate containing hairpins were synthesized according to standard protocols outlined in section 2.4.2. 25 nmoles of a phosphorothioate hairpin in 40 mM phosphate buffer pH 8.0 was treated with 10 mM *p*-azidophenacyl bromide in 50% methanol for 3 hours at room temperature. The mixtures (65 μl final volume) were then run through a G-25 Sephadex spin column and the alkylated hairpins were isolated by Reverse Phase HPLC on a Varian Pursuit C_{18} column (4.6 x 250 mm) using a 0-25% gradient of acetonitrile in 0.1 M triehtylammonium acetate pH 7.0 in 20 minutes at a rate of 1mL/min. The products were confirmed by ESI MS. All steps were performed under minimal lighting to avoid destroying the reactive aryl azide. In 1.5 mL microcentrifuge tubes, 2-0.5 nmoles of the alkylated hairpin was incubated with 50-100 pmoles of protein (HIV-1 RT or its isolated RNase H domain) at 37°C for 15 minutes in a buffer containing 40 mM cacodylate buffer, 20 mM NaCl and 5 mM $MgCl_2$ ($MnCl_2$ for the RNase H domain). Afterwards, the samples were cooled to r.t., transferred to the inner lids of the microtubes and placed in an ice bath. The samples were irradiated with UV_{366} light from a distance of 3 cm using a handheld UV lamp (0.2 amps) for 30 minutes. The cross-linked products were resolved on a 15% SDS-PAGE gel with a Rainbow™ marker (GE Healthcare) in one lane, visualized by staining with Coomassie blue or by autoradiography for 5'-^{32}P-labeled hairpins, excised into 1 mm cubes and the slices transferred to siliconized 0.6 mL microcentrifuge tubes.

2.4.12 Mass spectrometric analysis of cross-linked products

To identify the peptide fragments that were covalently attached to the hairpins, the unmodified and cross-linked proteins were treated with protease and subsequently

compared by MALDI-TOF MS. Gel slices containing unmodified and cross-linked proteins were washed twice with 100 μl water and the Coomassie blue destained by performing three serial washes of 100 μl 50 mM ammonium bicarbonate in 50% acetonitrile. The gel slices were dehydrated with 50 μl acetonitrile and reduced with 10 mM DTT in 50 mM ammonium bicarbonate for 30 minutes followed by alkylation with 50 μl of 50 mM iodoacetamide for 20 minutes and washed with acetonitrile. Proteolysis was achieved by submerging the gel slices (approximately 35 μl) in a 3ng/μl solution of trypsin in 50 mM ammonium bicarbonate for 16 hours at 37°C. Peptide fragments were extracted with 30 μl of 0.1% formic acid for 30 minutes, and subsequent washes with 60 μl of 0.1% formic acid in 50% acetonitrile for 30 minutes, and 0.1% formic acid in 75% acetonitrile for 30 minutes. Samples were evaporated to dryness in a speed vac, resuspended in 10 μl and passed through a Zip-tip and analyzed on a Micromass Q-Tof Ultima Global (Waters).

2.4.12 Protein NMR

The recombinant HIV-1 RNase H domain with the basic loop of *E. coli* RNase H I was prepared in ^{15}N enriched media using the plasmid developed by Keck and Marqusee.[72] ^{1}H-^{15}N HSQC experiments were acquired on a Varian INOVA 500 MHz spectrometer equipped with an H^{299} cold probe and z-axis pulse field gradients. Data sets were recorded at 25°C, 1024 X 64 data points were acquired with spectral windows of 8000 Hz (1H) and 1823 Hz (15N). The concentration of the recombinant RNAse H enzyme was 0.6 mM in buffer containing 25 mM Tris-HCl pH 6.8, 25 mM NaCl, 10% D_2O and varying amounts of the hairpin inhibitor.

Chapter 3 A single-label phenylpyrrolocytidine providing a molecular beacon-like response capable of reporting HIV-1 RT RNase H activity

3.1 Introduction

3.1.1 Development of high-throughput screening methods for the discovery of HIV-1 RT RNase H inhibitors

As mentioned in the previous Chapter, the ribonuclease H (RNase H) activity associated with HIV-1 reverse transcriptase (HIV-1 RT) degrades the viral RNA genome in RNA•DNA hybrids,[52] and has been identified as a potential target for antiretroviral therapy as it is required for virus infectivity;[79] yet there are no anti-RNase H agents in clinical use. The advent of high-throughput screening (HTS) fluorescent assays has led to the identification of many more RNase H inhibitors than previously possible through gel based assays.[251,252,300-302] The most widely used HTS assay of this type was developed by Parniak and co-workers,[251] which utilizes a two label, molecular beacon-like strategy[303] in which the RNA strand is labelled with a 3'-fluorophore (fluorescein, F) and a DNA strand with a 5'-quencher (DABCYL, Q) (Scheme 3.1). Another popular assay monitors the change in size of the RNA substrate by fluorescence polarization (FP) through a 3'-terminal fluorophore.[252]

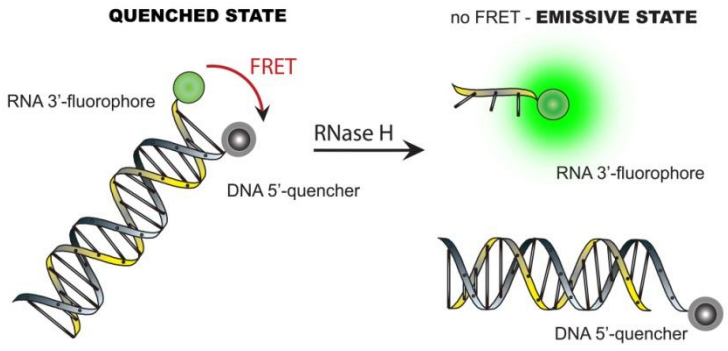

Figure 3.1. Representation of a fluorescent RNase H assay using a dual label system employing a fluorophore and a quencher.

Fluorescent studies involving nucleic acids most often utilize luminescent tags such as fluorescein or rhodamine sometimes in combination with a quencher such as

4-(dimethylaminoazo)benzene (DABCYL). However, these probes can be perturbing to the processes under investigation due to the steric bulk or non-polar groups they introduce to DNA and RNA. Through our own studies on hairpin inhibitors of HIV-1 RNase H (Chapter 2), we observed that the 5'-DABCYL quencher substantially reduces the catalytic efficiency for its RNA•DNA substrate as depicted in Figure 3.2. To address this problem, we directed our attention to the development of an RNase H assay that would exploit the intrinsic fluorescence of pyrrolocytosine nucleoside analogues.

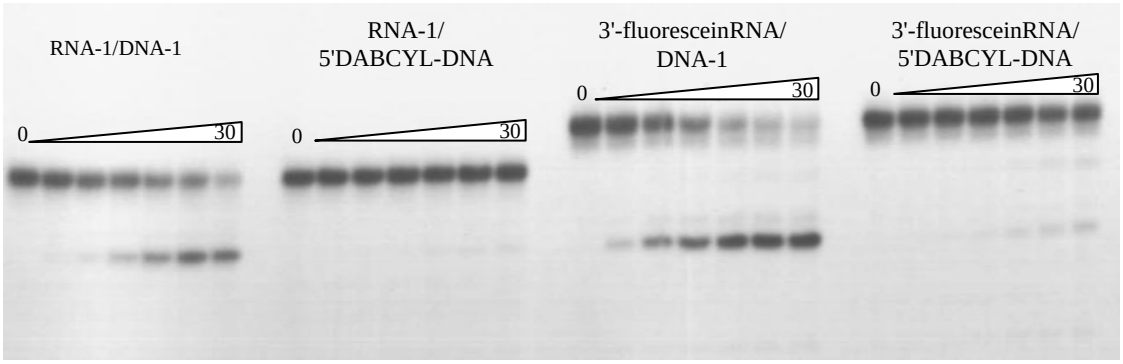

Figure 3.2. Comparison of the HIV-1 RT RNase H catalyzed cleavage of an unmodified RNA•DNA hybrid (left-most lane) with a 3'-terminated fluorescein on the RNA and a 5'-terminated DABCYL on the DNA. Reaction progress was monitored over time (0, 2, 5, 10, 15, 20 and 30 minutes) as indicated.

3.1.2 Fluorescent nucleobase analogues

The use of intrinsically fluorescent nucleotide base analogues offers a less invasive approach to fluorescence labelling of nucleic acids. The natural nucleobases have almost no fluorescence emission, and thus do not interfere with the signal of the fluorescent nucleobases. Using phosphoramidite solid-phase synthesis, a fluorescent nucleotide can be incorporated at any position on an oligomer without the use of linkers or post-synthetic modifications. In addition to their small size within nucleic acids compared to traditional probes, the fluorescence intensity of many base modified nucleotides are responsive to changes in their microenvironment, making them excellent reporters for nucleic acid structure and dynamics.[304] Many researchers are exploiting this property for the detection of single-nucleotide polymorphisms,[305] or as Saito coined the term, base-discriminating fluorescent nucleosides (BDF's).[306] Aside from their use as a BDF, few fluorescent nucleobase analogues have found

widespread use as a tool for molecular biology, the adenine analogues 2-aminopurine (2-AP)[304] and the pteridine base analogues (such as 6MI)[307] being historically the most important (Figure 3.3). Recent work from Tor and others have elegantly demonstrated the value and utility in the design and discovery of new fluorescent nucleobases.[308-311] Despite these and other recent advances, there remains a paucity of intrinsically fluorescent cytidine analogues that demonstrate responsiveness to their microenvironment and state of hybridization[305] thus motivating this work.

The success of a fluorescent nucleobase analogue as a useful reporter resides in its ability to form proper Watson-Crick base pairs, stability in double-stranded nucleic acids, its recognition by nucleic acid processing/binding enzymes, and its fluorescence intensity.[310,312,313309,311,312309,311,312307,309,310] The cytidine analogue pyrrolocytidine (pC, Figure 3.3) satisfies most of the above criteria as a fluorescent reporter [314,315] and has demonstrated compatibility with polymerases.[316,317] Due to oxidation at position 6 during solid-phase synthesis, 6-methylpyrrolodeoxycytidine (dMepC, Figure 3.3)[318] is a stable alternative that retains biological activity,[284,319,320] and is now commercially available. Recently, 6-methylpyrrolocytidine (MepC) has been described in RNA while conserving the properties of dMepC.[321] However, MepC and dMepC have low fluorescence intensity, as manifested by a modest quantum yield (Φ),[321] and lag behind competing chemistries ultimately making them less sensitive probes. The laboratory of Professor Robert H.E. Hudson, of the University of Western Ontario, ON, Canada, showed that the low quantum yield of dMepC can be remedied by substituting the C-6 position with an aromatic group without any penalties on sensitivity or base-pairing fidelity.[322-324] Their work also shows that in certain sequences, replacement of cytosine with dMepC can be destabilizing in a duplex, whereas 6-methoxymethylpyrrolodeoxycytidine (dMOMpC) and 6-deoxyphenylpyrrolocytidine (dPhpC) can be stabilizing.[322,325]

3.1.3 RNase H assays utilizing PhpC, MOMpC, dPhpC and dMOMpC

We now present a novel RNase H assay that utilizes a single fluorescent nucleobase with molecular beacon-like sensitivity and amenable to microplate format. This was realized using the ribonucleoside of 6-phenylpyrrolecytidine (PhpC), which we found that, like its DNA and PNA homologues, ranks among the brightest C-

analogue luminophores. The fluorescence of PhpC is sensitive to its microenvironment, and displays a λ_{max} excitation (360 nm) and λ_{max} emission (466 nm) significantly red-shifted from the absorption of other biomolecules. The

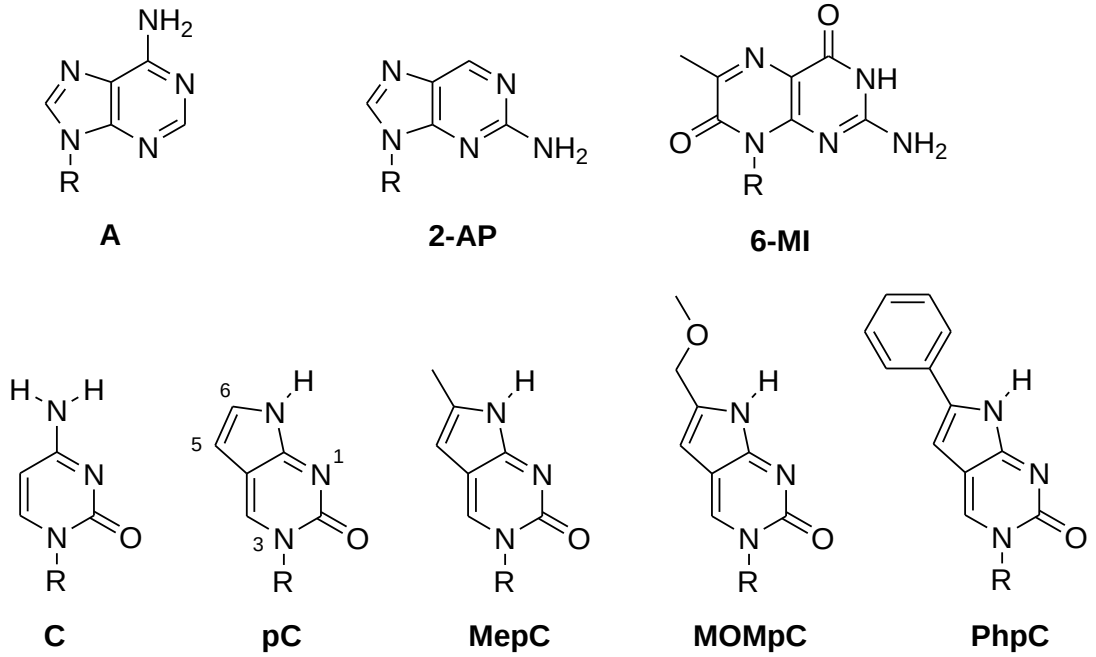

Figure 3.3. Comparison of some modified fluorescent nucleobases. Top Row: adenine (A) compared to 2-aminopurine (2-AP) and the pteridine analogue 6-methyl isoxanthopterin (6-MI). Bottom Row: cytosine (C) compared to pyrrolocytosine (pC), 6-methylpyrrolocytosine (MepC), 6-methoxymethylpyrrolocytosine (MOMpC) and 6-phenylpyrrolocytosine (PhpC). R= 1-ribosyl or 1-(2-deoxyribosyl).

combination of these properties makes PhpC unique among fluorescent nucleobase analogues and has enabled its use as a fluorescent reporter group in the enzymatic assay. Maintaining the same RNA sequence as the traditional fluorophore/quencher (FQ)-based assay[251] (RNA-1, Table 3.1), we replaced a single rC nucleoside with PhpC close to the 3'-terminus of the RNA•DNA hybrid, PhpC-1, where it exhibits low fluorescence (quenched state) as depicted in Figure 3.4. Treatment with HIV-1 RT RNase H generates an RNA tetranucleotide[253] bearing PhpC, and quickly dissociates from its DNA complement with a concomitant dramatic increase in fluorescence emission. We also explored the incorporation of MOMpC on the RNA strand, and dPhpC and dMOMpC on the DNA strand as alternative constructs for fluorescent RNase H assays.

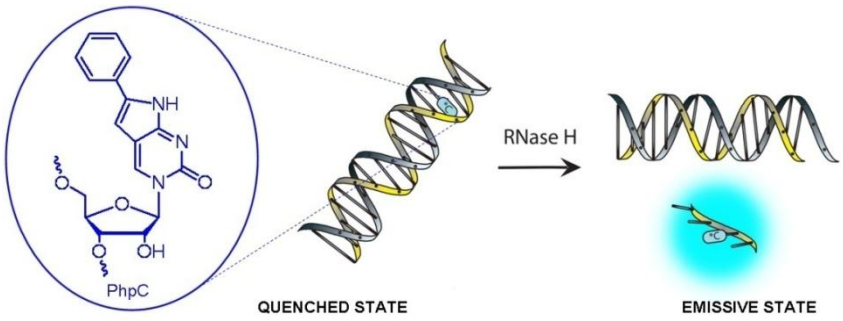

Figure 3.4. Reporting via a single internal fluorescent nucleotide analogue. C*=PhpC

3.2 Results and Discussion

3.2.1 Phosphoramidite Synthesis

The phosphoramidites for dPhpC and dMOMpC were obtained from Professor R.H.E. Hudson. 5'-*O*-(4,4'-dimethoxytrityl)-6-phenylpyrrolocytosine (3.5i, Figure 3.1) and 5'-*O*-(4,4'-dimethoxytrityl)-2′-*O*-*tert*-butyldimethylsilyl 6-methoxymethyl-pyrrolocytosine (3.6ii, Figure 3.1) were synthesized by Dr. Arash Ghorbani-Choghamarani. The methods used to prepare for the ribo derivatives, 6-phenylpyrrolocytidine (PhpC) and 6-methoxymethylenepyrrolocytidine (MOMpC) phosphoramidites was based on previously described protocols for the synthesis dPhpC and dMOMpC.[322,325] 5-Iodouridine was first dimethoxytritylated which was followed by Sonogashira coupling with the appropriate alkyne.[326,327] The 5-alkynyluracil moiety of the resulting nucleoside was subsequently subjected to Ag^{+}-mediated cyclization to form a furanouracil nucleoside derivative.[328] This was then converted to the corresponding pyrrolocytidine by treatment with aqueous ammonia.[318] Standard conditions were used to install the 2'-*O*-*tert*-butyldimethylsilyl group.[203,292] The desired 2'-*O*-regioisomer was characterized by 2D COSY ^{1}H NMR, which confirmed placement of the silyl group at the 2' position by the presence of a cross peak between the free 3'-OH and 3'-CH protons (see NMR spectra in section 3.4.2). Finally, the 5'-*O*-DMT-3'-*O*-phosphoramidite reagents were prepared according to literature methods.[196,292] The phosphoramidite of 6-phenylpyrrolocytidine (3.7i, Figure 3.1) was obtained in high yield (89%) in the final step to give a crispy yellow product. The phosphoramidite of 6-

methoxymethylpyrrolocytidine (3.7ii, Figure 3.1) was obtained as a yellow oil in only 24% yield, which we ascribe to the smaller scale of synthesis.

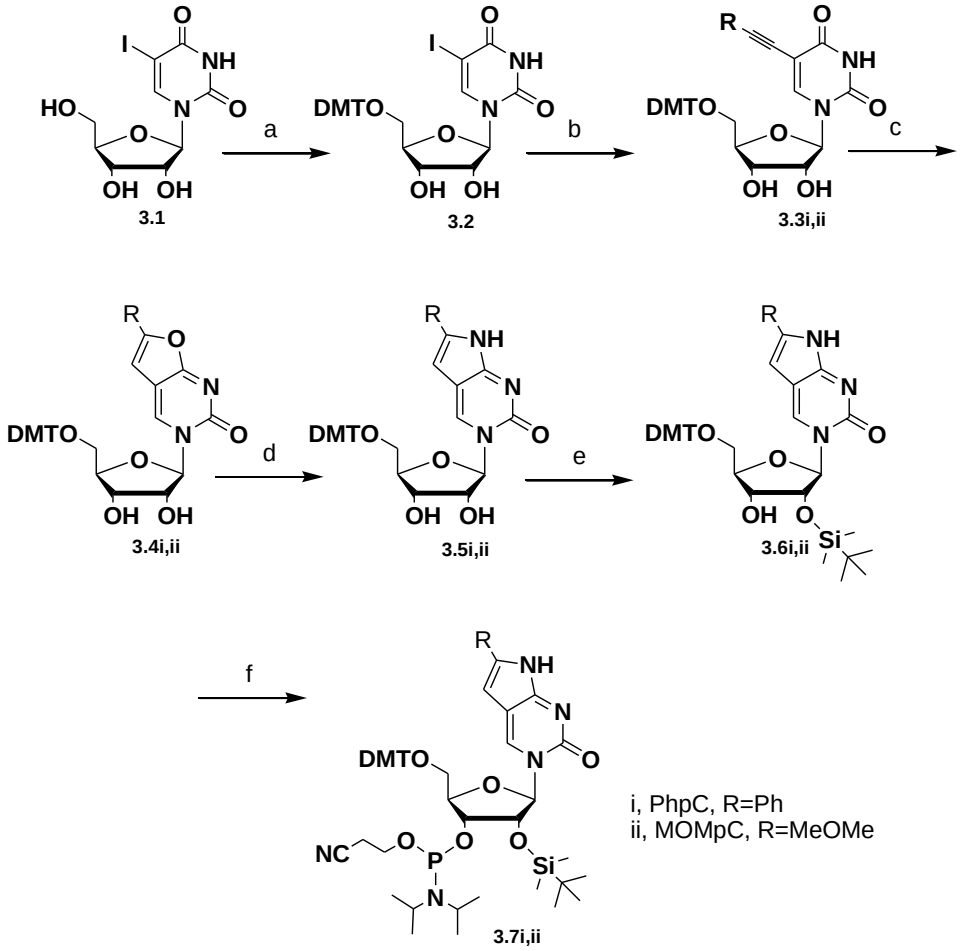

Scheme 3.1. Synthesis of PhpC and MOMpC phosphoramidites. Reagents and conditions: **a.** DMT-Cl, py, NEt_3. **b.** R-acetylene, acetone or DMF, $Pd(PPh_3)_4$, CuI, NEt_3. **c.** CuI, MeOH, NEt_3 or $AgNO_3$, acetone. **d.** NH_4OH, MeOH, 55°C. **e.** TBDMS-Cl, Imidazole, DMF. **f.** $(iPr)_2NP(Cl)O(CH_2)_2CN$, THF, $NiPr_2Et$.

3.2.2 Solid-phase oligonucleotide synthesis

Maintaining the same 18-mer RNA sequence as the traditional fluorophore-quencher(FQ)-based RNase H assay (RNA-1, Table 3.2),[251] we replaced single rC nucleosides with PhpC or MOMpC to give oligomers PhpC-1, PhpC-2, MOMpC-1 and MOMpC-2. The complementary oligodeoxynucleotide sequence, DNA-1, was also modified by replacing dC with dPhpC and dMOMpC units. We also synthesized RNA trinucleotides containing PhpC in order to assess the fluorescence of PhpC as a function of chain length (3nt vs 18 nt) and/or position within the RNA chain (Table 3.2).

Table 3.1. Oligonucleotides used in RNase H assays and T_m data.

Name	Sequence (5' to 3')[a]	T_m (°C)[b]		
		DNA-1	RNA-2	cRNA
RNA-1	GAU CUG AGC CUG GGA GCU	65.1	78.5	-
DNA-1	agc tcc cag gct cag atc	-	-	-
cRNA	UCG AGG GUC CGA GUC UAG	-	-	-
cDNA	cta gac tcg gac cct cga	-	-	64.3
PhpC-1	GAU CUG AGC CUG GGA G**PhpC**U	64.7	78.8	-
PhpC-2	GAU CUG AGC **PhpC**UG GGA GCU	67.5	80.8	-
MOMpC-1	GAU CUG AGC CUG GGA G**MOMpC**U	64.2	78.0	-
MOMpC-2	GAU CUG AGC **MOMpC**UG GGA GCU	66.0	79.3	-
dPhpC-1	**dPhpC**ta gac tcg gac cct cga	-	-	62.4
dPhpC-2	cta ga**dphpC** tcg gac cct cga	-	-	64.3
dMOMpC-1	**dMOMpC**ta gac tcg gac cct cga	-	-	65.7
dMOMpC-2	cta ga**dMOMpC** tcg gac cct cga	-	-	63.2

[a] Legend: RNA, dna, **PhpC**, **MOMpC**, **dPhpC**, **dMOMpC**. [b] T_m values represent the average of at least 3 independent experiments and are within 1°C.

Table 3.2. Sequences and MS data for pC-analogues and control oligonucleotides.

Name	Sequence (5' to 3')	Mass calculated	Mass measured
PhpC	**PhpC**	343.2	366.2 (Na+)
5'-PO_4-PhpC	PO_4- **PhpC**	423.2	423.1 (H+)
G-PhpC-U	G **PhpC** U	994.7	995.6 (H+)
C-PhpC-U	C **PhpC**U	954.7	977.2 (Na+)
U-PhpC-U	U **PhpC** U	955.7	956.07 (H+)
PhpC-1	GAU CUG AGC CUG GGA G**PhpC**U	5887.6	5910.5 (Na+)
PhpC-2	GAU CUG AGC **PhpC**UG GGA GCU	5887.6	5887.4
MOMpC-1	GAU CUG AGC CUG GGA G **MOMpC** U	5855.5	5878.3 (Na+)
MOMpC-2	GAU CUG AGC **MOMpC**UG GGA GCU	5855.5	5877.1 (Na+)
RNA-1	GAU CUG AGC CUG GGA GCU	5787.4	5787.8
DNA-1	agc tcc cag gct cag atc	5444.6	5444.1
RNA-2	AGC UCC CAG GCU CAG AUC	5690.5	5691
dPhpC-1	**dPhpC**ta gac tcg gac cct cga	5544.7	5543.7
dPhpC-2	cta ga**dPhpC** tcg gac cct cga	5544.7	5545
dMOMpC-1	**dMOMpC**ta gac tcg gac cct cga	5512.6	5512
dMOMpC-2	cta ga**dMOMpC** tcg gac cct cga	5512.6	5512
3'-Fluorescein RNA	GAU CUG AGC CUG GGA GCU-Fluorescein	6357.0	6352.9
5'-DABCYL DNA	DABCYL-agc tcc cag gct cag atc	5875.0	5874.9

Legend: RNA, dna, **PhpC**, **MOMpC**, **dPhpC**, **dMOMpC**.

Coupling times for the fluorescent phosphoramidites during solid-phase syntheses were extended to 1 hour to maximize yields, using dichloromethane instead of acetonitrile as the solvent in order to solubilize these monomers. Coupling yields for PhpC phosphoramidites were equivalent to those obtained with commercially available RNA monomers as judged from the quality of the crude oligonucleotides loaded onto a polyacrylamide gel (Figure 3.5) and measured by densitometry. The rather poor couplings obtained with MOMpC (~ 30%), dPhpC and dMOMpC (50%) were ascribed to the poor quality of the phosphoramidites, some of which had been stored for several months. Gel bands containing the fluorophores were visualized under 365 nm light in addition to the conventional 254 nm light used for UV shadowing. The molecular weights of purified oligonucleotides were confirmed by ESI-TOF mass spectrometry (Table 3.2).

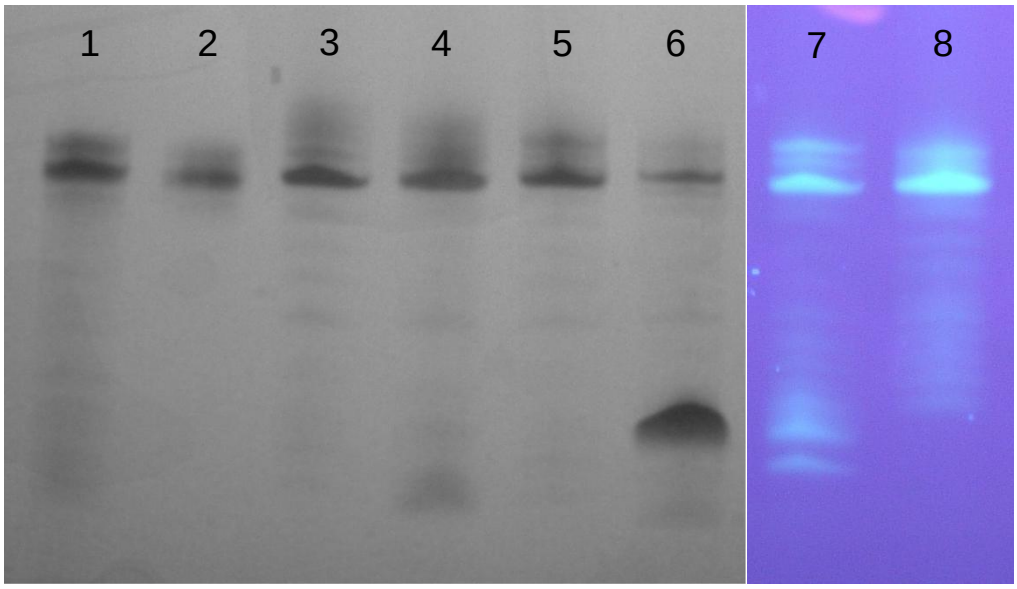

Figure 3.5. 24% denaturing analytical PAGE of RNA strands used in the current study. Lane 1, crude RNA-1; Lane 2, purified RNA-1; Lane 3 and 7, crude PhpC-1; Lane 4 and 8, crude PhpC-2; Lane 5, crude MOMpC-1; Lane 6, crude MOMpC-2. Lanes 1 to 6 were visualized by UV shadowing with 260 nm light, lanes 7 and 8 were visualized with 365 nm light using the fluorescence of PhpC.

3.2.3 Thermal Denaturation Studies

Thermal denaturation studies of DNA strands containing single inserts of dPhpC or dMeOMepC hybridized to their complementary RNA (cRNA) strands showed mixed results when compared to the unmodified DNA•cRNA control duplex (Table

3.1). Substitution in the middle of the DNA sequence with a dMOMpC unit gave a small reduction in melting temperature (ΔT_m *ca.* 1 ^oC). In contrast, an increase in T_m was observed when this modification was positioned at the 5'-termini (1.4 ^oC). In the case of dPhpC, an internal unit was neutral, whereas it was slightly destabilizing (1 ^oC) when placed at the 5'-termini. While these observations are particular significant in view of the potential increase in resistance to nuclease digestion (or 5'-phosphorylation of a sense siRNA strand by kinases) for oligomers with terminal modifications, we did not expect to observe this trend. Generally, the depression of T_m by a destabilizing modification is greater when it is placed in the middle than when it is placed at the (fraying) termini of a duplex.[329] Thermal denaturation studies of RNA strands containing PhpC and MOMpC hybridized to complementary DNA (DNA-1) and RNA (RNA-2) showed clearer trends. PhpC and MOMpC insertions close to the 3'-terminus (PhpC-1 and MOMpC-1) were neutral or slightly destabilizing, whereas at a central position (PhpC-2 and MOMpC-2)**,** they were stabilizing (ΔT_m +2°C and 1°C, respectively). Overall, PhpC substitutions were more stabilizing than MOMpC substitutions. This effect, combined with the increased hypochromicity observed for duplex PhpC-2•cRNA (Figure 3.8) is consistent the greater propensity of internal PhpC units to undergo π-stacking interactions.[322,324]

3.2.4 Circular Dichroism Studies

Circular dichroism was used to further evaluate the effect of these fluorescent nucleobases on the duplex structure. RNA·DNA hybrids with fluorophores on either strand showed similar patterns compared to control strands, differing mainly in the intensity of the CD peak at 265 nm. Fluorophores inserted into RNA•RNA duplexes were exceptionally well tolerated as the CD signature of modified duplexes overlapped with those of the native duplexes. It is noteworthy that despite the conformational changes that accompany the transition from B-form (dsDNA) to A-like in hybrid duplexes (RNA·DNA), to pure A-form (dsRNA), the modified *C5*-face of PhpC appears well accommodated based on our T_m and CD measurements. Although there is a scarcity of data reporting on conformation for *C5*-modified pyrimidines in dsRNA or hybrid RNA·DNA duplexes, T_m data indicate that modest

modifications such as halogens[330] and alkyl/alkynyl[331] groups may be modestly stabilizing, as we have observed for PhpC.

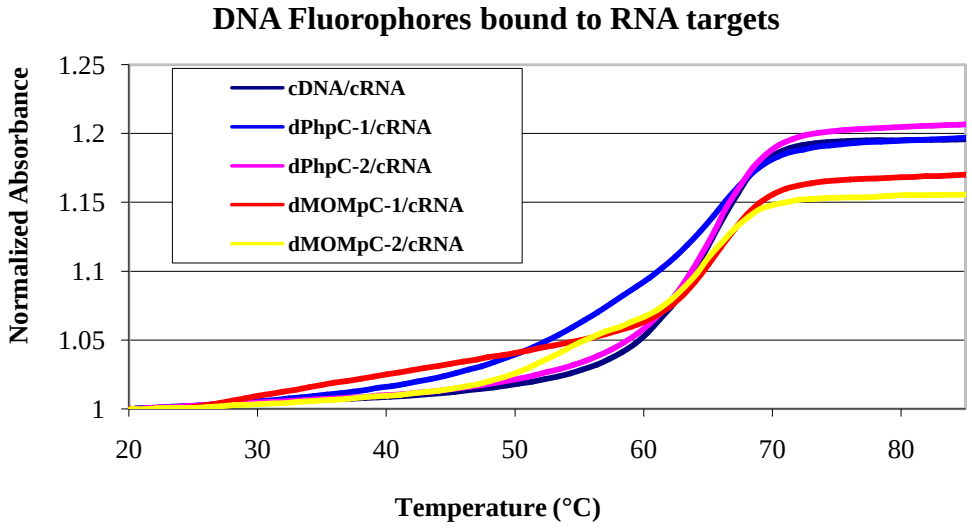

Figure 3.6. Thermal denaturation curves monitored by UV_{260} of DNA containing single inserts of PhpC and MOMpC bound to their complementary RNA.

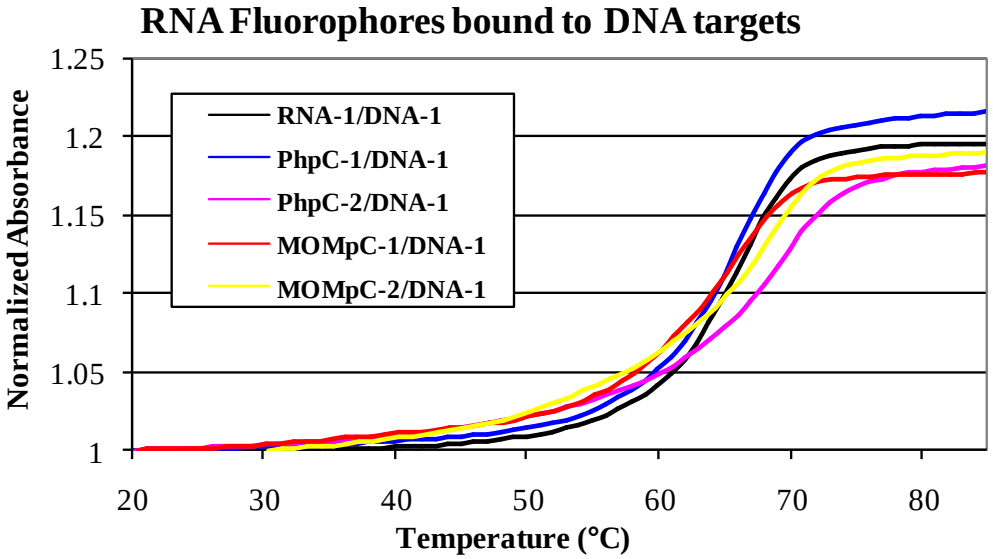

Figure 3.7. Thermal denaturation curves monitored by UV_{260} of RNA containing single inserts of PhpC and MOMpC bound to their complementary DNA.

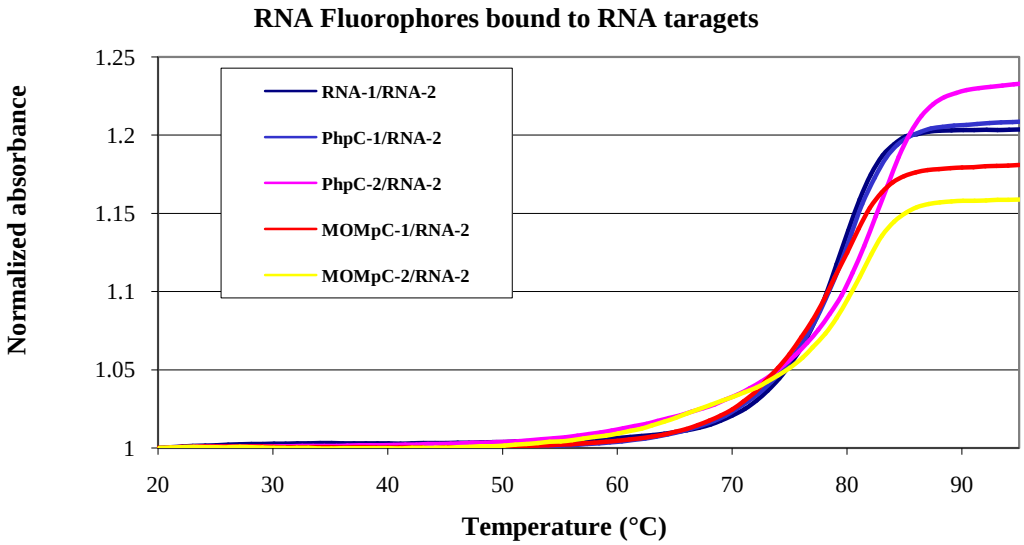

Figure 3.8. Thermal denaturation curves monitored by UV_{260} of RNA containing single inserts of PhpC and MOMpC bound to their complementary RNA.

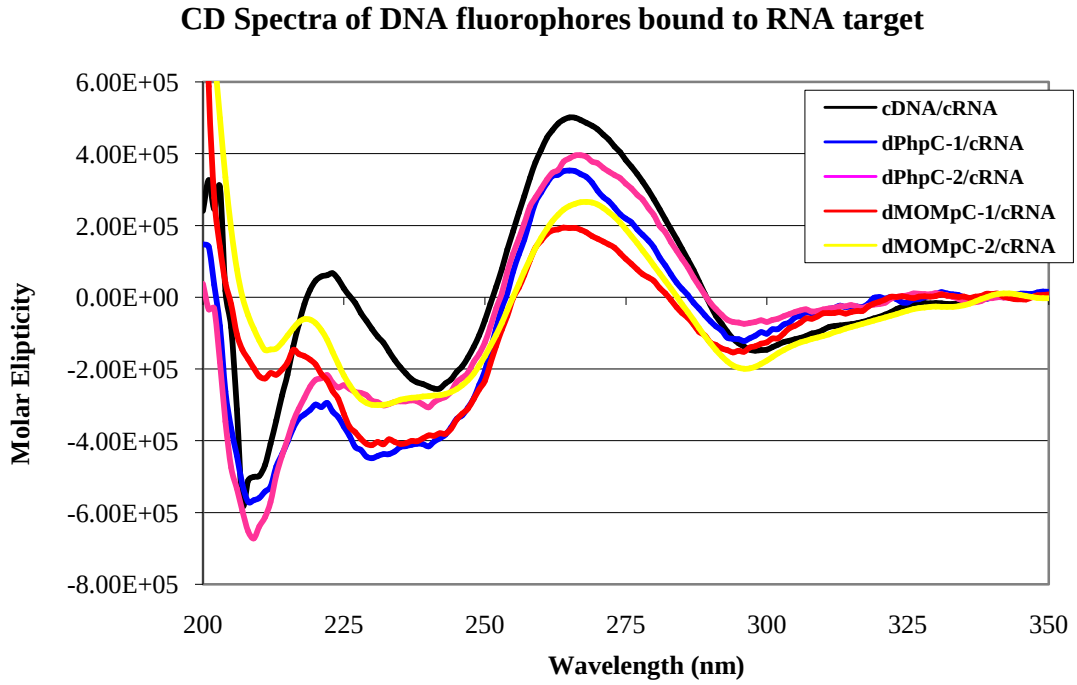

Figure 3.9. Circular dichroism spectra of DNA containing single inserts of PhpC and MOMpC bound to their complementary RNA.

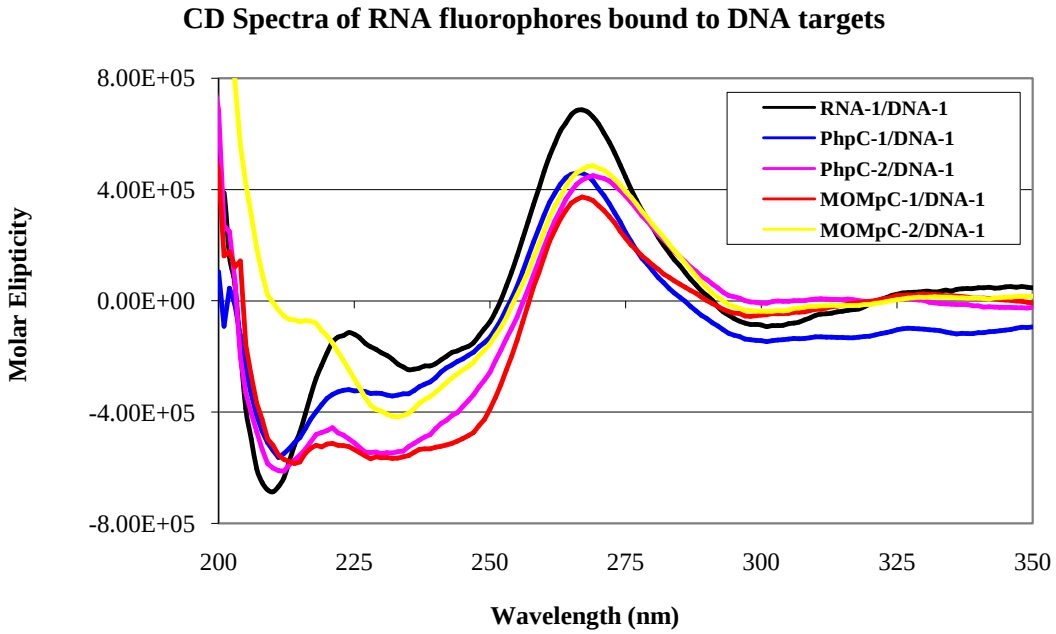

Figure 3.10. Circular dichroism spectra of RNA containing single inserts of PhpC and MOMpC bound to their complementary DNA.

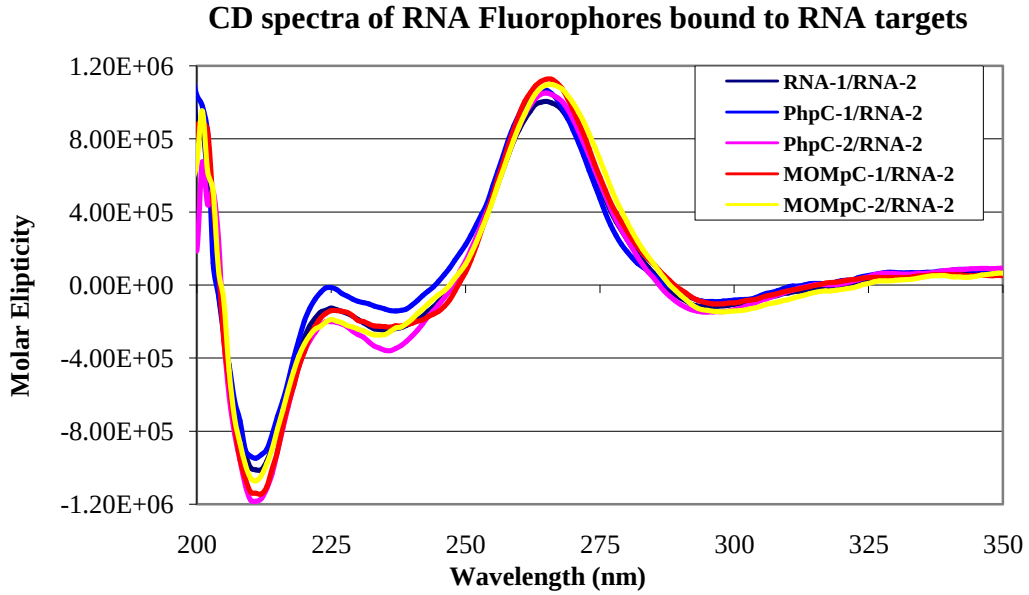

Figure 3.11. Circular dichroism spectra of RNA containing single inserts of PhpC and MOMpC bound to their complementary RNA.

3.2.5 Fluorescence properties of RNA containing PhpC and MOMpC

Based on previous work[323] we anticipated that RNA containing PhpC would be significantly brighter than RNA containing MOMpC. The fluorescence of PhpC aided in the analysis of this nucleoside and its derivatives (Scheme 3.1) as syntheses could

be readily monitored by TLC under UV_{365} light. As expected, all PhpC containing-oligonucleotides were more fluorescent than the corresponding MOMpC modified strands (Table 3.3).

The fluorescent parameters of PhpC as the free nucleoside, nucleotide, or incorporated in short oligomers (3 nt and 18 nt), or within RNA•DNA and RNA•RNA duplexes are given in Table 3.3. The maximum excitation and emission of PhpC (λ_{ex} max = 360; λ_{em} max = 466, Figure 3.12) and MOMpC (λ_{ex} max = 350; λ_{em} max = 455) were similar to their DNA and PNA homologues previously studied.[322-324] When incorporated into oligonucleotides, the λ_{ex} max of PhpC was slightly red-shifted (approx. 375 nm) compared to the monomers. Both the emission and excitation spectra were very broad, with a Stokes shift of about 100 nm.

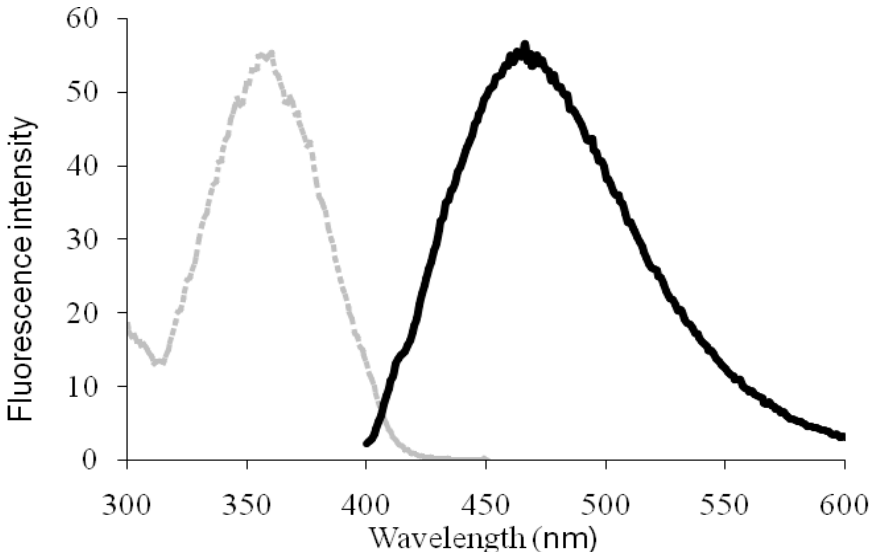

Figure 3.12. Excitation (dotted curve) and emission spectra (solid curve) of PhpC nucleoside.

The PhpC nucleoside and PhpC nucleoside 5'-monophosphate displayed similar fluorescence intensity and quantum yields (Φ) of 0.31 and 0.29 respectively (Table 3.3), a 12-fold increase from a reported value for methylpyrrolocytidine (Φ = 0.023).[332] Thus, it appears that the 5'-phosphate group does not play a role on the fluorescence intensity of the nucleobase. Comparing the trinucleotides, G-PhpC-U**,** C-PhpC-U**,** U-PhpC-U and A-PhpC-U the fluorescence intensity and quantum yield is dependent on the nature of neighboring bases, with G-PhpC-U (neighboring guanine) showing a reduced quantum yield as was previously reported with MepC.[332,333]

Theoretical studies on MepC suggested that base-stacking interactions can diminish Φ by affecting the strength of the oscillator for the fluorescence transition,[332] which is consistent with our observations, although quenching of the fluorescence by intrastrand electron transfer cannot be discounted. The U-PhpC-U had the highest observed quantum yield of the series at 0.41 (Table 3.3), which is likely due to shielding of the fluorophore from solvent (dynamical quenching) while not introducing other compensating nonradiative deactivation pathways. Interestingly, the 18-mer single-stranded PhpC-1 had the same fluorescence intensity and quantum yield as the trinucleotide G-PhpC-U, where PhpC had the same nearest neighbor nucleotide residues (5'G and 3'U). This trend did not continue with PhpC-2 (Φ=0.13) and its analogous trinucleotide C-PhpC-U (Φ=0.24). In this case, it appears that PhpC is quenched in the longer single-stranded RNA sequence by 50%, which may be due to better stacking interactions in a central position; however, length and base composition may play a greater role for shorter PhpC containing oligonucleotides that are conformationally more flexible.

Table 3.3. Fluorescent properties of oligonucleotides containing PhpC or MOMpC single inserts.

Name	Fluorescence Intensity[a]	Quantum Yield[b]	FP[c]
PhpC	51	0.31	< 0.02
5'-PO_4-PhpC	47	0.29	< 0.02
G-PhpC-U	36	0.11	0.03
C-PhpC-U	104	0.24	0.03
U-PhpC-U	134	0.41	0.03
A-PhpC-U	106	n.d.	0.03
PhpC-1	35	0.11	0.21
PhpC-1•DNA-1	7.8	0.035	0.28
PhpC-1•RNA-2	9.5	n.d.	0.30
PhpC-2	38	0.13	0.22
PhpC-2•DNA-1	80	0.20	0.27
PhpC-2•RNA-2	69	n.d.	0.28
MOMpC-1	4.0	n.d.	0.15
MOMpC-1•DNA-1	1.6	n.d.	n.d.
MOMpC-1•RNA-2	1.9	n.d.	n.d.
MOMpC-2	12	n.d.	0.14
MOMpC-2•DNA-1	3.0	n.d.	n.d.
MOMpC-2•RNA-2	3.6	n.d.	n.d.

Legend. n.d. signifies not determined. [a] 1 μM samples measured in 10 mM phosphate buffer (pH 7.0) and 50 mM NaCl at 25°C, PhpC: λ_{ex}=360 nm, λ_{emm}=465 nm, MOMpC: λ_{ex}=350 nm, λ_{emm}=455 nm [b] 9,10-Diphenylanthracene in ethanol (Φ_f=0.95) was used as the reference for Quantum Yield determination [c] fluorescence polarization (FP) measured in identical conditions as [a].

3.2.6 Fluorescence changes with formation of double strands

Oligonucleotides containing pC and pC analogues have consistently shown fluorescence quenching upon duplex formation.[316,318,321,322,334] Nearly all RNA strands containing PhpC and MOMpC hybridized to complementary DNA (DNA-1) and RNA (RNA-2) also showed a decrease in fluorescence compared to single strands (Table 3.3). PhpC-1 bound to its DNA complement exhibited the greatest quenching (~78 %), more than the MOMpC counterpart (60%). The fluorescence emission when PhpC-2 bound to DNA and RNA complements surprisingly increased (Table 3.3). This is unexpected and to our knowledge is the first example of a pC analogue displaying such behavior. Thus the dramatic quenching of fluorescence normally observed during duplex formation and specific hydrogen bonding to guanine may not necessarily be due to base-pairing mediated electron transfer, which leads to nonradiative relaxation of the electronically excited state.

3.2.7 Fluorescent thermal denaturation profiles

We have established that our pC analogs can fluorometrically report changes in their environment when incorporated in oligonucleotides. An increase in fluorescence as the duplexes denature could be monitored by thermal denaturation profiles, and the mid-point of the transition corresponds to the T_m determined by UV absorbance (Figure 3.13, 3.14, 3.15). Molecules that fluoresce generally suffer a decrease in intensity with increasing temperature,[335] so it was expected to see a steady decrease with no transition for the samples containing single strands, and a large transition close to the T_m value for samples containing double strands. This was clearly observed with the DNA oligonucleotides containing 2'-deoxy pC analogs, notably with MOMpC-2 (Figure 3.13), when at high temperature both samples are single-stranded and the thermal denaturation curves overlap.

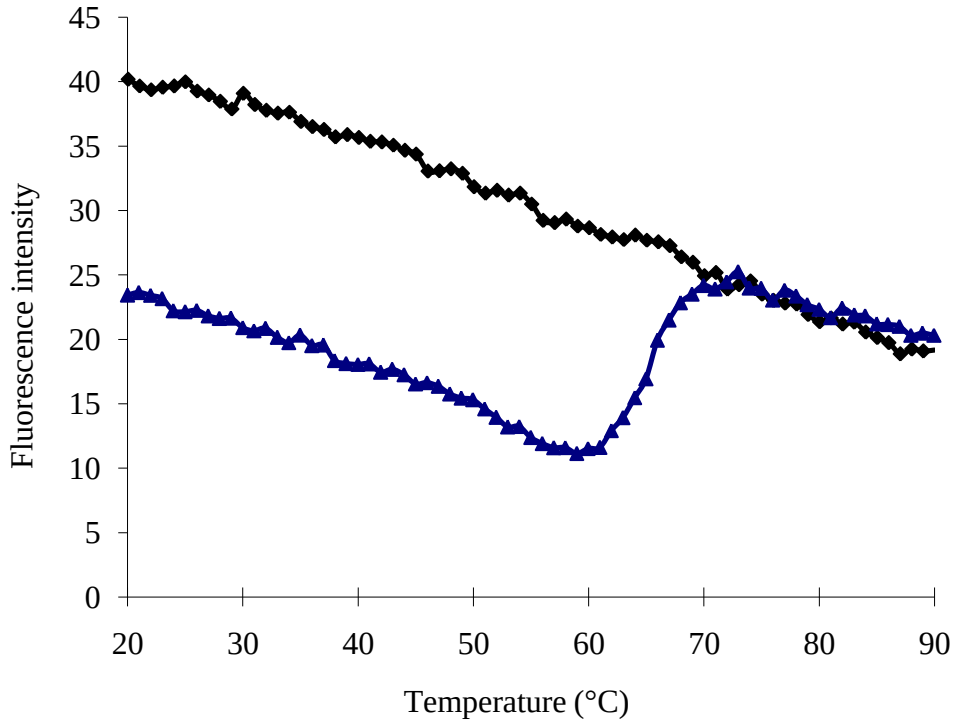

Figure 3.13. Fluorescence melting curve for dMOMpC -2 single-stranded (diamond) and bound to its RNA complement (triangles). λ_{ex} = 350 nm, λ_{em} = 455 nm.

The RNA containing pC analogs showed interesting melting curves for the single-stranded oligonucleotides. Instead of a steady decrease in fluorescence, as with the DNA analogues, the fluorescence intensity of the RNA PhpC and MOMpC strands showed a weak positive transition as temperature increased (Figure 3.14 and 3.15). This was observed with all of the single-stranded RNA pC strands. These transitions could not be monitored in the UV_{260} denaturation profiles. Most of the double strands (RNA•DNA and RNA•RNA) showed a relatively larger positive transition (at least 2.5 fold) centered at the T_m, with PhpC-1 bound to its DNA complementary strand showing the largest positive transition (6.5 fold) (Figure 3.14). In the case of PhpC-2, there was a sharper decrease in fluorescence with increasing temperature due to it being more emissive in the duplex form. The thermal denaturation profiles of PhpC-2 RNA•DNA and RNA•RNA double strands begin to overlap with the single-stranded PhpC-2 after the melting points (Figure 3.15). It is not evident why transitions in single strands were only observed with the RNA analogs and not the DNA. It is also not evident if these transitions are simply a manifestation of PhpC in RNA, or if PhpC

is capable of sensing otherwise unnoticed subtle RNA secondary structures in the sequences under investigation.

These observations are consistent with Thompson's recent study that proposed that the changes in quantum yield of MepC are not dominated by base stacking alone, which is responsible for much of the changes in fluorescence for 2-AP, but possibly by collisional deactivation from solvent.[332] This could explain the observed transition in the fluorescent thermal denaturation curves of single-stranded PhpC-1 (Figure 3.14) and PhpC-2 (Figure 3.15) indicating that some quenching in single strands is contributed by base stacking. Currently, this explanation awaits experimental support. It is clear from these results and the limited studies on MepC, that there are a variety of factors that affect the fluorescence of PhpC including the sequence context (neighbouring bases) and hybridization state along with microsequence effects.

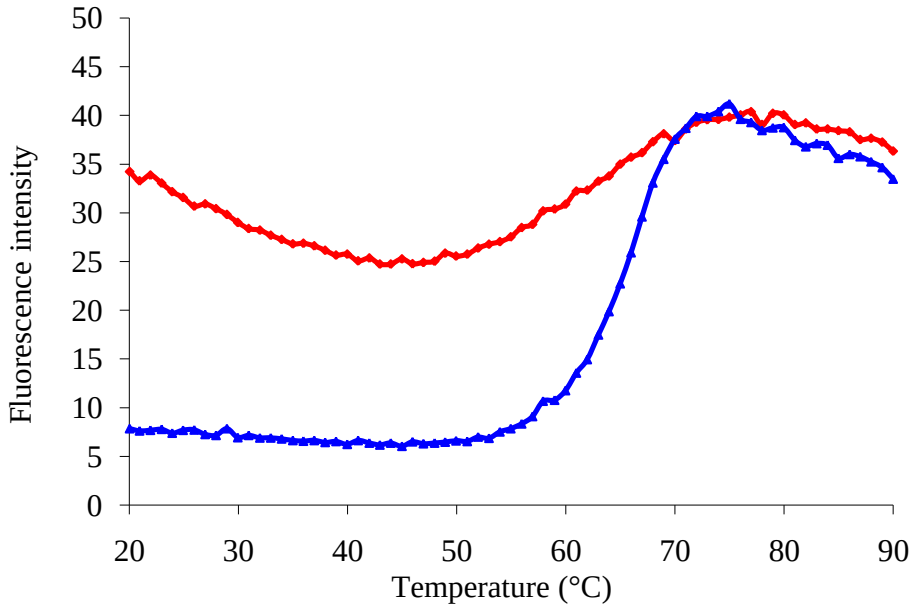

Figure 3.14. Thermal denaturation curves of PhpC-1single-stranded (red diamonds) and PhpC-1 bound to its DNA complement (blue triangles) monitored by fluorescence. λ_{ex} = 360 nm, λ_{em} = 465 nm

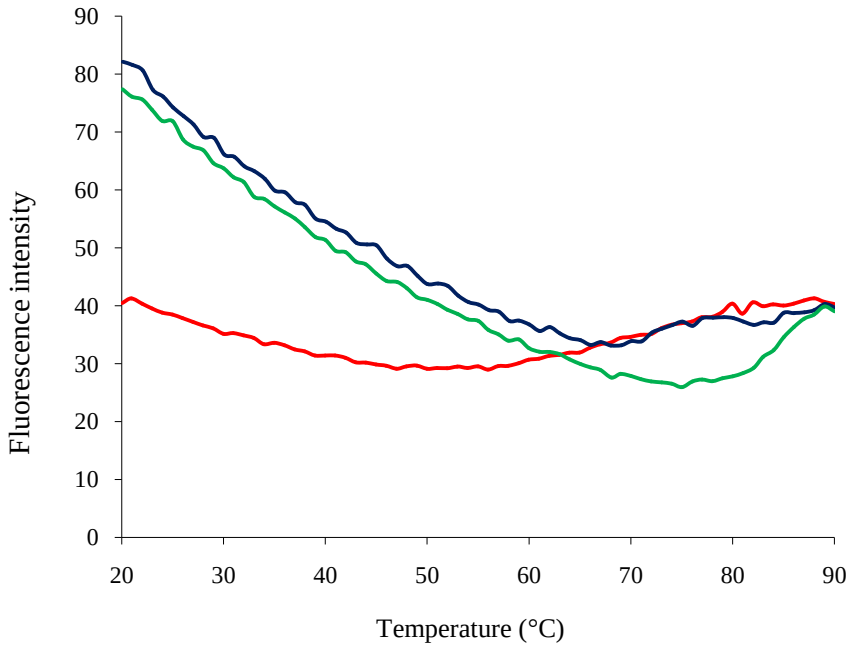

Figure 3.15. Fluorescence melting curve for the RNA oligonucleotide PhpC-2 single-stranded (red), bound to its DNA complement (blue) and bound to its RNA complement (green). λ_{ex} = 360 nm, λ_{em} = 465 nm.

3.2.8 Fluorescent snake venom phosphodiesterase and base degradation assays

Snake venom phosphodiesterase (SVPD) is a 3' endonuclease that cuts oligonucleotides into nucleoside 5'-monophosphates. As the RNA•DNA hybrids containing PhpC and MOMpC were digested by SVPD, the fluorescence increased (Figure 3.16). This again proves that the fluorescence is decreased in the double-stranded form. There was also an initial increase in fluorescence associated with the digestion of the single-stranded oligonucleotides into smaller fragments. The degradation of the single-stranded and double-stranded PhpC-1 was also verified by base degradation in NaOH. Once the solutions containing PhpC oligonucleotides were brought to 0.1 M NaOH, all the fluorescence signals were identical (Figure 3.17). This is because the oligonucleotides were denatured under the basic conditions, and thus all formed single strands. When an equivalent amount of 0.1 M HCl was added, all the fluorescent values increased. This can be due to the formation of shorter, more fluorescent PhpC containing oligonucleotides, or PhpC itself is more emissive in acidic media.

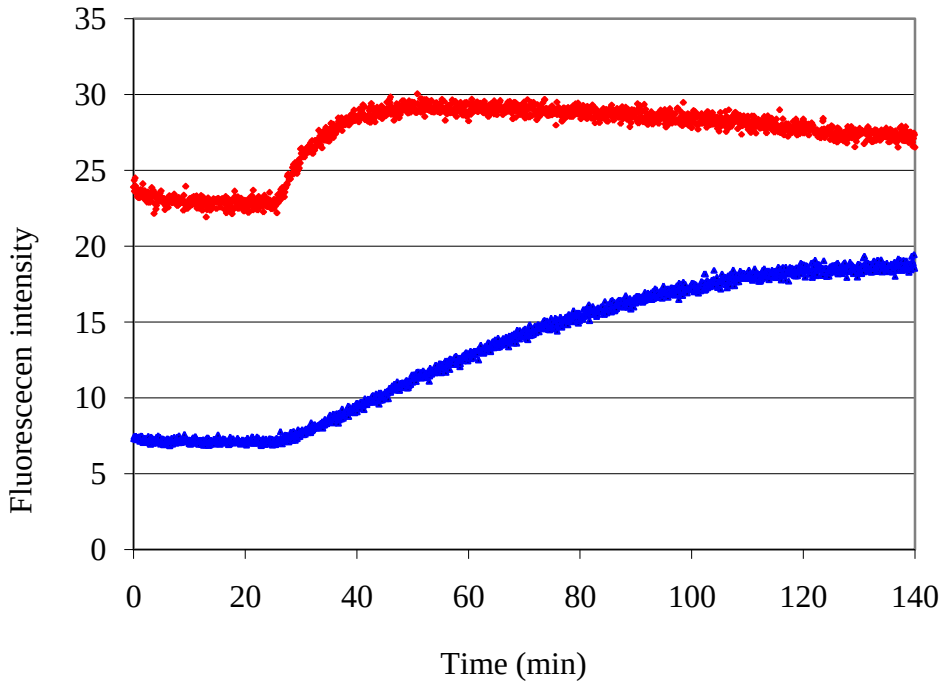

Figure 3.16. Monitoring the degradation of PhpC-1 single-stranded (red) and bound to DNA-1 (blue) by snake venom phosphodiesterase which was added to the samples at 30 minutes.

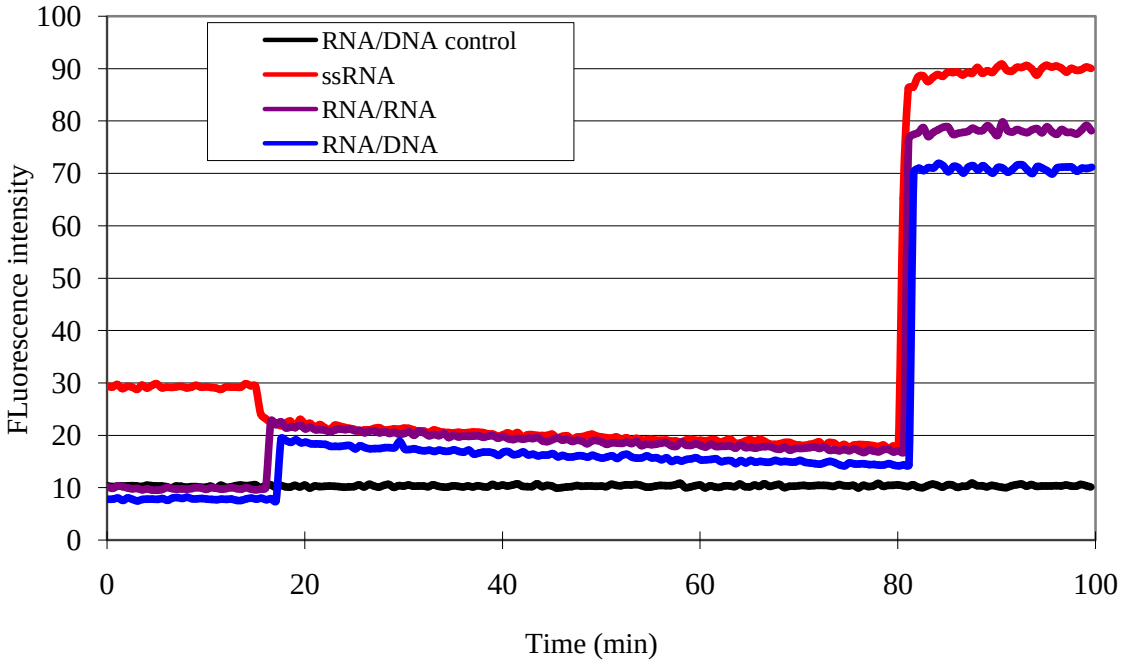

Figure 3.17. NaOH-mediated degradation of PhpC-1. 1 μM of ssRNA (red), RNA•RNA double strand (purple) and RNA•DNA double strand (blue) was brought to 0.1 M NaOH after 15 minutes, and neutralized with 0.1 M HCl after 80 minutes. An untreated control at pH 7 is also shown (black).

3.2.9 Gel-based RNase H assays

To determine their potential as fluorescent reporters in a biological context, dPhpC, PhpC, dMOMpC and MOMpC oligonucleotides were evaluated as substrates for HIV-1 RT RNase H. The dpC analogs incorporated into the DNA strand of a RNA•DNA hybrid were very well tolerated by the enzyme (Figure 3.18), unlike the FQ system which compromises enzymatic activity (Figure 3.2). Compared to the unmodified control (RNA•DNA), the DNA containing dMOMpC analogs induced RNase H catalyzed cleavage of the RNA strand at the same rate. The dPhpC DNA analogs generated cleavage products slightly slower than the other sequences under these conditions, but nonetheless most of the initial product was cut within 20 minutes. Furthermore, no aberrant cleavage products were generated as was previously observed when dMepC was incorporated into the polypurine tract of HIV-1.[284]

The RNA containing pC-analogues were also determined to be excellent substrates for HIV-1 RT RNase H activity (Figure 3.19). However, there is a noticeable drop in the rate of cleavage when the modified fluorescent residue is placed in the middle of the RNA substrate, but not when it is placed close to the 3'-terminus. In addition to cleavage by HIV-1 RT RNase H, the RNA modified strands were also good substrates for *E. coli* RNase H (gel not shown).

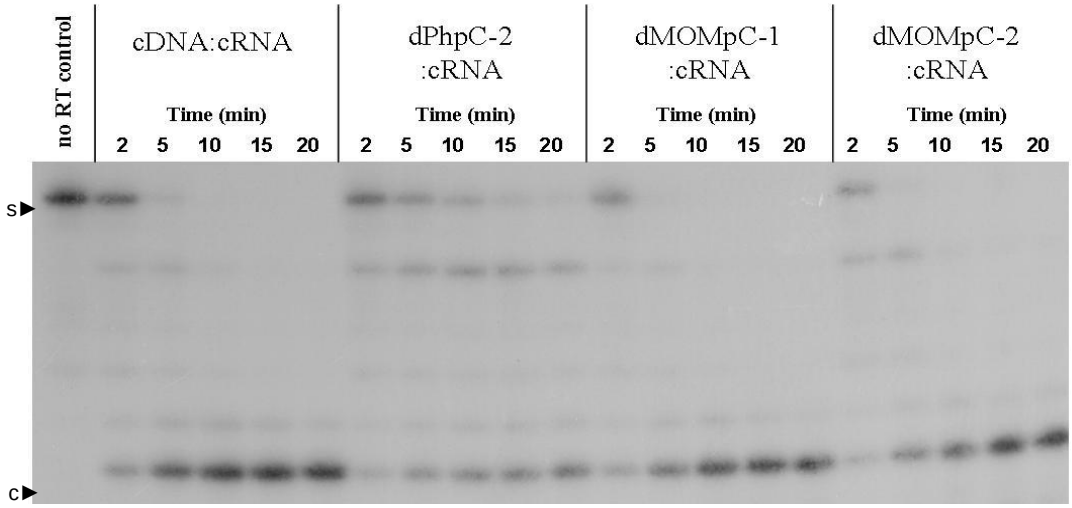

Figure 3.18. 5'-^{32}P-labeled PAGE assay for HIV-1 RT RNase H activity with dpC analogues on the DNA strand. Arrowheads indicate substrate (**s**) and major cleavage product (**c**).

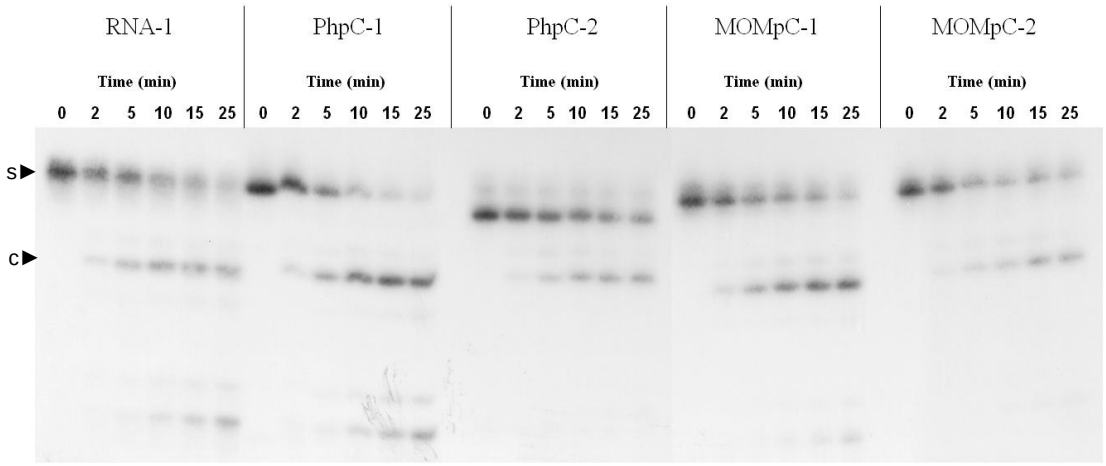

Figure 3.19. 5'-^{32}P-labeled PAGE assay for HIV-1 RT catalyzed RNase H cleavage of substrates containing a pC analog on the RNA strand. Arrowheads indicate the hybrid substrate (**s**) and major cleavage product (**c**).

3.2.10 Fluorescent RNase H assays

Since all the modified RNA•DNA hybrids proved to be substrates for HIV-1 RT RNase H, changes in their fluorescence intensities during cleavage was verified on a fluorescence spectrophotometer. Prior to initiating RNase H activity by adding $MgCl_2$, adding HIV-1 RT to the reaction mixtures with fluorescent substrates was found to have no effect on the fluorescence measurements under these assay conditions (λ_{ex} = 360 nm, λ_{em} = 465 nm for PhpC; λ_{ex} = 350 nm, λ_{em} = 455 nm for MOMpC). This indicates that the fluorescent amino acid residues in HIV-1 RT, such as tyrosine and tryptophan do not interfere with monitoring the fluorescence of PhpC. The RNA•DNA hybrids containing the fluorescent residues at the 5'-terminus of DNA (PhpC-DNA-1 and MOM-pC-DNA-1) and close to the 3'-end of RNA (PhpC-1 and MOMpC-1) showed increases in fluorescence as the RNA substrate is degraded by RNase H (Figure 3.20 and 3.21 respectively). Modifications at internal positions did not show significant changes in fluorescence intensity during cleavage (less than 10%). RNA strands PhpC-1 and MOMpC-1 showed the best responses to RNase H activity (~13 and ~4.5 fold increases respectively), than modifications on the DNA strands at the 5'-terminus (dPhpC-1~ 0.3 fold; dMOMpC-1~ 1.8 fold increases). These remarkable responses for PhpC-1 and MOMpC-1 were unexpected as they are greater increase in fluorescence than what is observed during denaturation of the

duplexes (Table 3.3). The increase in fluorescence of PhpC-1 in particular was so intense that it could be seen by the naked eye (Figure 3.22). We believe the short RNA product released upon RNase H catalyzed cleavage is more fluorescent. This is consistent with our previous observation that trinucleotides containing PhpC are significantly more fluorescent than single-stranded 18-mers (Table 3.3). Although G-PhpC-U was an exception to this trend, the product of the RNase H cleavage for this sequence is a tetramer, A-G-PhpC-U.[253] This leads us to believe that perhaps other tetramers that do not contain the G-PhpC-U trinucleotide may produce even greater fluorescence intensities. We also verified this RNase H assay at lower concentrations of PhpC-1 and MOMpC-1, and found that increasing the excitation and emission bandwidths to 10 nm improves the signal to noise ratio.

Subsequently, we compared the RNase H cleavage of PhpC-1 to the classic RNA-3'-fluorescein•DNA-5'-DABCYL (FQ) assay[251] by running them simultaneously at 1 μM substrate concentrations (Figure 3.23). We found that the FQ assay has higher fluorescence signal due to the greater brightness of fluorescein itself, but the PhpC-1 assay generated cleavage products with greater *relative* fluorescence compared to the intact substrates (13 fold vs 8 fold). As observed in gel based assays, the PhpC insert did not slow cleavage as did the FQ substrate resulting in a substantial gain in analysis time. The end point of cleavage (90% completion) was achieved in approximately 20 minutes for PhpC-1•DNA-1 versus 130 minutes for FQ.

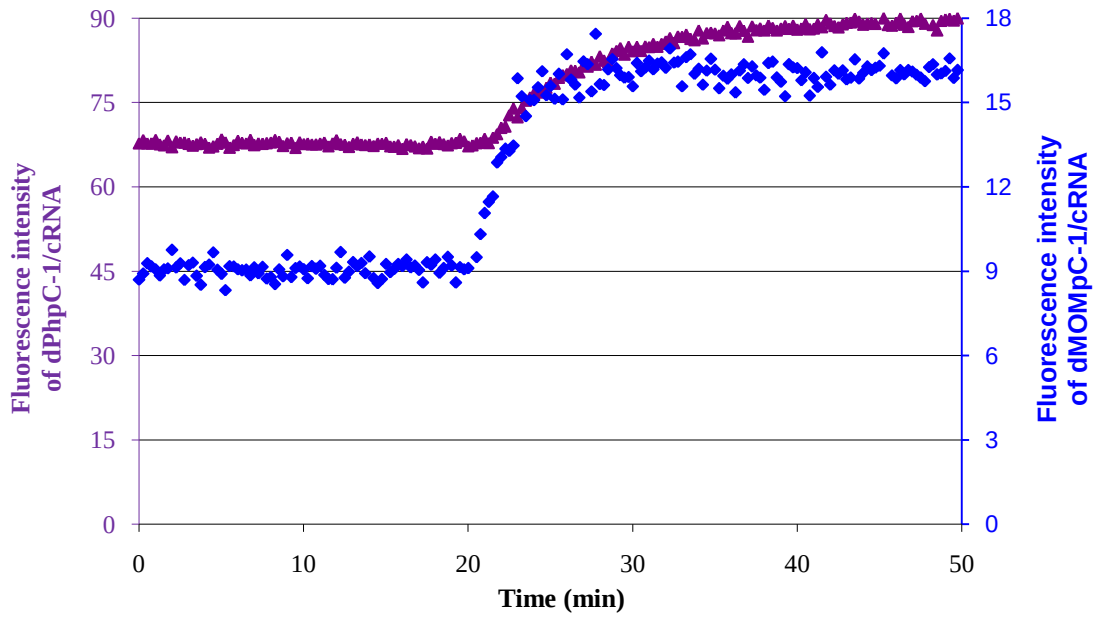

Figure 3.20. Monitoring RNase H catalyzed cleavage of 1 μM solutions of dPhpC-1•cRNA (purple triangles, λ_{exc} = 360 nm, λ_{em} = 465 nm) and dMOMpC-1•cRNA (blue diamonds, λ_{ex} = 350 nm, λ_{em} = 455 nm). HIV-1 RT was added after 10 minutes (25 nM final concentration) and $MgCl_2$ was added after 20 minutes (5 mM final concentration).

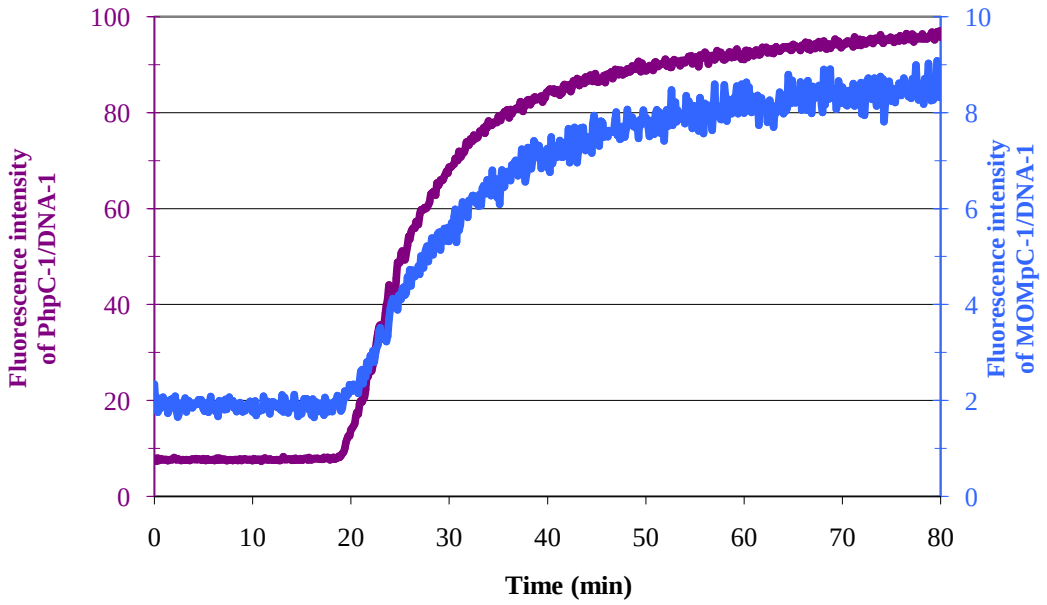

Figure 3.21. Monitoring RNase H catalyzed cleavage of 1 μM solutions of PhpC-1•DNA-1 (purple curve, λ_{exc} = 360 nm, λ_{em} = 465 nm) and MOMpC -1•DNA-1 (blue curve, λ_{ex} = 350 nm, λ_{em} = 455 nm). HIV-1 RT was added after 10 minutes (25 nM final concentration) and $MgCl_2$ was added after 20 minutes (5 mM final concentration).

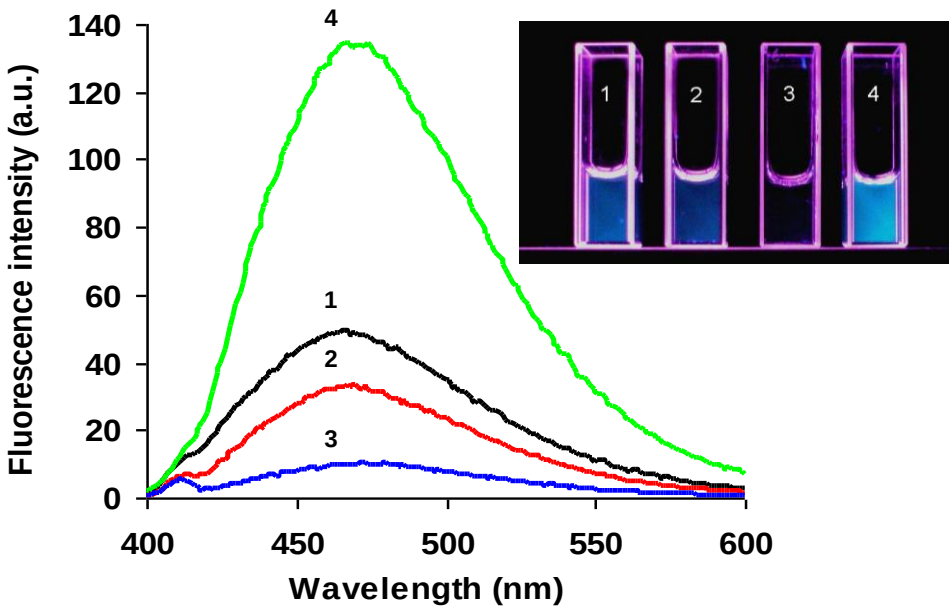

Figure 3.22. Fluorescence emission spectra of PhpC nucleotide (1, black), PhpC-1 single-stranded (2, red), PhpC-1•DNA-1 duplex (3, blue) and PhpC-1•DNA-1 after RNase H cleavage by HIV-1 RT (4, green). Visual changes in fluorescence of the same solutions under UV_{365} light, at 1 μM concentration (inset).

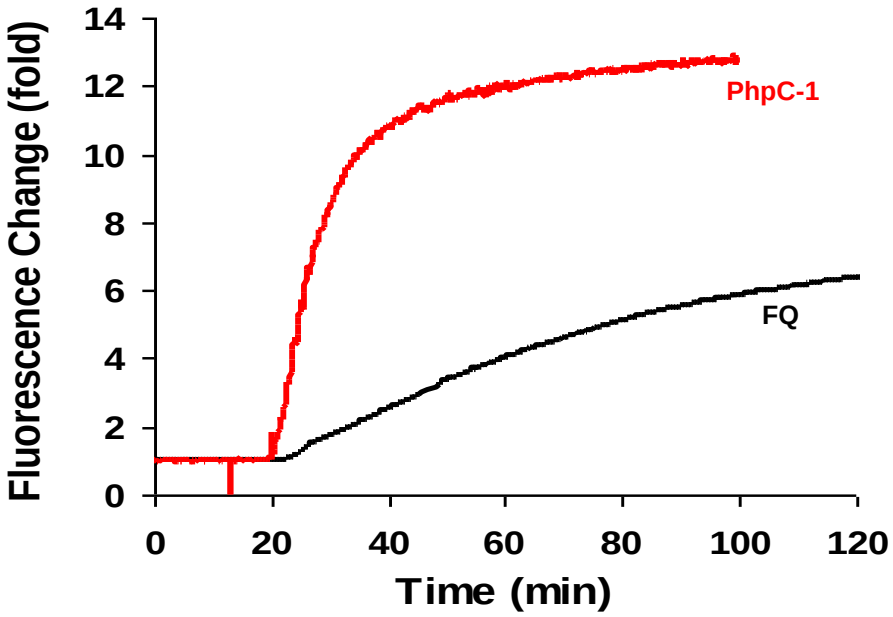

Figure 3.23. Comparison of the PhpC-1 RNase H assay (red curve) compared to the classic fluorescein-DABCYL (FQ) assay (black curve). Both substrates were treated with HIV-1 RT RNase H activity simultaneously in identical conditions at a concentration of 1 μM scanning at the λ_{max} excitation and emission for both fluorescein (485 nm/520 nm) and PhpC (360 nm/465 nm).

3.2.11 Fluorescence Polarization RNase H Assays

An advantage of incorporation of the fluorescent nucleoside into the RNA strand is that it gets processed by RNase H into fragments that are much smaller than the hybrid duplex. The substantial change in mass/size of the fluorescent moiety may be detected by changes in fluorescence polarization (FP).[321] As seen in Table 3.3, FP values increase with increasing molecular weight as expected for molecules undergoing less Brownian motion. RNase H catalyzed cleavage of PhpC-1•DNA-1 was readily monitored in real-time by FP (Figure 3.24) in a similar fashion to the RNase H assay developed by Pfizer.[252]

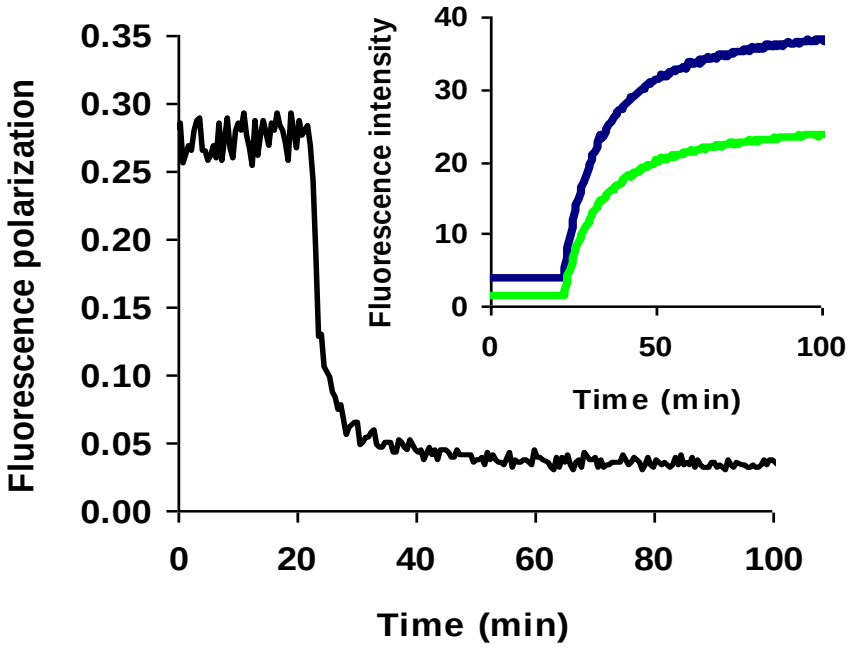

Figure 3.24. Monitoring the RNase H activity of HIV-1 RT on PhpC-1•DNA-1 by fluorescence polarization (black curve). The inset shows the fluorescence intensity with the excitation and emission polarizers parallel (blue curve) and perpendicular (green curve).

To test this further, we verified if the RNase H catalyzed degradation of duplex PhpC-2•DNA-1 can be monitored by FP, since this was not possible by measuring fluorescence intensity. We found that HIV-1 RT RNase H could not cut PhpC-2 to fragments smaller than a 10-mer, so *E. coli* RNase H was added to the reaction (Figure 3.25). Since *E. coli* RNase H can cut RNA into smaller fragments than HIV-1

RT,[336] the degradation of PhpC-2 was soon detected by FP even though the fluorescence intensity did not change very significantly (12% increase at endpoint). Nonetheless, FP enabled us to monitor the cleavage of the RNA strand at a central position using an embedded PhpC.

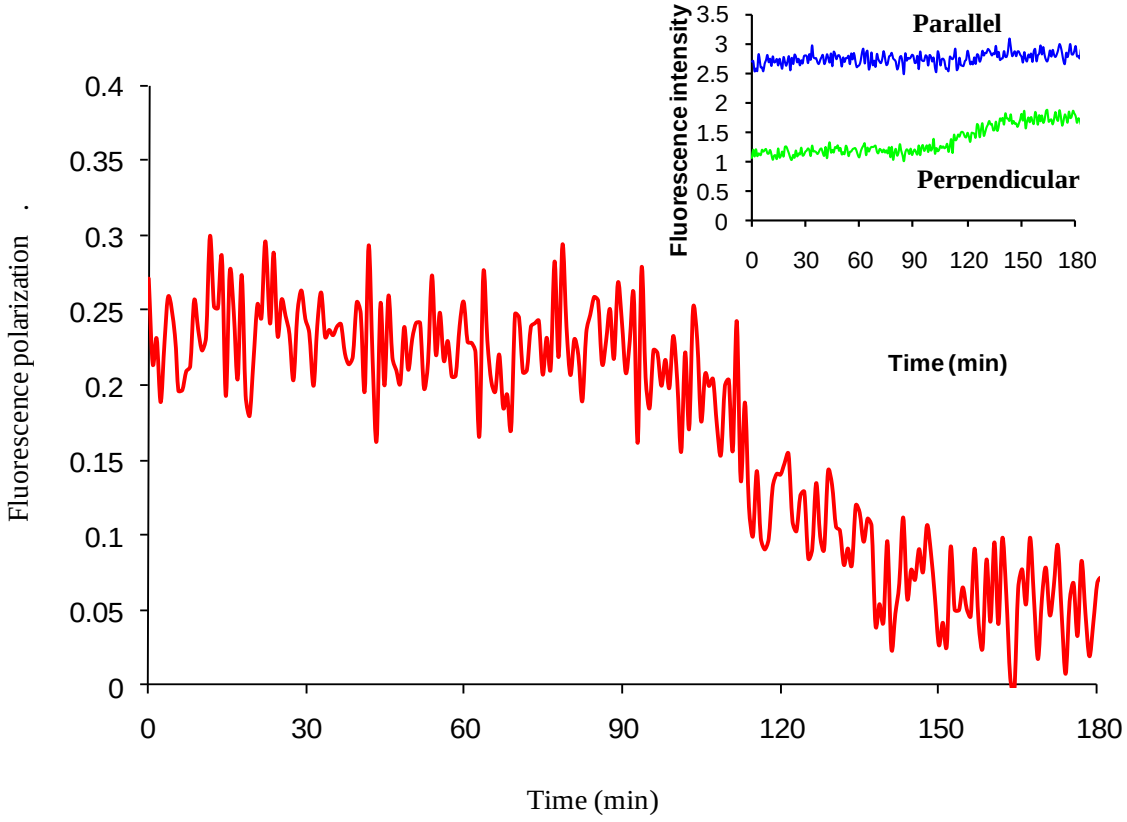

Figure 3.25. Monitoring the RNase H activity of HIV-1 RT from 0-80 minutes and *E. coli* RNase H from 80-180 minutes on PhpC-2•DNA-1 (200 nM) by fluorescence polarization (black curve). The inset shows the fluorescence intensity with the excitation and emission polarizers parallel (blue curve) and perpendicular (green curve).

3.2.12 RNase H Assays on 96-well microplates

Although fluorescent spectrophotometers are far more sensitive, it is desirable to adapt assays to fluorescent microplate readers that are amenable to HTS. Since PhpC-1 was the most fluorescent and responsive substrate for RNase H activity, it was tested in 96-well plate spectrofluorometers by fluorescence intensity and fluorescence polarization (Figure 3.26). Using identical reaction conditions used in the cuvettes (1 μM substrate and 25 nM HIV-1 RT), Figure 3.26A shows very good

signal to noise and response to RNase H cleaveage (10 fold increase). We later tested the limits of sensitivity of the assay and found we could still monitor RNase H activity down to 10 nM substrate concentration (60 nM in FP mode), which is comparable to ^{32}P PAGE assays. For application of this assay to screen inhibitors of RNase H activity, it is advantageous to monitor polarization as well as fluorescence intensity. FP can discern molecules that quench the fluorophore producing false hits.[252] We show that RNase H activity can be monitored on a 96-well plate by fluorescence polarization (Figure 3.26B).

With the versatility of PhpC we have demonstrated that both fluorescence intensity (which reports on hybridization/base stacking) and fluorescence polarization (which reports on the size of the molecule containing the fluorophore) can be monitored simultaneously using only one probe.

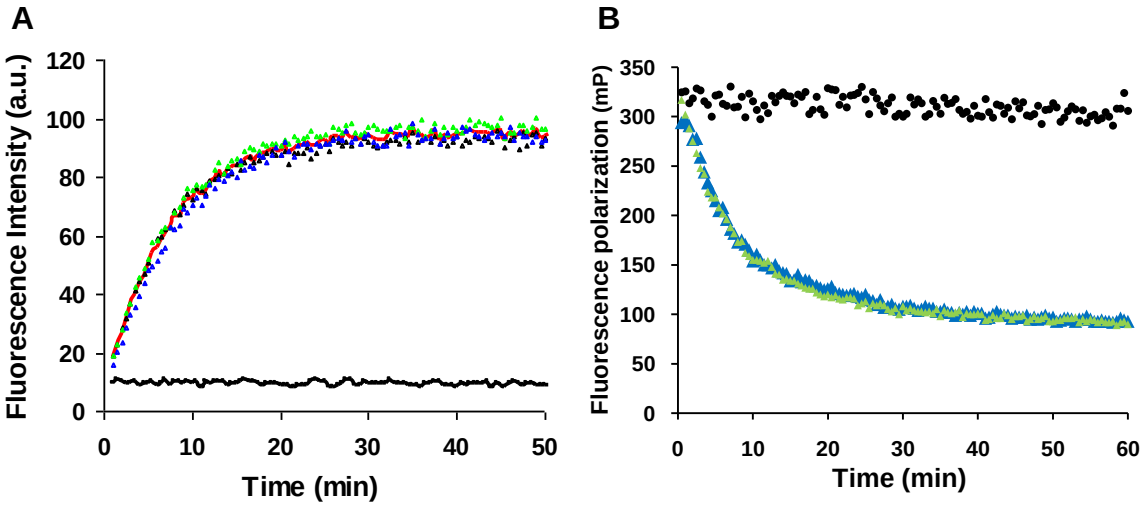

Figure 3.26. **A**. Fluorescence intensity HIV-1 RT RNase H assay of 1 μM PhpC-1•DNA-1 monitored by a 96-well plate spectrofluorometer. Colored triangles represent reactions in three individual wells, with the red curve representing their average. The average of three controls without enzyme is represented by the black curve. **B**. Fluorescence polarization HIV-1 RT RNase H assay of 1 μM PhpC-1•DNA-1 monitored by a 96-well plate spectrofluorometer. The green and light blue curves represent the reaction with HIV-1 RT added, and the black curve represents the average of two control wells without HIV-1 RT.

We determined the kinetic parameters K_m (54 +/- 3.3 nM), V_{max} (0.31 nmoles/min), and a k_{cat} of 6 min^{-1} of duplex PhpC-1•DNA-1 for HIV-1 RT RNase H (Figure 3.27). Since this assay will ultimately be used to screen potential inhibitors of RNase H, a

known inhibitor of HIV-1 RT RNase H, namely DHBNH, was tested in this assay. Our assay demonstrated that DHBNH was able to inhibit RNase H activity in a dose dependant manner with an IC_{50} of 5 μM, which is consistent with previous results (Figure 3.28).[248]

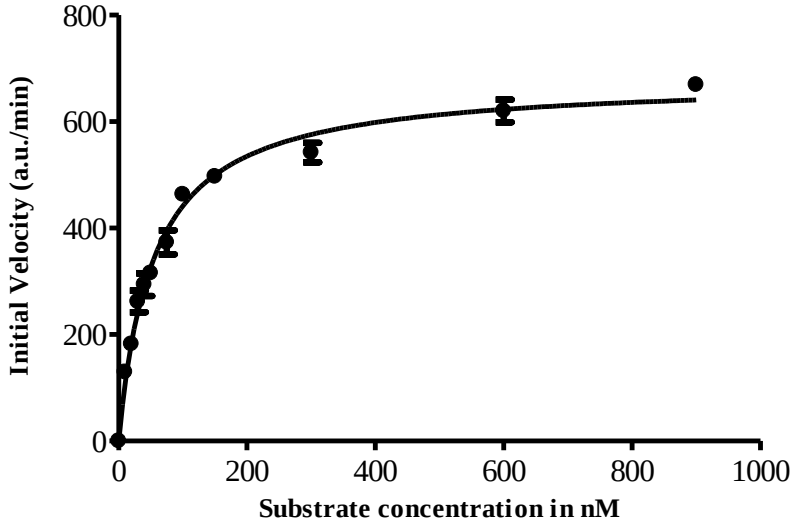

Figure 3.27. Michaelis-Menten plot of initial velocity versus substrate concentration. Initial velocities were measured in triplicates and the data fitted in Prism 5.0.

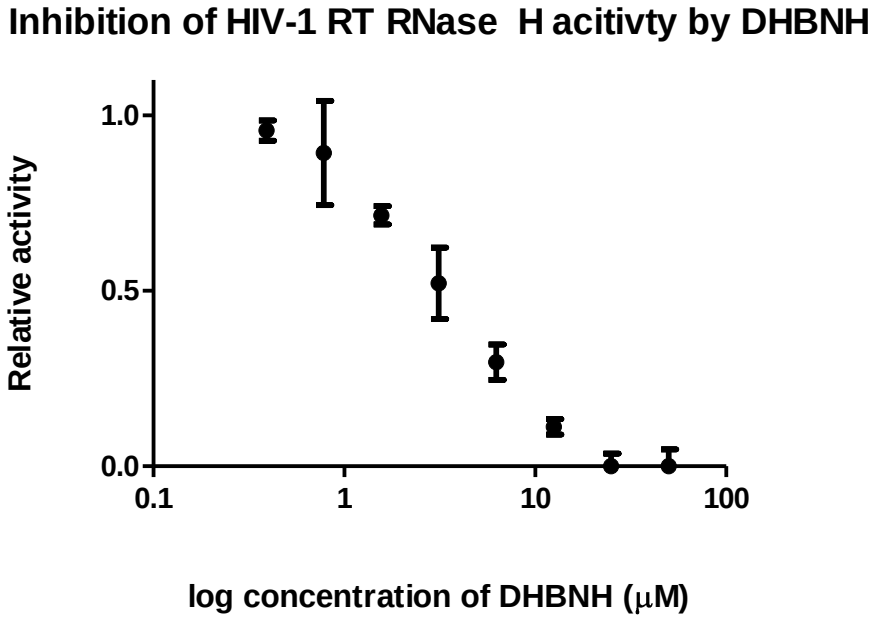

Figure 3.28. Dose-response curve of the inhibition of DHBNH for the RNase H activity of HIV-1 RT. The IC_{50} and curve was generated using Prism 5.0.

3.3 Conclusion and Future Directions

This work demonstrates the significant advantages of base-modified nucleosides, such as PhpC, compared to traditional fluorophores: one single PhpC insert can act as a sensitive reporter group that is non-disruptive to the structure and enzymatic activity. Although fluorescein is a substantially brighter luminophore, the PhpC–based assay for RNase H has clear advantages. The responsiveness, rapidity and ease (single label versus dual) of the RNase H assay has been dramatically improved. The fluorescence provided by PhpC is sufficient to compete with gel-based techniques on the basis of sensitivity and the assay can be adapted to multi-well plate format for HTS. This was also possible because the HIV-1 RT RNase H cleavage product showed remarkably greater fluorescence than even the free nucleoside. Overall, this report lays the framework for a sensitive and rapid assay for detecting inhibitors of RNase H. Work is currently under way to employ this assay to screen a small molecule library for such agents. Future work will look at utilizing PhpC in an assay to assess the capacity for antisense oligonucleotides to elicit RNase H activity. PhpC could be of great use as a fluorescent reporter to monitor the activity of other nucleic acid modifying enzyme, such as polymerases, much like the work of Kool and co-workers.[310] The synthesis of PhpC 5'-triphosphates would be required for these studies.

Also uncovered in this study, was the surprising and unprecedented observation that oligomer PhpC-2 showed an increase in fluorescence intensity upon duplex formation. We also noted that PhpC can monitor changes in its environment in single-strands in addition to double strands by fluorescent thermal denaturation studies. Together, these observations indicate that PhpC is significantly different from pC and warrants further investigation on the affects of sequence length and composition on changes in fluorescence. Studies should also be carried out to access the influence of pH on the intensity of fluorescence emission of PhpC. Work is currently underway to synthesize other fluorescent analogs of PhpC with greater quantum yields and more red-shifted excitation-emission. We feel that PhpC will contribute to the growing repertoire of useful fluorescent nucleobase analogues, such as tricyclic C and its analogues (tC and tC^o), which also show red-shifted

fluorescence and a high quantum yield (Φ=0.3) but whose fluorescence is insensitive to duplex formation.[337] Thus, encountering PhpC analogs that are insensitive to their microenvironment could also be of benefit.

3.4 Experimental methods

3.4.1 General methods

Chemicals and solvents were ACS grade or higher and were purchased from Sigma-Aldrich or Thermo-Fisher. Anhydrous pyridine was obtained by distilling over calcium hydride. All reagents used for oligonucleotide synthesis, including 2'-deoxyribonucleotide and 2'-tert-butyldimethylsilyl (TBDMS) ribonucleoside 3'-O-phosphoramidites, were purchased from Chemgenes Corp. Autoclaved Millipore water treated with diethylpyrocarbonate (DEPC)[290] was used to manipulate RNA and prepare aqueous buffers.

3.4.2 Phosphoramidite synthesis and characterization

5'-*O*-(4,4'-Dimethoxytrityl)-2'-*O*-*tert*-butyldimethylsilyl-6-phenylpyrrolocytidine: To a 25 ml round-bottom flask containing 315 mg (0.48 mmol) of compound 5'-*O*-(4,4'-Dimethoxytrityl)-6-phenylpyrrolocytidine dissolved in 2 ml of dry DMF, TBDMS-Cl (88 mg, 0.58 mmol) and imidazole (82 mg, 1.2 mmol) was added and stirred overnight. The formation of the 2'-*O*-silyl and 3'-*O*-silyl products were monitored by TLC (R_f values of 0.56 and 0.13 respectively in 1:3 ethyl acetate:dichloromethane) until the starting material was consumed. The reaction was worked-up in 5% $NaHCO_3$, filtered over $MgSO_4$ and evaporated to dryness. The 2'-*O*-silyl regioisomer was obtained by silica gel column chromatography using a gradient of hexanes-ethyl acetate from 1:3 to 1:1 keeping 1% triethylamine in the solvents. The remaining crude 2'-regioisomer and 3'-regioisomer were mixed for 2 hours in 5 ml of pyridine and 3 drops of water to form an equal mix of isomers. From this mix, the 2'-regioisomer was again purified by silica gel and both purified fractions were evaporated over high vacuum to give 213 mg of a yellow powder (58% yield). ^{1}H NMR (500 MHz, DMSO) δ = 11.76 (s, 1H), 8.75 (s, 1H), 7.61 (d, *J*=7.6, 2H), 7.47 – 7.10 (m, 16H), 6.92 (d, *J*=4.1, 4H), 5.78 (s, 1H), 5.41 (s, 1H), 5.20 (d, *J*=6.1, 1H), 4.37 (s, 1H), 4.15 (s, 1H), 4.11 (d, *J*=8.3, 1H), 3.70 (d, *J*=6.6, 7H), 3.45

(dd, *J*=9.9, 58.4, 2H), 0.89 (s, 9H), 0.15 (s, 3H), 0.10 (s, 3H) ppm. ^{13}C NMR (126 MHz, DMSO) δ = 160.38, 158.89, 158.84, 154.53, 144.68, 139.67, 136.79, 136.67, 136.35, 135.72, 130.82, 130.70, 130.54, 130.31, 129.70, 129.53, 128.74, 128.58, 127.53, 125.43, 125.31, 114.10, 114.01, 109.63, 97.04, 92.40, 92.28, 86.88, 82.06, 81.95, 77.58, 77.46, 68.37, 61.76, 55.76, 55.62, 26.45, 26.41, 18.66, -4.12, -4.20 ppm. ESI-TOF (m/z) 782.4 (M+Na).

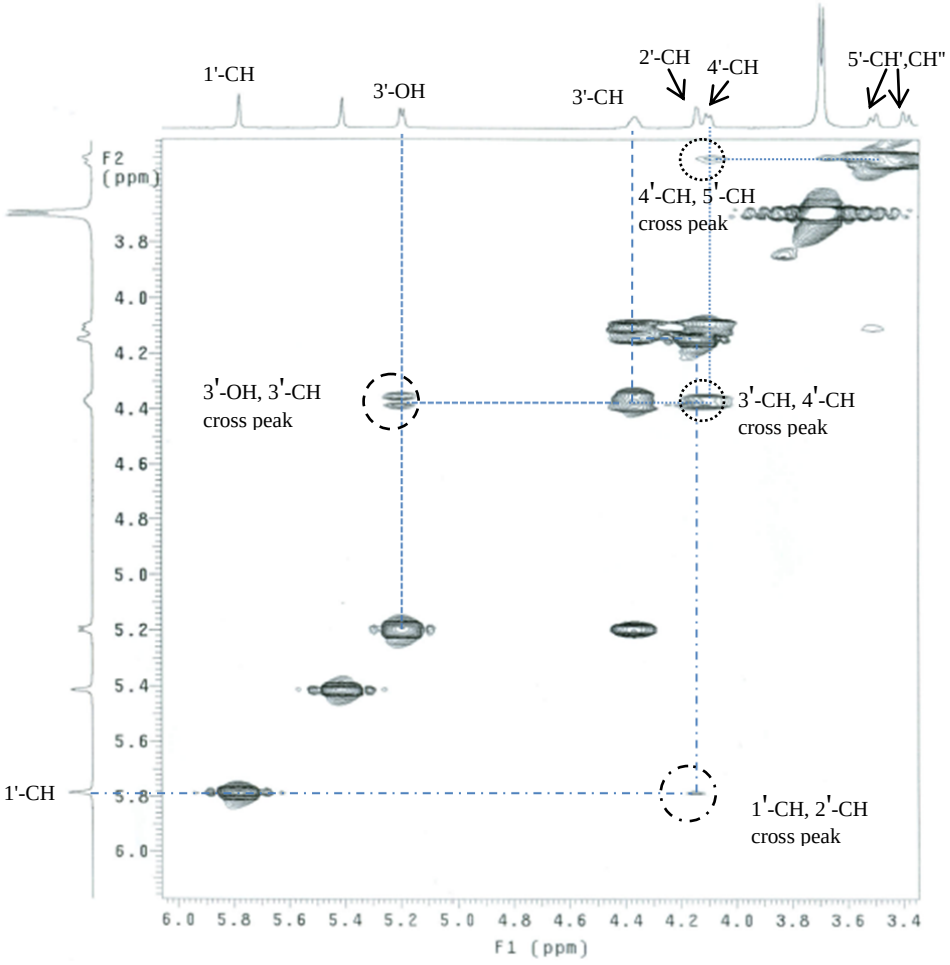

Figure 3.29 ^{1}H 2-D COSY NMR of 5'-*O*-(4,4'-Dimethoxytrityl)-2'-*O*-*tert*-butyldimethylsilyl-6-phenylpyrrolocytidine. Peaks representing sugar protons are indicated on the F1 axis, and proton-proton cross peaks are circled. The three bond coupling between the 3' C-H and 3' O-H suggests the TBDMS group is on the 2' oxygen.

5'-*O*-(4,4'-Dimethoxytrityl)-2'-*O*-*tert*-butyldimethylsilyl-3'-*O*-(2-cyanoethyldiisopropylphosphoramidite)-6-phenylpyrrolocytidine: 5'-*O*-(4,4'-Dimethoxytrityl)-2'-*O*-*tert*-butyldimethylsilyl-6-phenylpyrrolocytidine (213 mg, 0.28

mmol) was sublimed in 3 ml of distilled benzene over dry ice on high vacuum overnight, purged with argon and dissolved in freshly distilled THF. Dry diisopropylethylamine (0.2 ml, 1.12 mmol) and diisopropylamino-(2-cyanoethyl)-phosphoramidic chloride (63 μl, 0.28 mmol) were added and the reaction was stirred for two hours and monitored by TLC (5% methanol in dichloromethane). At the end of this time, the reaction was washed with 5% $NaHCO_3$, dried over sodium sulphate and loaded on a silica gel column neutralized in 2.5 % triethylamine in hexane. The purified phosphoramidite diastereomers were eluted in 6:4 hexane-ethyl acetate, rotary evaporated and sublimed in 3 ml of distilled benzene overnight to yield a yellow foam (240 mg, 89 % yield). ^{31}P NMR (200 MHz, CD_3CN) δ= 151.3 (s, 1P), 149.5 (s, 1P) ppm. ESI-TOF (m/z) 982 (M + Na).

5'-*O*-(4,4'-Dimethoxytrityl)-2'-*O*-*tert*-butyldimethylsilyl-3'-*O*-(2-cyanoethyldiisopropylphosphoramidite)-6-methoxymethylpyrrolocytidine: 5'-*O*-(4,4'-Dimethoxytrityl)-2'-*O*-*tert*-butyldimethylsilyl-6-methoxymethylpyrrolocytidine (100 mg, 0.14 mmol) was sublimed in 3 ml of distilled benzene over dry ice on high vacuum overnight and purged with argon, and dissolved in freshly distilled THF. Dry diisopropylethylamine (0.1 ml, 0.6 mmol) and diisopropylamino-(2-cyanoethyl)-phosphoramidic chloride (32 μl, 0.14 mmol) were added and the reaction was stirred for two hours and monitored by TLC (5% methanol in dichloromethane). At the end of this time, the reaction was washed with 5% $NaHCO_3$, dried over sodium sulphate and loaded on a silica gel column neutralized in 2.5 % triethylamine in hexane. The purified phosphoramidite diastereomers were eluted in 6:4 hexane-ethyl acetate, rotary evaporated and sublimed in 3 ml of distilled benzene overnight to give a yellow crusty foam (30 mg, 24 % yield). ^{31}P NMR (200 MHz, CD_3CN) δ= 149.9 (s, 1P) ppm. ESI-TOF: m/z 966.2 $[M + K]^+$

3.4.3 Synthesis and purification of oligonucleotides

All reagents used for oligonucleotide synthesis, including 2'-deoxyribonucleotide and 2'-*O*-TBDMS ribonulceotide phosphoramidtes, were purchased from Chemgenes Corp. Solid-phase synthesis of oligonucleotides was carried out on an Applied Biosystems 3400 DNA synthesizer using standard protocols.[205] Coupling yields for PhpC were comparable to standard 2'-*O*-TBDMS ribonulcleoside phosphoramidites

based on analytical denaturing PAGE (Figure 3.5). Cleavage from the solid-support was carried out in a 3:1 mixture of NH_4OH:EtOH at room temperature for 48 hours, and removal of the 2'-*O*-silyl protecting groups was achieved by treatment with distilled triethylammonium trihydrofluoride for 48 hours. The crude, deprotected oligonucleotides were precipitated in ice-cold butanol and 3M sodium acetate and quantitated by their UV absorbance at 260 nm on a Cary-300 UV-VIS spectrophotometer (Varian Inc). Crude products were then analyzed and purified by denaturing PAGE (7M urea) and visualized by UV shadowing using 254 nm light for non-fluorescent oligonucleotides, and 365 nm light for fluorescent oligonucleotides (Figure S1). Full length products were excised from the gels using a sterile surgical blade, and eluted in DEPC treated water. The eluted products were desalted by size-exclusion chromatography on G-25 Sephadex (GE Healthcare) and quantitated.

3.4.4 Thermal denaturation curves

For UV-Vis thermal denaturation experiments nucleotides and oligonucleotides were analyzed in 1 ml solutions at 1 μM concentrations in a buffer of 10 mM sodium phosaphate at pH 7.0 and 50 mM NaCl. Double-stranded oligonucleotides were annealed in equimolar amounts by heating to 95°C and then slowly cooling to room temperature on a heating block. Thermal denaturation experiments were performed on a Cary -300 UV-Vis spectrophotometer (Varian Inc.) equipped with a 6x6 cell changer and Peltier temperature controller. Samples were heated from 10°C to 95°C at a rate of 0.5°C per minute and the change in absorbance was measured every 1.0°C. The melting temperature (T_m) values were obtained by the baseline (alpha) method, and defined as the point when the mole fraction of duplex was equal to 0.5. These values represent the averages of at least three independent experiments. Fluorescent thermal denaturation plots were obtained in a similar fashion on a Cary Eclipse fluorescent spectrophotometer equipped with a multi-cell Peltier temperature controller and automated polarization accessories. Measurements for fluorescent experiments were carried out in 1 cm x 1 cm quartz cells in 2 ml volumes and 1 μM concentration of oligonucleotides

3.4.5 Circular dichroism spectra

Circular dichroism spectra were obtained using a Jasco J-800 spectropolarimeter. Samples were prepared in the same fashion as with T_m experiments. Scans were performed in triplicate at 20°C at a rate of 50 nm per minute from 350 nm to 190 nm. The data was averaged, corrected against a blank and smoothed using the Spectra Manager CD software provided by the manufacturer.

3.4.6 Fluorescent Measurements

Fluorescence intensity and polarization measurements and fluorescent thermal denaturation plots were obtained on a Cary Eclipse Spectrophotometer equipped with a multi-cell Peltier temperature controller and automated polarization accessories. Measurements were carried out in 1 cm x 1 cm quartz cells in 2 ml volumes. Excitation and emission bandwidths were set at 5 nm for all experiments. Emission spectra were obtained by exciting at 360 nm for PhpC and 350 nm for MOMpC and monitoring the emission from 400 to 600 nm. Fluorescent thermal denaturation plots were obtained in a similar fashion on a Cary Eclipse fluorescent spectrophotometer equipped with a multi-cell Peltier temperature controller and automated polarization accessories. Measurements for fluorescent experiments were carried out in 1 cm x 1 cm quartz cells in 2 ml volumes and 1 μM concentration of oligonucleotides.

3.4.7 Qauntum yield determination

The measurement of fluorescence quantum yields (Φ_f) was determined using 9,10-Diphenylanthracene in ethanol (Φ_f=0.95) as a reference standard. The quantum yield of the unknown Φ(x) can be calculated by the following equation:

$$\Phi_{(x)} = \Phi_{(ST)} (A_{ST}/A_X) (F_X/F_{ST}) (\eta^2_X/\eta^2_{ST})$$

Where $\Phi_{(ST)}$ is the quantum yield of the standard, A is the absorbance at the excitation wavelength, F is the integrated area in the emission curve, the subscripts X and ST refer to unknown and standard and η is the refractive index of the solvent. When measuring a series of diluted solutions with various absorbance readings the following equation may be used:

$$\Phi_{(x)} = \Phi_{(ST)} (Grad_X/Grad_{ST}) (\eta^2_X/\eta^2_{ST})$$

Where Grad is the gradient from the plot of integrated area in the emission curve versus absorbance at the excitation wavelength.

UV_{370} was measured on a Cary -300 UV-Vis spectrophotometer (Varian Inc.) from 0.1 to 0.03 absorbance units in 0.01 increments. The fluorescence emission curves were immediately measured afterwards in a Cary Eclipse (Varian Inc.) fluorescent spectrophotometer with an excitation wavelength of 370 nm. Prior to measuring the quantum yield of the unknown samples, the validity of the methodology was confirmed by measuring the quantum yield of anthracene in ethanol which gave a value of 0.27, which is in good agreement with the literature value (Φ_f=0.29).

3.4.8 Gel based RNase H assays

Wild type p66/p51 HIV-1 RT was a generous gift from Dr. Matthias Götte (McGill) prepared by his group as previously described.[52] RNA substrates were 5'-radiolabeled with γ-^{32}P ATP by T4 polynucleotide kinase (Fermentas) using the manufacturer's recommended procedure. The antisense and 5'-^{32}P-labeled RNA sense strands were combined in a 1.2:1 ratio and annealed by heating to 95°C followed by slow cooling to room temperature. HIV-1 RT (2.5 nM final concentration) was incubated for 10 minutes at 37°C in RNase H reaction buffer (50 mM Tris-HCl, pH 7.8, 60 mM KCl, 5 mM $MgCl_2$, 0.1 mM DTT and 0.01% Tween-20). The reactions were initiated by the addition of duplexed antisense/sense substrate to a concentration of 50 nM. Aliquots were removed at various times as indicated in Figure S7 and stopped by the addition of an equal volume of loading buffer (98% deionized formamide, 1 mg/mL bromophenol blue, and 1 mg/mL xylene cyanol) followed by heat inactivating at 95°C for 5 min. Cleavage products were resolved on a 16% denaturing polyacrylamide gel and visualized by autoradiography.

3.4.9 Fluorescent RNase H assays

HIV-1 RT RNase H activity was monitored by the changes in emission of fluorescent oligonucleotides on a Cary Eclipse fluorescent spectrophotometer equipped with a multi-cell Peltier temperature controller and automated polarization accessories. These assays were run in 2 mL volumes in identical buffer conditions as the gel based assays, but were initiated by the addition of $MgCl_2$ (5 mM final

concentration) in order to monitor fluorescence prior to cleavage by HIV-1 RT. Substrate concentrations varied from 1 μM to 0.2 μM and enzyme concentrations were changed to 25 nM or 5 nM respectively. The fluorescence intensity was monitored every 15 seconds. PhpC RNase H assays were monitored at an excitation wavelength of 360 nm (5 nm bandwidth) and emission wavelength of 465 nm (5 nm bandwidth). The fluorescein-RNA•DABCYL-DNA pair was monitored at an excitation wavelength of 485 nm (5 nm bandwidth) and emission wavelength of 520 nm (5 nm bandwidth). Fluorescence polarization RNase H assays were run under identical conditions as stated above.

The equation to calculate fluorescence polarization (P) as described by the Cary Eclipse follows:

$P = (I_{vv} – GI_{vh}) / (I_{vv} + GI_{vh})$

where

I_{vv} equals the intensity of fluorescence with the excitation polarizer = vertical and emission polarizer = vertical

I_{vh} equals the intensity of fluorescence with the excitation polarizer = vertical and emission polarizer = horizontal.

G is a factor that accounts for the polarization bias of the instrument and is calculated automatically before the experiment.

The G factor is given by:

$G = I_{hv}/I_{hh}$

3.4.10 Snake venom phosphodiesterase assays

Snake Venom Phosphodiesterase (SVPDE) Assays: Assays were performed in a Cary Eclipse Fluorescent Spectrophotometer equipped with a multi-cell Peltier temperature controller. 1 μM solution of the oligonucleotide was prepared in SVPDE buffer (100 mM Tris-HCl, pH 8.9, 100 mM NaCl, 14 mM $MgCl_2$) Samples were monitored for 30 minutes at 37 °C, after which 2.5 units of Snake venom phosphodiesterase I from *Crotalus admanteus* venom (USB Corporation) was added. Changes in fluorescence were monitored as described for RNase H assays.

3.4.11 Base degradation assays

Assays were performed in a Cary Eclipse Fluorescent Spectrophotometer equipped with a multi-cell Peltier temperature controller. A 1 μM solution of the ribo-oligonucleotide was prepared in water. Samples were monitored for 10 minutes at 37 °C, after which 200 μl NaOH was added to a final concentration of 0.1 mM. Changes in fluorescence were monitored as described for RNase H assays. After 80 minutes 200 μl of 1 M HCl was added

3.4.12 Fluorescent RNase H assays on 96-well microplates

RNase H activity of HIV-1 RT was monitored on a Gemini XS and M5 spectrofluorometers by Molecular Devices in 96-half well opaque plates. Fluorescence polarization measurements in 96-well microplates were performed on a BioTek Synergy 4. Experiments were run under identical buffer conditions as gel-based assays in a final volume of 100 μL. Reactions were initiated by the addition of a 50 μL solution containing HIV-1 RT and $MgCl_2$. The concentration of substrate was varied from 1 μM to 10 nM, and enzyme concentrations varied from 25 nM to 5 nM respectively. Excitation and emission wavelengths for PhpC were 360 nm and 465 nm respectively, and 485 nm and 520 nm for the DABCYL•fluorescein assay. To determine Km, Vmax and Kcat, the initial velocity of RNase H cleavage was measured under a fixed concentration HIV-1 RT (1 nM) and the substrate concentration was varied from 10 nM to 900 nM. The IC_{50} of DHBNH, a sample of which was generously provided by Dr. M.A. Parniak, was determined on two separate days and was run in triplicate using 200 nM substrate and 1.5 nM HIV-1 RT in 1% DMSO. Eight concentrations of DHBNH were dispensed by two-fold serial dilutions starting from 50 μM of the inhibitor.

Chapter 4 Incorporation of phenylpyrrolocytidine into siRNA: a molecular spy to monitor activity and biodistribution

4.1 Introduction

4.1.1 Chemical modifications to address the therapeutic shortcomings of siRNA

The discovery that double-stranded small interfering RNA (siRNA)[128] can selectively silence a gene in a process called RNA interference (RNAi)[123] has led to massive efforts in industry and academia to use this natural pathway for therapeutic applications. siRNAs that elicit the sequence specific degradation of complementary mRNA have routinely been shown to arrest the expression of a gene at nanomolar concentrations *in vitro*. However, for a relatively large negatively charged biological molecule such as RNA to perform *in vivo* it must first overcome many hurdles. RNA generally functions as a transient entity or is a marker of viral infections and there are many enzymes to ensure its destruction inside and outside the cell. As such siRNAs typically have a serum half-life on the order of minutes.[338] Even if they do survive these conditions, siRNAs have no method to ensure their delivery to the desired site of action. In addition, siRNAs can activate the immune system's inflammatory response by causing the release of cytokines through the NF-κB pathway by triggering Toll-like receptors.[339,340] This may exaggerate the silencing capabilities of siRNAs in a clinical setting[5] and furthermore cause immunotoxicity.[341] Finally, sequence specific off-target effects can arise from RISC loading the passenger strand (sense strand) as a guide strand (antisense strand). In brief, although RNAi is very potent and has the potential to turn-off disease-causing genes, unmodified RNA is not suitable for the development as a drug.

Chemical modifications can resolve many of the shortcomings of RNA by bestowing drug-like properties to siRNAs without compromising biological activity.[124,342] Modifications to the sugar-phosphate backbone is a common approach to increase the stability of therapeutic oligonucleotides in biological media. Of note are 2'-*O*-Me RNA, 2'F-RNA, 2'F-ANA and the locked nucleic acids (LNA) analogues which improve nuclease resistance and can also increase the melting temperature of

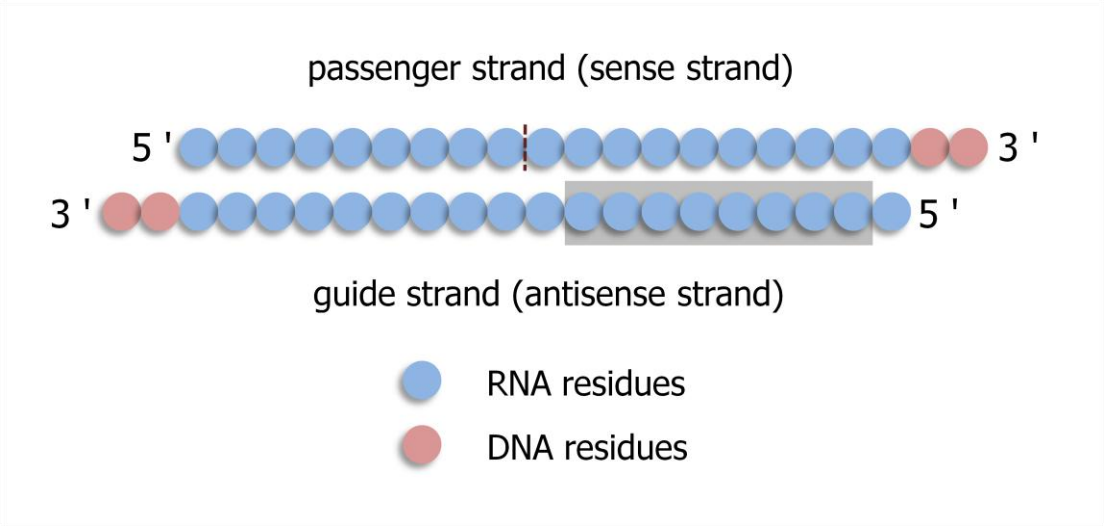

Figure 4.1. Morphology of a small interfering RNA (siRNA). siRNA is typically comprised of 19 nucleotides of RNA (blue circles) with two nucleotide overhangs of DNA (red cirles). The guide strand (antisense strand) contains the seed region (grey box) which is important for directing the recognition and cleavage of the target mRNA strand. The passenger strand (sense strand) is cleaved by the RNA induced silencing complex (RISC), the scissile phosphate being between nucleotides 9 and 10 (dashed line).

siRNA duplexes. If strategically placed away from the siRNA seed region (Figure 4.1), modifications can lower sequence-specific off-target effects.[343,344] Some of these chemical modifications can also reduce the immunogenic effects of siRNAs.[345,346] Like antisense oligonucleotides and aptamers, delivery of siRNAs is perhaps the greatest obstacle for their use as a therapy. Chemical modifications have aided in this regard as well, notably by adding lipophilic groups such as cholesterol at the termini of siRNA which demonstrated potency in animal models.[347,348]

4.1.2 Nucleobase modifications in siRNA

The use of chemically modified nucleobases in siRNAs is relatively an underexplored area of research. Figure 4.2 depicts some noteworthy nucleobase modifications that have been reported in the literature for RNA interference. An early report in nematodes indicated that incorporating some base modifications such as 5-bromouracil and 5-iodouracil did not abrogate gene silencing.[349] Later it was shown that 2-aminopurine, 5-bromouracil and 5-iodouracil showed increased duplex thermostability but decreased potency of the siRNA's to silence, while N^3-methyluracil showed duplex destabilization and abolished potency, presumably

through steric clashes with RISC in the major groove.[350] In many cases, base modifications increase the binding affinity of RNA duplexes, thus they can improve potency and guide strand loading into RISC if properly positioned in siRNAs.[351,352] An siRNA containing base modifications with enhanced duplex thermostability at the 3' segment (2-thiouracil and pseudouracil) and a destabilizing modification (dihydrouracil) at the 5' segment of the guide strand showed enhanced potency.[353] In a study on major groove modifications in siRNAs that included 5-methyluracil, 5-propynyluracil and 5-methylcytosine base modifications, it was shown that modulating gene silencing potency goes beyond the asymmetry in the binding affinity between the 5'-segment and the 3'-segment of the guide strand. Bulky groups like 5-propynyluracil that portrude into the major groove decreased potency when placed at specific sites at the 5'-portion of the guide strand, probably due to steric clashes with protein residues, but smaller groups in the major groove like 5-methyluracil and 5-methylcytosine increased duplex binding without any penalties to gene silencing.[331] The use of non-polar bases that do not hydrogen bond such as 2,4-difluorobenzene and difluorotoluene further show that sterics can play a role in siRNA potency as these modifications are well tolerated at certain positions.[354-356] Like modifications to the sugar and termini, difluorotoluene, 5-methyluracil, 5-propynyluracil and 5-methylcytosine base modifications also impart increased biostability to siRNAs.[331,356]

Studies on the immunostimulatory effects of base modified siRNAs are very limited. A study by Kariko and coworkers highlight that cells are capable of differentiating the origin of RNA, and nucleoside modifications can provide an additional molecular feature to discriminate between microbial and host RNA.[357] They showed that nucleoside-modified RNA incorporating 5-methylcytosine, 6-methyladenine, 5-methyluracil, 2-thiouracil or pseudouracil suppressed TLR-mediated immune responses in dendritic cells.[357] However in another study only thymine and not 5-methylcytosine nor 7-deazaguanine base modifications could reduce immune stimulation in peripheral blood mononuclear cells (PBMC).[358]

From the few studies on nucleobase modifications on siRNA, it is clear that they can offer the same enhancements as other types of chemistries. It is also evident that

these benefits can vary with sequence context, their position in an siRNA, and the cell types under study, warranting further investigation to maximize their efficiency.

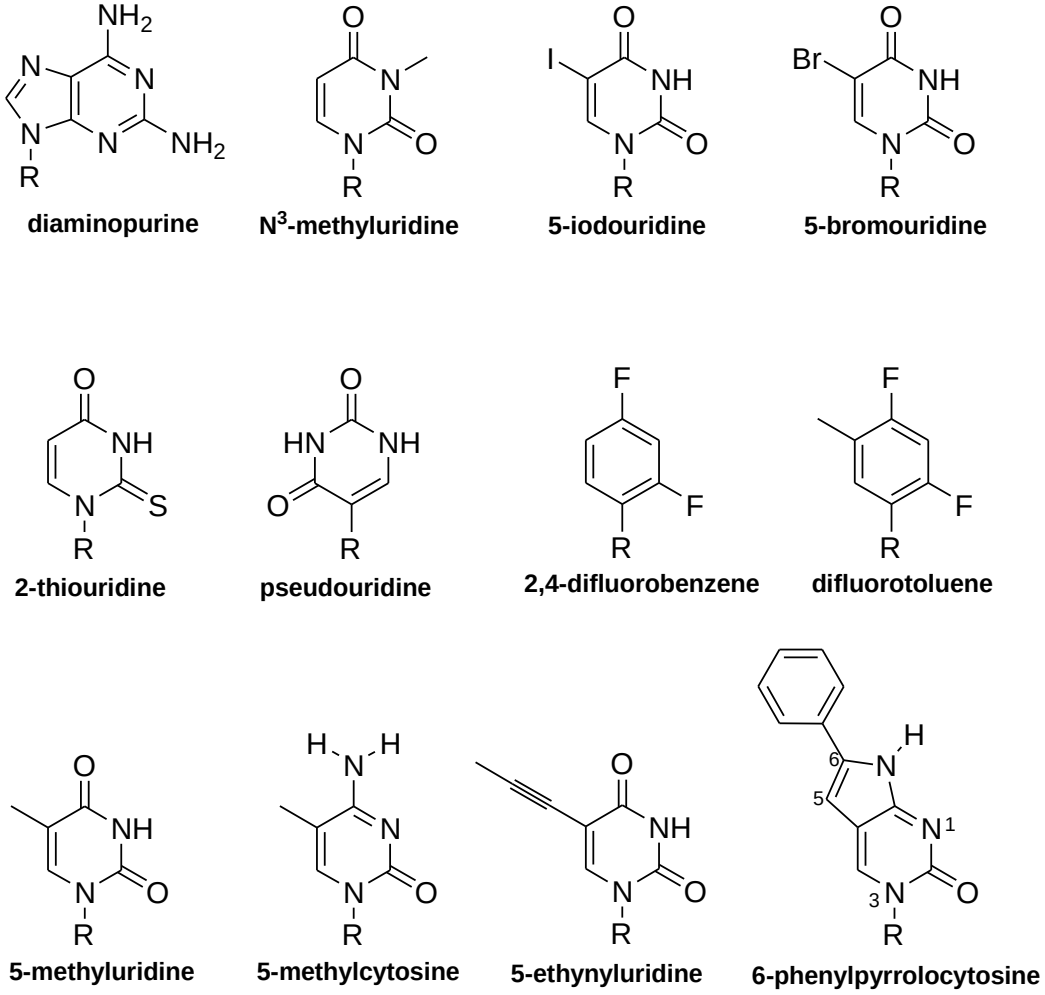

Figure 4.2. Notable nucleobase modifications that have been used in siRNAs and to modulate immune stimulation by RNA. R= ribose. The numbering for 6-phenylpyrrolocytidine (PhpC) is indicated.

4.1.3 6-Phenylpyrrolocytidine as a nucleobase modification in siRNA

6-Phenylpyrrolocytidine (PhpC) has a set of properties that make it unique among nucleobase analogues (Figure 4.2). It has shown increased binding to target RNA and DNA, has excellent mismatch discrimination, ranks among the most fluorescent C-analogues to date and fluorescence which changes with its microenvironment (e.g., as a free nucleoside, in a single strand, or hybridized in a duplex).[322,324,359] In addition, PhpC is an excellent cytosine mimic in terms of its recognition by nucleic acid modifying enzymes as demonstrated in Chapter 3. We used PhpC to develop a

molecular-beacon type RNase H assay that reports the cleavage of the enzyme substrate fluorometrically. In the present chapter, we are interested in evaluating the potential of PhpC as a nucleotide modification for siRNA therapy in order to address some of the shortcomings of siRNAs. For instance, the increased duplex stability of PhpC can aid in properly loading the guide strand into RISC by creating asymmetry in the melting temperature (T_m) of the 3' and 5' segments of a siRNA duplex. In addition, there is evidence that base-modifications are capable of decreasing the immunostimulatory effects of RNA,[357] and it would be of interest to ascertain if PhpC follows suit. Using the emissive properties of PhpC we also hope to create biologically active fluorescent siRNAs to visualize their distribution in cells. Currently, tracking siRNAs in cells is accomplished by terminal conjugation of traditional fluorophores such as fluorescein or the Cy-family of dyes.[360] As demonstrated in the previous chapter, these bulky hydrophobic dyes can drastically change the properties of oligonucleotides compared to a relatively conservative modification such as PhpC. This would also vacate the termini to allow conjugation of other lipophilic groups that can assist in delivery. This technique would enable the same molecule that is being tested for gene silencing to be used to look at cellular distribution.

Ultimately, we hope to develop a fluorescence-based assay to measure the kinetics of RISC cleavage similar to the RNase H assay developed in Chapter 3. Such an assay would greatly facilitate the screening of chemical modifications that make siRNAs better or poorer substrates for RISC, while monitoring other mitigating factors on gene silencing efficiency such as biostability and delivery.

We now describe, for the first time, the synthesis, physicochemical and biological studies on PhpC modified siRNAs. As shown below, duplexes containing this modification in the sense and antisense strand show increased T_m values compared to their analogous unmodified RNA strands. The fluorescence intensity and fluorescence polarization of PhpC-containing siRNA strands are sensitive to their environment. The synthesized substrate and cleavage product of RISC containing a single PhpC at the same position demonstrated markedly different fluorescent properties, suggesting its potential to follow RISC kinetics fluorometrically. siRNAs with PhpC inserts do

not impair gene silencing when introduced in the sense and the antisense strands and show promise as a fluorescent probe to monitor siRNA localization in cells.

4.2 Results and Discussion

4.2.1 Oligonucleotide Design

We employed the same 21-mer siRNA sequence described in previous studies that targets the mRNA of the firefly luciferase gene.[166,185] This sequence is designed so that the 5'-segment of the antisense siRNA is A/U rich and melts more readily than the G/C rich 3'-segment favouring guide strand loading into RISC over the passenger strand (Table 4.1). Since PhpC increases thermal stability, it is inadvisable to introduce it into the 5'-segment of the guide strand. The cleavage site of Ago2, the nuclease component of RISC, is between nucleotides 10 and 11 of the guide strand (the scissile phosphate being between nucleotides 9 and 10 of the passenger strand of an siRNA). Replacing the cytidine at position 10 of the passenger strad with PhpC should test the limits of how a single insert would be tolerated by RISC (ss.pC-1, Table 4.1). In the same vein, inserting PhpC closest to the scissile phosphate as possible, nucleotide 12, in the antisense strand was also accomplished (as.pC-1, Table 4.1). We also synthesized the cleavage product of ss.pC-1 when it is processed by RISC, ss.pC-2, to verify changes in fluorescence properties to evaluate its suitability to be employed in a fluorescent assay. Upon cleavage by RISC, the 5'-terminal PhpC generated should exhibit increased fluorescence intensity[322] and, in light of its smaller size, less fluorescence polarization. Finally, we added multiple PhpC inserts to the sense strand in an attempt to verify additive effects to thermal stability and fluorescence.

Table 4.1. Sequences and MS data for oligonucleotides used in siRNA studies.

Name	Sequence (5' to 3')	Mass calculated	Mass measured
sense	GCUUGAAGUCUUUAAUUAAtt	6617.0	6638.8 (Na+)
antisense	UUAAUUAAAGACUUAAGCgg	6673.0	6694.1 (Na+)
ss.pC-1	GCUUGAAGU**C**UUUAAUUAAtt	6717.1	6716.9
ss.pC-2	**C**UUUAAUUAAtt	3799.4	3799.2
ss.pC-3	G**C**UUGAAGU**C**UUUAAUUAAtt	6817.2	6817.1
as.pC-1	UUAAUUAAAGA**C**UUAAGCgg	6773.1	6773.3

Legend: RNA, dna, **PhpC**.

4.2.2 Thermal Denaturation Studies

Thermal denaturation studies were used to judge the stability of siRNA duplexes containing PhpC insertions in the place of natural C as judged by the melting temperatures (T_m) determined from the curves shown in Figure 4.3. Overall, the denaturation curves of modified duplexes overlapped with the unmodified control, except the former experienced transitions at slightly higher temperatures indicating that PhpC insertions are stabilizing, which is consistent with our previous findings (Chapter 3).[322,359] Compared to the unmodified control duplex, the addition of one (siPhpC-1) or two (siPhpC-3) PhpC insertions into the sense strand incrementally increased the melting temperature (T_m) by 0.5 ºC and 2.5 ºC respectively (Table 4.2). Adding one PhpC in the antisense strand (siPhpC-4) also showed an increase in T_m of 0.5 ºC. Single PhpC insertions in both the sense and antisense strands (siPhpC-5) showed a greater gain in stability than the sum of siPhpC-1 and siPhpC-4 (1.5 ºC vs 1.0 ºC). This duplex also exhibited the greatest increase in hypochromicity according to the thermal melt curve (Figure 4.3), which is indicative of better π-stacking of the bases in the duplex, and which may be aided by the proximity of the two PhpC inserts. Duplex siPhpC-2 showed very weak stability with a melting temperature of less than 20 ºC. This implies that at physiological conditions (37 ºC), the resulting 3'-segment of siPhpC-1 should dissociate from the antisense strand once the sense strand is cut by RISC, if it is not already unwound by RISC-associated helicase activity.

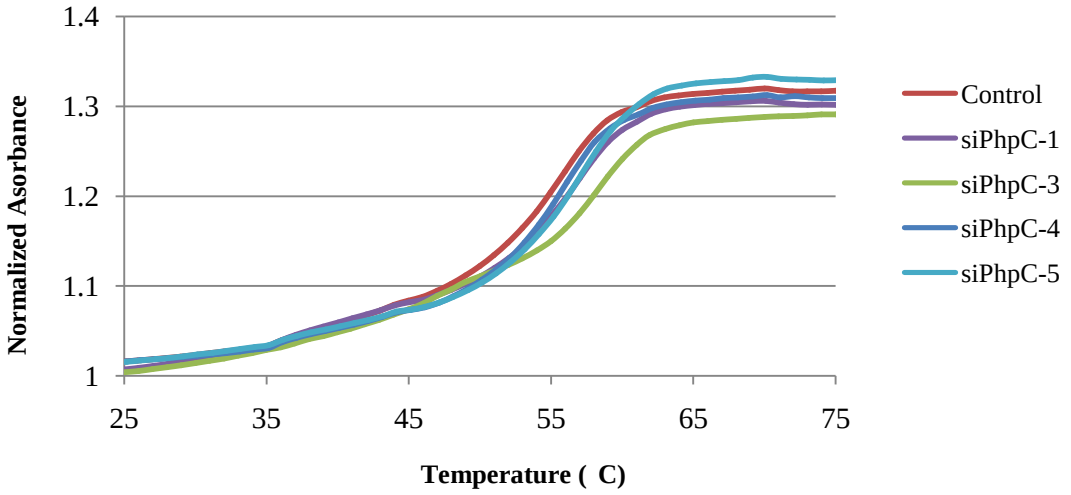

Figure 4.3. Thermal denaturation curves of siRNA duplexes containing PhpC and an unmodified control (red curve).

Table 4.2. SiRNA sequences with melting temperatures and gene silencing activity.

Duplex	Sequence[a]	T_m (°C) [b]	IC_{50} [b] (nM)
Control	5'-GCUUGAAGUCUUUAAUUAAtt-3' 3'-ggCGAACUUCAGAAAUUAAUU-5'	54.1	0.10
siPhpC-1	5'-GCUUGAAGU**C**UUUAAUUAAtt-3' 3'-ggCGAACUUCAGAAAUUAAUU-5'	54.6	0.16
siPhpC-2	5'-**C**UUUAAUUAAtt-3' 3'-ggCGAACUUCAGAAAUUAAUU-5'	18.5[c]	1.0
siPhpC-3	5'-G**C**UUGAAGU**C**UUUAAUUAAtt-3' 3'-ggCGAACUUCAGAAAUUAAUU-5'	56.4	3.8
siPhpC-4	5'-GCUUGAAGUCUUUAAUUAAtt-3' 3'-ggCGAACUU**C**AGAAAUUAAUU-5'	54.6	2.7
siPhpC-5	5'-GCUUGAAGU**C**UUUAAUUAAtt-3' 3'-ggCGAACUU**C**AGAAAUUAAUU-5'	55.6	0.77
siPhpC-6	5'-G**C**UUGAAGU**C**UUUAAUUAAtt-3' 3'-ggCGAACUU**C**AGAAAUUAAUU-5'	nd	0.18
Scrambled	5'-GCUUGAUUUCUGAAAUUAAtt-3' 3'-ggCGAACUAAAGACUUUAAUU-5'	-	-

[a] Sense strands are listed on top and antisense strands below.Legend: RNA, dna, **PhpC**. T_m's were measured at concentrations of 1 μM in 10 mM phosphate buffer (pH 7.0) and 50 mM NaCl. [b] T_m and IC_{50} values are the average of three independent experiments. Tm values represent the average of at least 3 independent experiments within 1 °C. [c] The T_m of siPhpC-2 could only be determined by the derivative method. nd= not determined

4.2.3 Fluorescence Studies of siRNAs Containing PhpC

The fluorescence of single-stranded oligonucleotides containing PhpC are generally quenched when hybridized to complementary RNA or DNA,[322,359] however there may be exceptions depending on sequence length and composition[361] (see section 3.2.6). The fluorescence of PhpC containing RNA strands, both single-stranded and double-stranded, is depicted graphically in Figure 4.4. The fluorescence of single-stranded oligonucleotides in this study is greater than that found for the sequences described in Chapter 3. This may be attributed to the base composition of the siRNA strands, with PhpC neighboring uridines being more conducive to higher quantum yields while a neighboring guanine reduced the quantum yield (Table 3.2.2).

This trend is nicely illustrated in the present study when replacing one or two cytidine residues with PhpC in the sense strand (ss.pC-1 and ss.pC-3). The ss.pC-1 single strand is highly emissive, which follows our previous report where trinucleotide A-PhpC-U showed excellent fluorescent emission.[361] Replacing the other cytidine in the strand with PhpC gives ss.pC-3, but does not show any increase in fluorescence intensity presumably due to the neighboring guanine. Guanines can reduce the quantum yield fluorophores in a distant-dependent manner through an electron transfer mechanism.[362,363] The truncated version of ss.pC-1 (ss.pC-2) showed an increase in fluorescence of approximately 25%, consistent with previous studies that demonstrated terminal PhpC's are more fluorescent than a corresponding internal PhpC.[322] In summary, the fluorescence intensity of the PhpC in single-stranded RNA varies with its position and sequence composition in accordance with previous studies.

The double-stranded RNA containing the PhpC modification exibited less fluorescence emission compared to their single-stranded oligonucleotide components (Figure 4.4, blue bars). The oligonucleotides containing single internal PhpC insertions in the passenger strand (ss.pC-1) or guide strand (as.pC-1) each showed a decrease of about 30% in fluorescence upon duplex formation (duplex siPhpC-1 and duplex siPhpC-4 respectively). The fluorescence of the duplex containing both ss.pC-1 and as.pC-1 (siPhpC-5) was approximately equal to the sum of the fluorescence of siPhpC-1 and siPhC-4, indicating that the fluorescence of PhpC can be additive in the context of a duplex. The truncated passenger strand with a terminal PhpC (ss.pC-2), showed a decrease in fluorescence of only 25% upon duplex formation compared to the single strand. This is typical, terminal PhpC insertions have shown less quenching upon duplex formation than internal ones.[322] Also, it should be noted that siPhpC-2 would not be a duplex since these measurements were carried out at 25 °C, which is above its melting temperature (18.5 °C).

We also verified the fluorescence polarization (FP) of the PhpC containing oligonucleotides. FP can discern the size of a molecule harboring a fluorescent moiety by the rate at which it tumbles freely in solution (Brownian motion). Larger molecules experience less motion, and this translates to higher FP measurements.

Thus, we expect to see a decrease in FP when the passenger strand in a siRNA duplex gets cleaved by RISC. Single-stranded RNAs with one PhpC insert showed an FP value of 0.13, while duplexes with a single PhpC insert were 0.28. The fluorescent passenger strand cleavage product of RISC, ss.pC-2, showed an FP value of 0.09. This indicates that it may be possible to monitor the cleavage of an siRNA by RISC using fluorescence polarization as the FP values change from 0.28 to 0.09, a substantial (3 fold) difference. In contrast, the change in fluorescence intensity was only about 2 fold (101 to 212) when comparing duplex siPhpC-1 to ss.pC-2 alone.

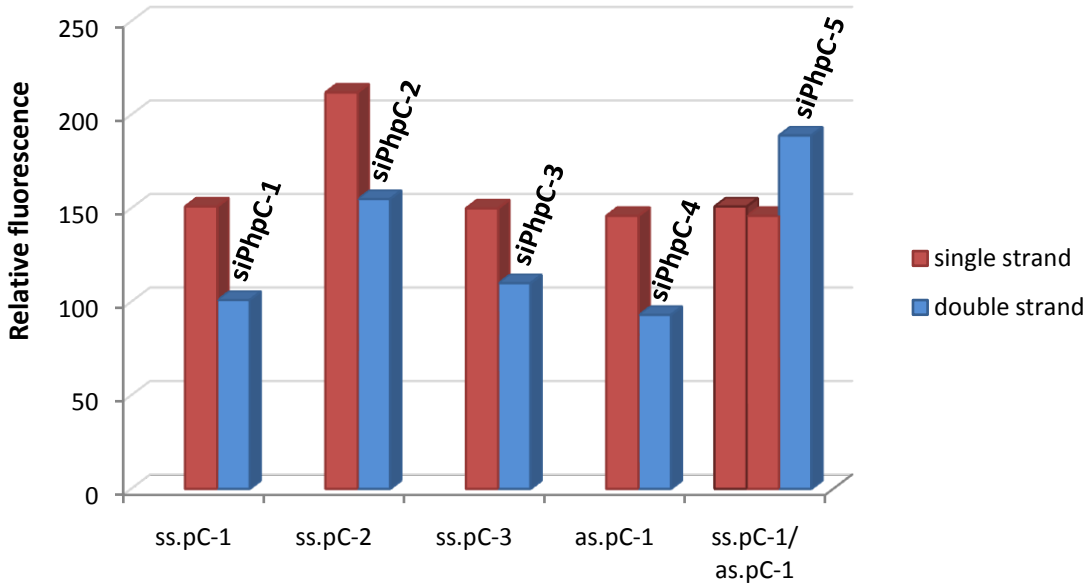

Figure 4.4. Comparison of the fluorescence intensity of PhpC containing single-stranded oligonucleotides (red bars) and duplexed to unmodified complementary strands (blue bars). Duplex siPhpC-5 contains a modified sense strand, ss.pC-1, and a modified antisense strand, as.pC-1. Samples were measured at a concentrations of 1 μM in 10 mM phosphate buffer (pH 7.0) and 50 mM NaCl at 25°C, λ_{ex}=360 nm, λ_{emm}=465 nm. Data represents the average of at least three independent experiments.

4.2.4 RNAi Assays

PhpC was placed in the sense and antisense strands of siRNA's targeting the firefly luciferase gene (Table 4.2). These duplexes were transfected in HeLa cells over-expressing firefly luciferase as described in section 4.4.5, and the ensuing gene silencing was judged by the decrease of firefly luminescence and compared to that of renilla luciferase expressed from a co-transfected plasmid (Figure 4.5a,b,c) The

renilla luciferase counts did not go down for all samples. A scrambled duplex with identical base composition and no silencing activity was used as a negative control. Full length duplexes with single or triple insertions of PhpC in the sense and/or antisense strand generally showed good silencing efficacy compared to the unmodified control. Not surprisingly, the siRNA containing the truncated sense-strand with a terminal PhpC (siPhpC-2) showed no gene-silencing in one instance (Figure 4.5b), no doubt due to the difficulty to form stable duplexes at physiological conditions and get recognized by RISC. The increased duplex stability on the 3'-end of the guide strand did not generate more potent siRNA's (siPhpC-3 and siPhpC-6), but the sequence currently under investigation is GC-rich in this region and may already possess sufficient thermodynamic bias.[351] Overall, this data suggests PhpC holds promise as a chemical modification in siRNAs as it can be placed in *both* the sense and antisense strand without severely affecting potency. Furthermore, as PhpC insertions were placed at the scissile phosphate of both sense and antisense strands, these very encouraging results suggest that the PhpC modification does not impair Ago2 catalysis.

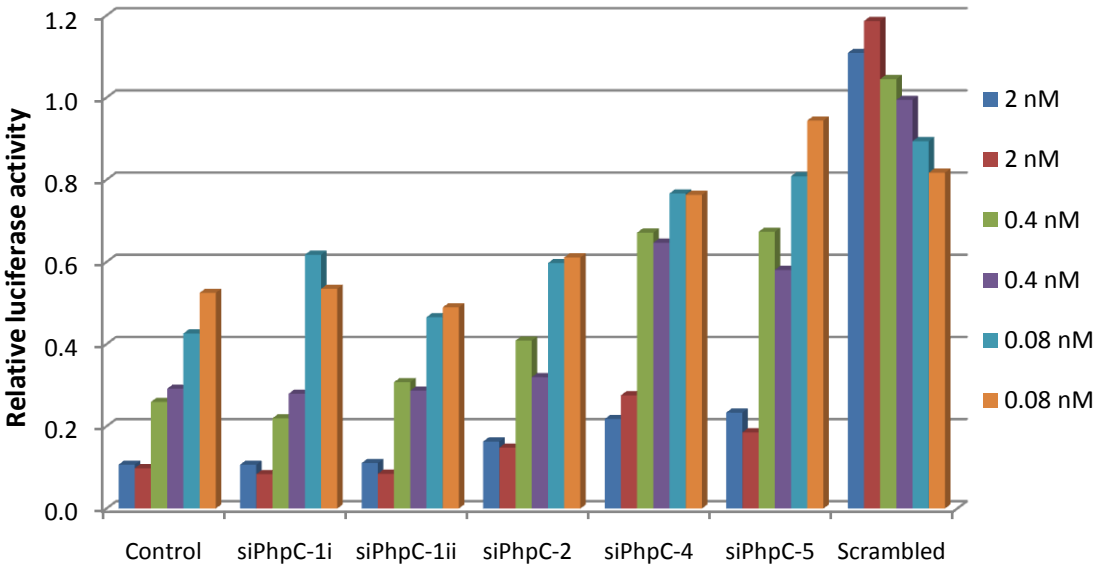

Figure 4.5a. Knockdown of luciferase gene in HeLa cells by siRNA's containing PhpC (Trial 1). Two preps of siPhpC-1 were tested (i and ii).

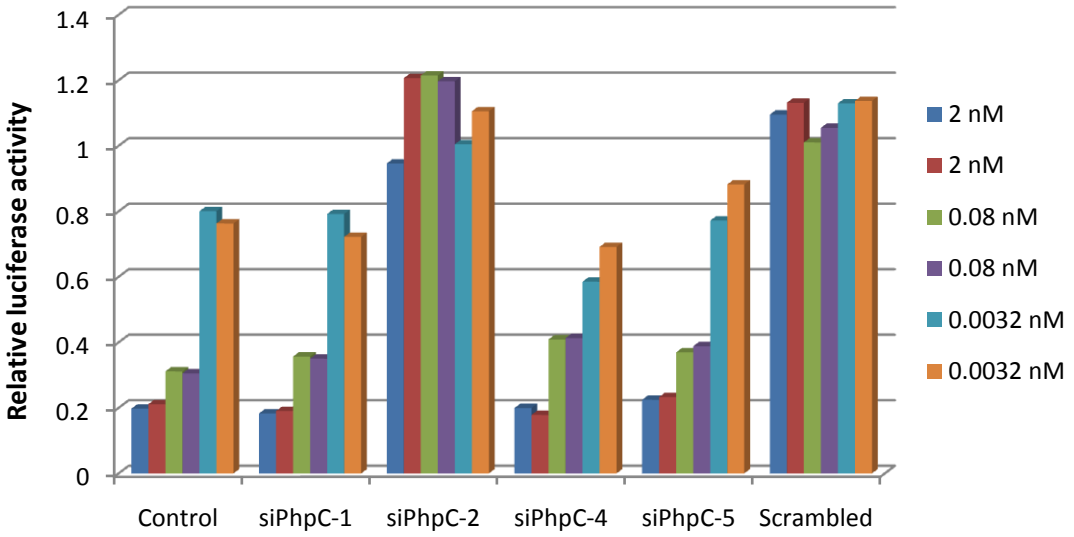

Figure 4.5b. Knockdown of luciferase gene in HeLa cells by siRNA's containing PhpC (Trial 2).

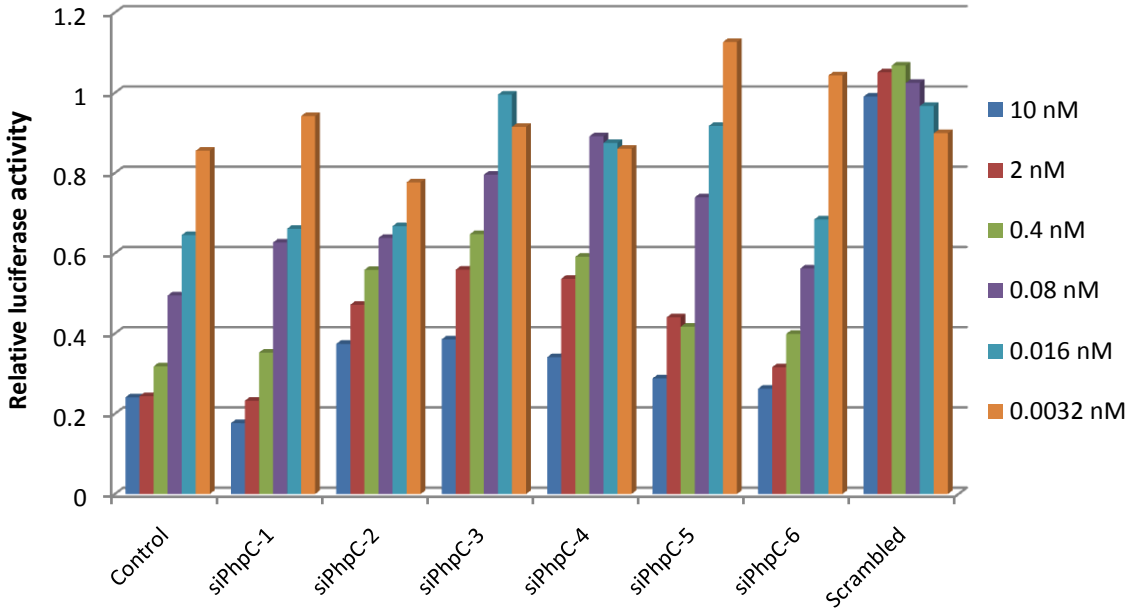

Figure 4.5c. Knockdown of luciferase gene in HeLa cells by siRNA's containing PhpC (Trial 3). This data represents the average of one experiment run in duplicate. IC_{50} values from Table 4.2 were calculated from this data.

4.2.5 Fluorescence Microscopy of PhpC siRNAs

It would be advantageous if a chemical modification could also serve as a fluorescent reporter to monitor siRNA uptake and localization. This would

circumvent the need to re-synthesize the same siRNA conjugated to a fluorescent dye with potentially altered properties. Towards this end, HeLa cells were transfected with 1 μM of siPhpC-1 or a Cy3 5'-end labeled single-stranded DNA and the live cells were observed in a Zeiss Axiovert 200 M inverted fluorescent microscope. Live cells were used in this study to lay the groundwork for future studies to monitor the localization of fluorescent siRNA in real time. After four hours of incubation, cells containing no fluorescent siRNA and cells containing siPhpC-1 were visualized using DAPI filters (λ_{exc}= 360 nm and λ_{em} = 460), and the Cy3-DNA oligonucleotides using Cy3 filters (λ_{exc}= 540 nm and λ_{em} = 620). Due to the lower fluorescence of PhpC, compared to Cy3, longer exposure times were required to obtain images for cells transfected with siPhpC-1 (1 s versus 0.1 s). The cells containing no fluorescent oligonucleotides showed some background fluorescence at these exposure times (Figure 4.6 A), most likely due to internal fluorescence caused by NADH.[364] Under the same conditions, the cells containing siPhpC-1 showed bright spots on the periphery of the cells, in addition to the background fluorescence, suggesting the siPhpC-1 is entrapped in endosomes or are localized in processing bodies, the location of mRNA degradation (Figure 4.6 B). This distribution is similar to that seen for the Cy-3-labeled DNA (Figure 4.6 C) and is consistent with studies by others on the localization of siRNAs using traditional fluorescent tags.[360] This result suggests that the traditional fluorophores do not alter the localization of siRNAs in HeLa cells. We verified that the bright spots in the cells containing siPhpC-1 were not due to artifacts. The intensity of these spots was measured to be three-fold more fluorescent than the NADH fluorescence after subtracting the background.

In conclusion, these preliminary studies show that PhpC shows promise as a probe to monitor siRNA in cells provided the overall fluorescence can be increased relative to that of cellular NADH. This should be feasible by multiple (> 4) PhpC incorporations, since PhpC fluorescence is additive. In addition, it was recently reported by our collaborator, Prof. Robert Hudson (U Western Ontario), that insertions of several PhpCs in peptide nucleic acids (PNA) can fluorescently report PNA localization in fibroblasts by confocal microscopy.[365]

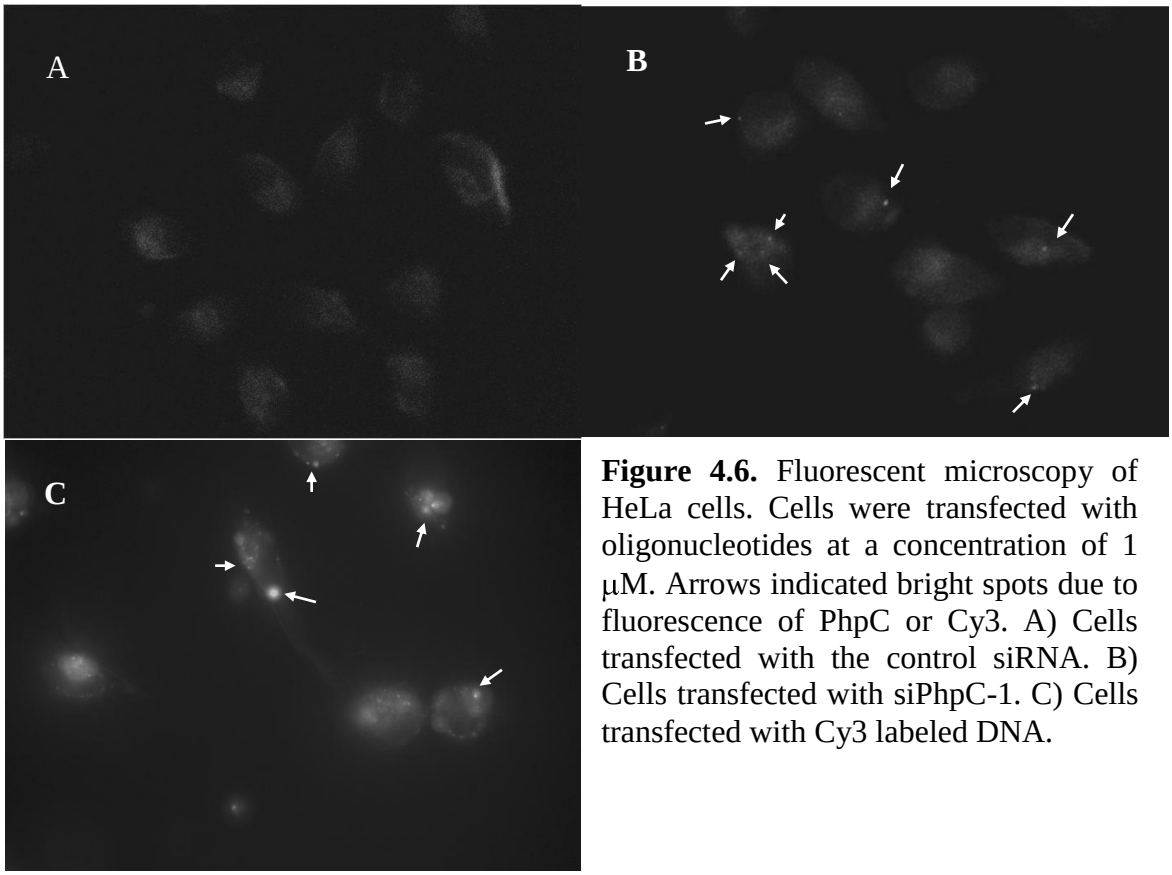

Figure 4.6. Fluorescent microscopy of HeLa cells. Cells were transfected with oligonucleotides at a concentration of 1 μM. Arrows indicated bright spots due to fluorescence of PhpC or Cy3. A) Cells transfected with the control siRNA. B) Cells transfected with siPhpC-1. C) Cells transfected with Cy3 labeled DNA.

4.3 Conclusion and Future Directions

4.3.1 Conclusions

This work establishes that PhpC can be beneficial to monitor the biodistribution of siRNAs. Replacing C for PhpC in the passenger strand, guide strand, or both increases the T_m of duplexes by 0.5 to 1 °C per insertion. Perhaps the most significant observation is that insertions of PhpC did not show any marked decrease in the gene silencing activity of siRNAs in HeLa cells, even though previous work suggests that base modifications that protrude in the major groove of RNA diminish binding to RISC.[331] We observe that PhpC modified siRNAs are active whether the PhpC modification is placed at the scissile phosphate group of the sense strand or at the sensitive antisense strand of the duplex. These very encouraging results warrant further RNAi studies with PhpC modified siRNAs.

The fluorescent properties of PhpC such as high quantum yield, red-shifted fluorescence emission and responsiveness to environment make it unique among chemical modifications to study siRNA. PhpC insertions gave fluorescent siRNAs that were able to be followed in the cell, albeit with the presence of background fluorescence. Adding several PhpC units in a duplex can increase the overall fluorescence emission to counteract background fluorescence. However, careful consideration is necessary when inserting PhpC in order to maximize the fluorescence signal (i.e. avoiding intrastrand neighboring guanines). The binding and catalytic efficiency of siRNAs for RISC is not routinely addressed since other factors such as biostability, delivery to the target and off-target effects are considered the limiting factors in RNAi therapy. PhpC can be used to discriminate between the substrates and products of RISC by fluorescence intensity and fluorescence polarization, laying the framework for a real-time RISC cleavage assay. Finally, this work should encourage the use of other strongly emissive and red-shifted fluorescent nucleobase analogues, such as the tricyclic cytosines studied by Wilhelmsson,[309,337,366] to study RNA interference.

4.3.2 Future Work

Currently, siRNAs containing several PhpC inserts are being synthesized in the Damha laboratory (Table 4.3). These duplexes are being designed to have greater fluorescence intensity to allow their visualization in HeLa cells at lower exposure times, thus eliminating the autofluorescence of NADH. This can be accomplished by replacing additional C residues with PhpC's in the antisense strand at locations away from guanine residues. Furthermore, the two 3'-dG overhangs on the antisense strand can be replaced with dPhpC as they have shown to be very receptive to modifications.

Table 4.3. siRNA sequences containing multiple PhpC insertions designed to have enhanced fluorescence intensity.

Duplex	Sequence
Control	5'-GCUUGAAGUCUUUAAUUAAtt-3' 3'-ggCGAACUUCAGAAAUUAAUU-5'
siPhpC-7	5'-G**C**UUGAAGU**C**UUUAAUUAAtt-3' 3'-gg**C**GAA**C**UU**C**AGAAAUUAAUU-5'
siPhpC-8	5'-G**C**UUGAAGU**C**UUUAAUUAA***cc***-3' 3'-***cc*****C**GAA**C**UU**C**AGAAAUUAAUU-5'

Legend: RNA, dna, **PhpC**, ***dPhpC***.

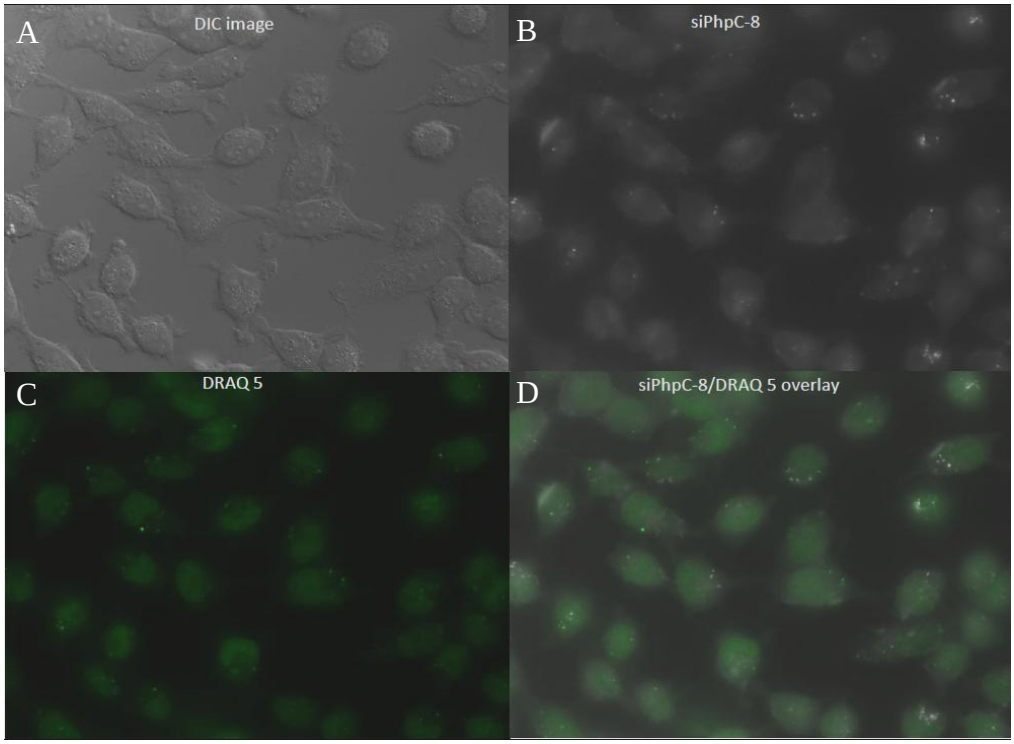

Figure 4.7. Fluorescent microscopy of DRAQ5 stained HeLa cells transfected with siPhpC-8. A. Differential interference contrast image. B. siPhpC-8 image showing intracellular localization of siRNA (DAPI filters). C. DRAQ5 nuclear stain image (Cy5 filters). D. siPhpC-8/DRAQ5 overlay image indicates siRNAs are accumulating in the cytoplasm.

Preliminary images using siPhpC-8 (Figure 4.7) suggest PhpC could serve as an invaluable tool to study siRNA delivery and trafficking. The 3' and 5'-termini would not be occupied by a fluorescent probe, thus lipophilic groups or targeting molecules could easily be appended to siRNAs. In addition, the merits of "gymnotic" delivery of oligonucleotides, which are devoid of terminal conjugations or transfecting agents, has recently been described.[367] In the absence of terminal conjugated fluorescent probes, we believe PhpC is a suitable replacement to follow the uptake of these "naked" oligonucleotides. The potency and localization of PhpC containing siRNAs should then be tested in different sequence contexts and cell types to establish how broadly this modification can be applied.

As discussed in section 4.1.3, base modifications can affect the immune-modulatory properties of siRNAs,[357,368] an important off-target effect that is emerging as a serious hurdle for their therapeutic development.[340] Therefore, the effect of siRNAs containing PhpC on immune stimulation should be verified. Our understanding of immune stimulation by siRNAs is still at the discovery stage, but

recent studies have shown that certain sequences can be more immunogenic than others and varies among cell types.[369,370] Hornung *et al.* showed that a sequence of nine bases (5'-GUC CUU CAA-3') at the 3' end of the sense strand is responsible for immunostimulatory activity in plasmacytoid dendritic cells,[370] and these effects are reduced by modifying the sequence with locked nucleic acids (LNA). Using the same methodology, replacing the C residues for PhpC in this sequence could indicate whether this modification can also modulate the immune response of siRNAs.

Lastly, the kinetics of cleavage could be tested using the fluorescence of PhpC-1. As previously discussed, developing a quick assay to screen the kinetics of modified siRNAs by RISC could aid in designing more effective substrates. A fluorescence based screening assay can also be developed to uncover enhancers of RISC activity, as the existence of such factors have recently been suggested.[371] In addition, fluorescence polarization or potentially FRET experiments between a PhpC containing antisense strand and a fluorescently labeled RISC could determine on/off rates of siRNA and monitor the duration the antisense strand is loaded in RISC.

4.4 Experimental methods

4.4.1 General methods

Chemicals and solvents were ACS grade or higher and were purchased from Sigma-Aldrich or Thermo-Fisher. Anhydrous pyridine was obtained by distilling over calcium hydride. All reagents used for oligonucleotide synthesis, including 2'-deoxyribonucleotide and 2'-silylribonulceotide phosphoramidites, were purchased from Chemgenes Corp. PhpC was synthesized according to previously described methods. Autoclaved Millipore water treated with diethylpyrocarbonate (DEPC)[290] was used to manipulate RNA and prepare aqueous buffers.

4.4.2 Synthesis and purification of oligonucleotides

Solid-phase synthesis of oligonucleotides was carried out on an Applied Biosystems 3400 DNA synthesizer using standard protocols.[205] Cleavage from the solid-support was carried out in a 3:1 mixture of NH_4OH:EtOH at room temperature for 48 hours, and removal of the 2'-*O*-silyl protecting groups was achieved by treatment with distilled triethylammonium trihydrofluoride for 48 hours. The crude,

deprotected oligonucleotides were precipitated in ice-cold butanol and 3M sodium acetate and quantitated by their UV absorbance at 260 nm on a Cary-300 UV-VIS spectrophotometer (Varian Inc). Crude products were then analyzed and purified by denaturing PAGE (7M urea) and visualized by UV shadowing using 254 nm light for non-fluorescent oligonucleotides, and 365 nm light for fluorescent oligonucleotides. Full length products were excised from the gels using a sterile surgical blade, and eluted in DEPC treated water. The eluted products were desalted by size-exclusion chromatography on G-25 Sephadex (GE Healthcare) and quantitated.

4.4.3 Thermal denaturation curves

For UV-Vis thermal denaturation experiments nucleotides and oligonucleotides were analyzed in 1 mL solutions at 1 μM concentrations in a buffer of 10 mM sodium phosaphate at pH 7.0 and 50 mM NaCl. Double-stranded oligonucleotides were annealed in equimolar amounts by heating to 95°C and then slowly cooling to room temperature on a heating block. Thermal denaturation experiments were performed on a Cary-300 UV-Vis spectrophotometer (Varian Inc.) equipped with a 6x6 cell changer and Peltier Temperature controller. Samples were heated from 10°C to 95°C at a rate of 0.5°C per minute and the change in absorbance was measured every 1.0°C. The melting temperature (T_m) values were obtained by the baseline (alpha) method, and defined as the point when the mole fraction of duplex was equal to 0.5. These values represent the averages of at least three independent experiments. Fluorescent thermal denaturation plots were obtained in a similar fashion on a Cary Eclipse fluorescent spectrophotometer equipped with a multi-cell Peltier temperature controller and automated polarization accessories. Measurements for fluorescent experiments were carried out in 1 cm X 1 cm quartz cells in 2 mL volumes and 1 μM concentration of oligonucleotides

4.4.4 Fluorescent Measurements

Fluorescence intensity and polarization measurements were obtained on a Cary Eclipse Spectrophotometer equipped with a multi-cell Peltier temperature controller and automated polarization accessories. Measurements were carried out in 1 cm X 1 cm quartz cells in 2 mL volumes at r.t. in 1 μM concentrations in a buffer of 10 mM sodium phosaphate at pH 7.0 and 50 mM NaCl. Excitation and emission bandwidths

were set at 5 nm for all experiments. Emission spectra were obtained by exciting at 360 nm and monitoring the emission from 400 to 600 nm.

4.4.5 SiRNA gene silencing assays

siRNA assays were performed by Dr. Francis Robert in the lab of Dr. Jerry Pelletier of the McGill Cancer Centre. HelaX1/5 cells that stably express firefly luciferase were grown as previously described [185]. The day prior to transfection, 0.5 x 10^5 cells were plated in each well of a 24-well plate. The next day, the cells were incubated with increasing amounts of siRNAs premixed with lipofectamine 2000 reagent (Invitrogen) using 1 μL of lipofectamine. For the siRNA titrations, each siRNA was diluted into dilution buffer (30 mM HEPES-KOH, pH 7.4, 100 mM KOAc, 2 mM $MgOAc_2$) and mixed with 200 ng of plasmid pCI-hRL-con expressing the *Renilla* luciferase. 24 hours after transfection, the cells were lysed in hypotonic lysis buffer (15 mM K_3PO_4, 1 mM EDTA, 1% Triton, 2 mM NaF, 1 mg/mL BSA, 1 mM DTT, 100 mM NaCl, 4 μg/mL aprotinin, 2 μg/mL leupeptin and 2 μg/mL pepstatin) and the firefly and renilla light units were determined using a Fluostar Optima 96-well plate bioluminescence reader (BMG Labtech) as described [372]. The luciferase counts were normalized to the protein concentration of the cell lysate as determined by the DC protein assay (BioRad). Cotransfecting the siRNAs and the plasmid pCI-hRL-con expressing the *Renilla* luciferase mRNA [373] in the same cell line showed no difference in expression of this reporter, demonstrating the specificity of the RNAi effects (data not shown).

4.4.6 Fluorescence microscopy

HelaX1/5 cells were grown in 35 mm glass bottom culture dishes. The next day, the native control siRNA, PhpC-containing siRNAs, or a ss-DNA conjugated to Cy3 (5'-Cy3-AGC TCC CAG GCT CAG ATC-3') were mixed with 1 μL of lipofectamine 2000 (Invitrogen) and incubated for 30 minutes. The cells were transfected with the siRNA/lipofectamine mixture to a final concentration of 1 μM oligonucleotide. After 3 hours, DRAQ5 was added to the cell medium in a 1/10 000 fold dilution and incubated for 15 to 30 minutes, after which time the medium was. The cells were observed under a Zeiss Axiovert 200 wide field microscope using the DAPI filters to image PhpC and Cy5 filters to image the DRAQ5 nuclear stain.

Chapter 5 Towards the development of improved inhibitors against HIV-1 RT-mediated nucleotide excision

5.1 Introduction

5.1.1 Thymidine analogue mutations and nucleotide excision

Nucleoside (or nucleotide) reverse transcriptase inhibitors were the first antiviral compounds used to treat HIV in the clinic, and to this day are an important component of combination therapy. However, insensitivity to treatment soon developed in the first patients administered with NRTIs.[107] These resistance mutations are located in the fingers, thumb and palm domains of RT and were named thymidine analogue mutations (TAMs). Nucleotide excision, also called primer unblocking or phosphorolysis, is the major phenotypic mechanism of resistance of HIV-1 RT with TAMs.[81,105,106] During excision, a pyrophosphate donor (pyrophosphate or ATP) attacks the NRTI monophosphate at the 3'-terminus of the primer to form an NRTI-triphosphate. For this reaction to occur the NRTI must occupy the N-site of RT.[64,65] Nucleotide excision is basically the reverse reaction of nucleotide incorporation. In TAMs, the rate of ATP-mediated NRTI excision is much higher compared to wild type (WT) RT, resulting in the rescue of DNA synthesis in chain-terminated complexes. Although they confer a high level resistance to AZT, RT with TAMs show resistance to other NRTIs as well.[110]

There are two common approaches to address the emergence of TAMs and nucleotide excision. The first option is to develop NRTI analogues that would block DNA synthesis but would be resistant to excision. For example, TAMs provide low-level phenotypic resistance to 3TC. In addition, the 3TC resistant mutation M184V reduces the ability of HIV-1 RT to carry out the excision reaction.[111] This observation illustrates how the use of multiple nucleoside analogues like AZT and 3TC contribute to successful drug regimens. Some nucleoside analogues that contain a 3'-hydroxyl group can act as delayed chain terminators.[374-379] In this model, the nucleotide analogue would not inhibit polymerization immediately following incorporation, but after allowing several incorporations of dNTPs thus avoiding excision. The second

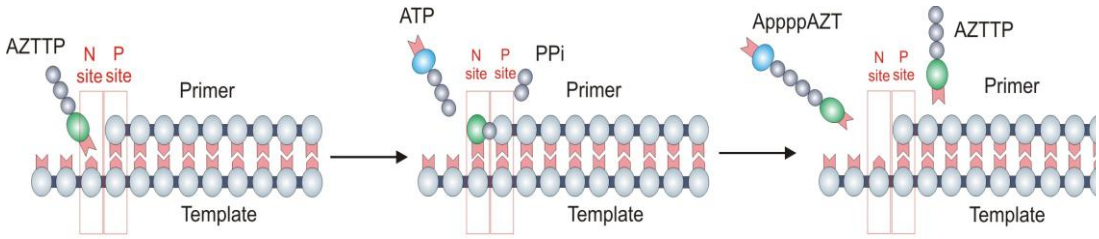

Figure 5.1. Nucelotide excision as illustrated by the phosphorolytic removal of AZTMP from the 3'-end of a primer. The product of pyrophosphate mediated excision is AZT-triphosphate (AZTTP), while the product of ATP mediated excision is 5'-AZT-tetraphosphate-5'-adenosine dinucleotide (AppppAZT).

approach is to find compounds that block the excision reaction.[380-382] NNRTI binding to the non-nucleoside binding pocket reduces the rate of excision in addition to inhibiting polymerization.[383,384] ATP and pyrophosphate analogues have been shown to reduce excision as well, such as the ATP-mediated excision product 5'-AZT-tetraphosphate-5'-adenosine dinucleotide (Figure 5.1).[380,381] Thus inhibitors that reduce nucleotide excision may represent a new therapeutic target towards HIV.

This chapter utilizes nucleotide analogues to study excision. Nucleotides with sugar modifications are directed towards the development of analogues that are less easily excised by RT and fluorescent nucleobase analogues are used to develop a screening method to detect inhibitors of nucleotide excision.

5.1.2 Probing the relationship between sugar conformation and excision

The first study will investigate if RT nucleotide excision has a preference for certain sugar pucker conformations. Preference for northern or RNA-like puckers during DNA polymerization has been uncovered by X-ray crystallography and by incorporating nucleotides with conformational biases. RT discriminates between dNTP and rNTP substrates through the “steric gate” effect mediated by residue Y115 in the dNTP binding pocket.[59,385] Residue Y115 clashes with 2' substituents in rNTPs, and also directs dNTPs to adopt a North conformation to reduce steric hindrance by the 3'-hydroxyl group. In addition, modified nucleotides with sugar conformational equilibrium favouring Northern sugar puckers are incorporated by RT easier than Southern sugar puckers.[85,376,386]

In the following experiments, we synthesize a library of primers having a variety 3'-terminal nucleotide analogues and measure their rates of nucleotide excision. We employ a divergent strategy on solid support (controlled-pore glass, CPG) that does

not require the synthesis of individual nucleoside triphosphates or phosphoramidite building blocks (Figure 5.2). The nucleotide analogues incorporated at the 3'-end of the primers show a range of preferred sugar conformations. Nucleosides with Southern sugar puckers include 2'-deoxythymidine (dT), arabinouridine[18,387] and 2'-fluoro-2'-deoxyarabinothymidine (2'F-araT, South-East)[19] (Figure 5.2). 3'-azido-2',3'dideoxythymidine (AZT) exists as an equal population of both North and South conformers.[388] Uridine (rU), 2'-fluoro-2'-deoxyribouridine (2'F-rU) and 2',3'-dideoxythymidine (ddT) all prefer the northern conformation (Figure 5.2). [18,387] The assumption is that the nucleosides will maintain these conformations when incorporated at the 3'-terminus of the oligonucleotide primer.

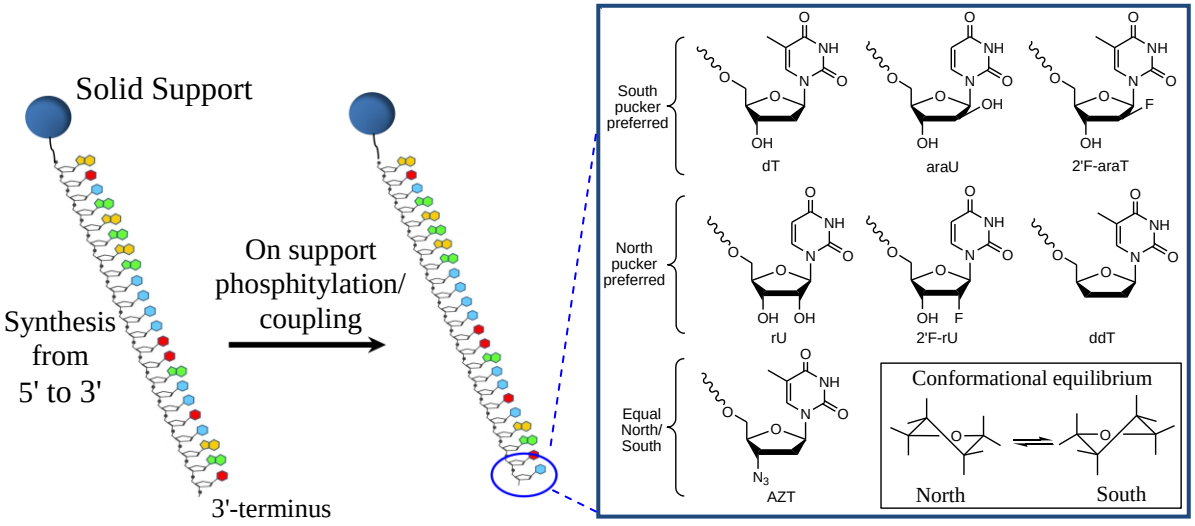

Figure 5.2. Divergent strategy for the synthesis of primers with varying 3'-terminal nucleotides. Incorporated nucleosides are shown in the blue box with sugar conformational preferences. The primer is grown from the 5' to 3'direction. The free 3'-hydroxyl group is converted to a phosphoramidite on the solid support and coupled to a various nucleosides. AZT coupling was accomplished using H-phosphonate chemistry.

5.1.3 Developing a fluorescent nucleotide excision assay to screen inhibitors

The second set of experiments addresses the need for new methods to discover inhibitors that can disrupt nucleotide excision. Currently, excision is assessed by gel-based assays, which are inconvenient for screening large chemical libraries. Using fluorescent nucleobase analogues, an assay amenable to 96-well microplate readers was designed. In one construct, a fluorescent nucleobase sensitive to hybridization[305]

such as 6-phenylpyrrolocytidine (PhpC, Chapter 3) or 2-aminopurine (2AP), are placed in the template strand opposite to the nucleotide to be excised (Figure 5.3A). In another construct, the fluorescent nucleobase is placed at the 3'-terminus of the primer and its excision by RT is monitored by fluorescence polarization (Figure 5.3B).

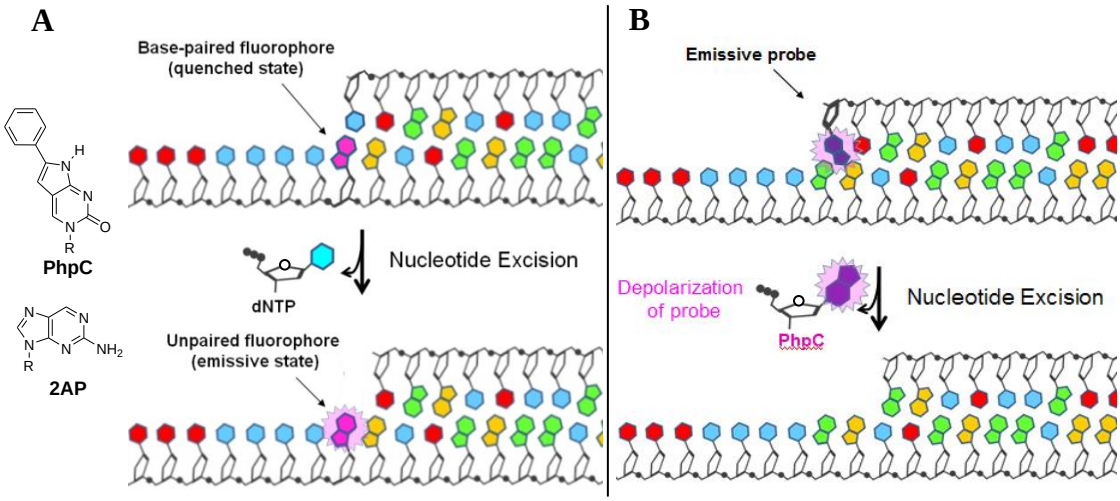

Figure 5.3. A. Fluorescence nucleotide excision assay with the fluorophore on the template stand. The hybridization sensitive fluorescent nucleobase (PhpC or 2AP) is base paired to the nucleotide to be excised. Excision is accompanied by a change in fluorescence. B. Nucleotide excision assay based on fluorescence depolarization with the fluorophore placed at the 3'-terminus of the primer strand. Excision of the fluorescent nucleotide generates a large decrease in fluorescence polarization.

5.2 Results and Discussion

5.2.1 Oligonucleotide *in situ* phosphitylation-coupling on solid support

The conversion of nucleosides to their 3'-(or 5'-) phosphoramidite derivatives can be quickly achieved using N,N-diisopropylamino-(2-cyanoethyl)-phosphoramidic chloride in high yields.[196] However, purification from side-products can prove challenging as phosphoramidites are prone to degradation on silica gel columns. This is particularly evident on smaller scales. In addition, some phosphoramidites are hygroscopic viscous oils making their storage and manipulation tedious. An alternative approach is to generate a phosphoramidite *in situ* or at the terminus of the growing support-bound oligonucleotide, eliminating the need for column purification.[389-391] The phosphoramidite can then be directly coupled to a free

hydroxyl group in the presence of standard activators such as 4,5-dicyanoimidazole[392] or 5-(ethylthio)-1H-tetrazole.[393]

Our research group has employed *in situ* phosphitylation techniques for the synthesis of lariat nucleic acids[394] and oligonucleotides containing 4'-selenonucleotides.[342] These studies, and reports from others, showed that 30 equivalents of phosphitylating reagent to the free hydroxyl gave the highest yields. In the current study, we adapted this method as a route to synthesize an oligonucleotide with different 3'-terminal nucleosides without having to synthesize each corresponding phosphoramidite. We first evaluated how the ratio of base to phosphitylating reagent affects the coupling yield. The 5'-hydroxyl of 3'-CPG-bound thymidine was reacted with N,N-diisopropylamino-(2-cyanoethyl)-phosphoramidic chloride in the presence of N,N-diisopropylethylamine (DIPEA) or pyridine as the base (Scheme 5.1). The phosphitylated support-bound thymidine was coupled to 5'-*O*-DMT-thymidine in 5-(ethylthio)-1H-tetrazole, and the yields were determined by measuring the release of trityl cation after treatment with 3% TCA (Table 5.1). Phosphitylation with 1 or 2 equivalents of DIPEA as the base gave excellent yields (> 95%), whereas coupling with pyridine as the base gave low yields (< 15%) (Table 5.1).

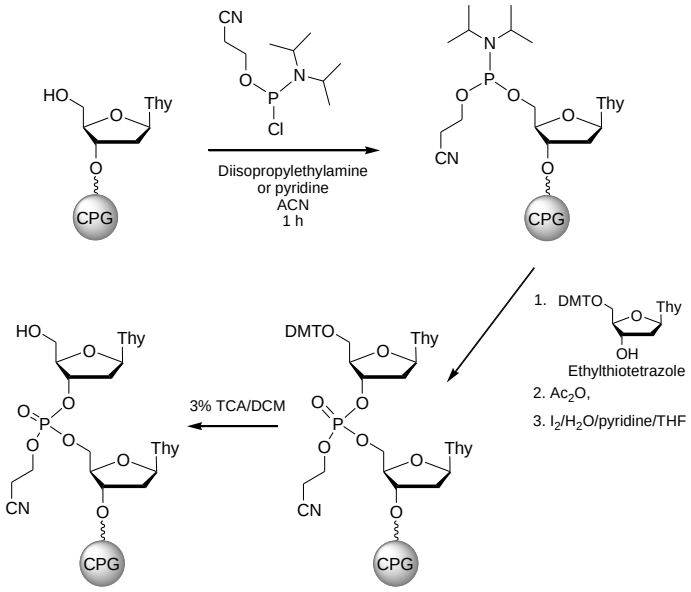

Scheme 5.1. Synthesis of a thymidine dinucleotide by phosphitylation-coupling on solid support. All steps were performed on an ABI 3400 synthesizer except the final detritylation, which was performed manually in culture tubes.

Table 5.1. Coupling yields for the synthesis of dTpdT on solid support via *in situ* phosphitylation-coupling under various basic conditions.

Column	Base conditions[a]	Trityl cation (μmoles/g)[b]	Coupling yield (%)[c]
1	2 equivalents DIPEA to phosphitylating agent	92.0	100
2	1 equivalent DIPEA to phosphitylating agent	90.4	98
3	0.5 equivalents DIPEA to phosphitylating agent	65.2	71
4	1 equivalent pyridine to phosphitylating agent	12.6	14

[a] The phosphitylating agent used was N,N-diisopropylamino-(2-cyanoethyl)-phosphoramidic chloride. [b] The amount of dimethoxytrityl (DMT) cation released per g of CPG was measured in triplicate by UV_{505} (ε=76 000 $M^{-1}cm^{-1}$). [c] The coupling yields were calculated as (DMT cation released after coupling)/(loading of T-CPG before coupling) × 100, where the loading of the column was 91.8 μmoles/g of CPG.

The reaction times for the on-support phosphitylation reaction were further optimized using 2 equivalents of DIPEA to phosphitylating agent in acetonitrile. The mixture of diisopropylamino-(2-cyanoethyl)-phosphoramidic chloride and DIPEA was added to the synthesis column in three 20 minute injections and showed no trace of unreacted 5'-hydroxyl according to mass spectrometry. We also report that the generation of the diisopropylammonium chloride salt produced during the reaction did not cause any blockage on the lines on the DNA synthesizer. The coupling of the CPG-bound oligonucleotide-5'-phosphoramidite to nucleosides dissolved in ACN, DCM, THF and DMF were accomplished. It was observed that the water content of the solvents greatly affected the overall yield. Unlike standard solid-phase synthesis which uses an excess of phosphoramidites, trace amounts of water will consume relatively more support bound phosphoramidite in this methodology and has a greater impact on coupling yields.

5.2.2 Synthesis of primers with varying 3'-terminal nucleotide analogues

Oligonucleotide p22 was synthesized in the reverse direction (5' to 3') using 3'-dimethoxytrityl-5'-phosphoramidites (Figure 5.2). 5' CPG-bound p22 was used to incorporate various nucleosides at the free 3'-end of p22 using the optimized phosphitylation-coupling conditions described in section **5.2.1**. Gel electrophoresis of p22 after on-column phosphitylation showed one major product with a molecular

weight corresponding to phosphitylated p22 as determined by mass spectral analysis (MW 6780.1 g/mole). CPG-bound phosphitylated p22 was coupled to 3'-acetyl thymidine in ACN to give p23, dideoxythymidine (ddT) in DMF to give ddT-p23, 2',3'-diacetylribo uridine in THF to give rU-p23 and 2',3'-diacetylarabinouridine in THF to give araU-p23. The extent of coupling was assessed by denaturing PAGE (Figure 5.4) and the presence of the products confirmed by mass spectrometry (Table 5.2). The full length products accounted for the major band on the gel for most of the crude oligonucleotides. The crude for ddT-p23 showed incomplete coupling, which was attributed to water present in DMF during the reaction. Primers 2'F-rU-p23 and 2'F-araT-p23 were synthesized using standard solid-phase synthesis since only the corresponding phosphoramidite building blocks were available. Primer p23 was also synthesized using standard solid-phase synthesis to serve as a 23-nucleotide positive control. The synthesis of primer AZT-p23 was accomplished from AZT 5'-H-phosphonate and p22. Azides react with trivalent phosphorus making AZT incompatible with the phosphoramidite approach, unlike the H-phosphonate approach which uses pentavalent phosphorus building blocks.[395] AZT 5'-H-phosphonate was prepared by treating AZT with diphenyl-H-phosphonate for 15 minutes followed by the addition of NEt_3 and H_2O (Scheme 5.2).[396] The product was purified by column chromatography. Coupling of AZT 5'-H-phosphonate to p22, followed by oxidation with 0.02 M I_2 in H_2O/THF/pyridine afforded AZT-p23 in good yield as assessed by PAGE (Scheme 5.2). This method is substantially less time-consuming than using the enzymatic approach for producing primers in much larger quantities.

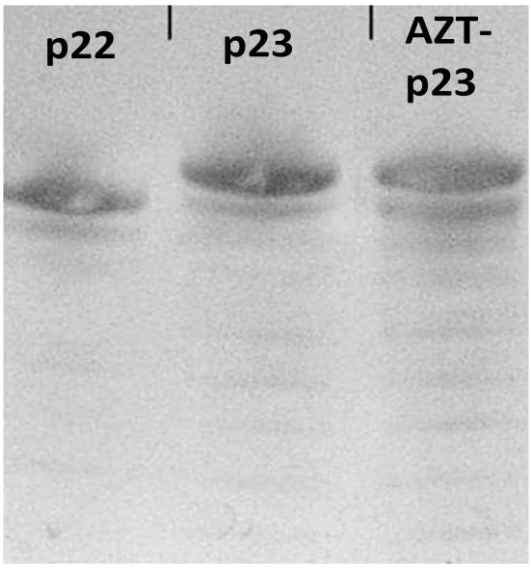

Figure 5.4. Analytical denaturing PAGE displaying crude material from the synthesis of p22, from grown the 5' to 3'direction, p23 synthesized from the on-column phosphitylation/coupling of p22 and 3'-acetyl thymidine and AZT-p23, synthesized from p22 and AZT 5'-H-phosphonate.

In summary, the on-support phosphitylation-coupling procedure generated the desired oligonucleotides. This methodology has merits as an alternative to making individual phosphoramidite building blocks for single nucleotide incorporations, provided the nucleosides can be dissolved in a solvent with very low water content. A divergent approach using H-phosphonate chemistry should be considered if nucleosides containing azides, such as AZT-analogues, wish to be incorporated.

Table 5.2. Sequences and MS data of oligonucleotides used in the nucleotide excision studies.

Name	Sequence (5' to 3')	Mass calculated	Mass measured
p22	gct aga gat ttt cca ttc tga c	6700.3	6700.4
p23	gct aga gat ttt cca ttc tga ct	7004.5	7004.6
rU-p23	gct aga gat ttt cca ttc tga cU	7006.5	7006.6
araU-p23	gct aga gat ttt cca ttc tga c<u>U</u>	7006.5	7006.7
2'F-rU-p23	gct aga gat ttt cca ttc tga c**U**	7008.6	7006.7
2'F-araT-p23	gct aga gat ttt cca ttc tga c**<u>T</u>**	7022.7	7022.7
ddT-p23	gct aga gat ttt cca ttc tga c**d**	6988.6	inc
AZT-p23	gct aga gat ttt cca ttc tga c**Z**	7029.5	7029.4
pC-p23	gct aga gat ttt cca ttc tga **pc**t	7104.7	7104.8
pC-p22	gct aga gat ttt cca ttc tga **pc**	6800.5	6800.6
dG-p23	gct aga gat ttt cca ttc tga cg	7029.5	7029.8
t42	ctc aga ccc ttt tag tca gaa tgg aaa atc tct agc agt ggc	1289.74	inc
pC-t42	ctc aga ccc ttt t**pc**g tca gaa tgg aaa atc tct agc agt ggc	12967.2	12986.5 (Na+)
2AP-t42	ctc aga ccc ttt t**2AP**g tca gaa tgg aaa atc tct agc agt ggc	12897.4	inc

Legend: T = thymidine, U = uridine, <u>U</u> = arabinouridine, **U** = 2'-deoxy-2'-fluoro uridine, **<u>U</u>** = 2'-deoxy-2'-fluoroarabinothymidine, **Z** = 3'-azido-3'-deoxythymidine, **d**=dideoxythymidine, **pc** = 6-phenylpyrrolodexoycytidine, **2AP** = 2-aminopurine, inc = inconclusive.

5.2.3 HIV-1 RT nucleotide excision of various 3'-terminal nucleotides

The extent of 3'-terminal nucleotide excision by HIV-1 RT is summarized in Table 5.3. Nucleosides are sorted by sugar conformation with those having greater preference for the northern conformations at the top. The majority of the nucleosides tested show preferential sugar puckers that equilibrate between the C3'-*endo* (North, P = 18) and C2'-*endo* (South, P = 162) conformations. The most notable exception is 2'F-araT that equilibrates between a C3'-*endo*/C2'-*exo* twist (North, P = -6) and South-East conformations (P = 126).[19] The nucleosides that were excised the

quickest, dT and 2'F-araT (Figure 5.5), show South or South-East sugar puckers respectively. AZT, which has equal populations of North and South conformations, also showed a high rate of excision (Table 5.3). However ddT, which has a greater preference for the North pucker, also showed moderate excision (Table 5.3). 2'F-rU, rU and araU were all poorly excised by WT HIV-1 RT. Among these, araU is the only one that does not show a preference for the North sugar pucker (Table 5.3).

Table 5.3. Phase (P) parameters, conformational equilibria and rate of HIV-1 RT excision of 3'-terminal nucleotides.

Nucleoside[a]	Northern P	Southern P	% North	Relative excision
2' F-rU[387]	21	159	87	-
ddT[397]	11	154	75	+
rU[387]	18	162	58	-
AZT[388]	22	160	50	++
araU[397]	22	151	46	-
2'F-araT[19]	-6	126	41	+++
dT[387]	18	162	40	+++

Legend: - no excision, + moderate excision, ++ fast excision, +++ very fast excision. [a] Nucleoside sugar conformational preferences were obtained from indicated references.

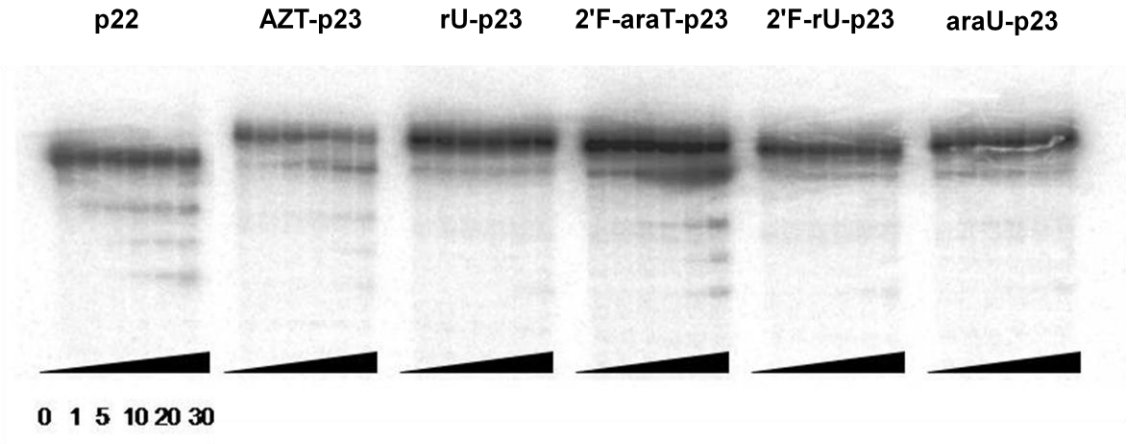

Figure 5.5. Denaturing PAGE displaying HIV-1 RT catalyzed nucleotide excision of 3'-termnial modified primers. All reactions were stopped at the times indicated for p22 (in minutes).

Considering sugar conformation alone, there is a trend towards Southern sugar puckers being excised easier than Northern puckers. This is in agreement with a study of nucleosides with fixed (or "locked") North conformations showing poor

excision.[376] Two notable exceptions to this trend suggest that other factors, such as steric effects with the RT, also contribute to excision. Mutational studies on RT found that araC could be resensitized to the excision reaction, implying a possible "steric gate" effect for excision similar to that found in incorporation (Y115).[385,398] In addition, ddT would present the least steric clashes with RT and in that regard is perhaps excised despite its preference for a North sugar pucker. Another consideration is that sugar conformation and sterics may not directly affect the catalytic efficiency of the excision reaction, but the propensity of the 3'-terminal nucleotide to reside in the P-site or the N-site. It has been shown that the excision reaction can only occur when a chain terminator occupies the N-site.[65] Site-specific footprinting experiments showed that a 3'-terminal AZT occupies the N-site, while a 3'-terminal ddT occupies the P-site.[65] This is in agreement with the excision data presented in this study and suggests that the translocation state of our primers must be addressed.

The data presented attempts to provide a direct investigation of how sugar conformation can affect the excision reaction carried out by RT independent of the incorporation reaction. In this regard, synthesizing terminated primers using solid phase synthesis is advantageous over enzymatic methods that incorporate the nucleotide from NTPs. Chemistries that are incapable for being incorporated by RT can be evaluated for excision. For the purpose of developing better NRTI drugs, incorporation must be considered. Invariably, this is the route NRTIs must take to generate a chain terminated complex. Further studies should therefore consider the rate of incorporation vs. excision.[399] Excision also needs to be tested using RTs with TAMs. Ultimately, novel structures that show reduced excision with these NRTI resistant variants will have greater therapeutic implications.

5.2.4 Design of fluorescent nucleotide excision assays

Nucleotide excision is emerging as a new potential antiretroviral target. To quickly screen a library of compounds that can block excision, we envisaged two models for fluorescence-based high throughput screening assays (Figure 5.3). The first assay incorporates a fluorescent nucleobase that is sensitive to its hybridization state, such as 2AP and PhpC. The fluorescent nucleobase is placed in the template strand based-paired to the 3'-terminal nucleotide of the primer strand (Figure 5.3A). In the duplexed state, both 2AP and PhpC would be expected to have their fluorescence in a less emissive state. Upon excision of the 3'-terminal nucleotide by HIV-1 RT, the unpaired fluorescent nucleobase would become more emissive (Figure 5.3A). In a second model, the 3'-terminal nucleotide is a fluorescent nucleobase analogue, such as PhpC (Figure 5.3B). The excision of the terminal fluorophore from the primer-template would be accompanied by a large change in the size of the fluorescent species, and this is expected to cause a measurable decrease in fluorescence polarization (depolarization) (Figure 5.3B).

The fluorescent templates (pC-t42 and 2AP-t42) and primer (pC-p22) were synthesized using standard solid-phase oligonucleotide synthesis and their fluorescence properties measured on a fluorescence spectrophotometer. The fluorescence of the single-stranded templates was compared to double-stranded primer-template duplexes. In comparison to the single-stranded oligonucleotide, the fluorescence of pC-t42 slightly increased when bound to p22 and decreased by 30% when bound to dG-p23 (Figure 5.6). The decrease in fluorescence upon hybridization to p23, when dPhpC is base-paired, is in agreement with previous studies. PhpC shows relatively less quenching when placed at the terminus of a duplex.[322] This trend appears to follow in the present study, except PhpC is on a longer template. However, the increased fluorescence when binding to p22 was not expected as PhpC is unpaired. A similar trend in fluorescence changes was observed with the 2AP-containing template, where 2AP-t42 bound to p23 showed a 50% decrease in fluorescence compared to the single-stranded template (Figure 5.6). These values suggest that a fluorescence assay based on the 2AP-containing template may show a better signal to noise ratio when evaluating excision.

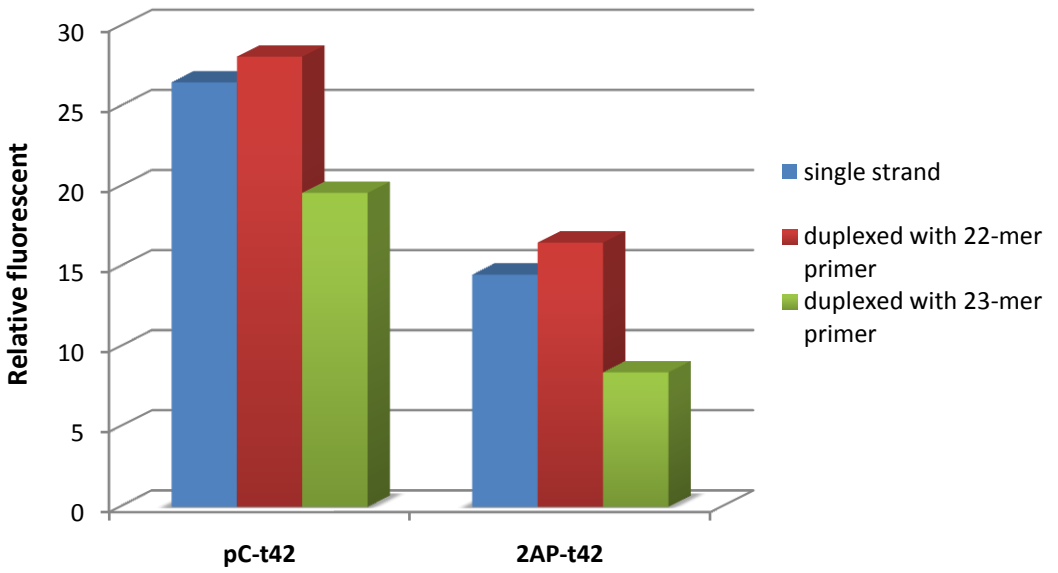

Figure 5.6. Comparison of the fluorescence intensity of PhpC and 2AP containing templates single-stranded (blue bars), duplexed to p22 (red bars) and duplexed to complementary 23-mer primers (green bars). Samples were measured at a concentrations of 1 μM in 10 mM phosphate buffer (pH 7.0) and 50 mM NaCl at 25°C, λ_{ex}=360 nm, λ_{emm}=465 nm for PhpC and λ_{ex}=307 nm, λ_{emm}=371 nm for 2-AP.

The fluorescence signals of the substrate and product of the fluorescence polarization assay was also verified. The free PhpC nucleotide has an fluorescence polarization value below 0.03 FP units,[400] substantially less than the value for the pC-p22•t40 primer template (0.28 FP units). Thus, the FP change would be easily measurable should dPhpC be a competent substrate for excision.

5.2.5 Nucleotide excision assays on 96-well microplate reader

The fluorescence template incorporating 2AP was tested on a 96 well microplate reader. Due to the low excitation and emission wavelengths of 2AP, the intrinsic fluorescence of HIV-1 RT interfered with these readings. Since it was evident that no fluorescence assays using 2AP could be carried out in conjunction with HIV-1 RT, this strategy was abandoned.

The methodology incorporating a 3'-terminal dPhpC on the primer was also tested for HIV-1 RT catalyzed excision on a 96 well microplate reader (Figure 5.7). The polarization values for the primer-template (pC-p22•p42) in the microplate reader were in agreement with those measured on the fluorescence spectrophotometer. Interestingly, the fluorescence polarization increased in samples containing HIV-1 RT

(Figure 5.7, red curve and green curve). This was attributed to RT binding to the primer-template and suggests that PhpC may be a suitable probe to study nucleic acid-protein binding interactions. The fluorescence polarization was unaffected in samples containing only primer-template (Figure 5.7, blue curve) or primer-template and pyrophosphate (Figure 5.7, purple curve). The samples containing RT and primer-template without pyrophosphate show a slow decrease in polarization, associated with nucleotide excision (Figure 5.7, red curve). This was attributed to contaminating pyrophosphate that may be present in the enzyme preparation and could be remedied by supplementing with pyrophosphatase. The samples containing HIV-1 RT and pyrophosphate demonstrated the greatest rate of nucleotide excision (Figure 5.7, green curve), as judged by depolarization, albeit to a lesser extent than in the gel based assays. We hypothesize that several factors may contribute to this observation. The conditions of the gel-based and microplate reader excision reactions differed in substrate and enzyme concentrations. In addition, the HIV-1 RT preparations originated from different batches. It is also possible that dPhpC is a poor substrate for excision, as there is evidence that nucleobase composition affects the rate of excision.[399] Gel-based excision assays incorporating dP-p23 should determine how the excision of dPhpC compares to other nucleobases. If the rate of excision of dPhpC is insignificant in comparison to the common nucleobases, other highly emissive analogues, such as 6-phenylalkynyluridine, could be substituted.[305] This assay should also be performed in the presence of NRTI resistant variants of RT with enhanced rates of excision. Finally, known inhibitors of excision, such as foscarnet and adenine-tetraphosphate-AZT dinucleotide, should verify that this system can indeed detect potential drug candidates. This will determine the merits of this system for high throughput screening.

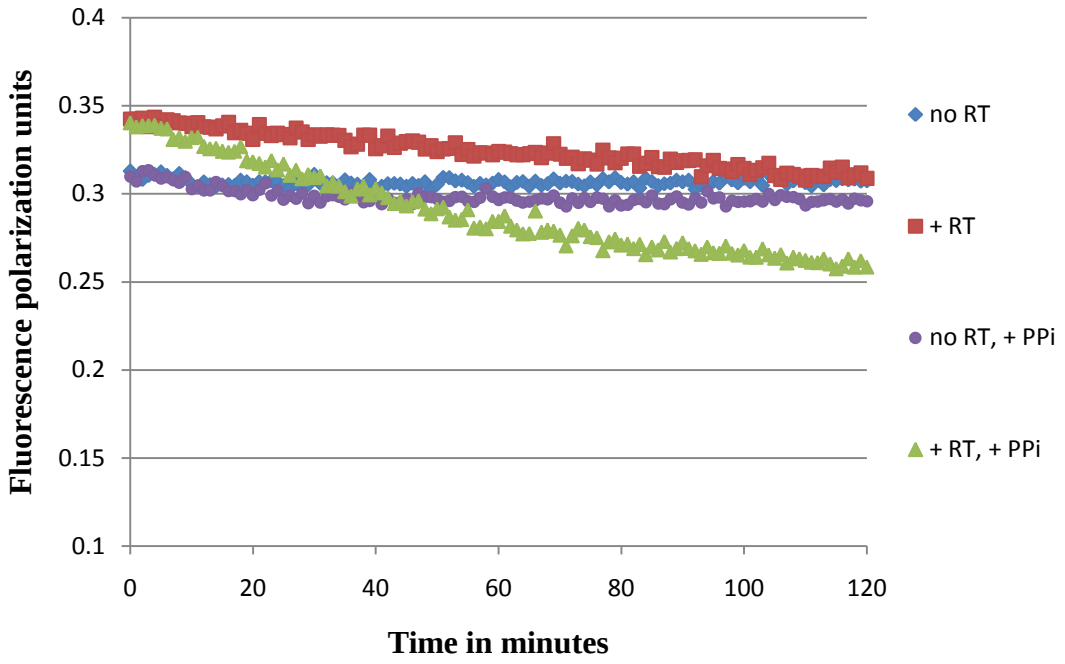

Figure 5.7. Fluorescence polarization assay to measure HIV-1 RT catalyzed nucleotide excision of duplex (dP-p23•p42). The primer (dP-p23) incorporates a terminal dPhpC, an emissive fluorescent nucleobase analogue. Each curve is the average of samples run in duplicate. Legend: blue diamonds, dP-p23•p42; red squares, HIV-1 RT and dP-p23•p42; purple circles, dP-p23•p42 and pyrophosphate; green trianlges, HIV-1 RT, dP-p23•p42 and pyrophosphate.

5.3 Conclusion and Future Directions

5.3.1 Conclusions

This preliminary nucleotide excision study provides a framework for future experiments geared to understanding pyrophosphorolysis as a key mechanism of drug resistance. The gel based nucleotide excision assay suggests North biased sugar puckers are poorly excised by RT. Sterics also appear to play a role in excision as the ddT (north pucker) showed modest excision. South and South-East puckers, as found in dT and 2'F-araT respectively, are excised easily and may not be suitable excision-resistant modifications. Evidently, these results need to be repeated with more nucleotide analogues and with RTs containing excision enhancing mutations.

The on-column phosphitylation/coupling strategy used in these studies demonstrates that the synthesis of nucleoside phosphoramidite synthons can be avoided. This can be very useful if the synthesis of a larger library of primers is

required. Also, the synthesis of the AZT-chain terminated primer using H-phosphonate chemistry is an attractive, alternative strategy to conventional enzymatic approaches that produce generally limited amounts of material.

Our initial attempts at developing a high-throughput screening method for nucleotide excision inhibitors has met with some degree of success. PhpC outcompetes 2AP in terms of fluorescence intensity and having a red-shifted emission spectrum that does not overlap with intrinsic protein fluorescence. Using the fluorescence polarization of PhpC, RT catalyzed nucleotide excision was monitored in a 96 well microplate reader. This reaction proceeded slower compared to gel based assays, and may perform better after optimizing the conditions. The true utility of this assay will only be established when it is tested to screen inhibitors of excision.

5.3.2 Future Work

A larger library of 3'-terminal nucleotides with preference for a wider range of sugar puckers should be analyzed to obtain clearer trends on the role of conformation on nucleotide excision. Nucleotide analogues with fixed conformations, such as locked nucleic acids (LNA), would be advantageous for these purposes. Development of a divergent on-column synthesis methodology utilizing H-phosphonate chemistry would aid in synthesizing 3'-terminal nucleotides with azide groups. Future studies should also explore nucleobase modifications, such as PhpC, since base composition also affects excision. As discussed previously, the rates of incorporation[109] and translocation from the P-site to the N-site should also be considered when assessing excision rates.[65]

Further validation is required before the fluorescent polarization assay described in this study can be used for screening compounds that block excision. The fluorescent nucleobase, in this case dPhpC, must be representative of the NRTIs that are excised in resistance mutations. For this purpose, the rate of excision of fluorescent nucleobase analogues must first be verified in gel-based excision assays with wild type RT and variants that display enhanced excision. Eventually, the excision assay needs to be tested against known inhibitors. Finally, the assay should be utilized to serve its purpose of screening new compounds that can serve as new drug candidates to block nucleotide excision.

5.4 Experimental methods

5.4.1 General methods

Chemicals and solvents were ACS grade or higher and were purchased from Sigma-Aldrich or Thermo-Fisher. Anhydrous pyridine and DMF was obtained by distilling over calcium hydride. All reagents used for oligonucleotide synthesis, including 5'-*O*-DMT-2'-deoxyribonucleotides, 3'-*O*-DMT-2'-deoxyribonucleotides phosphoramidites, β-cyanoethyl-(N,N-diisopropylamino) phosphorochloridite and acetyl protected nucleosides were purchased from Chemgenes Corp. dPhpC was synthesized according to previously described methods by Hudson and co-workers (University of Western Ontario).[322] AZT was obtained from Sigma-Aldrich. Autoclaved Millipore water treated with diethylpyrocarbonate (DEPC)[290] was used to manipulate DNA and prepare aqueous buffers.

5.4.2 Synthesis of 5'-H-phosphonate-3'-azido-3'-deoxythymidine[401]

Distilled pyridine (5 mL) was added to AZT (534 mg; 2 mmol) in a dry 25 mL round bottom flask and purged with argon.[396,402] To this solution, 7 mmols of diphenyl-H-phosphonate was added drop wise under inert conditions. The mixture was stirred at room temperature for 15 minutes, followed by addition of 2 mL of a 1:1 mixture of triethylamine and water (Scheme 5.2). The solution was stirred for an additional 15 minutes after which the mixture was evaporated to dryness by rotary evaporation, resuspended in minimal dichloromethane and applied to a silica gel column. 5'-hydrogenphosphonate-3'-azido-3'-deoxythymidine was eluted in a mobile phase containing 10% methanol in chloroform. The product was evaporated to dryness and sublimed in 2 mL of dry benzene to give the triethylammonium salt of the purified product as a thick white oil (170 mg, 52% yield). The ^{1}H NMR of the product was consistent with previous reported spectra.[401] ^{1}H NMR (400 MHz, $CDCl_3$) δ (ppm) = 10.0 (s, 1H, N-H), 7.65 (s, 1H, H-6), 7.12 (d, 1H, *J*=7.2, P-H), 6.24 (t, 1H, *J*=6.8, H-1'), 4.42 (dd, 1H, *J*=9.4, *J*=5.8, H-3'), 4.10 (m, 2H, H-5'), 3.99 (d, 1H, *J*=2.5, H-4'), 2.3 (t, 2H, *J*=6.2, H-2'), 1.90 (d, 3H, *J*=0.8, CH_3 on C5). ^{31}P NMR (200 MHz, CD_3CN) δ = 3.39 ppm. ESI-TOF (m/z) 330.18 (M-).

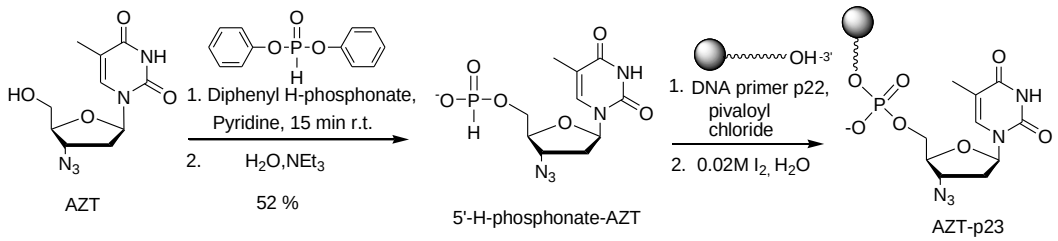

Scheme 5.2. Synthesis of 5'-hydrogenphosphonate-3'-azido-3'-deoxy thymidine (AZT 5'-H-phosphonate) from 3'-azido-3'-deoxy thymidine (AZT) and AZT-p23.

5.4.3 General synthesis and purification of oligonucleotides

Solid-phase synthesis of oligonucleotides p22, p23, rU-p23, araFT-p23, pC-p23, pC-22, pC-t42 and 2AP-t42 were carried out on an Applied Biosystems 3400 DNA synthesizer using standard protocols.[205] Cleavage from the solid-support was carried out in a 3:1 mixture of NH_4OH:EtOH at room temperature for 48 hours. The crude oligonucleotides were quantitated by their UV absorbance at 260 nm on a Cary-300 UV-VIS spectrophotometer (Varian Inc). Crude products were then analyzed and purified by denaturing PAGE (7M urea) and visualized by UV shadowing using 254 nm light for non-fluorescent oligonucleotides, and 365 nm light for fluorescent oligonucleotides. Full length products were excised from the gels using a sterile surgical blade, and eluted in DEPC treated water. The eluted products were desalted by size-exclusion chromatography on G-25 Sephadex (GE Healthcare) and quantitated. Alternatively, oligonucleotides were purified by reverse-phase HPLC on Varian Pursuit C-18 column (4.6 mm diameter 250 mm length) in buffer consisting of 100 mM triethyl ammonium acetate, pH 7.2 (95:5 water:acetonitrile) and eluted with increasing concentrations of 100% acetonitrile. RP-HPLC purified oligonucleotides were evaporated to dryness and quantitated. The mass of synthesized oligonucleotides was obtained by LC-ESI at the Concordia University MS facility.

5.4.4 Oligonucleotide synthesis using on column phosphitylation/coupling

Oligonucleotides rU-p23, araU-p23 and ddT-p23 were synthesized using the on support phosphitylation-coupling methodology. rU-p23, araU-p23 and ddT-p23 were synthesized from p22 5'-bound to the solid support grown in the 5' to 3' direction. Oligonucleotides were phosphitylated at the 3'-end on an ABI 3400 DNA synthesizer. A mixture containing 40 μl of diisopropylethylamine (DIPEA), 20 μl of N,N-

diisopropylamino-(2-cyanoethyl)-phosphoramidic chloride and 2 mL of ACN was placed on an amidite port on the DNA synthesizer. The mixture was delivered to columns containing p22 and reacted for 20-30 minutes. This step was repeated 2 or 3 times after which the column was purged with argon and flushed with ACN. 0.1 M 2',3'-acetyl ribouridine in anhydrous THF, 0.1 M 2',3'-acetyl arabinouridine in anhydrous THF or 2',3'-didexoythymidine in anhydrous DMF were placed on different amidite ports. 2',3'-acetyl ribouridine, 2',3'-acetyl arabinouridine and 2',3'-didexoythymidine were delivered to separate columns containing p22 in the presence of the activator, 5-(ethylthio)-1H-tetrazole (ETT), and coupled for one hour. After coupling, the internucleotide linkages were oxidized with 0.02 M iodine in H_2O/pyridine/THF (1:7:2). The oligonucleotides were deprotected and cleaved from the solid support and purified using the standard protocols described in the previous section.

5.4.5 Synthesis of AZT-p23

AZT-p23 was synthesized by manually coupling AZT 5'-H-phosphonate to p22 according to published H-phosphonate chemistry.[396,402,403] A column containing p22 grown in the 5' to 3' direction bound to the solid support at the 5'-end was sequentially washed with 4 mL of DCM over 2 minutes, 2 mL of ACN over 1 minute, and 2 mL 3:1 ACN:Py over 1 minute. 0.3 mL of a freshly prepared solution of 75 mM AZT 5'-H-phosphonate in distilled pyridine and 0.3 mL of a freshly prepared solution of 225 mM pivaloyl chloride in 3:1 ACN:Py were added to the column using syringes. After 2.5 minutes, the column was flushed with 3:1 ACN:Py over 1 minute and 1 mL ACN over 1 minute. The column was placed on an ABI 3400 DNA synthesizer and oxidized for 10 minutes using 0.02 M iodine in H_2O/pyridine/THF (1:7:2). AZT-p23 was deprotected and cleaved from the solid support and purified using the standard protocols described in the previous sections.

5.4.6 Fluorescent Measurements

Fluorescence intensity measurements were carried out on a Cary Eclipse spectrophotometer equipped with a multi-cell Peltier temperature controller and automated polarization accessories. Measurements were carried out in 1 cm X 1 cm quartz cells in 2 mL volumes at r.t. in 1 or 0.25 μM concentrations in a buffer of 10

mM sodium phosphate at pH 7.0 and 50 mM NaCl. Excitation and emission bandwidths were set at 5 nm for all experiments. The emission spectra of PhpC-containing oligonucleotides were obtained by exciting at 360 nm and monitoring the emission from 400 to 600 nm. The emission spectra of 2AP-containing oligonucleotides were obtained by exciting at 307 nm and monitoring the emission from 320 to 500 nm.

5.4.7 Gel-based RT nucleotide excision assay

Gel-based nucleotide excision assays were carried out by Dr. Tatiana Ilina, a member of the laboratory of Dr. Michael A. Parniak at the University of Pittsburgh, Department of Microbiology and Molecular Genetics. Wild type p66/p51 HIV-1 RT was prepared by previously described methods.[52] DNA primers were 5'-radiolabeled with γ-^{32}P ATP by T4 polynucleotide kinase (Fermentas) using the manufacturer's recommended procedure. The DNA template (ctc aga ccc ttt tphpcg tca gaa tgg aaa atc tct agc agt ggc) and 5'-^{32}P-labeled primers were combined in a 2:1 ratio and annealed by heating to 95°C followed by slow cooling to room temperature. Wild type HIV-1 RT (40 nM final concentration) and annealed primer-templates (20 nM final concentration) were incubated for 10 minutes at 37°C in reaction buffer (50 mM Tris-HCl, pH 8.0, 50 mM KCl). The reactions were initiated by the addition of sodium pyrophosphate to a concentration of 50 μM and 6 mM $MgCl_2$. Aliquots were removed at various times as indicated in Figure 5.6 and stopped by the addition of an equal volume of loading buffer (98% deionized formamide, 1 mg/mL bromophenol blue, and 1 mg/mL xylene cyanol). Reaction products were resolved on 14% denaturing PAGE and analyzed by phosphoimaging. The extent of nucleotide excision was assessed by the amount of full-length primer remaining as measured by densitometry.

5.4.8 Fluorescent nucleotide excision assay

Nucleotide excision was monitored by fluorescence on a Biotek Synergy 4 in 96-well opaque plates. Experiments were run under identical buffer conditions as gel-based assays in a final volume of 100 μL. The final concentration of the primer-template substrate was 100 nM final and 25 nM HIV-1 RT. Reactions were initiated by the addition of 50 μL of 300 μM sodium pyrophosphate (or water for controls).

Excitation and emission wavelengths for PhpC were 360 nm and 465 nm respectively, and for 2-aminopurine were 310 nm and 370 nm respectively.

Chapter 6 Contributions to knowledge

6.1 Summary of contributions to knowledge

6.1.1 Chemically modified hairpins with inhibition towards HIV-1 RT RNase H

Based on site-specific footpriting assays, we have shown that short nucleic acid hairpin inhibitors of RNase H and a primer-template substrate are capable of binding to HIV-1 RT simultaneously. This suggests that the RNase H activity can be an antiretroviral target independent of the rest of the enzyme. Hairpins conjugated with cholesterol display enhanced thermal stability compared to corresponding unconjugated hairpins. DLS experiments suggest the cholesterol-conjugated hairpins aggregate and have greater potency towards the polymerase and RNase H activities of HIV-1 RT through a bimodal mechanism of action.

6.1.2 Synthesis and physical properties of RNA containing PhpC

The fluorescent cytidine analogue, 6-phenylpyrrolocytidine (PhpC) was synthesized and incorporated in RNA. Compared to unmodified RNA, oligonucleotides bearing PhpC showed increased thermal stability. Like dPhpC, the fluorescence intensity of single-stranded oligonucleotides containing PhpC is quenched upon duplex with complementary strands. The extent of quenching is dependent on the length and composition of the sequence. The neighboring guanosine residues reduce the fluorescence intensity of PhpC.

6.1.3 A real-time fluorescent assay incorporating PhpC to measure RNaseH activity

A fluorescent RNase H assay incorporating PhpC in RNA was developed. This represents the first example of a fluorescent nucleotide analogue amenable to high-throughput screening that outperforms widely-used fluorophores. This assay could readily measure RNase H activity in real-time in both fluorescence intensity and fluorescence polarization modes. Inhibition of HIV-1 RT RNase H activity by the inhibitor DHBNH was shown to be detected by this method.

6.1.4 Incorporation of PhpC into siRNA

To further validate PhpC as a biologically relevant nucleotide analogue, siRNAs containing PhpC insertions were shown capable of maintaining gene-silencing

activity. Inserting PhpC in both the sense and antisense strands were well tolerated. The high fluorescence intensity of PhpC motivated us to determine if its emission can be detected in live cells. A single incorporation of PhpC into siRNA allowed us to follow its distribution into HeLa cells, despite the background fluorescence of NADH.

6.1.5 Sugar conformational preferences in HIV-1 RT nucleotide excision

The sugar conformational preference for nucleotide excision by HIV-1 RT was addressed. Various 3'-terminal nucleotides were synthesized by a divergent on-column phosphitylation/coupling technique. This procedure is not compatible with azides, therefore we developed a convenient and high-yielding route to synthesize AZT chain-terminated primers via H-phosphonate chemistry. This work suggests that nucleotides with northern sugar puckers, such as RNA and 2'F-RNA are poorly excised by HIV-1 RT. Also, it appears steric contributions at the 2' and 3' positions may contribute to the rate of excision.

6.1.6 Development of an assay to screen inhibitors of nucleotide excision

As nucleotide excision is gaining interest as a therapeutic target for HIV, we explored methods to screen agents that block this activity using fluorescent nucleobases. 2-aminopurine is not a suitable fluorescent analogue for use in enzymatic assays on plate readers due to the overlapping intrinsicl fluorescence of proteins. A PhpC fluorescence polarization assay demonstrated real-time monitoring of nucleotide excision. To our knowledge, this represents the first example of a convenient and non-gel based screening method to measure nucleotide excision.

6.2 Papers and conference presentations

6.2.1 Papers published

Alexander S. Wahba, Tatiana Ilina, Michael A Parniak and Masad J. Damha. “Sugar conformational preferences during nucleotide excision by HIV-1 RT.” *Nucleic Acids Symposium Series*. 54, 2010, *in press*.

Alexander S. Wahba, Abbasali Esmaeili, Masad J. Damha and Robert H.E. Hudson. A single-label phenylpyrrolocytidine provides a molecular beacon-like response

reporting HIV-1 RT RNase H activity. *Nucleic Acids Research.* 38: 1048-1056 , 2010.

Alexander S. Wahba, Masad J. Damha and Robert H.E. Hudson. RNA Containing pyrrolocytidine base analogs: good binding affinity and fluorescence that responds to hybridization. *Nucleic Acids Symposium Series*. 52, 399-400, 2008.

Jonathan K. Watts, Blair D. Johnston, Kumarasamy Jayakanthan, Alexander S. Wahba, B. Mario Pinto and Masad J. Damha; "Synthesis and biophysical characterization of oligonucleotides containing a 4'-selenonucleotide," *Journal of the American Chemical Society*, 130, 8578–8579, 2008.

Jonathan K. Watts, Niloufar Choubdar, Kashinath Sadalapure, Francis Robert, Alexander S. Wahba, Jerry Pelletier, B. Mario Pinto and Masad J. Damha; "2'-Fluoro-4'-thioarabino-modified oligonucleotides: Conformational switches linked to siRNA activity," *Nucleic Acids Research*, 35: 1441-1451, 2007.

6.2.2 Manuscripts in preparation

Alexander S. Wahba, Fereshteh Azizi, Glen F. Deleavey, Francis Robert, Jerry Pelletier and Masad J. Damha "siRNAs incorporating 6-phenylpyrrolocytidine: a "molecular spy" with improved stability capable of monitoring activity and biodistribution."

Alexander S. Wahba, Bruno Marchand, Michael A. Parniak. Matthias Götte and Masad J. Damha. "Inhibition of HIV-1 RT RNase H Activity by chemically modified nucleic acid hairpins."

Alexander S. Wahba, Adam Katolik, Tatiana Ilina, Robert H.E. Hudson, Michael A Parniak and Masad J. Damha. "A method to screen inhibitors of HIV-1 RT nucleotide excision incorporating a fluorescent nucleobase analogue."

6.2.3 Conference Presentations

The presenting author is underlined

Alexander S. Wahba, Tatiana Ilina, Michael A Parniak and Masad J. Damha. "Sugar conformational preferences during nucleotide excision by HIV-1 RT." 19th IRT 3NA Universite de Lyon, Lyon, France. Aug. 29 – Sept 3, 2010.

Alexander S. Wahba, Masad J. Damha and Robert H.E. Hudson. "Properties of RNA containing phenylpyrroloribocytidine and its applicability to fluorescent microplate assays." 4th Annual Meeting of the Oligonucleotide Therapeutics Society, Boston, MA, United States, October 15- 18, 2008.

Alexander S. Wahba, Masad J. Damha and Robert H.E. Hudson. "RNA Containing 6-Phenylpyrrolocytidine Base Analogs: Hybridization responsive fluorescence applied to the study of RNase H" 18th IRT 3NA and 35th SNAC, Kyoto University, Kyoto, Japan. Sept. 8-12, 2008.

Alexander S. Wahba and Masad J. Damha. Short RNA hairpins targeting the RNase H activity of HIV-1 RT. 234th ACS National Meeting, Boston, MA, United States, August 19-23, 2007.

Alexander S. Wahba, Bruno Marchand, Matthias Götte and Masad J. Damha. Short RNA hairpins as potential antiretroviral agents. 89th Canadian Chemistry Conference and Exhibition. May 24-31, Halifax, NS, 2006.

Alexander S. Wahba, Bruno Marchand, Matthias Götte and Masad J. Damha. Short RNA hairpins as potential antiretroviral agents. 16th Quebec-Ontario Mini Symposium of Bioorganic and Organic Chemistry. November 10-12, Sainte Adele, QC, 2005.

References

1. G. M. Blackburn, M. J. Gait, D. Loakes, D. M. Williams, Nucleic Acids in Chemistry and Biology, (3rd edition), Royal Society of Chemistry, Cambridge, UK, **2006**.

2. F. Barresinoussi, J. C. Chermann, F. Rey, M. T. Nugeyre, S. Chamaret, J. Gruest, C. Dauguet, C. Axlerblin, F. Vezinetbrun, C. Rouzioux, W. Rozenbaum, L. Montagnier. Isolation of a T-Lymphotropic Retrovirus from a Patient at Risk for Acquired Immune-Deficiency Syndrome (Aids). *Science* **1983**, *220*(4599), 868-871.

3. M. Popovic, M. G. Sarngadharan, E. Read, R. C. Gallo. Detection, Isolation, and Continuous Production of Cytopathic Retroviruses (Htlv-Iii) from Patients with Aids and Pre-Aids. *Science* **1984**, *224*(4648), 497-500.

4. O. T. Avery, C. M. MacLeod, M. McCarty. Studies on the Chemical Nature of the Substance Inducing Transformation of Pneumococcal Types Induction of Transformation by a Desoxyribonucleic Acid Fraction Isolated from Pneumococcus Type Iii. *J. Exp. Med.* **1944**, *79*(2), 137-158.

5. J. D. Watson, F. H. C. Crick. Molecular Structure of Nucleic Acids - a Structure for Deoxyribose Nucleic Acid. *Nature* **1953**, *171*(4356), 737-738.

6. M. H. F. Wilkins, A. R. Stokes, H. R. Wilson. Molecular Structure of Deoxypentose Nucleic Acids. *Nature* **1953**, *171*(4356), 738-740.

7. R. E. Franklin, R. G. Gosling. Molecular Configuration in Sodium Thymonucleate. *Nature* **1953**, *171*(4356), 740-741.

8. J. D. Watson, F. H. C. Crick. Genetical Implications of the Structure of Deoxyribonucleic Acid. *Nature* **1953**, *171*(4361), 964-967.

9. P. A. Levene. The structure of yeast nucleic acid. IV. Ammonia hydrolysis. *J. Biol. Chem.* **1919**, *40*(2), 415-424.

10. F. Griffith. The significance of pneumococcal types. *J. Hyg. (Lond).* **1928**, *27*, 113-159.

11. J. M. Gulland, D. O. Jordan, H. F. W. Taylor. Deoxypentose Nucleic Acids .2. Electrometric Titration of the Acidic and the Basic Groups of the Deoxypentose Nucleic Acid of Calf Thymus. *J. Chem. Soc.* **1947**(Sep), 1131-1141.

12. W. T. Astbury. X-Ray Studies of Nucleic Acids. *Symp. Soc. Exp. Biol.* **1947**, *1*, 66.

13. B. Magasanik, E. Vischer, R. Doniger, D. Elson, E. Chargaff. The Separation and Estimation of Ribonucleotides in Minute Quantities. *J. Biol. Chem.* **1950**, *186*(1), 37-50.

14. R. E. Franklin, R. G. Gosling. Evidence for 2-Chain Helix in Crystalline Structure of Sodium Deoxyribonucleate. *Nature* **1953**, *172*(4369), 156-157.

15. V. A. Bloomfield, D. M. Crothers, I. Tinoco, Nucleic Acids: Structures, properties, and functions, University Science Books, Sausalito, CA, **2000**.

16. C. Altona, M. Sundaralingham. Conformational-Analysis of Sugar Ring in Nucleosides and Nucleotides - New Description Using Concept of Pseudorotation. *J. Am. Chem. Soc.* **1972**, *94*(23), 8205-&.

17. C. Thibaudeau, J. Plavec, N. Garg, A. Papchikhin, J. Chattopadhyaya. How Does the Electronegativity of the Substituent Dictate the Strength of the Gauche Effect. *J. Am. Chem. Soc.* **1994**, *116*(9), 4038-4043.

18. J. Chattopadhyaya, C. Thibaudeau, P. Acharaya, Stereoelectronic Effects in Nucleosides & Nucleotides and their Structural Implications, (2nd Edition), Uppsala University Press, Uppsala, **2005**.

19. J. K. Watts, K. Sadalapure, N. Choubdar, B. M. Pinto, M. J. Damha. Synthesis and conformational analysis of 2'-fluoro-5-methyl-4'-thio-arabino-uridine (4'S-FMAU). *J. Org. Chem.* **2006**, *71*(3), 921-925.

20. M. Egli, N. Usman, S. G. Zhang, A. Rich. Crystal-Structure of an Okazaki Fragment at 2-a Resolution. *Proc. Natl. Acad. Sci. U. S. A.* **1992**, *89*(2), 534-538.

21. M. Egli, S. Portmann, N. Usman. RNA hydration: A detailed look. *Biochemistry* **1996**, *35*(26), 8489-8494.

22. P. Acharya, P. Cheruku, S. Chatterjee, S. Acharya, J. Chattopadhyaya. Measurement of nucleobase pK(a) values in model mononucleotides shows RNA-RNA duplexes to be more stable than DNA-DNA duplexes. *J. Am. Chem. Soc.* **2004**, *126*(9), 2862-2869.

23. M. Egli, P. S. Pallan. Crystallographic Studies of Chemically Modified Nucleic Acids: A Backward Glance. *Chem. Biodivers.* **2010**, *7*(1), 60-89.

24. L. Gold, B. Polisky, O. Uhlenbeck, M. Yarus. Diversity of Oligonucleotide Functions. *Annu. Rev. Biochem* **1995**, *64*, 763-797.

25. C. Tuerk, P. Gauss, C. Thermes, D. R. Groebe, M. Gayle, N. Guild, G. Stormo, Y. Daubentoncarafa, O. C. Uhlenbeck, I. Tinoco, E. N. Brody, L. Gold. Cuucgg Hairpins - Extraordinarily Stable RNA Secondary Structures Associated with Various Biochemical Processes. *Proc. Natl. Acad. Sci. U. S. A.* **1988**, *85*(5), 1364-1368.

26. C. J. Cheong, G. Varani, I. Tinoco. Solution Structure of an Unusually Stable RNA Hairpin, 5'ggac(Uucg)Gucc. *Nature* **1990**, *346*(6285), 680-682.

27. G. Varani, C. J. Cheong, I. Tinoco. Structure of an Unusually Stable RNA Hairpin. *Biochemistry* **1991**, *30*(13), 3280-3289.

28. F. H. T. Allain, G. Varani. Structure of the P1 Helix from Group-I Self-Splicing Introns. *J. Mol. Biol.* **1995**, *250*(3), 333-353.

29. S. Nozinovic, B. Furtig, H. R. A. Jonker, C. Richter, H. Schwalbe. High-resolution NMR structure of an RNA model system: the 14-mer cUUCGg tetraloop hairpin RNA. *Nucleic Acids Res.* **2010**, *38*(2), 683-694.

30. N. H. Williams, B. Takasaki, M. Wall, J. Chin. Structure and nuclease activity of simple dinuclear metal complexes: Quantitative dissection of the role of metal ions. *Acc. Chem. Res.* **1999**, *32*(6), 485-493.

31. F. Westheimer. Why nature chose phosphates. *Science* **1987**, *235*(4793), 1173-1178.

32. A. Kornberg, I. R. Lehman, M. J. Bessman, E. S. Simms. Enzymic Synthesis of Deoxyribonucleic Acid. *Biochim. Biophys. Acta* **1956**, *21*(1), 197-198.

33. S. B. Weiss, T. Nakamoto. Net Synthesis of Ribonucleic Acid with a Microbial Enzyme Requiring Deoxyribonucleic Acid and 4 Ribonucleoside Triphosphates. *J. Biol. Chem.* **1961**, *236*(3), Pc18-&.

34. F. Jacob, J. Monod. Genetic Regulatory Mechanisms in Synthesis of Proteins. *J. Mol. Biol.* **1961**, *3*(3), 318-&.

35. S. Brenner, M. Meselson, F. Jacob. Unstabel Intermediate Carrying Information from Genes to Ribosomes for Protein Synthesis. *Nature* **1961**, *190*(477), 576-&.

36. J. Brachet. The localisation of pentose nuclein acids during the development of amphibians. *C. R. Seances Soc. Biol. Fil.* **1940**, *133*, 90-91.

37. F. Crick. Central Dogma of Molecular Biology. *Nature* **1970**, *227*(5258), 561-&.

38. S. M. Berget, C. Moore, P. A. Sharp. Spliced Segments at 5' Terminus of Adenovirus 2 Late Messenger-RNA. *Proc. Natl. Acad. Sci. U. S. A.* **1977**, *74*(8), 3171-3175.

39. L. T. Chow, R. E. Gelinas, T. R. Broker, R. J. Roberts. Amazing Sequence Arrangement at 5' Ends of Adenovirus-2 Messenger-RNA. *Cell* **1977**, *12*(1), 1-8.

40. G. E. Palade. A Small Particulate Component of the Cytoplasm. *J Biophys Biochem Cytol.* **1955**, *1*(1), 59-68.

41. T. R. Cech, A. J. Zaug, P. J. Grabowski. Invitro Splicing of the Ribosomal-RNA Precursor of Tetrahymena - Involvement of a Guanosine Nucleotide in the Excision of the Intervening Sequence. *Cell* **1981**, *27*(3), 487-496.

42. C. Guerriertakada, K. Gardiner, T. Marsh, N. Pace, S. Altman. The RNA Moiety of Ribonuclease-P Is the Catalytic Subunit of the Enzyme. *Cell* **1983**, *35*(3), 849-857.

43. P. Nissen, J. Hansen, N. Ban, P. B. Moore, T. A. Steitz. The structural basis of ribosome activity in peptide bond synthesis. *Science* **2000**, *289*(5481), 920-930.

44. M. B. Hoagland, M. L. Stephenson, J. F. Scott, L. I. Hecht, P. C. Zamecnik. Soluble Ribonucleic Acid Intermediate in Protein Synthesis. *J. Biol. Chem.* **1958**, *231*(1), 241-257.

45. R. C. Lee, V. Ambros. An extensive class of small RNAs in Caenorhabditis elegans. *Science* **2001**, *294*(5543), 862-864.

46. Y. Lee, C. Ahn, J. J. Han, H. Choi, J. Kim, J. Yim, J. Lee, P. Provost, O. Radmark, S. Kim, V. N. Kim. The nuclear RNase III Drosha initiates microRNA processing. *Nature* **2003**, *425*(6956), 415-419.

47. H. Siomi, M. C. Siomi. On the road to reading the RNA-interference code. *Nature* **2009**, *457*(7228), 396-404.

48. 2009 AIDS epidemic update, WHO Library Cataloguing-in-Publication Data, **2009**.

49. Baltimor.D. Viral RNA-Dependent DNA Polymerase - RNA-Dependent DNA Polymerase in Virions of RNA Tumour Viruses. *Nature* **1970**, *226*(5252), 1209-&.

50. H. M. Temin, S. Mizutani. Viral RNA-Dependent DNA Polymerase - RNA-Dependent DNA Polymerase in Virions of Rous Sarcoma Virus. *Nature* **1970**, *226*(5252), 1211-&.

51. F. D. Veronese, T. D. Copeland, A. L. Devico, R. Rahman, S. Oroszlan, R. C. Gallo, M. G. Sarngadharan. Characterization of Highly Immunogenic P66 P51 as the Reverse-Transcriptase of Htlv-Iii Lav. *Science* **1986**, *231*(4743), 1289-1291.

52. O. Schatz, J. Mous, S. F. J. Le Grice. HIV-1 RT-associated ribonuclease H displays both endonuclease and 3' -> 5' exonuclease activity. *EMBO J.* **1990**, *9*(4), 1171-1176.

53. R. A. Katz, A. M. Skalka. The Retroviral Enzymes. *Annu. Rev. Biochem* **1994**, *63*, 133-173.

54. V. P. Basu, M. Song, L. Gao, S. T. Rigby, M. N. Hanson, R. A. Bambara. Strand transfer events during HIV-1 reverse transcription. *Virus Res.* **2008**, *134*(1-2), 19-38.

55. P. Charneau, F. Clavel. A single-stranded gap in human immunodeficiency virus unintegrated linear DNA defined by a central copy of the polypurine tract. *J. Virol.* **1991**, *65*(5), 2415-2421.

56. L. A. Kohlstaedt, J. Wang, J. M. Friedman, P. A. Rice, T. A. Steitz. Crystal-Structure at 3.5 Angstrom Resolution of HIV-1 Reverse-Transcriptase Complexed with an Inhibitor. *Science* **1992**, *256*(5065), 1783-1790.

57. A. Jacobomolina, J. P. Ding, R. G. Nanni, A. D. Clark, X. D. Lu, C. Tantillo, R. L. Williams, G. Kamer, A. L. Ferris, P. Clark, A. Hizi, S. H. Hughes, E. Arnold. Crystal-Structure of Human-Immunodeficiency-Virus Type-1 Reverse-Transcriptase Complexed with Double-Stranded DNA at 3.0 Angstrom Resolution Shows Bent DNA. *Proc. Natl. Acad. Sci. U. S. A.* **1993**, *90*(13), 6320-6324.

58. W. J. Tong, C. D. Lu, S. K. Sharma, S. Matsuura, A. G. So, W. A. Scott. Nucleotide-induced stable complex formation by HIV-1 reverse transcriptase. *Biochemistry* **1997**, *36*(19), 5749-5757.

59. H. F. Huang, R. Chopra, G. L. Verdine, S. C. Harrison. Structure of a covalently trapped catalytic complex of HIV-I reverse transcriptase: Implications for drug resistance. *Science* **1998**, *282*(5394), 1669-1675.

60. S. G. Sarafianos, K. Das, J. P. Ding, P. L. Boyer, S. H. Hughes, E. Arnold. Touching the heart of HIV-1 drug resistance: the fingers close down on the dNTP at the polymerase active site. *Chem. Biol.* **1999**, *6*(5), R137-R146.

61. M. R. Sawaya, R. Prasad, S. H. Wilson, J. Kraut, H. Pelletier. Crystal structures of human DNA polymerase beta complexed with gapped and nicked DNA: Evidence for an induced fit mechanism. *Biochemistry* **1997**, *36*(37), 11205-11215.

62. Y. Li, Y. Kong, S. Korolev, G. Waksman. Crystal structures of the Klenow fragment of Thermus aquaticus DNA polymerase I complexed with deoxyribonucleoside triphosphates. *Protein Sci.* **1998**, *7*(5), 1116-1123.

63. B. Marchand, E. P. Tchesnokov, M. Gotte. The pyrophosphate analogue foscarnet traps the pre-translocational state of HIV-1 reverse transcriptase in a Brownian ratchet model of polymerase translocation. *J. Biol. Chem.* **2007**, *282*(5), 3337-3346.

64. S. G. Sarafianos, A. D. Clark, K. Das, S. Tuske, J. J. Birktoft, P. Ilankumaran, A. R. Ramesha, J. M. Sayer, D. M. Jerina, P. L. Boyer, S. H. Hughes, E. Arnold. Structures of HIV-1 reverse transcriptase with pre- and post-translocation AZTMP-terminated DNA. *EMBO J.* **2002**, *21*(23), 6614-6624.

65. B. Marchand, M. Gotte. Site-specific footprinting reveals differences in the translocation status of HIV-1 reverse transcriptase - Implications for polymerase translocation and drug resistance. *J. Biol. Chem.* **2003**, *278*(37), 35362-35372.

66. H. S. Peter Hausen. Ribonuclease H. *Eur. J. Biochem.* **1970**, *14*(2), 278-283.

67. O. Y. Fedoroff, M. Salazar, B. R. Reid. Structure of a DNA-RNA Hybrid Duplex - Why RNase-H Does Not Cleave Pure RNA. *J. Mol. Biol.* **1993**, *233*(3), 509-523.

68. J. T. Nielsen, P. C. Stein, M. Petersen. NMR structure of an alpha-L-LNA : RNA hybrid: structural implications for RNase H recognition. *Nucleic Acids Res.* **2003**, *31*(20), 5858-5867.

69. M. Nowotny, S. M. Cerritelli, R. Ghirlando, S. A. Gaidamakov, R. J. Crouch, W. Yang. Specific recognition of RNA/DNA hybrid and enhancement of human RNase H1 activity by HBD. *EMBO J.* **2008**, *27*(7), 1172-1181.

70. M. Gotte, S. Fackler, T. Hermann, E. Perola, L. Cellai, H. J. Gross, S. F. J. Legrice, H. Heumann. HIV-1 Reverse Transcriptase-Associated RNase-H Cleaves RNA/RNA in Arrested Complexes - Implications for the Mechanism by Which RNase-H Discriminates Beween RNA/RNA and RNA/DNA. *EMBO J.* **1995**, *14*(4), 833-841.

71. J. F. Davies, Z. Hostomska, Z. Hostomsky, S. R. Jordan, D. A. Matthews. Crystal-Structure of the Ribonuclease-H Domain of HIV-1 Reverse-Transcriptase. *Science* **1991**, *252*(5002), 88-95.

72. J. L. Keck, S. Marqusee. Substitution of a Highly Basic Helix Loop Sequence into the RNase-H Domain of Human-Immunodeficiency-Virus Reverse-Transcriptase Restores Its Mn2+-Dependent RNase-H Activity. *Proc. Natl. Acad. Sci. U. S. A.* **1995**, *92*(7), 2740-2744.

73. R. F. Doolittle, D. F. Feng, M. S. Johnson, M. A. Mcclure. Origins and Evolutionary Relationships of Retroviruses. *Q. Rev. Biol.* **1989**, *64*(1), 1-30.

74. M. Nowotny, S. A. Gaidamakov, R. J. Crouch, W. Yang. Crystal structures of RNase H bound to an RNA/DNA hybrid: Substrate specificity and metal-dependent catalysis. *Cell* **2005**, *121*(7), 1005-1016.

75. M. Nowotny, W. Yang. Stepwise analyses of metal ions in RNase H catalysis from substrate destabilization to product release. *EMBO J.* **2006**, *25*(9), 1924-1933.

76. M. De Vivo, M. Dal Peraro, M. L. Klein. Phosphodiester cleavage in ribonuclease H occurs via an associative two-metal-aided catalytic mechanism. *J. Am. Chem. Soc.* **2008**, *130*(33), 10955-10962.

77. S. J. Schultz, J. J. Champoux. RNase H activity: Structure, specificity, and function in reverse transcription. *Virus Res.* **2008**, *134*(1-2), 86-103.

78. S. Broder. The development of antiretroviral therapy and its impact on the HIV-1/AIDS pandemic. *Antiviral Res.* **2010**, *85*(1), 1-18.

79. M. Tisdale, T. Schulze, B. A. Larder, K. Moelling. Mutations within the RNase-H Domain of Human-Immunodeficiency-Virus Type-1 Reverse-Transcriptase Abolish Virus Infectivity. *J. Gen. Virol.* **1991**, *72*, 59-66.

80. S. G. Sarafianos, B. Marchand, K. Das, D. M. Himmel, M. A. Parniak, S. H. Hughes, E. Arnold. Structure and Function of HIV-1 Reverse Transcriptase: Molecular Mechanisms of Polymerization and Inhibition. *J. Mol. Biol.* **2009**, *385*(3), 693-713.

81. P. R. Meyer, S. E. Matsuura, A. M. Mian, A. G. So, W. A. Scott. A Mechanism of AZT Resistance: An Increase in Nucleotide-Dependent Primer Unblocking by Mutant HIV-1 Reverse Transcriptase. *Mol. Cell* **1999**, *4*(1), 35-43.

82. P. L. Anderson, T. N. Kakuda, K. A. Lichtenstein. The cellular pharmacology of nucleoside- and nucleotide-analogue reverse-transcriptase inhibitors and its relationship to clinical toxicities. *Clin. Infect. Dis.* **2004**, *38*(5), 743-753.

83. P. A. Furman, J. A. Fyfe, M. H. Stclair, K. Weinhold, J. L. Rideout, G. A. Freeman, S. N. Lehrman, D. P. Bolognesi, S. Broder, H. Mitsuya, D. W. Barry. Phosphorylation of 3'-Azido-3'-Deoxythymidine and Selective Interaction of the 5'-Triphosphate with Human-Immunodeficiency-Virus Reverse-Transcriptase. *Proc. Natl. Acad. Sci. U. S. A.* **1986**, *83*(21), 8333-8337.

84. S. Eriksson, B. Kierdaszuk, B. Munchpetersen, B. Oberg, N. G. Johansson. Comparison of the Substrate Specificities of Human Thymidine Kinase-1 and Kinase-2 and Deoxycytidine Kinase toward Antiviral and Cytostatic Nucleoside Analogs. *Biochem. Biophys. Res. Commun.* **1991**, *176*(2), 586-592.

85. L. Mu, S. G. Sarafianos, M. C. Nicklaus, P. Russ, M. A. Siddiqui, H. Ford, H. Mitsuya, R. Le, E. Kodama, C. Meier, T. Knispel, L. Anderson, J. J. Barchi, V. E. Marquez. Interactions of conformationally biased north and south 2 '-fluoro-2 ',3 '-dideoxynucleoside 5 '-triphosphates with the active site of HIV-1 reverse transcriptase. *Biochemistry* **2000**, *39*(37), 11205-11215.

86. B. D. Preston, B. J. Poiesz, L. A. Loeb. Fidelity of HIV-1 Reverse-Transcriptase. *Science* **1988**, *242*(4882), 1168-1171.

87. H. Mitsuya, K. J. Weinhold, P. A. Furman, M. H. Stclair, S. N. Lehrman, R. C. Gallo, D. Bolognesi, D. W. Barry, S. Broder. 3'-Azido-3'-Deoxythymidine (Bw A509u) - an Antiviral Agent That Inhibits the Infectivity and Cytopathic Effect of Human Lymphotropic-T Virus Type-Iii Lymphadenopathy-Associated Virus Invitro. *Proc. Natl. Acad. Sci. U. S. A.* **1985**, *82*(20), 7096-7100.

88. H. Mitsuya, S. Broder. Inhibition of the Invitro Infectivity and Cytopathic Effect of Human Lymphotrophic-T Virus "Type-Iii/Lymphadenopathy-Associated Virus (Htlv-Iii/Lav) by 2',3'-Dideoxynucleosides. *Proc. Natl. Acad. Sci. U. S. A.* **1986**, *83*(6), 1911-1915.

89. C. Cazenave, N. Loreau, N. T. Thuong, J. J. Toulme, C. Helene. Enzymatic Amplification of Translation Inhibition of Rabbit Beta-Globin Messenger-RNA Mediated by Anti-Messenger Oligodeoxynucleotides Covalently Linked to Intercalating Agents. *Nucleic Acids Res.* **1987**, *15*(12), 4717-4736.

90. M. M. Mansuri, J. E. Starrett, I. Ghazzouli, M. J. M. Hitchcock, R. Z. Sterzycki, V. Brankovan, T. S. Lin, E. M. August, W. H. Prusoff, J. P. Sommadossi, J. C. Martin. 1-(2,3-Dideoxy-Beta-D-Glycero-Pent-2-Enofuranosyl)Thymine - a Highly Potent and Selective Anti-HIV Agent. *J. Med. Chem.* **1989**, *32*(2), 461-466.

91. M. B. Faletto, W. H. Miller, E. P. Garvey, M. H. S. Clair, S. M. Daluge, S. S. Good. Unique intracellular activation of the potent anti-human

immunodeficiency virus agent 1592U89. *Antimicrob. Agents Chemother.* **1997**, *41*(5), 1099-1107.

92. H. Soudeyns, X. J. Yao, Q. Gao, B. Belleau, J. L. Kraus, N. B. Nghe, B. Spira, M. A. Wainberg. Anti-Human-Immunodeficiency-Virus Type-1 Activity and Invitro Toxicity of 2'-Deoxy-3'-Thiacytidine (Bch-189), a Novel Heterocyclic Nucleoside Analog. *Antimicrob. Agents Chemother.* **1991**, *35*(7), 1386-1390.

93. D. D. Richman. Antiretroviral activity of emtricitabine, a potent nucleoside reverse transcriptase inhibitor. *Antiviral Therapy* **2001**, *6*(2), 83-88.

94. J. Balzarini, A. Holy, J. Jindrich, L. Naesens, R. Snoeck, D. Schols, E. Declercq. Differential Antiherpesvirus and Antiretrovirus Effects of the (S) and (R) Enantiomers of Acyclic Nucleoside Phosphonates - Potent and Selective Invitro and Invivo Antiretrovirus Activities of (R)-9-(2-Phosphonomethoxypropyl)-2,6-Diaminopurine. *Antimicrob. Agents Chemother.* **1993**, *37*(2), 332-338.

95. R. Esnouf, J. S. Ren, C. Ross, Y. Jones, D. Stammers, D. Stuart. Mechanism of Inhibition of HIV-1 Reverse-Transcriptase by Nonnucleoside Inhibitors. *Nat. Struct. Biol.* **1995**, *2*(4), 303-308.

96. C. A. Shaw-Reid, B. Feuston, V. Munshi, K. Getty, J. Krueger, D. J. Hazuda, M. A. Parniak, M. D. Miller, D. Lewis. Dissecting the effects of DNA polymerase and ribonuclease H inhibitor combinations on HIV-1 reverse-transcriptase activities. *Biochemistry* **2005**, *44*(5), 1595-1606.

97. G. N. Nikolenko, S. Palmer, F. Maldarelli, J. W. Mellors, J. M. Coffin, V. K. Pathak. Mechanism for nucleoside analog-mediated abrogation of HIV-1 replication: Balance between RNase H activity and nucleotide excision. *Proc. Natl. Acad. Sci. U. S. A.* **2005**, *102*(6), 2093-2098.

98. K. A. Delviks-Frankenberry, G. N. Nikolenko, P. L. Boyer, S. H. Hughes, J. M. Coffin, A. Jere, V. K. Pathak. HIV-1 reverse transcriptase connection subdomain mutations reduce template RNA degradation and enhance AZT excision. *Proc. Natl. Acad. Sci. U. S. A.* **2008**, *105*(31), 10943-10948.

99. V. W. Byrnes, V. V. Sardana, W. A. Schleif, J. H. Condra, J. A. Waterbury, J. A. Wolfgang, W. J. Long, C. L. Schneider, A. J. Schlabach, B. S. Wolanski, D. J. Graham, L. Gotlib, A. Rhodes, D. L. Titus, E. Roth, O. M. Blahy, J. C. Quintero, S. Staszewski, E. A. Emini. Comprehensive Mutant Enzyme and Viral Variant Assessment of Human-Immunodeficiency-Virus Type-1 Reverse-Transcriptase Resistance to Nonnucleoside Inhibitors. *Antimicrob. Agents Chemother.* **1993**, *37*(8), 1576-1579.

100. A. S. Perelson, A. U. Neumann, M. Markowitz, J. M. Leonard, D. D. Ho. HIV-1 dynamics in vivo: Virion clearance rate, infected cell life-span, and viral generation time. *Science* **1996**, *271*(5255), 1582-1586.

101. L. Menéndez-Arias. Molecular basis of human immunodeficiency virus drug resistance: An update. *Antiviral Res.* **2010**, *85*(1), 210-231.

102. E. Domingo, L. MenendezArias, J. J. Holland. RNA virus fitness. *Rev. Med. Virol.* **1997**, *7*(2), 87-96.

103. S. G. Sarafianos, K. Das, A. D. Clark, J. P. Ding, P. L. Boyer, S. H. Hughes, E. Arnold. Lamivudine (3TC) resistance in HIV-1 reverse transcriptase involves steric hindrance with beta-branched amino acids. *Proc. Natl. Acad. Sci. U. S. A.* **1999**, *96*(18), 10027-10032.

104. T. Ilina, M. A. Parniak, J. Kuan-Teh, in *Advances in Pharmacology, Vol. Volume 56*, Academic Press, **2008**, pp. 121-167.

105. D. Arion, N. Kaushik, S. McCormick, G. Borkow, M. A. Parniak. Phenotypic mechanism of HIV-1 resistance to 3 '-azido-3 '-deoxythymidine (AZT): Increased polymerization processivity and enhanced sensitivity to pyrophosphate of the mutant viral reverse transcriptase. *Biochemistry* **1998**, *37*(45), 15908-15917.

106. P. R. Meyer, S. E. Matsuura, R. G. So, W. A. Scott. Unblocking of chain-terminated primer by HIV-1 reverse transcriptase through a nucleotide-dependent mechanism. *Proc. Natl. Acad. Sci. U. S. A.* **1998**, *95*(23), 13471-13476.

107. B. A. Larder, S. D. Kemp. Multiple Mutations in HIV-1 Reverse-Transcriptase Confer High-Level Resistance to Zidovudine (AZT). *Science* **1989**, *246*(4934), 1155-1158.

108. P. L. Boyer, S. G. Sarafianos, E. Arnold, S. H. Hughes. Selective excision of AZTMP by drug-resistant human immunodeficiency virus reverse transcriptase. *J. Virol.* **2001**, *75*(10), 4832-4842.

109. N. Sluis-Cremer, D. Koontz, D. Arion, U. Parikh, R. Schinazi, J. Mellors, M. A. Parniak. The 3 '-azido group is not the primary structural determinant for the excision phenotype correlated with HIV-1 resistance to AZT. *Antiviral Therapy* **2003**, *8*(3), U42-U43.

110. A. G. Marcelin, C. Delaugerre, M. Wirden, P. Viegas, A. Simon, C. Katlama, V. Calvez. Thymidine analogue reverse transcriptase inhibitors resistance mutations profiles and association to other nucleoside reverse transcriptase

inhibitors resistance mutations observed in the context of virological failure. *J. Med. Virol.* **2004**, *72*(1), 162-165.

111. M. Gotte, D. Arion, M. A. Parniak, M. A. Wainberg. The M184V mutation in the reverse transcriptase of human immunodeficiency virus type 1 impairs rescue of chain-terminated DNA synthesis. *J. Virol.* **2000**, *74*(8), 3579-3585.

112. V. W. Byrnes, E. A. Emini, W. A. Schleif, J. H. Condra, C. L. Schneider, W. J. Long, J. A. Wolfgang, D. J. Graham, L. Gotlib, A. J. Schlabach, B. S. Wolanski, O. M. Blahy, J. C. Quintero, A. Rhodes, E. Roth, D. L. Titus, V. V. Sardana. Susceptibilities of Human-Immunodeficiency-Virus Type-1 Enzyme and Viral Variants Expressing Multiple Resistance-Engendering Amino-Acid Substitutions to Reverse-Transcriptase Inhibitors. *Antimicrob. Agents Chemother.* **1994**, *38*(6), 1404-1407.

113. B. Selmi, J. Deval, K. Alvarez, J. Boretto, S. Sarfati, C. Guerreiro, B. Canard. The Y181C substitution in 3 '-azido-3 '-deoxythymidine-resistant human immunodeficiency virus, type 1, reverse transcriptase suppresses the ATP-mediated repair of the 3 '-azido-3 '-deoxythymidine 5 '-monophosphate-terminated primer. *J. Biol. Chem.* **2003**, *278*(42), 40464-40472.

114. J. G. Gall, M. L. Pardue. Formation and Detection of RNA-DNA Hybrid Molecules in Cytological Preparations. *Proc. Natl. Acad. Sci. U. S. A.* **1969**, *63*(2), 378-&.

115. E. M. Southern. Detection of Specific Sequences among DNA Fragments Separated by Gel-Electrophoresis. *J. Mol. Biol.* **1975**, *98*(3), 503-&.

116. M. L. Stephenson, P. C. Zamecnik. Inhibition of Rous sarcoma viral RNA translation by a specific oligodeoxyribonucleotide. *Proc. Natl. Acad. Sci. U. S. A.* **1978**, *75*(1), 285-288.

117. Antisense Drug Technology; Principles, Strategies, and Applications, (2^{nd} Edition), CRC Press, Boca Raton, FL, **2006**.

118. C. C. Smith, L. Aurelian, M. P. Reddy, P. S. Miller, P. O. P. Tso. Antiviral Effect of an Oligo(Nucleoside Methylphosphonate) Complementary to the Splice Junction of Herpes-Simplex Virus Type-1 Immediate Early Pre-Messenger RNA-4 and Pre-Messenger RNA-5. *Proc. Natl. Acad. Sci. U. S. A.* **1986**, *83*(9), 2787-2791.

119. Z. Dominski, R. Kole. Restoration of Correct Splicing in Thalassemic Premessenger RNA by Antisense Oligonucleotides. *Proc. Natl. Acad. Sci. U. S. A.* **1993**, *90*(18), 8673-8677.

120. M. T. Haeuptle, R. Frank, B. Dobberstein. Translation arrest by oligodeoxynucleotides complementary to mRNA coding sequences yields polypeptides of predetermined length. *Nucleic Acids Res.* **1986**, *14*(3), 1427-1448.

121. J. Minshull, T. Hunt. The use of single-stranded DNA and RNase H to promote quantitative 'hybrid arrest of translation' of mRNA/DNA Hybrids in reticulocyte lysate cell-free translations. *Nucleic Acids Res.* **1986**, *14*(16), 6433-6451.

122. I. Berkower, J. Leis, J. Hurwitz. Isolation and Characterization of an Endonuclease from Escherichia-Coli Specific for Ribonucleic-Acid in Ribonucleic Acid Deoxyribonucleic Acid Hybrid Structures. *J. Biol. Chem.* **1973**, *248*(17), 5914-5921.

123. A. Fire, S. Xu, M. K. Montgomery, S. A. Kostas, S. E. Driver, C. C. Mello. Potent and specific genetic interference by double-stranded RNA in Caenorhabditis elegans. *Nature* **1998**, *391*(6669), 806-811.

124. A. de Fougerolles, H. P. Vornlocher, J. Maraganore, J. Lieberman. Interfering with disease: a progress report on siRNA-based therapeutics. *Nature Reviews Drug Discovery* **2007**, *6*(6), 443-453.

125. P. D. Zamore, T. Tuschl, P. A. Sharp, D. P. Bartel. RNAi: Double-stranded RNA directs the ATP-dependent cleavage of mRNA at 21 to 23 nucleotide intervals. *Cell* **2000**, *101*(1), 25-33.

126. I. J. MacRae, K. H. Zhou, F. Li, A. Repic, A. N. Brooks, W. Z. Cande, P. D. Adams, J. A. Doudna. Structural basis for double-stranded RNA processing by dicer. *Science* **2006**, *311*(5758), 195-198.

127. S. M. Hammond, E. Bernstein, D. Beach, G. J. Hannon. An RNA-directed nuclease mediates post-transcriptional gene silencing in Drosophila cells. *Nature* **2000**, *404*(6775), 293-296.

128. S. M. Elbashir, J. Harborth, W. Lendeckel, A. Yalcin, K. Weber, T. Tuschl. Duplexes of 21-nucleotide RNAs mediate RNA interference in cultured mammalian cells. *Nature* **2001**, *411*(6836), 494-498.

129. T. A. Rand, K. Ginalski, N. V. Grishin, X. D. Wang. Biochemical identification of Argonaute 2 as the sole protein required for RNA-induced silencing complex activity. *Proc. Natl. Acad. Sci. U. S. A.* **2004**, *101*(40), 14385-14389.

130. G. Hutvagner, P. D. Zamore. A microRNA in a multiple-turnover RNAi enzyme complex. *Science* **2002**, *297*(5589), 2056-2060.

131. H. Tabara, M. Sarkissian, W. G. Kelly, J. Fleenor, A. Grishok, L. Timmons, A. Fire, C. C. Mello. The rde-1 gene, RNA interference, and transposon silencing in C-elegans. *Cell* **1999**, *99*(2), 123-132.

132. G. Hutvagner, P. D. Zamore. RNAi: nature abhors a double-strand. *Curr. Opin. Genet. Dev.* **2002**, *12*(2), 225-232.

133. T. Sijen, J. Fleenor, F. Simmer, K. L. Thijssen, S. Parrish, L. Timmons, R. H. A. Plasterk, A. Fire. On the role of RNA amplification in dsRNA-triggered gene silencing. *Cell* **2001**, *107*(4), 465-476.

134. H. Valadi, K. Ekstrom, A. Bossios, M. Sjostrand, J. J. Lee, J. O. Lotvall. Exosome-mediated transfer of mRNAs and microRNAs is a novel mechanism of genetic exchange between cells. *Nat. Cell Biol.* **2007**, *9*(6), 654-U672.

135. M. Halic, D. Moazed. Dicer-Independent Primal RNAs Trigger RNAi and Heterochromatin Formation. *Cell* **2010**, *140*(4), 504-516.

136. Y. Bennasser, S. Y. Le, M. Benkirane, K. T. Jeang. Evidence that HIV-1 encodes an siRNA and a suppressor of RNA silencing. *Immunity* **2005**, *22*(5), 607-619.

137. C. Chable-Bessia, O. Meziane, D. Latreille, R. T. Robinson, A. Zamborlini, A. Wagschal, J. M. Jacquet, J. Reynes, Y. Levy, A. Saib, Y. Bennasser, M. Benkirane. Suppression of HIV-1 replication by microRNA effectors. *Retrovirology* **2009**, *6*, -.

138. B. R. Cullen. Viral and cellular messenger RNA targets of viral microRNAs. *Nature* **2009**, *457*(7228), 421-425.

139. D. M. Pegtel, K. Cosmopoulos, D. A. Thorley-Lawson, M. A. J. van Eijndhoven, E. S. Hopmans, J. L. Lindenberg, T. D. de Gruijl, T. Wurdinger, J. M. Middeldorp. Functional delivery of viral miRNAs via exosomes. *Proc. Natl. Acad. Sci. U. S. A.* **2010**, *107*(14), 6328-6333.

140. J. L. Huang, F. X. Wang, E. Argyris, K. Y. Chen, Z. H. Liang, H. Tian, W. L. Huang, K. Squires, G. Verlinghieri, H. Zhang. Cellular microRNAs contribute to HIV-1 latency in resting primary CD4(+) T lymphocytes. *Nat. Med.* **2007**, *13*(10), 1241-1247.

141. R. Nathans, C. Y. Chu, A. K. Serquina, C. C. Lu, H. Cao, T. M. Rana. Cellular MicroRNA and P Bodies Modulate Host-HIV-1 Interactions. *Mol. Cell* **2009**, *34*(6), 696-709.

142. M. Mascini, Aptamers in Bioanalysis, John Wiley and Sons. Inc., Hoboken, NJ, **2009**.

143. K. W. Thiel, P. H. Giangrande. Therapeutic Applications of DNA and RNA Aptamers. *Oligonucleotides* **2009**, *19*(3), 209-222.

144. A. D. Ellington, J. W. Szostak. Invitro Selection of RNA Molecules That Bind Specific Ligands. *Nature* **1990**, *346*(6287), 818-822.

145. G. Werstuck, M. R. Green. Controlling gene expression in living cells through small molecule-RNA interactions. *Science* **1998**, *282*(5387), 296-298.

146. I. Harvey, P. Garneau, J. Pelletier. Inhibition of translation by RNA-small molecule interactions. *RNA* **2002**, *8*(4), 452-463.

147. A. Nahvi, N. Sudarsan, M. S. Ebert, X. Zou, K. L. Brown, R. R. Breaker. Genetic control by a metabolite binding mRNA. *Chem. Biol.* **2002**, *9*(9), 1043-1049.

148. C. Tuerk, L. Gold. Systematic Evolution of Ligands by Exponential Enrichment - RNA Ligands to Bacteriophage-T4 DNA-Polymerase. *Science* **1990**, *249*(4968), 505-510.

149. R. D. Jenison, S. C. Gill, A. Pardi, B. Polisky. High-Resolution Molecular Discrimination by RNA. *Science* **1994**, *263*(5152), 1425-1429.

150. W. Mok, Y. F. Li. Recent Progress in Nucleic Acid Aptamer-Based Biosensors and Bioassays. *Sensors* **2008**, *8*(11), 7050-7084.

151. H. Schurer, K. Stembera, D. Knoll, G. Mayer, M. Blind, H. H. Forster, M. Famulok, P. Welzel, U. Hahn. Aptamers that bind to the antibiotic moenomycin A. *Biorg. Med. Chem.* **2001**, *9*(10), 2557-2563.

152. C. Tuerk, S. Macdougal, L. Gold. RNA Pseudoknots That Inhibit Human-Immunodeficiency-Virus Type-1 Reverse-Transcriptase. *Proc. Natl. Acad. Sci. U. S. A.* **1992**, *89*(15), 6988-6992.

153. D. P. Bartel, M. L. Zapp, M. R. Green, J. W. Szostak. HIV-1 Rev Regulation Involves Recognition of Non-Watson-Crick Base-Pairs in Viral-RNA. *Cell* **1991**, *67*(3), 529-536.

154. L. C. Bock, L. C. Griffin, J. A. Latham, E. H. Vermaas, J. J. Toole. Selection of Single-Stranded-DNA Molecules That Bind and Inhibit Human Thrombin. *Nature* **1992**, *355*(6360), 564-566.

155. G. Fish, J. A. Haller, A. C. Ho, M. Klein, J. Loewenstein, D. Martin, D. Orth, R. B. Rosen, S. Sanislo, S. D. Schwartz, L. J. Singerman, G. Williams, A. P. Adamis, M. Blumenkranz, M. Goldberg, E. S. Gragoudas, J. W. Miller, L. Yannuzzi, D. R. Guyer, D. O'Shaughnessy, S. Patel, E. S. Grp. Anti-vascular endothelial growth factor therapy for subfoveal choroidal neovascularization secondary to age-related macular degeneration - Phase II study results. *Ophthalmology* **2003**, *110*(5), 979-986.

156. G. The Eyetech Study. Preclinical and Phase 1A Clinical Evaluation of An Anti-Vegf Pegylated Aptamer (Eye001) for the Treatment of Exudative Age-Related Macular Degeneration. *Retina* **2002**, *22*(2), 143-152.

157. J. O. McNamara, E. R. Andrechek, Y. Wang, K. D Viles, R. E. Rempel, E. Gilboa, B. A. Sullenger, P. H. Giangrande. Cell type-specific delivery of siRNAs with aptamer-siRNA chimeras. *Nat. Biotechnol.* **2006**, *24*(8), 1005-1015.

158. G. A. Prody, J. T. Bakos, J. M. Buzayan, I. R. Schneider, G. Bruening. Autolytic Processing of Dimeric Plant-Virus Satellite RNA. *Science* **1986**, *231*(4745), 1577-1580.

159. S. W. Santoro, G. F. Joyce. A general purpose RNA-cleaving DNA enzyme. *Proc. Natl. Acad. Sci. U. S. A.* **1997**, *94*(9), 4262-4266.

160. S. Schubert, D. C. Gul, H. P. Grunert, H. Zeichhardt, V. A. Erdmann, J. Kurreck. RNA cleaving '10-23' DNAzymes with enhanced stability and activity. *Nucleic Acids Res.* **2003**, *31*(20), 5982-5992.

161. D. M. Perrin, T. Garestier, C. Helene. Bridging the gap between proteins and nucleic acids: A metal-independent RNAseA mimic with two protein-like functionalities. *J. Am. Chem. Soc.* **2001**, *123*(8), 1556-1563.

162. C. A. Lipinski, F. Lombardo, B. W. Dominy, P. J. Feeney. Experimental and computational approaches to estimate solubility and permeability in drug discovery and development settings. *Adv. Drug Del. Rev.* **1997**, *23*(1-3), 3-25.

163. J. Kurreck. Antisense technologies. Improvement through novel chemical modifications. *Eur. J. Biochem.* **2003**, *270*(8), 1628-1644.

164. J. K. Watts, G. F. Deleavey, M. J. Damha. Chemically modified siRNA: tools and applications. *Drug Discovery Today* **2008**, *13*(19-20), 842-855.

165. B. P. Monia, E. A. Lesnik, C. Gonzalez, W. F. Lima, D. Mcgee, C. J. Guinosso, A. M. Kawasaki, P. D. Cook, S. M. Freier. Evaluation of 2'-Modified Oligonucleotides Containing 2'-Deoxy Gaps as Antisense Inhibitors of Gene-Expression. *J. Biol. Chem.* **1993**, *268*(19), 14514-14522.

166. J. K. Watts, N. Choubdar, K. Sadalapure, F. Robert, A. S. Wahba, J. Pelletier, B. M. Pinto, M. J. Damha. 2 '-Fluoro-4 '-thioarabino-modified oligonucleotides: conformational switches linked to siRNA activity. *Nucleic Acids Res.* **2007**, *35*(5), 1441-1451.

167. K. P. Anderson, M. C. Fox, V. BrownDriver, M. J. Martin, R. F. Azad. Inhibition of human cytomegalovirus immediate-early gene expression by an antisense oligonucleotide complementary to immediate-early RNA. *Antimicrob. Agents Chemother.* **1996**, *40*(9), 2004-2011.

168. M. D. De Smet, C. Meenken, G. J. Van Den Horn. Fomivirsen - a phosphorothioate oligonucleotide for the treatment of CMV retinitis. *Ocul. Immunol. Inflamm.* **1999**, *7*, 189-198.

169. B. V. L. Potter, P. J. Romaniuk, F. Eckstein. Stereochemical Course of DNA Hydrolysis by Nuclease S1. *J. Biol. Chem.* **1983**, *258*(3), 1758-1760.

170. C. A. Stein, C. Subasinghe, K. Shinozuka, J. S. Cohen. Physicochemical Properties of Phosphorothioate Oligodeoxynucleotides. *Nucleic Acids Res.* **1988**, *16*(8), 3209-3221.

171. R. L. Letsinger, G. G. Zhang, D. K. Sun, T. Ikeuchi, P. S. Sarin. Cholesteryl-Conjugated Oligonucleotides - Synthesis, Properties, and Activity as Inhibitors of Replication of Human Immunodeficiency Virus in Cell-Culture. *Proc. Natl. Acad. Sci. U. S. A.* **1989**, *86*(17), 6553-6556.

172. A. M. Krieg, J. Tonkinson, S. Matson, Q. Y. Zhao, M. Saxon, L. M. Zhang, U. Bhanja, L. Yakubov, C. A. Stein. Modification of Antisense Phosphodiester Oligodeoxynucleotides by a 5' Cholesteryl Moiety Increases Cellular-Association and Improves Efficacy. *Proc. Natl. Acad. Sci. U. S. A.* **1993**, *90*(3), 1048-1052.

173. H. Inoue, Y. Hayase, A. Imura, S. Iwai, K. Miura, E. Ohtsuka. Synthesis and Hybridization Studies on 2 Complementary Nona(2'-O-Methyl)Ribonucleotides. *Nucleic Acids Res.* **1987**, *15*(15), 6131-6148.

174. A. M. Kawasaki, M. D. Casper, S. M. Freier, E. A. Lesnik, M. C. Zounes, L. L. Cummins, C. Gonzalez, P. D. Cook. Uniformly Modified 2'-Deoxy-2'-Fluoro Phosphorothioate Oligonucleotides as Nuclease-Resistant Antisense Compounds with High-Affinity and Specificity for RNA Targets. *J. Med. Chem.* **1993**, *36*(7), 831-841.

175. A. A. Koshkin, V. K. Rajwanshi, J. Wengel. Novel convenient syntheses of LNA [2.2.1]bicyclo nucleosides. *Tetrahedron Lett.* **1998**, *39*(24), 4381-4384.

176. A. A. Koshkin, J. Wengel. Synthesis of novel 2 ',3 '-linked bicyclic thymine ribonucleosides. *J. Org. Chem.* **1998**, *63*(8), 2778-2781.

177. S. Obika, D. Nanbu, Y. Hari, J. Andoh, K. Morio, T. Doi, T. Imanishi. Stability and structural features of the duplexes containing nucleoside analogues with a fixed N-type conformation, 2 '-O,4 '-C-methyleneribonucleosides. *Tetrahedron Lett.* **1998**, *39*(30), 5401-5404.

178. M. Frieden, H. F. Hansen, T. Koch. Nuclease stability of LNA oligonucleotides and LNA-DNA chimeras. *Nucleosides Nucleotides & Nucleic Acids* **2003**, *22*(5-8), 1041-1043.

179. B. Vester, J. Wengel. LNA (Locked nucleic acid): High-affinity targeting of complementary RNA and DNA. *Biochemistry* **2004**, *43*(42), 13233-13241.

180. J.-F. Trempe, C. J. Wilds, A. Y. Denisov, R. T. Pon, M. J. Damha, K. Gehring. NMR solution structure of an oligonucleotide hairpin with a 2'F-ANA/RNA stem: implications for RNase H specificity toward DNA/RNA hybrid duplexes. *J. Am. Chem. Soc.* **2001**, *123*(21), 4896-4903.

181. H. Ikeda, R. Fernandez, A. Wilk, J. J. Barchi, X. L. Huang, V. E. Marquez. The effect of two antipodal fluorine-induced sugar puckers on the conformation and stability of the Dickerson-Drew dodecamer duplex [d(CGCGAATTCGCG)](2). *Nucleic Acids Res.* **1998**, *26*(9), 2237-2244.

182. C. J. Wilds, M. J. Damha. Duplex recognition by oligonucleotides containing 2 '-deoxy-2 '-fluoro-D-arabinose and 2 '-deoxy-2 '-fluoro-D-ribose. Intermolecular 2 '-OH-phosphate contacts versus sugar puckering in the stabilization of triple-helical complexes. *Bioconjugate Chem.* **1999**, *10*(2), 299-305.

183. C. J. Wilds, M. J. Damha. 2 '-Deoxy-2 '-fluoro-beta-D-arabinonucleosides and oligonucleotides (2 ' F-ANA): synthesis and physicochemical studies. *Nucleic Acids Res.* **2000**, *28*(18), 3625-3635.

184. M. J. Damha, C. J. Wilds, A. Noronha, I. Brukner, G. Borkow, D. Arion, M. A. Parniak. Hybrids of RNA and arabinonucleic acids (ANA and 2 ' F-ANA) are substrates of ribonuclease H (vol 120, pg 12976, 1998). *J. Am. Chem. Soc.* **1998**, *120*(51), 13545-13545.

185. T. Dowler, D. Bergeron, A.-L. Tedeschi, L. Paquet, N. Ferrari, M. J. Damha. Improvements in siRNA properties mediated by 2'-deoxy-2'-fluoro-b-D-arabinonucleic acid (FANA). *Nucleic Acids Res.* **2006**, *34*(6), 1669-1675.

186. J. K. Watts, M. J. Damha. 2 ' F-arabinonucleic acids (2 ' F-ANA) - History, properties, and new frontiers. *Can. J. Chem.* **2008**, *86*(7), 641-656.

187. K. Mullis, F. Faloona, S. Scharf, R. Saiki, G. Horn, H. Erlich. Specific Enzymatic Amplification of DNA Invitro - the Polymerase Chain-Reaction. *Cold Spring Harbor Symp. Quant. Biol.* **1986**, *51*, 263-273.

188. G. H. McGall, A. D. Barone, M. Diggelmann, S. P. A. Fodor, E. Gentalen, N. Ngo. The efficiency of light-directed synthesis of DNA arrays on glass substrates. *J. Am. Chem. Soc.* **1997**, *119*(22), 5081-5090.

189. J. G. Lackey, D. Mitra, M. M. Somoza, F. Cerrina, M. J. Damha. Acetal Levulinyl Ester (ALE) Groups for 2 '-Hydroxyl Protection of Ribonucleosides in the Synthesis of Oligoribonucleotides on Glass and Microarrays. *J. Am. Chem. Soc.* **2009**, *131*(24), 8496-8502.

190. A. M. Michelson, A. R. Todd. Nucleotides .32. Synthesis of a Dithymidine Dinucleotide Containing a 3'-5'-Internucleotidic Linkage. *J. Chem. Soc.* **1955**, 2632-2638.

191. K. L. Agarwal, H. Buchi, Caruther.Mh, N. Gupta, H. G. Khorana, K. Kleppe, A. Kumar, E. Ohtsuka, Rajbhand.Ul, Vandesan.Jh, Sgaramel.V, H. Weber, T. Yamada. Total Synthesis of Gene for an Alanine Transfer Ribonucleic Acid from Yeast. *Nature* **1970**, *227*(5253), 27-&.

192. M. Smith, H. G. Khorana, D. H. Rammler, I. H. Goldberg. Studies on Polynucleotides .14. Specific Synthesis of C3'-C5' Interrribonucleotide Linkage - Syntheses of Uridylyl-(3'-]5')-Uridine and Uridylyl-(3'-]5')-Adenosine. *J. Am. Chem. Soc.* **1962**, *84*(3), 430-&.

193. H. Schaller, G. Weimann, H. G. Khorana, B. Lerch. Studies on Polynucleotides .24. Stepwise Synthesis of Specific Deoxyribopolynucleotides (4) - Protected Derivatives of Deoxyribonucleosides and New Syntheses of Deoxyribonucleoside-3 Phosphates. *J. Am. Chem. Soc.* **1963**, *85*(23), 3821-&.

194. Letsinge.Rl, K. K. Ogilvie. Synthesis of Oligothymidylates Via Phosphotriester Intermediates. *J. Am. Chem. Soc.* **1969**, *91*(12), 3350-&.

195. R. L. Letsinger, W. B. Lunsford. Synthesis of Thymidine Oligonucleotides by Phosphite Triester Intermediates. *J. Am. Chem. Soc.* **1976**, *98*(12), 3655-3661.

196. S. L. Beaucage, M. H. Caruthers. Deoxynucleoside Phosphoramidites - a New Class of Key Intermediates for Deoxypolynucleotide Synthesis. *Tetrahedron Lett.* **1981**, *22*(20), 1859-1862.

197. R. L. Letsinger, M. J. Kornet, V. Mahadevan, D. M. Jerina. Reactions on Polymer Supports. *J. Am. Chem. Soc.* **1964**, *86*(23), 5163-&.

198. G. Alvaradourbina, G. M. Sathe, W. C. Liu, M. F. Gillen, P. D. Duck, R. Bender, K. K. Ogilvie. Automated Synthesis of Gene Fragments. *Science* **1981**, *214*(4518), 270-274.

199. S. P. Adams, K. S. Kavka, E. J. Wykes, S. B. Holder, G. R. Galluppi. Hindered Dialkylamino Nucleoside Phosphite Reagents in the Synthesis of 2 DNA 51-Mers. *J. Am. Chem. Soc.* **1983**, *105*(3), 661-663.

200. R. T. Pon, N. Usman, K. K. Ogilvie. Derivatization of Controlled Pore Glass-Beads for Solid-Phase Oligonucleotide Synthesis. *BioTechniques* **1988**, *6*(8), 768-775.

201. R. T. Pon, M. J. Damha, K. K. Ogilvie. Modification of Guanine Bases by Nucleoside Phosphoramidite Reagents during the Solid-Phase Synthesis of Oligonucleotides. *Nucleic Acids Res.* **1985**, *13*(18), 6447-6465.

202. S. L. Beaucage. Solid-phase synthesis of siRNA oligonucleotides. *Current Opinion in Drug Discovery & Development* **2008**, *11*(2), 203-216.

203. K. K. Ogilvie, A. L. Schifman, C. L. Penney. Synthesis of Oligoribonucleotides .3. Use of Silyl Protecting Groups in Nucleoside and Nucleotide Chemistry .8. *Canadian Journal of Chemistry-Revue Canadienne De Chimie* **1979**, *57*(17), 2230-2238.

204. K. K. Ogilvie, M. J. Nemer. Silyl Protecting Groups in Nucleoside and Nucleotide Chemistry .11. The Synthesis of Oligoribonucleotides .6. The Synthesis of a Hexadecamer by a Block Condensation Approach. *Canadian Journal of Chemistry-Revue Canadienne De Chimie* **1980**, *58*(14), 1389-1397.

205. L. Bellon. Oligoribonucleotides with 2'-O-(tert-butyldimethylsilyl) groups. *Curr. Protoc. Nucleic Acid Chem., Beaucage, S.L, Herdewijn, P., Matsuda, A. Ed.s, John Wiley & Sons* **2001**, *Unit 3.6*, 1-8.

206. K. K. Ogilvie, N. Usman, K. Nicoghosian, R. J. Cedergren. Total Chemical Synthesis of a 77-Nucleotide-Long RNA Sequence Having Methionine-Acceptance Activity. *Proc. Natl. Acad. Sci. U. S. A.* **1988**, *85*(16), 5764-5768.

207. M. J. Cavaluzzi, P. N. Borer. Revised UV extinction coefficients for nucleoside-5'-monophosphates and unpaired DNA and RNA. *Nucleic Acids Res.* **2004**, *32*(1), -.

208. C. R. Cantor, M. M. Warshaw, H. Shapiro. Oligonucleotide Interactions .3. Circular Dichroism Studies of Conformation of Deoxyoligonucleotides. *Biopolymers* **1970**, *9*(9), 1059-1070.

209. D. M. Gray, S. H. Hung, K. H. Johnson. Absorption and Circular-Dichroism Spectroscopy of Nucleic-Acid Duplexes and Triplexes. *Biochemical Spectroscopy* **1995**, *246*, 19-34.

210. A. Rich, I. Tinoco. The Effect of Chain Length Upon Hypochromism in Nucleic Acids and Polynucleotides. *J. Am. Chem. Soc.* **1960**, *82*(24), 6409-6411.

211. I. Tinoco. Hypochromism in Polynucleotides. *J. Am. Chem. Soc.* **1960**, *82*(18), 4785-4790.

212. P. J. Chou, W. C. Johnson. Base Inclinations in Natural and Synthetic DNAs. *J. Am. Chem. Soc.* **1993**, *115*(4), 1205-1214.

213. C. R. Cantor, I. Tinoco. Absorption and Optical Rotatory Dispersion of 7 Trinucleoside Diphosphates. *J. Mol. Biol.* **1965**, *13*(1), 65-&.

214. M. M. Warshaw, I. Tinoco. Optical Properties of 16 Dinucleoside Phosphates. *J. Mol. Biol.* **1966**, *20*(1), 29-&.

215. J. D. Puglisi, I. Tinoco. Absorbance melting curves in RNA. *Methods Enzymol.* **1989**, *180*, 304-325.

216. R. Thomas. Sur Lexistence, Dans La Molecule Des Acides Nucleiques, Dune Structure Secondaire a Liaisons Labiles. *Experientia* **1951**, *7*(7), 261-262.

217. J. L. Mergny, A. T. Phan, L. Lacroix. Following G-quartet formation by UV-spectroscopy. *FEBS Lett.* **1998**, *435*(1), 74-78.

218. G. R. Bishop, J. B. Chaires. Characterization of DNA Structures by Circular Dichroism. *Curr. Protoc. Nucleic Acid Chem., Beaucage, S.L, Herdewijn, P., Matsuda, A. Ed.s, John Wiley & Sons* **2002**, *Vol. 7.11*, 1-8.

219. S. Paramasivan, I. Rujan, P. H. Bolton. Circular dichroism of quadruplex DNAs: Applications to structure, cation effects and ligand binding. *Methods* **2007**, *43*(4), 324-331.

220. R. Martin, Gel electrophoresis: Nucleic Acids, BIOS Scientific Publishers Ltd, Oxford, UK, **1996**.

221. R. E. Kay, E. R. Walwick, C. K. Gifford. Spectral Changes in Cationic Dye Due to Interaction with Macromolecules .2. Effects of Environment + Macromolecule Structure. *J. Phys. Chem.* **1964**, *68*(7), 1907-&.

222. R. E. Kay, E. R. Walwick, C. K. Gifford. Spectral Changes in Cationic Dye Due to Interaction with Macromolecules .I. Behavior of Dye Alone in Solution + Effect of Added Macromolecules. *J. Phys. Chem.* **1964**, *68*(7), 1896-&.

223. J. R. Lakowicz, Principles of Fluorescence Spectrospcopy, (3rd edition), Springer, **2006**.

224. P. R. Callis. Electronic States and Luminescence of Nucleic-Acid Systems. *Annu. Rev. Phys. Chem.* **1983**, *34*, 329-357.

225. E. A. Abbondanzieri, G. Bokinsky, J. W. Rausch, J. X. Zhang, S. F. J. Le Grice, X. W. Zhuang. Dynamic binding orientations direct activity of HIV reverse transcriptase. *Nature* **2008**, *453*(7192), 184-U182.

226. M. J. Damha, C. J. Wilds, A. Noronha, I. Brukner, G. Borkow, D. Arion, M. A. Parniak. Hybrids of RNA and arabinonucleic acids (ANA and 2 ' F-ANA) are substrates of ribonuclease h. *J. Am. Chem. Soc.* **1998**, *120*(49), 12976-12977.

227. M. M. Mangos, K. L. Min, E. Viazovkina, A. Galarneau, M. I. Elzagheid, M. A. Parniak, M. J. Damha. Efficient RNase H-directed cleavage of RNA promoted by antisense DNA or 2 ' F-ANA constructs containing acyclic nucleotide inserts. *J. Am. Chem. Soc.* **2003**, *125*(3), 654-661.

228. D. Sabatino, M. J. Damha. Oxepane nucleic acids: Synthesis, characterization, and properties of oligonucleotides bearing a seven-membered carbohydrate ring. *J. Am. Chem. Soc.* **2007**, *129*(26), 8259-8270.

229. M. M. Mangos, K.-L. Min, E. Viazovkina, A. Galarneau, M. I. Elzagheid, M. A. Parniak, M. J. Damha. Efficient RNase H-directed cleavage of RNA promoted by antisense DNA or 2'F-ANA constructs containing acyclic nucleotide inserts. *J. Am. Chem. Soc.* **2003**, *125*(3), 654-661.

230. M. Wasner, D. Arion, G. Borkow, A. Noronha, A. H. Uddin, M. A. Parniak, M. J. Damha. Physicochemical and biochemical properties of 2',5'-linked RNA and 2',5'-RNA:3',5'-RNA "hybrid" duplexes. *Biochemistry* **1998**, *37*(20), 7478-7486.

231. R. N. Hannoush, S. Carriero, K. L. Min, M. J. Damha. Selective inhibition of HIV-1 reverse transcriptase (HIV-1 RT) RNase H by small RNA hairpins and dumbbells. *ChemBioChem* **2004**, *5*(4), 527-533.

232. R. N. Hannoush, K. L. Min, M. J. Damha. Diversity-oriented solid-phase synthesis and biological evaluation of oligonucleotide hairpins as HIV-1 RT RNase H inhibitors. *Nucleic Acids Res.* **2004**, *32*(21), 6164-6175.

233. J. Coffin, A. Haase, J. A. Levy, L. Montagnier, S. Oroszlan, N. Teich, H. Temin, K. Toyoshima, H. Varmus, P. Vogt, R. Weiss. Human Immunodeficiency Viruses. *Science* **1986**, *232*(4751), 697-697.

234. R. C. Gallo, L. Montagnier. AIDS in 1988. *Sci. Am.* **1988**, *259*(4), 40-48.

235. M. S. Krug, S. L. Berger. Reverse-Transcriptase from Human-Immunodeficiency-Virus - a Single Template-Primer Binding-Site Serves 2 Physically Separable Catalytic Functions. *Biochemistry (Mosc).* **1991**, *30*(44), 10614-10623.

236. Y. El Safadi, V. Vivet-Boudou, R. Marquet. HIV-1 reverse transcriptase inhibitors. *Appl. Microbiol. Biotechnol.* **2007**, *75*(4), 723-737.

237. H. Mitsuya, R. Yarchoan, S. Broder. Molecular Targets for AIDS Therapy. *Science* **1990**, *249*(4976), 1533-1544.

238. V. J. Merluzzi, K. D. Hargrave, M. Labadia, K. Grozinger, M. Skoog, J. C. Wu, C. K. Shih, K. Eckner, S. Hattox, J. Adams, A. S. Rosehthal, R. Faanes, R. J. Eckner, R. A. Koup, J. L. Sullivan. Inhibition of HIV-1 Replication by a Nonnucleoside Reverse-Transcriptase Inhibitor. *Science* **1990**, *250*(4986), 1411-1413.

239. S. M. Hammer, M. S. Saag, M. Schechter, J. S. G. Montaner, R. T. Schooley, D. M. Jacobsen, M. A. Thompson, C. C. J. Carpenter, M. A. Fischl, B. G. Gazzard, J. M. Gatell, M. S. Hirsch, D. A. Katzenstein, D. D. Richman, S. Vella, P. G. Yeni, P. A. Volberding. Treatment for Adult HIV Infection: 2006 Recommendations of the International AIDS Society-USA Panel. *JAMA* **2006**, *296*(7), 827-843.

240. The UK Collaborative Group on HIV Drug Resistance and UK CHIC Study Group. Long-Term Probability of Detecting Drug-Resistant HIV in Treatment-Naive Patients Initiating Combination Antiretroviral Therapy. *Clin. Infect. Dis.* **2010**, *50*(9), 1275-1285.

241. C. Flexner. HIV drug development: the next 25 years. *Nature Reviews Drug Discovery* **2007**, *6*(12), 959-966.

242. O. Schatz, F. V. Cromme, F. Gruningerleitch, S. F. J. Legrice. Point Mutations in Conserved Amino-Acid Residues within the C-Terminal Domain of HIV-1 Reverse-Transcriptase Specifically Repress RNase-H Function. *FEBS Lett.* **1989**, *257*(2), 311-314.

243. E. Tramontano. HIV-1 RNase H: recent progress in an exciting, yet little explored, drug target. *Mini-Rev. Med. Chem.* **2006**, *6*(6), 727-737.

244. M. Ntemgwa, M. A. Wainberg, M. Oliveira, D. Moisi, R. Lalonde, V. Micheli, B. G. Brenner. Variations in reverse transcriptase and RNase H domain mutations in human immunodeficiency virus type 1 clinical isolates are associated with divergent phenotypic resistance to zidovudine. *Antimicrob Agents Ch* **2007**, *51*(11), 3861-3869.

245. A. Hachiya, K. Shimane, S. G. Sarafianos, E. N. Kodama, Y. Sakagami, F. Negishi, H. Koizumi, H. Gatanaga, M. Matsuoka, M. Takiguchi, S. Oka. Clinical relevance of substitutions in the connection subdomain and RNase H domain of HIV-1 reverse transcriptase from a cohort of antiretroviral treatment-naive patients. *Antiviral Res.* **2009**, *82*(3), 115-121.

246. M. Ehteshami, G. L. Beilhartz, B. J. Scarth, E. P. Tchesnokov, S. McCormick, B. Wynhoven, P. R. Harrigan, M. Gotte. Connection domain mutations N348I and A360V in HIV-1 reverse transcriptase enhance resistance to 3 '-azido-3 '-deoxythymidine through both RNase H-dependent and -independent mechanisms. *J. Biol. Chem.* **2008**, *283*(32), 22222-22232.

247. G. Borkow, R. S. Fletcher, J. Barnard, D. Arion, D. Motakis, G. I. Dmitrienko, M. A. Parniak. Inhibition of the ribonuclease H and DNA polymerase activities of HIV-1 reverse transcriptase by N-(4-tert-butylbenzoyl)-2-hydroxy-1-naphthaldehyde hydrazone. *Biochemistry (Mosc).* **1997**, *36*(11), 3179-3185.

248. D. M. Himmel, S. G. Sarafianos, S. Dharmasena, M. M. Hossain, K. McCoy-Simandle, T. Ilina, A. D. Clark, J. L. Knight, J. G. Julias, P. K. Clark, K. Krogh-Jespersen, R. M. Levy, S. H. Hughes, M. A. Parniak, E. Arnold. HIV-1 reverse transcriptase structure with RNase H inhibitor dihydroxy benzoyl naphthyl hydrazone bound at a novel site. *Acs Chem Biol* **2006**, *1*(11), 702-712.

249. C. A. Shaw-Reid, V. Munshi, P. Graham, A. Wolfe, M. Witmer, R. Danzeisen, D. B. Olsen, S. S. Carroll, M. Embrey, J. S. Wai, M. D. Miller, J. L. Cole, D. J. Hazuda. Inhibition of HIV-1 ribonuclease H by a novel diketo acid, 4-[5-(benzoylamino)thien-2-yl]-2,4-dioxobutanoic acid. *J. Biol. Chem.* **2003**, *278*(5), 2777-2780.

250. M. D. Miller, B. Feuston, V. Munshi, K. Getty, J. Krueger, D. J. Hazuda, M. A. Parniak, D. Lewis, J. A. Grobler, C. A. Shaw-Reid. An HIV-1 RNase H inhibitor synergizes with three different classes of RT polymerase inhibitors in an in vitro reverse transcription assay. *Antiviral Therapy* **2005**, *10*(4), S90-S90.

251. M. A. Parniak, K. L. Min, S. R. Budihas, S. F. J. Le Grice, J. A. Beutler. A fluorescence-based high-throughput screening assay for inhibitors of human immunodeficiency virus-1 reverse transcriptase-associated ribonuclease H activity. *Anal. Biochem.* **2003**, *322*(1), 33-39.

252. G. R. Nakayama, P. Bingham, D. Tan, K. A. Maegley. A fluorescence polarization assay for screening inhibitors against the ribonuclease H activity of HIV-1 reverse transcriptase. *Anal. Biochem.* **2006**, *351*(2), 260-265.

253. K. C. King, S. R. Budihas, S. F. J. Le Grice, M. A. Parniak, R. J. Crouch, S. A. Gaidamakov, H. J. Isaaq, A. Wamiru, J. B. McMahon, J. A. Beutler. A capillary electrophoretic assay for ribonuclease H activity. *Anal. Biochem.* **2004**, *331*(2), 296-302.

254. S. R. Budihas, I. Gorshkova, S. Gaidamakov, A. Wamiru, M. K. Bona, M. A. Parniak, R. J. Crouch, J. B. McMahon, J. A. Beutler, S. F. J. Le Grice. Selective inhibition of HIV-1 reverse transcriptase-associated ribonuclease H activity by hydroxylated tropolones. *Nucleic Acids Res.* **2005**, *33*(4), 1249-1256.

255. G. L. Beilhartz, M. Wendeler, N. Baichoo, J. Rausch, S. Le Grice, M. Gotte. HIV-1 Reverse Transcriptase Can Simultaneously Engage Its DNA/RNA Substrate at Both DNA Polymerase and RNase H Active Sites: Implications for RNase H Inhibition. *J. Mol. Biol.* **2009**, *388*(3), 462-474.

256. M. Wendeler, H. F. Lee, A. Bermingham, J. T. Miller, O. Chertov, M. K. Bona, N. S. Baichoo, M. Ehteshami, J. Beutler, B. R. O'Keefe, M. Gotte, M. Kvaratskhelia, S. Le Grice. Vinylogous Ureas as a Novel Class of Inhibitors of Reverse Transcriptase-Associated Ribonuclease H Activity. *Acs Chem Biol* **2008**, *3*(10), 635-644.

257. D. J. Schneider, J. Feigon, Z. Hostomsky, L. Gold. High-Affinity Ssdna Inhibitors of the Reverse-Transcriptase of Type-1 Human-Immunodeficiency-Virus. *Biochemistry (Mosc).* **1995**, *34*(29), 9599-9610.

258. P. J. Joshi, T. W. North, V. R. Prasad. Aptamers directed to HIV-1 reverse transcriptase display greater efficacy over small hairpin RNAs targeted to viral RNA in blocking HIV-1 replication. *Mol. Ther.* **2005**, *11*(5), 677-686.

259. P. Joshi, V. R. Prasad. Potent inhibition of human immunodeficiency virus type 1 replication by template analog reverse transcriptase inhibitors derived by SELEX (systematic evolution of ligands by exponential enrichment). *J. Virol.* **2002**, *76*(13), 6545-6557.

260. J. D. Kissel, D. M. Held, R. W. Hardy, D. H. Burke. Single-stranded DNA aptamer RT1t49 inhibits RT polymerase and RNase H functions of HIV type 1, HIV type 2, and SIVCPZ RTs. *AIDS Res. Hum. Retroviruses* **2007**, *23*(5), 699-708.

261. O. Kensch, B. A. Connolly, H. J. Steinhoff, A. McGregor, R. S. Goody, T. Restle. HIV-1 reverse transcriptase-pseudoknot RNA aptamer interaction has a

binding affinity in the low picomolar range coupled with high specificity. *J. Biol. Chem.* **2000**, *275*(24), 18271-18278.

262. J. J. DeStefano, G. R. Nair. Novel aptamer inhibitors of human immunodeficiency virus reverse transcriptase. *Oligonucleotides* **2008**, *18*(2), 133-143.

263. M.-L. Andreola, F. Pileur, C. Calmels, M. Ventura, L. Tarrago-Litvak, J.-J. Toulme, S. Litvak. DNA Aptamers Selected against the HIV-1 RNase H Display in Vitro Antiviral Activityâ€ *Biochemistry (Mosc).* **2001**, *40*(34), 10087-10094.

264. A. Somasunderam, M. R. Ferguson, D. R. Rojo, V. Thiviyanathan, X. Li, W. A. O'Brien, D. G. Gorenstein. Combinatorial Selection, Inhibition, and Antiviral Activity of DNA Thioaptamers Targeting the RNase H Domain of HIV-1 Reverse Transcriptase. *Biochemistry (Mosc).* **2005**, *44*(30), 10388-10395.

265. C. Cazenave, C. A. Stein, N. Loreau, N. T. Thuong, L. M. Neckers, C. Subasinghe, C. Helene, J. S. Cohen, J. J. Toulme. Comparative Inhibition of Rabbit Globin Messenger-RNA Translation by Modified Antisense Oligodeoxynucleotides. *Nucleic Acids Res.* **1989**, *17*(11), 4255-4273.

266. M. Wasner, D. Arion, G. Borkow, A. Noronha, A. H. Uddin, M. A. Parniak, M. J. Damha. Physicochemical and biochemical properties of 2 ',5 '-linked RNA and 2 ',5 '-RNA : 3 ',5 '-RNA "hybrid" duplexes. *Biochemistry (Mosc).* **1998**, *37*(20), 7478-7486.

267. A. E. Pitts, D. R. Corey. Inhibition of human telomerase by 2 '-O-methyl-RNA. *Proc. Natl. Acad. Sci. U. S. A.* **1998**, *95*(20), 11549-11554.

268. M. Majlessi, N. C. Nelson, M. M. Becker. Advantages of 2 '-O-methyl oligoribonucleotide probes for detecting RNA targets. *Nucleic Acids Res.* **1998**, *26*(9), 2224-2229.

269. C. N. Lok, E. Viazovkina, K. L. Min, E. Nagy, C. J. Wilds, M. J. Damha, M. A. Parniak. Potent gene-specific inhibitory properties of mixed-backbone antisense oligonucleotides comprised of 2 '-deoxy-2 '-fluoro-D-arabinose and 2 '-deoxyribose nucleotides. *Biochemistry (Mosc).* **2002**, *41*(10), 3457-3467.

270. S. G. Sarafianos, K. Das, C. Tantillo, A. D. Clark, J. Ding, J. M. Whitcomb, P. L. Boyer, S. H. Hughes, E. Arnold. Crystal structure of HIV-1 reverse transcriptase in complex with a polypurine tract RNA : DNA. *EMBO Journal* **2001**, *20*(6), 1449-1461.

271. W. P. Bohlayer, J. J. DeStefano. Tighter Binding of HIV Reverse Transcriptase to RNA-DNA versus DNA-DNA Results Mostly from Interactions in the Polymerase Domain and Requires Just a Small Stretch of RNA-DNA. *Biochemistry (Mosc).* **2006**, *45*(24), 7628-7638.

272. S. X. Liu, E. A. Abbondanzieri, J. W. Rausch, S. F. J. Le Grice, X. W. Zhuang. Slide into Action: Dynamic Shuttling of HIV Reverse Transcriptase on Nucleic Acid Substrates. *Science* **2008**, *322*(5904), 1092-1097.

273. W. Metzger, T. Hermann, O. Schatz, S. F. J. Legrice, H. Heumann. Hydroxyl Radical Footprint Analysis of Human-Immunodeficiency-Virus Reverse-Transcriptase Template.Primer Complexes. *Proc. Natl. Acad. Sci. U. S. A.* **1993**, *90*(13), 5909-5913.

274. M. Gotte, G. Maier, H. J. Gross, H. Heumann. Localization of the active site of HIV-1 reverse transcriptase-associated RNase H domain on a DNA template using site-specific generated hydroxyl radicals. *J. Biol. Chem.* **1998**, *273*(17), 10139-10146.

275. M. M. Mangos, M. J. Damha. Flexible and frozen sugar-modified nucleic acids - modulation of biological activity through furanose ring dynamics in the antisense strand. *Curr. Top. Med. Chem.* **2002**, *2*, 1145-1169.

276. F. S. Santiago, H. C. Lowe, M. M. Kavurma, C. N. Chesterman, A. Baker, D. G. Atkins, L. M. Khachigian. New DNA enzyme targeting Egr-1 mRNA inhibits vascular smooth muscle proliferation and regrowth after injury (vol 5, pg 1264, 1999). *Nat. Med.* **1999**, *5*(12), 1438-1438.

277. M. Manoharan, K. L. Tivel, L. K. Andrade, V. Mohan, T. P. Condon, C. F. Bennett, P. D. Cook. Oligonucleotide Conjugates - Alteration of the Pharmacokinetic Properties of Antisense Agents. *Nucleosides Nucleotides* **1995**, *14*(3-5), 969-973.

278. R. N. Hannoush, M. J. Damha. Remarkable Stability of Hairpins Containing 2',5'-Linked RNA Loops. *Journal of the American Chemical Society* **2001**, *123*(49), 12368-12374.

279. D. J. Williams, J. L. Boots, K. B. Hall. Thermodynamics of 2 '-ribose substitutions in UUCG tetraloops. *RNA-a Publication of the RNA Society* **2001**, *7*(1), 44-53.

280. P. A. Giannaris, M. J. Damha. Oligoribonucleotides Containing 2',5'-Phosphodiester Linkages Exhibit Binding Selectivity for 3',5'-RNA over 3',5'-Ssdna. *Nucleic Acids Res.* **1993**, *21*(20), 4742-4749.

281. S. M. Gryaznov, D. H. Lloyd. Modulation of Oligonucleotide Duplex and Triplex Stability Via Hydrophobic Interactions. *Nucleic Acids Res.* **1993**, *21*(25), 5909-5915.

282. R. N. Hannoush, M. J. Damha. Preference for ribose over deoxyribose in loop-closing base pairs of extra stable nucleic acid hairpins. *Nucleosides, Nucleotides and Nucleic Acids* **2005**, *24*(10), 1519 - 1530.

283. M. Manoharan, in *Antisense Drug Technology* (Ed.: S. T. Crooke), Taylor and Francis Group, **2001**.

284. C. Dash, J. W. Rausch, S. F. J. Le Grice. Using pyrrolo-deoxycytosine to probe RNA/DNA hybrids containing the human immunodeficiency virus type-1 3 ' polypurine tract. *Nucleic Acids Res.* **2004**, *32*(4), 1539-1547.

285. G. T. Hermanson, Bioconjugate Techniques, (2), Academic Press, Inc., **2008**.

286. A. N. Mayer, F. Barany. Photoaffinity Cross-Linking of Taqi Restriction-Endonuclease Using an Aryl Azide Linked to the Phosphate Backbone. *Gene* **1995**, *153*(1), 1-8.

287. K. Pari, G. A. Mueller, E. F. DeRose, T. W. Kirby, R. E. London. Solution structure of the RNase H domain of the HIV-1 reverse transcriptase in the presence of magnesium. *Biochemistry (Mosc).* **2003**, *42*(3), 639-650.

288. C. A. Stein, R. Pal, A. L. Devico, G. Hoke, S. Mumbauer, O. Kinstler, M. G. Sarngadharan, R. L. Letsinger. Mode of Action of 5'-Linked Cholesteryl Phosphorothioate Oligodeoxynucleotides in Inhibiting Syncytia Formation and Infection by HIV-1 and HIV-2 Invitro. *Biochemistry (Mosc).* **1991**, *30*(9), 2439-2444.

289. M. Nowotny, S. A. Gaidamakov, R. Ghirlando, S. M. Cerritelli, R. J. Crouch, W. Yang. Structure of human RNase h1 complexed with an RNA/DNA hybrid: Insight into HIV reverse transcription. *Mol. Cell* **2007**, *28*(2), 264-276.

290. B. Wolf, J. A. Lesnaw, Reichman.Me. A Mechanism of Irreversible Inactivation of Bovine Pancreatic Ribonuclease by Diethylpyrocarbonate - a General Reaction of Diethylpyrocarbonate with Proteins. *European Journal of Biochemistry* **1970**, *13*(3), 519-&.

291. C. Mackellar, D. Graham, D. W. Will, S. Burgess, T. Brown. Synthesis and Physical-Properties of Anti-HIV Antisense Oligonucleotides Bearing Terminal Lipophilic Groups. *Nucleic Acids Res.* **1992**, *20*(13), 3411-3417.

292. M. J. Damha, K. K. Ogilvie. Oligoribonucleotide synthesis. The silyl-phosphoramidite method. *Methods in molecular biology (Clifton, N.J.)* **1993**, *20*, 81-114.

293. J. Y. Tang, Y. X. Han, J. X. Tang, Z. D. Zhang. Large-scale synthesis of oligonucleotide phosphorothioates using 3-amino-1,2,4-dithiazole-5-thione as an efficient sulfur-transfer reagent. *Org Process Res Dev* **2000**, *4*(3), 194-198.

294. S. Gabbara, W. R. Davis, L. Hupe, D. Hupe, J. A. Peliska. Inhibitors of DNA strand transfer reactions catalyzed by HIV-1 reverse transcriptase. *Biochemistry (Mosc).* **1999**, *38*(40), 13070-13076.

295. W. R. Davis, J. Tomsho, S. Nikam, E. M. Cook, D. Somand, J. A. Peliska. Inhibition of HIV-1 reverse transcriptase-catalyzed DNA strand transfer reactions by 4-chlorophenylhydrazone of mesoxalic acid. *Biochemistry (Mosc).* **2000**, *39*(46), 14279-14291.

296. M. M. Hanna, C. F. Meares. Synthesis of a Cleavable Dinucleotide Photoaffinity Probe of Ribonucleic-Acid Polymerase - Application to Trinucleotide Labeling of an Escherichia-Coli Transcription Complex. *Biochemistry (Mosc).* **1983**, *22*(15), 3546-3551.

297. B. Canard, R. Sarfati, C. C. Richardson. Binding of RNA template to a complex of HIV-1 reverse transcriptase/primer/template. *Proc. Natl. Acad. Sci. U. S. A.* **1997**, *94*(21), 11279-11284.

298. S. W. Yang, H. A. Nash. Specific Photo-Cross-Linking of DNA-Protein Complexes - Identification of Contacts between Integration Host Factor and Its Target DNA. *Proc. Natl. Acad. Sci. U. S. A.* **1994**, *91*(25), 12183-12187.

299. L. A. Agrofoglio, F. Amblard, S. P. Nolan, S. Charamon, I. Gillaizeau, T. A. Zevaco, P. Guenot. Synthesis of L-cyclopentenyl nucleosides using ring-closing metathesis and palladium-mediated allylic alkylation methodologies. *Tetrahedron* **2004**, *60*(38), 8397-8404.

300. J. Rizzo, L. K. Gifford, X. Zhang, A. M. Gewirtz, P. Lu. Chimeric RNA-DNA molecular beacon assay for ribonuclease H activity. *Mol. Cell. Probes* **2002**, *16*(4), 277-283.

301. N. McLellan, X. Wei, B. Marchand, M. A. Wainberg, M. Gotte. Nonradioactive detection of retroviral-associated RNase H activity in a microplate-based, high-throughput format. *BioTechniques* **2002**, *33*(2), 424-429.

302. C. J. Y. Yan Chen, Yanrong Wu, Patrick Conlon, Youngmi Kim, Hui Lin, Weihong Tan. Light-Switching Excimer Beacon Assays For Ribonuclease H Kinetic Study. *ChemBioChem* **2008**, *9*(3), 355-359.

303. S. Tyagi, F. R. Kramer. Molecular beacons: Probes that fluoresce upon hybridization. *Nature Biotechnology* **1996**, *14*(3), 303-308.

304. M. J. Rist, J. P. Marino. Fluorescent nucleotide base analogs as probes of nucleic acid structure, dynamics and interactions. *Curr. Org. Chem.* **2002**, *6*(9), 775-793.

305. D. W. Dodd, R. H. E. Hudson. Intrinsically Fluorescent Base-Discriminating Nucleoside Analogs. *Mini - Reviews in Organic Chemistry* **2009**, *6*, 378-391.

306. A. Okamoto, Y. Saito, I. Saito. Design of base-discriminating fluorescent nucleosides. *Journal of Photochemistry and Photobiology C-Photochemistry Reviews* **2005**, *6*(2-3), 108-122.

307. M. E. Hawkins, F. M. Balis. Use of pteridine nucleoside analogs as hybridization probes. *Nucl. Acids Res.* **2004**, *32*(7), e62-.

308. Y. Tor. Exploring RNA-ligand interactions. *Pure Appl. Chem.* **2009**, *81*(2), 263-272.

309. P. Sandin, G. Stengel, T. Ljungdahl, K. Borjesson, B. Macao, L. M. Wilhelmsson. Highly efficient incorporation of the fluorescent nucleotide analogs tC and tCO by Klenow fragment. *Nucl. Acids Res.* **2009**, *37*(12), 3924-3933.

310. J. N. Wilson, E. T. Kool. Fluorescent DNA base replacements: reporters and sensors for biological systems. *Org Biomol Chem* **2006**, *4*(23), 4265-4274.

311. E. Socher, L. Bethge, A. Knoll, N. Jungnick, A. Herrmann, O. Seitz. Low-Noise Stemless PNA Beacons for Sensitive DNA and RNA Detection. *Angew Chem Int Edit* **2008**, *47*(49), 9555-9559.

312. S. G. Srivatsan, N. J. Greco, Y. Tor. A highly emissive fluorescent nucleoside that signals the activity of toxic ribosome-inactivating proteins. *Angew Chem Int Edit* **2008**, *47*(35), 6661-6665.

313. G. Stengel, J. P. Gill, P. Sandin, L. M. Wilhelmsson, B. Albinsson, B. Norden, D. Millar. Conformational dynamics of DNA polymerase probed with a novel fluorescent DNA base analogue. *Biochemistry (Mosc).* **2007**, *46*(43), 12289-12297.

314. H. Inoue, A. Imura, E. Ohtsuka. Synthesis of Dodecadeoxyribonucleotides Containing a Pyrrolo[2,3-D]Pyrimidine Nucleoside and Their Base-Pairing Ability. *Nippon Kagaku Kaishi* **1987**(7), 1214-1220.

315. J. Woo, R. B. Meyer, Jr., H. B. Gamper. G/C-modified oligodeoxynucleotides with selective complementarity: synthesis and hybridization properties. *Nucl. Acids Res.* **1996**, *24*(13), 2470-2475.

316. C. H. Liu, C. T. Martin. Fluorescence characterization of the transcription bubble in elongation complexes of T7 RNA polymerase. *J. Mol. Biol.* **2001**, *308*(3), 465-475.

317. C. H. Liu, C. T. Martin. Promoter clearance by T7 RNA polymerase - Initial bubble collapse and transcript dissociation monitored by base analog fluorescence. *J. Biol. Chem.* **2002**, *277*(4), 2725-2731.

318. D. A. Berry, K. Y. Jung, D. S. Wise, A. D. Sercel, W. H. Pearson, H. Mackie, J. B. Randolph, R. L. Somers. Pyrrolo-dC and pyrrolo-C: fluorescent analogs of cytidine and 2 '-deoxycytidine for the study of oligonucleotides. *Tetrahedron Lett.* **2004**, *45*(11), 2457-2461.

319. P. Chen, C. A. He. A general strategy to convert the MerR family proteins into highly sensitive and selective fluorescent biosensors for metal ions. *J. Am. Chem. Soc.* **2004**, *126*(3), 728-729.

320. C. M. Zhang, C. P. Liu, T. Christian, H. Gamper, J. Rozenski, D. L. Pan, J. B. Randolph, E. Wickstrom, B. S. Cooperman, Y. M. Hou. Pyrrolo-C as a molecular probe for monitoring conformations of the tRNA 3 ' end. *RNA-a Publication of the RNA Society* **2008**, *14*(10), 2245-2253.

321. R. A. Tinsley, N. G. Walter. Pyrrolo-C as a fluorescent probe for monitoring RNA secondary structure formation. *RNA* **2006**, *12*(3), 522-529.

322. R. H. E. Hudson, A. Ghorbani-Choghamarani. Selective fluorometric detection of guanosine-containing sequences by 6-phenylpyrrolocytidine in DNA. *Synlett* **2007**(6), 870-873.

323. R. H. E. Hudson, A. K. Dambenieks, R. D. Viirre. Fluorescent 7-deazapurine derivatives from 5-iodocytosine via a tandem cross-coupling-annulation reaction with terminal alkynes. *Synlett* **2004**(13), 2400-2402.

324. F. Wojciechowski, R. H. E. Hudson. Fluorescence and hybridization properties of peptide nucleic acid containing a substituted phenylpyrrolocytosine designed to engage guanine with an additional H-bond. *J. Am. Chem. Soc.* **2008**, *130*(38), 12574-12575.

325. R. H. E. Hudson, A. G. Choghamarani. The 6-methoxymethyl derivative of pyrrolo-dC for selective fluorometric detection of guanosine-containing sequences. *Nucleosides Nucleotides & Nucleic Acids* **2007**, *26*(6-7), 533-537.

326. M. J. Robins, P. J. Barr. Nucleic-Acid Related-Compounds .39. Efficient Conversion of 5-Iodo to 5-Alkynyl and Derived 5-Substituted Uracil Bases and Nucleosides. *J. Org. Chem.* **1983**, *48*(11), 1854-1862.

327. M. J. Robins, P. J. Barr. Nucleic-Acid Related-Compounds .31. Smooth and Efficient Palladium-Copper Catalyzed Coupling of Terminal Alkynes with 5-Iodouracil Nucleosides. *Tetrahedron Lett.* **1981**, *22*(5), 421-424.

328. V. Aucagne, F. Amblard, L. A. Agrofoglio. Highly efficient AgNO3-catalyzed preparation of substituted furanopyrimidine nucleosides. *Synlett* **2004**(13), 2406-2408.

329. D. J. Patel, C. W. Hilbers. Proton Nuclear Magnetic-Resonance Investigations of Fraying in Double-Stranded D-Aptpgpcpapt in H2o Solution. *Biochemistry (Mosc).* **1975**, *14*(12), 2651-2656.

330. K. Ziomek, E. Kierzek, E. Biala, R. Kierzek. The thermal stability of RNA duplexes containing modified base pairs placed at internal and terminal positions of the oligoribonucleotides. *Biophys. Chem.* **2002**, *97*(2-3), 233-241.

331. M. Terrazas, E. T. Kool. RNA major groove modifications improve siRNA stability and biological activity. *Nucleic Acids Res.* **2009**, *37*(2), 346-353.

332. S. J. O. Hardman, S. W. Botchway, K. C. Thompson. Evidence for a Nonbase Stacking Effect for the Environment-sensitive Fluorescent Base Pyrrolocytosine-Comparison with 2-Aminopurine. *Photochem. Photobiol.* **2008**, *84*(6), 1473-1479.

333. S. J. O. Hardman, K. C. Thompson. Influence of base stacking and hydrogen bonding on the fluorescence of 2-aminopurine and pyrrolocytosine in nucleic acids. *Biochemistry (Mosc).* **2006**, *45*(30), 9145-9155.

334. Y. Saito, Y. Shinohara, S. S. Bag, Y. Takeuchi, K. Matsumoto, I. Saito. Ends free and self-quenched molecular beacon with pyrene labeled pyrrolocytidine in the middle of the stem. *Tetrahedron* **2009**, *65*(4), 934-939.

335. Lakowics. Principles of Fluorescence Spectrospcopy.

336. S. T. Crooke, K. M. Lemonidis, L. Neilson, R. Griffey, E. A. Lesnik, B. P. Monia. Kinetic Characteristics of Escherichia-Coli RNase H1 - Cleavage of Various Antisense Oligonucleotide-RNA Duplexes. *Biochem. J* **1995**, *312*, 599-608.

337. P. Sandin, K. Borjesson, H. Li, J. Martensson, T. Brown, L. M. Wilhelmsson, B. Albinsson. Characterization and use of an unprecedentedly bright and structurally non-perturbing fluorescent DNA base analogue. *Nucleic Acids Res.* **2008**, *36*(1), 157-167.

338. J. M. Layzer, A. P. McCaffrey, A. K. Tanner, Z. Huang, M. A. Kay, B. A. Sullenger. In vivo activity of nuclease-resistant siRNAs. *RNA-a Publication of the RNA Society* **2004**, *10*(5), 766-771.

339. L. Alexopoulou, A. C. Holt, R. Medzhitov, R. A. Flavell. Recognition of double-stranded RNA and activation of NF-kappa B by Toll-like receptor 3. *Nature* **2001**, *413*(6857), 732-738.

340. M. E. Kleinman, K. Yamada, A. Takeda, V. Chandrasekaran, M. Nozaki, J. Z. Baffi, R. J. C. Albuquerque, S. Yamasaki, M. Itaya, Y. Z. Pan, B. Appukuttan, D. Gibbs, Z. L. Yang, K. Kariko, B. K. Ambati, T. A. Wilgus, L. A. DiPietro, E. Sakurai, K. Zhang, J. R. Smith, E. W. Taylor, J. Ambati. Sequence- and target-independent angiogenesis suppression by siRNA via TLR3. *Nature* **2008**, *452*(7187), 591-U591.

341. M. Robbins, A. Judge, I. MacLachlan. siRNA and Innate Immunity. *Oligonucleotides* **2009**, *19*(2), 89-101.

342. J. K. Watts, B. D. Johnston, K. Jayakanthan, A. S. Wahba, B. M. Pinto, M. J. Damha. Synthesis and biophysical characterization of oligonucleotides containing a 4 '-selenonucleotide. *J. Am. Chem. Soc.* **2008**, *130*(27), 8578-+.

343. K. Ui-Tei, Y. Naito, S. Zenno, K. Nishi, K. Yamato, F. Takahashi, A. Juni, K. Saigo. Functional dissection of siRNA sequence by systematic DNA substitution: modified siRNA with a DNA seed arm is a powerful tool for mammalian gene silencing with significantly reduced off-target effect. *Nucl. Acids Res.* **2008**, gkn042.

344. K. Ui-Tei, Y. Naito, K. Nishi, A. Juni, K. Saigo. Thermodynamic stability and Watson-Crick base pairing in the seed duplex are major determinants of the efficiency of the siRNA-based off-target effect. *Nucl. Acids Res.* **2008**, *36*(22), 7100-7109.

345. D. V. Morrissey, J. A. Lockridge, L. Shaw, K. Blanchard, K. Jensen, W. Breen, K. Hartsough, L. Machemer, S. Radka, V. Jadhav, N. Vaish, S. Zinnen, C. Vargeese, K. Bowman, C. S. Shaffer, L. B. Jeffs, A. Judge, I. MacLachlan, B. Polisky. Potent and persistent in vivo anti-HBV activity of chemically modified siRNAs. *Nat. Biotechnol.* **2005**, *23*(8), 1002-1007.

346. A. D. Judge, G. Bola, A. C. H. Lee, I. MacLachlan. Design of noninflammatory synthetic siRNA mediating potent gene silencing in vivo. *Mol. Ther.* **2006**, *13*(3), 494-505.

347. J. Soutschek, A. Akinc, B. Bramlage, K. Charisse, R. Constien, M. Donoghue, S. Elbashir, A. Geick, P. Hadwiger, J. Harborth, M. John, V. Kesavan, G. Lavine, R. K. Pandey, T. Racie, K. G. Rajeev, I. Rohl, I. Toudjarska, G. Wang, S. Wuschko, D. Bumcrot, V. Koteliansky, S. Limmer, M. Manoharan, H. P. Vornlocher. Therapeutic silencing of an endogenous gene by systemic administration of modified siRNAs. *Nature* **2004**, *432*(7014), 173-178.

348. T. S. Zimmermann, A. C. H. Lee, A. Akinc, B. Bramlage, D. Bumcrot, M. N. Fedoruk, J. Harborth, J. A. Heyes, L. B. Jeffs, M. John, A. D. Judge, K. Lam, K. McClintock, L. V. Nechev, L. R. Palmer, T. Racie, I. Rohl, S. Seiffert, S. Shanmugam, V. Sood, J. Soutschek, I. Toudjarska, A. J. Wheat, E. Yaworski, W. Zedalis, V. Koteliansky, M. Manoharan, H. P. Vornlocher, I. MacLachlan. RNAi-mediated gene silencing in non-human primates. *Nature* **2006**, *441*(7089), 111-114.

349. S. Parrish, J. Fleenor, S. Q. Xu, C. Mello, A. Fire. Functional anatomy of a dsRNA trigger: Differential requirement for the two trigger strands in RNA interference. *Mol. Cell* **2000**, *6*(5), 1077-1087.

350. Y. L. Chiu, T. M. Rana. siRNA function in RNAi: A chemical modification analysis. *RNA-a Publication of the RNA Society* **2003**, *9*(9), 1034-1048.

351. A. Khvorova, A. Reynolds, S. D. Jayasena. Functional siRNAs and miRNAs exhibit strand bias. *Cell* **2003**, *115*(2), 209-216.

352. D. S. Schwarz, G. Hutvagner, T. Du, Z. Xu, N. Aronin, P. D. Zamore. Asymmetry in the assembly of the RNAi enzyme complex. *Cell* **2003**, *115*(2), 199-208.

353. K. Sipa, E. Sochacka, J. Kazmierczak-Baranska, M. Maszewska, M. Janicka, G. Nowak, B. Nawrot. Effect of base modifications on structure, thermodynamic stability, and gene silencing activity of short interfering RNA. *RNA-a Publication of the RNA Society* **2007**, *13*(8), 1301-1316.

354. A. Somoza, J. Chelliserrykattil, E. T. Kool. The roles of hydrogen bonding and sterics in RNA interference. *Angew Chem Int Edit* **2006**, *45*(30), 4994-4997.

355. A. Somoza, A. P. Silverman, R. M. Miller, J. Chelliserrykattil, E. T. Kool. Steric effects in RNA interference: Probing the influence of nucleobase size and shape. *Chem-Eur J* **2008**, *14*(26), 7978-7987.

356. J. Xia, A. Noronha, I. Toudjarska, F. Li, A. Akinc, R. Braich, M. Frank-Kamenetsky, K. G. Rajeev, M. Egli, M. Manoharan. Gene sitencing activity of siRNAs with a ribo-difluorotoluyl nucteotide. *Acs Chem Biol* **2006**, *1*(3), 176-183.

357. K. Kariko, M. Buckstein, H. P. Ni, D. Weissman. Suppression of RNA recognition by Toll-like receptors: The impact of nucleoside modification and the evolutionary origin of RNA. *Immunity* **2005**, *23*(2), 165-175.

358. F. Eberle, K. Giessler, C. Deck, K. Heeg, M. Peter, C. Richert, A. H. Dalpke. Modifications in small interfering RNA that separate immunostimulation from RNA interference. *J. Immunol.* **2008**, *180*(5), 3229-3237.

359. A. S. Wahba, M. J. Damha, R. H. E. Hudson. RNA containing pyrrolocytidine base analogs: good binding affinity and fluorescence that responds to hybridization. *NUCLEIC ACIDS SYMP SER (OXF)* **2008**, *52*(1), 399-400.

360. S. Y. Berezhna, L. Supekova, F. Supev, P. G. Schultz, A. A. Deniz. siRNA in human cells selectively localizes to target RNA sites. *Proc. Natl. Acad. Sci. U. S. A.* **2006**, *103*(20), 7682-7687.

361. A. S. Wahba, A. Esmaeili, M. J. Damha, R. H. E. Hudson. A single-label phenylpyrrolocytidine provides a molecular beacon-like response reporting HIV-1 RT RNase H activity. *Nucl. Acids Res.* **2009**, gkp1022.

362. C. A. M. Seidel, A. Schulz, M. H. M. Sauer. Nucleobase-specific quenching of fluorescent dyes .1. Nucleobase one-electron redox potentials and their correlation with static and dynamic quenching efficiencies. *J. Phys. Chem.* **1996**, *100*(13), 5541-5553.

363. F. D. Lewis, T. F. Wu, Y. F. Zhang, R. L. Letsinger, S. R. Greenfield, M. R. Wasielewski. Distance-dependent electron transfer in DNA hairpins. *Science* **1997**, *277*(5326), 673-676.

364. L. N. M. Duysens, J. Amesz. Fluorescence Spectrophotometry of Reduced Phosphopyridine Nucleotide in Intact Cells in the near-Ultraviolet and Visible Region. *Biochim. Biophys. Acta* **1957**, *24*(1), 19-26.

365. J. X. Hua, D. W. Dodd, R. H. E. Hudson, D. R. Corey. Cellular localization and allele-selective inhibition of mutant huntingtin protein by peptide nucleic acid oligomers containing the fluorescent nucleobase [bis-o-(aminoethoxy)phenyl]pyrrolocytosine. *Bioorg. Med. Chem. Lett.* **2009**, *19*(21), 6181-6184.

366. P. Sandin, P. Lincoln, T. Brown, L. M. Wilhelmsson. Synthesis and oligonucleotide incorporation of fluorescent cytosine analogue tC: a promising nucleic acid probe. *Nature Protocols* **2007**, *2*(3), 615-623.

367. C. A. Stein, J. B. Hansen, J. Lai, S. Wu, A. Voskresenskiy, A. Hog, J. Worm, M. Hedtjarn, N. Souleimanian, P. Miller, H. S. Soifer, D. Castanotto, L. Benimetskaya, H. Orum, T. Koch. Efficient gene silencing by delivery of locked nucleic acid antisense oligonucleotides, unassisted by transfection reagents. *Nucl. Acids Res.* **2009**, gkp841.

368. V. Hornung, J. Ellegast, S. Kim, K. Brzozka, A. Jung, H. Kato, H. Poeck, S. Akira, K. K. Conzelmann, M. Schlee, S. Endres, G. Hartmann. 5 '-triphosphate RNA is the ligand for RIG-I. *Science* **2006**, *314*(5801), 994-997.

369. A. D. Judge, V. Sood, J. R. Shaw, D. Fang, K. McClintock, I. MacLachlan. Sequence-dependent stimulation of the mammalian innate immune response by synthetic siRNA. *Nat. Biotechnol.* **2005**, *23*(4), 457-462.

370. V. Hornung, M. Guenthner-Biller, C. Bourquin, A. Ablasser, M. Schlee, S. Uematsu, A. Noronha, M. Manoharan, S. Akira, A. de Fougerolles, S. Endres, G. Hartmann. Sequence-specific potent induction of IFN-alpha by short interfering RNA in plasmacytoid dendritic cells through TLR7. *Nat. Med.* **2005**, *11*(3), 263-270.

371. G. Shan, Y. J. Li, J. L. Zhang, W. D. Li, K. E. Szulwach, R. H. Duan, M. A. Faghihi, A. M. Khalil, L. H. Lu, Z. Paroo, A. W. S. Chan, Z. J. Shi, Q. H. Liu, C. Wahlestedt, C. He, P. Jin. A small molecule enhances RNA interference and promotes microRNA processing. *Nat. Biotechnol.* **2008**, *26*(8), 933-940.

372. O. Novac, A.-S. Guenier, J. Pelletier. Inhibitors of protein synthesis identified by a high throughput multiplexed translation screen. *Nucl. Acids Res.* **2004**, *32*(3), 902-915.

373. R. S. Pillai, S. N. Bhattacharyya, C. G. Artus, T. Zoller, N. Cougot, E. Basyuk, E. Bertrand, W. Filipowicz. Inhibition of Translational Initiation by Let-7 MicroRNA in Human Cells. *Science* **2005**, *309*(5740), 1573-1576.

374. J. Deval. Antimicrobial Strategies Inhibition of Viral Polymerases by 3 '-Hydroxyl Nucleosides. *Drugs* **2009**, *69*(2), 151-166.

375. A. M. Noronha, D. Arion, M. A. Parniak, M. J. Damha. Effect of substituting arabinonucleosides for deoxynucleotides in the DNA priming strand on the polymerase action of HIV-1 RT. *Nucleosides Nucleotides & Nucleic Acids* **2001**, *20*(4-7), 1205-1209.

376. P. L. Boyer, J. G. Julias, V. E. Marquez, S. H. Hughes. Fixed conformation nucleoside analogs effectively inhibit excision-proficient HIV-1 reverse transcriptases. *Journal of Molecular Biology* **2005**, *345*(3), 441-450.

377. E. P. Tchesnokov, A. Obikhod, R. F. Schinazi, M. Gotte. Delayed Chain Termination Protects the Anti-hepatitis B Virus Drug Entecavir from Excision by HIV-1 Reverse Transcriptase. *J. Biol. Chem.* **2008**, *283*(49), 34218-34228.

378. P. L. Boyer, J. G. Julias, Z. Ambrose, M. A. Siddiqui, V. E. MarqueZ, S. H. Hughes. The nucleoside analogs 4 ' C-Methyl thymidine and 4 ' C-Ethyl thymidine block DNA synthesis by wild-type HIV-1 RT and excision proficient NRTI resistant RT variants. *J. Mol. Biol.* **2007**, *371*(4), 873-882.

379. E. Michailidis, B. Marchand, E. N. Kodama, K. Singh, M. Matsuoka, K. A. Kirby, E. M. Ryan, A. M. Sawani, E. Nagy, N. Ashida, H. Mitsuya, M. A. Parniak, S. G. Sarafianos. Mechanism of Inhibition of HIV-1 Reverse Transcriptase by 4 '-Ethynyl-2-fluoro-2 '-deoxyadenosine Triphosphate, a Translocation-defective Reverse Transcriptase Inhibitor. *J. Biol. Chem.* **2009**, *284*(51), 35681-35691.

380. S. Dharmasena, Z. Pongracz, E. Arnold, S. G. Sarafianos, M. A. Parniak. 3 '-azido-3 '-deoxythymidine-(5 ')-tetraphospho-(5 ')-adenosine, the product of ATP-Mediated excision of chain-terminating AZTMP, is a potent chain-terminating substrate for HIV-1 reverse transcriptase. *Biochemistry (Mosc).* **2007**, *46*(3), 828-836.

381. Y. C. Song, J. M. W. Chan, Z. Tovian, A. Secrest, E. Nagy, K. Krysiak, K. Bergan, M. A. Parniak, E. Oldfield. Bisphosphonate inhibitors of ATP-mediated HIV-1 reverse transcriptase catalyzed excision of chain-terminating 3 '-azido, 3 '-deoxythymidine: A QSAR investigation. *Biorg. Med. Chem.* **2008**, *16*(19), 8959-8967.

382. C. Cruchaga, E. Anso, M. Font, V. S. Martino, A. Rouzaut, J. J. Martinez-Irujo. A new strategy to inhibit the excision reaction catalysed by HIV-1 reverse transcriptase: compounds that compete with the template-primer. *Biochem. J* **2007**, *405*, 165-171.

383. G. Borkow, D. Arion, M. A. Wainberg, M. A. Parniak. The thiocarboxanilide nonnucleoside inhibitor UC781 restores antiviral activity of 3 '-azido-3 '-deoxythymidine (AZT) against AZT-resistant human immunodeficiency virus type 1. *Antimicrob. Agents Chemother.* **1999**, *43*(2), 259-263.

384. L. Odriozola, C. Cruchaga, M. Andreola, V. Dolle, C. H. Nguyen, L. Tarrago-Litvak, A. Perez-Mediavilla, J. J. Martinez-Irujo. Non-nucleoside inhibitors of HIV-1 reverse transcriptase inhibit phosphorolysis and resensitize the 3 '-azido-

3 '-deoxythymidine (AZT)-resistant polymerase to AZT-5 '-triphosphate. *J. Biol. Chem.* **2003**, *278*(43), 42710-42716.

385. P. L. Boyer, S. G. Sarafianos, E. Arnold, S. H. Hughes. Analysis of mutations at positions 115 and 116 in the dNTP binding site of HIV-1 reverse transcriptase. *Proc. Natl. Acad. Sci. U. S. A.* **2000**, *97*(7), 3056-3061.

386. C. G. Peng, M. J. Damha. Probing DNA polymerase activity with stereoisomeric 2'-fluoro-beta-D-arabinose (2'F-araNTPs) and 2'-fluoro-beta-D-ribose (2'F-rNTPs) nucleoside 5-triphosphates. *Canadian Journal of Chemistry-Revue Canadienne De Chimie* **2008**, *86*(9), 881-891.

387. W. Guschlbauer, K. Jankowski. Nucleoside Conformation Is Determined by the Electronegativity of the Sugar Substituent. *Nucleic Acids Res.* **1980**, *8*(6), 1421-1433.

388. J. Plavec, L. H. Koole, A. Sandstrom, J. Chattopadhyaya. Structural Studies of Anti-HIV 3'-Alpha-Fluorothymidine and 3'-Alpha-Azidothymidine by 500 Mhz H-1-NMR Spectroscopy and Molecular Mechanics (Mm2) Calculations. *Tetrahedron* **1991**, *47*(35), 7363-7376.

389. T. M. Cao, S. E. Bingham, M. T. Sung. A Novel Route for Solid-Phase Synthesis of Polynucleotides Using Phosphite Chemistry. *Tetrahedron Letters* **1983**, *24*(10), 1019-1020.

390. S. L. Beaucage. A Simple and Efficient Preparation of Deoxynucleoside Phosphoramidites Insitu. *Tetrahedron Lett.* **1984**, *25*(4), 375-378.

391. W. T. Tan, R. P. Iyer, Z. W. Jiang, D. Yu, S. Agrawal. An Efficient Synthesis of Radioisotopically Labeled Oligonucleotides through Direct Solid-Phase 5'-Phosphitylation. *Tetrahedron Lett.* **1995**, *36*(30), 5323-5326.

392. C. Vargeese, J. Carter, J. Yegge, S. Krivjansky, A. Settle, E. Kropp, K. Peterson, W. Pieken. Efficient activation of nucleoside phosphoramidites with 4,5-dicyanoimidazole during oligonucleotide synthesis. *Nucleic Acids Res.* **1998**, *26*(4), 1046-1050.

393. F. Wincott, A. Direnzo, C. Shaffer, S. Grimm, D. Tracz, C. Workman, D. Sweedler, C. Gonzalez, S. Scaringe, N. Usman. Synthesis, Deprotection, Analysis and Purification of RNA and Ribozymes. *Nucleic Acids Res.* **1995**, *23*(14), 2677-2684.

394. S. Carriero, Ph.D. Thesis, McGill University (Montreal, QC), **2003**.

395. T. Wada, A. Mochizuki, S. Higashiya, H. Tsuruoka, S. Kawahara, M. Ishikawa, M. Sekine. Synthesis and properties of 2-azidodeoxyadenosine and

its incorporation into oligodeoxynucleotides. *Tetrahedron Letters* **2001**, *42*(52), 9215-9219.

396. J. Stawinski, A. Kraszewski. How to get the most out of two phosphorus chemistries. studies on H-phosphonates. *Acc. Chem. Res.* **2002**, *35*(11), 952-960.

397. J. B. Houseknecht, C. Altona, C. M. Hadad, T. L. Lowary. Conformational analysis of furanose rings with PSEUROT: Parametrization for rings possessing the arabino, lyxo, ribo, and xylo stereochemistry and application to arabinofuranosides. *J. Org. Chem.* **2002**, *67*(14), 4647-4651.

398. G. X. Gao, M. Orlova, M. M. Georgiadis, W. A. Hendrickson, S. P. Goff. Conferring RNA polymerase activity to a DNA polymerase: A single residue in reverse transcriptase controls substrate selection. *Proc. Natl. Acad. Sci. U. S. A.* **1997**, *94*(2), 407-411.

399. N. Sluis-Cremer, D. Arion, U. Parikh, D. Koontz, R. F. Schinazi, J. W. Mellors, M. A. Parniak. The 3 '-azido group is not the primary determinant of 3 '-azido-3 '-deoxythymidine (AZT) responsible for the excision phenotype of AZT-resistant HIV-1. *J. Biol. Chem.* **2005**, *280*(32), 29047-29052.

400. A. S. Wahba, A. Esmaeili, M. J. Damha, R. H. E. Hudson. A single-label phenylpyrrolocytidine provides a molecular beacon-like response reporting HIV-1 RT RNase H activity. *Nucleic Acids Res.* **2010**, *38*(3), 1048-1056.

401. A. A. Krayevsky, N. B. Tarussova, Q. Y. Zhu, P. Vidal, T. C. Chou, P. Baron, B. Polsky, X. J. Jiang, J. Matulicadamic, I. Rosenberg, K. A. Watanabe. Nucleosides .156. 5'-Hydrogenphosphonates and 5'-Methylphosphonates of Sugar Modified Pyrimidine Nucleosides as Potential Anti-HIV-1 Agents. *Nucleosides Nucleotides* **1992**, *11*(2-4), 177-196.

402. J. Stawinski, R. Strömberg. Deoxyribo-and ribonucleoside H-phosphonates. *Curr. Protoc. Nucleic Acid Chem., Beaucage, S.L, Herdewijn, P., Matsuda, A. Ed.s, John Wiley & Sons* **2001**, *Unit 2.6*, 1-15.

403. R. Strömberg, J. Stawinski. Synthetic strategies and parameters involved in the synthesis of oligodeoxyribo-and oligoribonucleotides according to the H-phosphonate method. *Curr. Protoc. Nucleic Acid Chem., Beaucage, S.L, Herdewijn, P., Matsuda, A. Ed.s, John Wiley & Sons* **2000**, *Unit 3.4*, 1-11.